ANTENNAS WITH FREQUENCY DOMAIN

CONTROL FOR FUTURE COMMUNICATION

SYSTEMS

By

Zhen Hua Sampson Hu

A Thesis submitted to the College of

Engineering and Physical Sciences, University

of Birmingham, for the degree of

DOCTOR OF PHILOSOPHY

School of Electronic, Electrical, & Computer Engineering,

University of Birmingham, Edgbaston,

Birmingham, B15 2TT,

U.K.

UNIVERSITY^{OF} BIRMINGHAM

University of Birmingham Research Archive

e-theses repository

ABSTRACT

This dissertation describes research into "Antennas with Frequency Domain Control for Future Communication Systems" and several novel antennas are shown, each of which addresses a specific issue for current and future communication systems, in terms of wideband coverage, channel capacity, antenna isolation and band-rejection. These antenna designs may be candidates for implementation in future multiband radios, and software defined radio (SDR) and cognitive radio (CR) systems, which are two new concepts in wireless communications in the foreseeable future, although it is evident that there are as yet no clear specifications for those future systems.

A novel two-port reconfigurable antenna which can operate within a narrowband or wideband mode is presented. Three different structures of wideband reconfigurable balanced antennas, with a wide tuning range, have been proposed. When the balanced antenna is combined with the two-port chassis antenna, it becomes a reconfigurable MIMO antenna for small terminals and at least 15 dB of isolation is achieved. Several designs of conical monopole antennas, incorporating different types of slots to achieve good band-rejection behaviour, have been introduced. These are the 2 C-shaped, 4 C-shaped slots, 4 U-shaped slots, 4 tilted-U-shaped slots and 4 U-C-shaped slots. The study of wideband antennas with notched-band behaviour using a simple equivalent circuit model has been proposed. It has been noted that increasing the number of resonators and the coupling factor will increase the band-rejection. However, it will also widen the bandwidth of the frequency notched band. A novel pyramidal monopole antenna, with four loop shaped slots, offering wide tunable band-notch, is also presented.

DEDICATION

This thesis is dedicated to

My Parents

And

My Wife (Shi Zhou)

ACKNOWLEDGEMENTS

First of all, I want to thank Professor Peter S. Hall for providing a very interesting research topic for my thesis and for his kind supervision, and especially his support, encouragement and invaluable guidance.

I would like to thank my 2nd supervisor Dr. Peter Gardner for sharing his extensive experience in RF/microwave design and academic work.

I would also like to thank all members in the Communication Engineering Research Group for their help and support over the last three years, particularly to Dr. James Kelly, Dr. Yuriy Nechayev and Mr. Zhengpeng Wang. I am very grateful to Mr. Alan Yates for providing all the technical support in using the equipment and making the antennas and Mr. Warren Hay for workshop support.

Special thanks also go to my other brilliant colleagues and very nice friends, Jin Tang, Xiao Tong, Baifan Yang, Yu Ying Tu, Sio Fong Leong, Chunyang Xu, Ziyu Chen, Ming Xiao, Elham Ebrahimi, Donya Jasteh, Lida Akhoonzadeh-Asl, Rijal Hamid, Xianyue Wu, Somayeh Chanaani, Ghaith Mansour, Oluwabunmi Tade, etc. With all your support and encouragement, my study life becomes happy in all respects!

Finally, I would like to give my deepest gratitude to my parents for their unconditional support and love. I would also like to give my utmost gratitude to my wife Shi Zhou. Thanks for believing in me. Their generous support and boundless love mean the most to me.

PATENTS AND PUBLICATIONS

Patents:

1. **Z. H. Hu** and P. S. Hall, "Reconfigurable Balanced Antenna", International PCT/GB2011/001598, 2011

2. **Z. H. Hu** and P. S. Hall, "Multi-Output Chassis-Antenna", U.K Patent application GB1112839.4. 2011

3. **Z. H. Hu** and P. S. Hall, "Reconfigurable Balanced Antenna", U.K Patent application GB1108456.3. 2011

4. **Z. H. Hu** and P. S. Hall, "Balanced Antenna System", U.K. Patent application GB1020202.6. 2010

Publications:

Journal Papers:

1. **Z. H. Hu,** Y. Nechayev, P. S. Hall and P. Gardner, "Reconfigurable MIMO antenna for small handheld terminals", submitted to *IEEE Transactions on Antenna and Propagation,* 2011.

2. **Z. H. Hu,** C. T. P. Song, J. R. Kelly, P. S. Hall and P. Gardner, "Dual band reconfigurable chassis-antenna for small handheld terminals", submitted to *IEEE Transactions on Antenna and Propagation,* 2011.

3. **Z. H. Hu,** J. R. Kelly, P. S. Hall and P. Gardner, "Wideband conical monopole antenna with integrated stopband filter", *Progress In Electromagnetics Research* C, Vol. 27, 2012, pp. 223-238.

4. **Z. H. Hu,** P. S. Hall, J. R. Kelly, and P. Gardner, "Wideband pyramidal monopole antenna with wide tunable frequency band-notch", submitted to *IET Microwaves, Antenna and Propagation,* 2011.

5. **Z. H. Hu,** P. S. Hall, and P. Gardner, "Novel reconfigurable dipole-chassis antennas for small terminal MIMO applications", *Electronics Letters*, Vol. 47, No. 17, 18th August 2011, pp. 953-955

6. **Z. H. Hu,** P. S. Hall, J. R. Kelly, and P. Gardner, "Improved band-notched wideband conical monopole antenna", *Microwave and Optical Technology Letters,* Vol. 53, Issue 8, 17 May 2011, pp. 1825-1829

7. **Z. H. Hu,** P. S. Hall, J. R. Kelly, and P. Gardner, "Novel UWB pyramidal monopole antenna with wide tunable band notched behaviour", *Electronics Letters*, Vol. 46, Issue 24, 2010, pp. 1588-1590

8. **Z. H. Hu,** P. S. Hall, J. R. Kelly, and P. Gardner, "Novel wideband conical monopole antenna with frequency band notched behaviour", *Electronics Letters,* vol. 46, Issue 23, 2010, pp. 1542-1543.

9. L. Borja, J. R. Kelly, Q. Liu, P. S. Hall and **Z. H. Hu**, "Dipole antenna with left-handed loading operating at a zero order mode", *Progress In Electromagnetics Research* C, Vol. 19, 2011, pp. 85-92

10. **Z. H. Hu**, C. T. P. Song, J. Kelly, P. S. Hall, and P. Gardner, "Wide tunable dual-band reconfigurable antenna", *Electronics Letters,* vol. 45, Issue 22, Oct. 22 2009, pp. 1109-1110.

Conference Papers:

1. **Z. H. Hu**, P. S. Hall, P. Gardner, and Y. Nechayev, "Wide tunable balanced antenna for mobile terminals and its potential for MIMO applications", Accepted by *Loughborough Antenna & Propagation Conference 2011, LAPC 2011*.

2. O. O. Tade, **Z. H. Hu**, P. Gardner, and P. S. Hall, "Small antennas for cognitive radio using negative impedance converters", Accepted by *The 12th Annual Post Graduate Symposium on the Convergence of Telecommunications, Networking and Broadcasting (PGNet2011), Liverpool, UK.*

3. **Z. H. Hu**, P. S. Hall, J. R. Kelly, and P. Gardner, "Novel wideband pyramidal monopole antenna with wide tunable frequency band-notch", *Antennas and Propagation (EUCAP), Proceedings of the 5th European Conference in 2011*, pp. 3509-3512

4. **Z. H. Hu**, P. S. Hall, J. R. Kelly, and P. Gardner, "Wideband omni conical monopole antenna with high Q band-notched behaviour", *Antenna Technology (iWAT) 2011 International Workshop,* 2011, pp. 37-40

5. **Z. H. Hu,** J. R. Kelly, P. Gardner, and P. S. Hall, "Pattern Reconfigurable Wideband Conical Monopole Antenna with frequency notch-band", *Second UK URSI Festival of Radio Science 2011*, University of Leicester, 12th Jan. 2011.

6. P. Hall, **Z. H. Hu**, P. Song, M. R. Hamid, and Z. Wang, "Creating reconfigurable adaptive antennas for cognitive radio applications considering cost and portability", *The IET Seminar on Cognitive Radio Communications*, 4th Oct. 2010, London, U.K.

7. **Z. H. Hu,** J. Kelly, C. T. P. Song, P. S. Hall and P. Gardner, "Equivalent circuit modelling of chassis-antenna with two coupling elements", accepted by *2010 IEEE International Symposium on Antennas and Propagation and CNC/USNC/URSI Radio Science Meeting,* July 11-17, 2010, Toronto, Ontario, Canada.

8. **Z. H. Hu,** C. T. P. Song, J. Kelly, P. S. Hall and P. Gardner, "Novel reconfigurable dual-port UWB chassis-antenna", accepted by *2010 IEEE International Symposium on Antennas and Propagation and CNC/USNC/URSI Radio Science Meeting,* July 11-17, 2010, Toronto, Ontario, Canada.

9. **Z. H. Hu**, J. Kelly, C. T. P. Song, P. S. Hall, and P. Gardner, "Novel wide tunable dual-band reconfigurable chassis-antenna for future mobile terminals", *Antennas and Propagation (EuCAP), 2010 Proceedings of the Fourth European Conference on 2010,* pp. 1-5.

10. Hall P S, Gardner P., **Hu Z. H**., Song P., Kelly J. and Hamid M.R., 'Reconfigurable antennas for wideband wireless systems' *Adaptable and Tunable Antenna Technology for Handsets and Mobile Computing Products Savoy Place*, London, 22 Oct 2009.

11. **Z. H. Hu,** C. T. P. Song, J. Kelly, P. S. Hall, and P. Gardner, "A novel reconfigurable UWB chassis-antenna for future mobile terminals", *UK*

URSI Festival of Radio Science, University of Birmingham, Thesday, 15 December 2009.

12.   C. T. P. Song, **Z. H. Hu**, J. Kelly, P. S. Hall, and P. Gardner, "Wide tunable dual-band reconfigurable antenna for future wireless devices", *Loughborough Antenna and Propag. Conference, LAPC 2009, Loughborough, UK,* 16-17 Nov. 2009, pp. 601-604

TABLE OF CONTENTS

LIST OF FIGURES

LIST OF TABLES

LIST OF ACRONYMS

ADS	Advanced Design System
AF	Array Factor
AIM	Antenna Interface Module
CST	Computer Simulation Technologies
CR	Cognitive Radio
CP	Circular Polarization
CPW	Co-Planar Waveguide
dB	decibel
dBi	decibel isotropic
EBG	Electromagnetic Band Gap
DVB-H	Digital Video Broadcasting High definition
EMC	Electromagnetic Compatibility
FCC	Federal Communication Commission
G	Gain
GaAs FET	Gallium Arsenide Field Effect Transistor
GHz	Gigahertz
GPS	Global Positioning System
GSM	Global Systems for Mobile Communications
HF	High Frequency
IEEE	Institute of Electrical and Electronics Engineers
IMT2000	International Mobile Telecommunications 2000
ISM	Industrial Scientific Medical
LF	Low Frequency
LNA	Low Noise Amplifier
LHCP	Left Hand Circular Polarization
LTE	Long Term Evolution
MEMs	Micro Electro Mechanical system
MIMO	Multiple Input Multiple Output
MHz	Megahertz
OFDM	Orthogonal Frequency Division Multiplexing

PCB	Printed Circuit Board
PIFA	Planar Inverted F Antenna
PIN DIODE	Positive Intrinsic Negative DIODE
PCS	Personal Communication Service
PILA	Planar Inverted L Antenna
Q	Quality Factor
RF	Radio Frequency
RHCP	Right Hand Circular Polarization
SDR	Software Defined Radio
SMT	Surface Mount Technology
SRR	Split Ring Resonator
TEM	Transverse ElectroMagnetic
TV	Television
UMTS	Universal Mobile Telecommunications System
USB	Universal Serial Bus
UWB	Ultra WideBand
VHF	Very High Frequency
VSWR	Voltage Standing Wave Ratio
WLAN	Wireless Local Area Network
WiMAX	Worldwide Interoperability for Microwave Access
WRAN	Wireless Regional Area Network

CHAPTER I

INTRODUCTION

1.1. Background

Software defined radio, (SDR), and cognitive radio, (CR), are two new concepts in wireless communications that will, in the foreseeable future, have significant effects on antenna requirements in a host of applications from mobile phones to satellite communications. Software defined radio was first described by Mitola [1], as a system in which the majority of the functionality is defined by software algorithms. A cognitive radio (CR) is a wireless transponder that can sense the environment where it wishes to operate and can adapt itself to optimise its operation. Thus, it offers much promise to increase spectrum usage efficiency to users in a wide variety of applications, covering commercial, military and space communications [2]. Software defined radio is seen as an enabling technology for cognitive radio. Both terms, since their first description, have attracted increasing interest and driven significant world-wide research. Fig. 1.1 shows a typical block diagram of cognitive radio architecture [3]. A wideband low noise amplifier (LNA) is needed in the search stream, followed by the sensing receiver, with coarse and fine sensing, shown in Fig. 1.1.
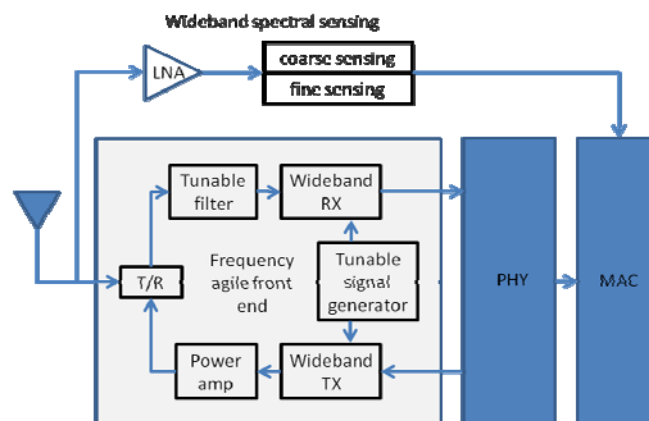
Fig. 1.1 Cognitive Radio Architecture [3]

There are no clear standards for SDR although possible specifications have been suggested [4] and shown in Table 1.1. The big effect on antenna design will be the frequency range, which approximately covers FM radio broadcast, private mobile radio, radio microphones, TV broadcast and the current mobile phone bands. It may also include ISM bands, WiFi and other possible bands. Cognitive radio has also been suggested in the ultra wideband (UWB) 3 to 10 GHz range [5], and in the 60 GHz [6] band. Such wide frequency ranges will pose enormous problems for antenna design, both for handsets and fixed installations.

Parameter	Requirement
Radio frequency range	100 MHz to 2.2 GHz
Signal or channel bandwidth	< 8 MHz
Tx power	1 watt

Table 1.1 Possible SDR requirements [4]

1.1.1. Antennas Challenges for Mobile Communications Handsets

It is well known that the bandwidth and gain of an antenna are limited by its volume. Chu, [7], gave an expression for the minimum quality factor, Q, of an antenna, which shows that as the size relative to the wavelength reduces, so does the bandwidth. For linearly polarized lossless antennas the Chu limit can be expressed by equation (1.1). Similarly, the gain is shown by Harrington, [8], to also introduce with size. The relation can be expressed by equation (1.2):

$$Q = \frac{1}{(ka)^3} + \frac{1}{ka} \tag{1.1}$$

$$G = (ka)^2 + 2(ka) \tag{1.2}$$

where, k is the wave number associated with the electromagnetic field and a is the radius of a sphere which fits the whole antenna. The Chu-Harrington Limit implies

that it is not possible to cover such wide frequency ranges, suggested in Table 1.1, with a typical smart phone size. If this range is put into the Chu expression, the antenna must be much larger than the size of a handset. For example, if a handset size of 100x50 mm^2 is considered, which represents a typical smart phone size, then the bandwidth (or frequency range), at the lowest frequency, is about 11 MHz, a number that in creases with frequency. It implies that the antenna must be either tunable, or capable of supporting many modes.

Modern mobile handsets enable users to access a very wide range of different wireless communication standards, such as penta-band cellular services, Bluetooth, Wifi, FM radio, etc. With growing requirements for connectivity in a highly mobile environment, more standards and services are being rolled out (such as DVB-H, RFID, LTE, etc). If the trend continues, some believe that future mobile terminals will have a need for more than 20 antennas [9]. This will create a difficult challenge for the mobile terminal designer, who is already short of space to locate the antenna. To overcome this, reconfigurable antennas, incorporating switches or varactors, become a promising solution. Reconfigurable antennas also have potential applications to cover such wide bandwidth in cognitive radio.

Besides, the next generation mobile phones are expected to support wideband radio links designed to handle large amounts of data. Multiple-input-multiple-out (MIMO) wireless systems have attracted increasing interest due to their potential for increased capacity in rich multipath environments. Such systems can be used to enable enhanced communication performance in terms of improved signal quality and reliability, by use of multi-path propagation, without requiring additional spectrum

bandwidth. A frequency agile MIMO antenna, with wide tuning range, will be demanded. It can also be employed for future cognitive radio (CR), for spectrum sensing and data transmission at the same time [10]. However, there is no literature regarding a reconfigurable MIMO antenna with a wide tuning range.

1.1.2. Antennas Challenges for Indoor/Outdoor Base Station

Congestion in the spectrum is becoming a serious problem and is leading to a variety of methods to allow interoperation and to release additional resources. One such method, the underlay approach keeps transmission power below the noise level and uses wideband waveforms to communicate, such as in the ultrawide band (UWB) system. Overlay methods use higher power and search for unused spectrum, as in cognitive radio. One CR standard, IEEE 802.22 [11], wireless regional area network (WRAN), will operate from 52-862 MHz, and requires a sensing antenna with as wide a bandwidth as possible, while maintaining an omni-directional pattern. In those applications there is a need for stopband capabilities to serve to protect the search receiver from saturation by high power legacy transmitters, operating in the local area. Whilst one solution to this problem is to insert a band-stop filter before the low noise amplifier (LNA) in the UWB receiver, this would increase the size, weight, and complexity of the system. An alternative solution is to design an antenna which incorporates an integrated band rejection filter. Many researchers have proposed the planar printed UWB antenna incorporating a notch-band. However, many of the proposed solutions suffer from at least one of the following limitations: 1) poor rejection at the notch frequency, 2) complex structure which cannot be easily reconfigured; 3) poor omni-directional radiation pattern at frequencies within the operating band, which make them unsuitable for IEEE 802.22 applications [11]

1.2. Objectives of the Project

The primary object of this research is to investigate antennas that can begin to approach the requirements for the systems described above. The study has been split into a number of areas as follows:

1. Reconfigurable antennas which are suitable for use within small mobile terminals, capable of simultaneous wide tunable dual narrow-band operation as well as wideband performance;

2. Frequency agile MIMO antennas, with a wide tuning range, providing low-correlation and high efficiency;

3. Wideband antennas with slots to achieve good band-rejection behaviour and omni-directional patterns at frequencies throughout the operating band, even at a high frequency, i.e. 10 GHz;

4. Wideband antennas, with wide tunable frequency band-notch providing good band-rejection and stable omni-directional radiation patterns at frequencies throughout the operating band.

1.3. Layout of the Thesis

The thesis consists of seven chapters. An overview of each chapter is given below. Chapter 1 provides introduction to the project and the layout of the thesis. Chapter 2 discusses the background of antenna designs for future communications systems. The literature review covers reconfigurable antennas, MIMO antennas, wideband antennas with fixed band-notch and wideband antennas with tunable band-notch behaviour. Chapter 3 introduces a two-port reconfigurable antenna, which can operate within a narrowband or wide band mode. A new equivalent circuit for two-port chassis-

antenna is proposed and discussed. Three different structures of wideband reconfigurable balanced antennas for use in current and future mobile wireless communication systems and their potential for reconfigurable MIMO applications are discussed in Chapter 4. Elliptical cone antennas incorporating different shaped of slots are proposed in Chapter 5. The significant characteristics study of wideband antenna with notched-band behaviour using a simple equivalent circuit model is also discussed. Chapter 6 introduces a novel pyramidal monopole antenna with tunable band-notch behaviour. Fixed capacitors and varactor diodes, were used to adjust the notch band frequencies, are also discussed. Chapter 7 summarises some important conclusions derived from the research study and also gave some possible future extension of the work.

References:

[1]   J. Mitola III, "Sofeware radios – survey, critical evaluation and future directions", in *Telesyst, Conf., 1992. NTC-92., National,* May 1992, pp. 13/15-13/23.

[2]   P. S. Hall, P. Gardner, J. Kelly, E. Ebrahimi, M. R. Hamid, F. Ghanem, F. J. Herraiz-Martinez, and D. Segovia-Vargas, "Reconfigurable antenna challenges for future radio systems", *Antennas and Propagation, 2009. EuCAP 2009. 3rd European Conference* on 23-27 March 2009, pp. 949-955.

[3]   J. Laskar, R. Mukhopadphyay, Y. Hur, C.-H, Lee, K. Lim, "Reconfigurable RFICs and modules for cognitive radio", *2006 Topical Meeting on Silicon Monolithic Integ Circuits in RF Syst.,* Jan. 2006.

[4]   P. B. Kenington, *RF and Baseband Techniques or Software Defined Radio.* Boston: Artech House, 2005.

[5]   R. Jin, D. Grace, and P. D. Mitchell, "Applying cognitive spectrum sharing to UWB", *IEEE Int. Symp. on Wireless Communications Systems – WUN COGCOM 2010 Workshop,* Sept. 2010.

[6]   D. Cabric, M. S. W. Chen, D. A. Sobel, J. Yang, and R. W. Brodersen, Future Wireless Systems: UWB, 60 GHz, and Cognitive Radios*, IEEE Custom Integrated Circuits Conference*, Sept. 18-21, 2005, San Jose.

[7]   L. J. Chu, "Physical limitations of omnidirectional antennas", *J. Appl. Phys.,* Vol. 19, Dec. 1948, pp. 1163-1175.

[8]   R. F. Harrington, "Effect of antenna size on gain, bandwidth, and efficiency", *J. Res. Nar. Bur. Stand.,* Vol. 64D, Jan.-Feb. 1960, pp. 1-12.

[9]   P. Vainikainen, J. Holopainen, C. Icheln, O. Kivekas, M. Kyro, M. Mustonen, S. Ranvier, R. Valkonen, and J. Villanen, "More than 20 antenna elements in future mobile phones, threat or opportunity?", *Antennas and Propagation, 2009, EuCAP 2009. 3rd European Confer*ence on 23-27 March 2009, pp. 2940-2943.

[10]   W. Lee, and D.-H. Cho, "Enhanced spectrum sensing scheme in cognitive radio systems with MIMO antennae", *IEEE Transactions on Vehicular Technology,* Vol. 60, Issue 3, March 2011, pp 1072-1085.

[11]   IEEE 802.22 Wireless Regional Area Networks - Enabling rural broadband wireless access using cognitive radio technology, IEEE 802.22-10/0073r03, 2010-06-15.

CHAPTER II

OVERVIEW OF ANTENNAS FOR FUTURE

COMMUNICATION SYSTEMS

2.1. Literature Review

2.1.1. Overview of Reconfigurable Antennas

In recent years, reconfigurable antennas, both single element and arrays, have attracted increasing interest. The three main types of reconfiguration are:

- Pattern reconfigurable

- Polarisation reconfigurable

- Frequency reconfigurable

Radiation pattern reconfigurable antennas can be used to avoid noise sources or electronic jamming, improve security, and save energy by changing the directivity toward intended users. Therefore, this type of reconfiguration is a promising candidate for reinforcing the signal in a desired direction or suppressing the signal in undesired directions, in the fields of wireless communications, satellite communications, radar, etc.

Polarisation reconfigurable antennas have been used to mitigate the detrimental fading caused by multipath and are used in broadband wireless communication systems, such as wireless local area networks (WLAN), satellite links, and space robots.

Frequency reconfigurable antenna is one of the promising solutions to support multiple functions at multiple frequency bands and will significantly reduce the hardware size and cost.

2.1.1.1. Pattern Reconfigurable Antenna

The field of pattern reconfigurable antennas is large and a few that are representative of what is done are now described. The most common way to obtain effective radiation pattern manipulation is to use an array of antennas (i.e. a phased array). Fig. 2.1 shows the structure of a N-element linear array. All the elements are assumed to have identical amplitudes, and each succeeding element has β progressive phase lead current excitation relative to the preceding one. The total field can be formed by multiplying the array factor of the isotropic sources by the field of a single element. The array factor, *F*, can be obtained by the following equation [1]:

$$F = 1 + e^{+j(kd\cos\theta+\beta)} + e^{+j2(kd\cos\theta+\beta)} + ... + e^{+j(N-1)(kd\cos\theta+\beta)} \qquad (2.1)$$

where *k* is the wave vector of the incident wave, *d* is the separation of each element and *β* is the phase excitation difference between the elements. By varying the separation d and/or the phase β between the elements, the characteristics of the array factor and of the total field of the array can be controlled. Thus, pattern reconfiguration can be achieved.
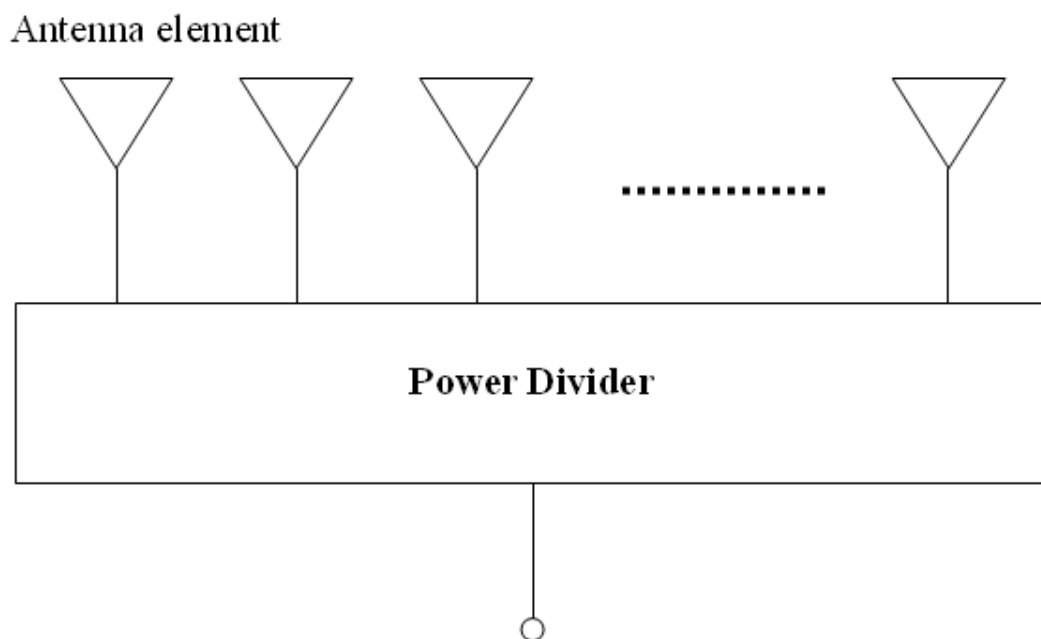
Antenna element

Fig. 2.1 Structure of N-element linear array

Ref. [2] introduces an electrically small, pattern reconfigurable Yagi antenna. Two directors are located on the two opposite sides of the driver, as shown in Fig. 2.2. The beam pattern can be switched by using a pin diode which is located on the bottom of the director. When switch 1 is on and switch 2 is off, the resonant frequency is 450 MHz with 14.3 dB of return loss and the beam pattern is steered towards the director 1 direction, as shown by the solid curve in Fig. 2.3. In the opposite state, the situation is reversed. The beam is steered towards director 2 as shown by the dashed curve in Fig. 2.3.
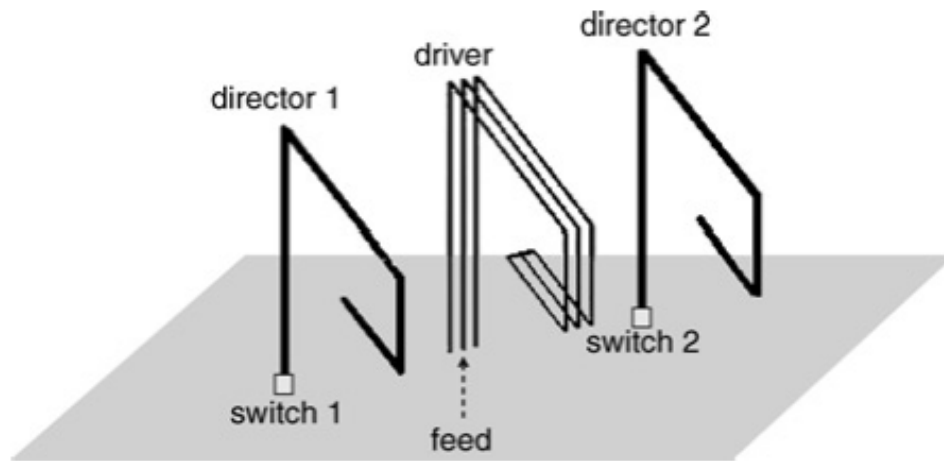
Fig. 2.2 Geometry of small reconfigurable Yagi antenna [2]
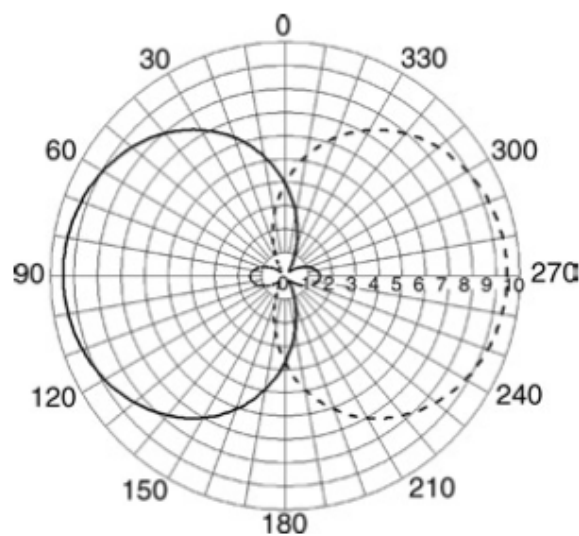
Fig. 2.3 Patterns in azimuth plane of the small reconfigurable Yagi antenna [2]
—— switch 1: on, switch 2: off
--- switch 1: off, switch 2: on

Another simple radiation pattern reconfigurable example is presented in ref. [3]. Fig. 2.4(a) shows the concept of how to reconfigure the radiation pattern. The structure of the antenna is shown in Fig. 2.4(b). By controlling the switch states, the antenna can be worked as a monopole antenna with an omni-directional radiation pattern or a dipole antenna with reflector, which has directional radiation pattern, as shown in Fig. 2.4(a). The measured results show that at switches 'off' state, the bandwidth is 2.18 - 2.53 GHz while 2.37 – 2.73 GHz at switches 'on' state. Thus, this antenna provides both pattern and frequency reconfigurations.

(a)

(b)
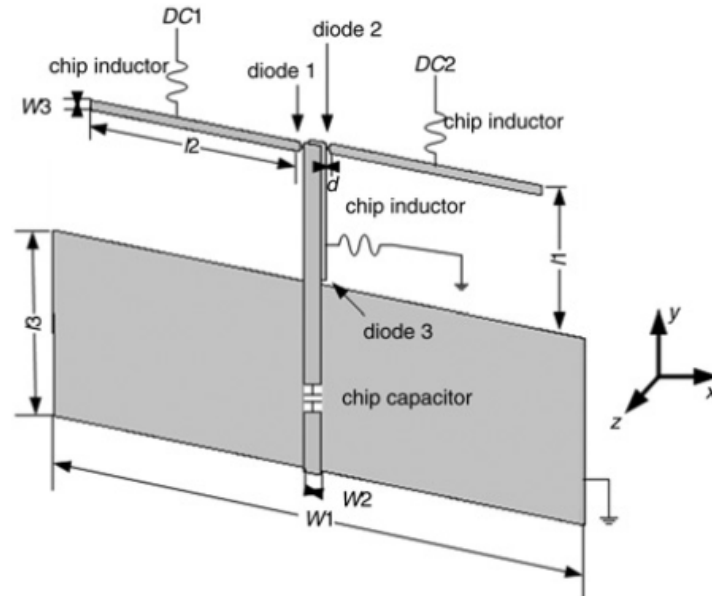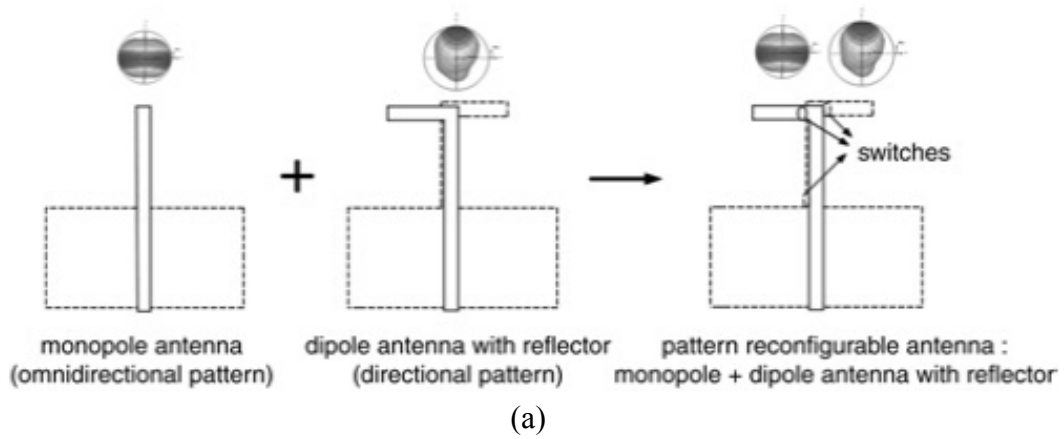
Fig. 2.4 (a) Concept of proposed pattern reconfiguration antenna; (b) Schematic of the pattern reconfiguration dipole antenna [3]

The last but not the least example is a wideband circular antenna array with a reconfigurable radiation pattern in ref. [4]. The array consists of eight TEM horn antennas and is fed through eight reconfigurable bandstop filters and a power splitter, as shown in Fig. 2.5(a). The prototype of the TEM horn array is shown in Fig. 2.5(b). When each of eight ports is excited by a signal which has the same magnitude and phase, the antenna provides an omni-directional radiation pattern, i.e. the solid line shown in Fig. 2.6. By disconnecting certain elements within the array, a pattern notch can be created, i.e. the dashed line shown in Fig. 2.6. This pattern reconfigurable antenna array would be useful in combating interference in wideband communication systems or spectrum search in cognitive radio systems.

(a)

(b)
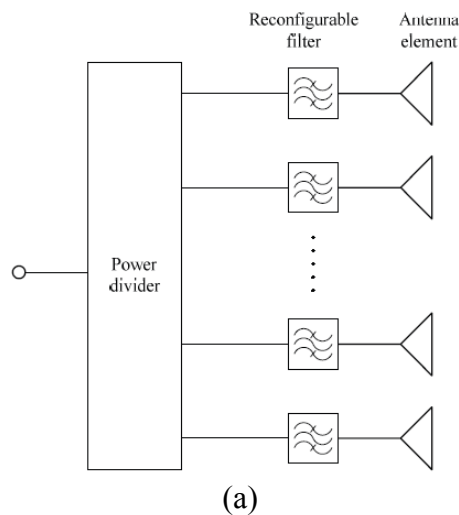
Fig. 2.5 (a) Architecture of the wideband antenna with reconfigurable pattern notch; (b) Prototype of the TEM circular array [4]
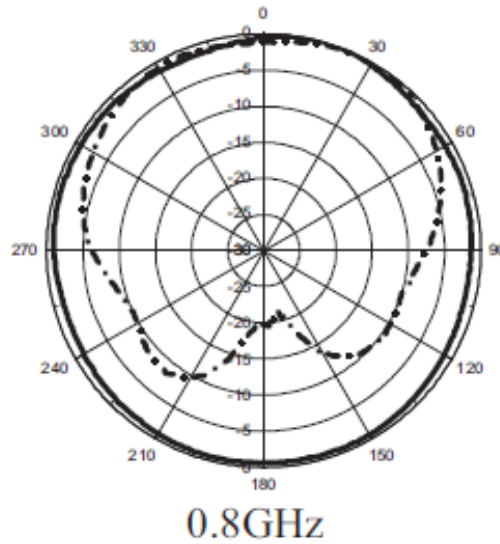
0.8GHz

Fig. 2.6 Radiation patterns at 0.8 GHz for the TEM circular array [4]

2.1.1.2. Polarisation Reconfigurable Antenna

The patch antenna has been widely used for polarisation reconfiguration due to the desirable features such as low profile and simplicity of manufacture. Ref. [5] presents a patch antenna with switchable slots that can achieve right hand circular polarization (RHCP) and left hand circular polarization (LHCP) with a single feeding port, as shown in Fig. 2.7. The patch size is 18×18 mm^2 for operation at 4.64 GHz and the ground plane size is 40×40 mm^2. Two orthogonal and identical slots are etched into the patch and two pin diodes are inserted into the centre of the slots. A bias circuit is used to control the status of the diodes and two capacitors are soldered onto the edges of the slots to isolate the dc while maintaining continuity for the RF, as shown in Fig. 2.7. During the measurement, conductive metal tabs are used to represent switch diodes. By controlling status of the switch diodes, the antenna can switch between radiating a RHCP and LHCP pattern with the same feeding port. The best axial ratio, shown in ref. [5], is achieved at 4.64 GHz with 3% CP bandwidth according to an axial ratio criterion of 3 dB.
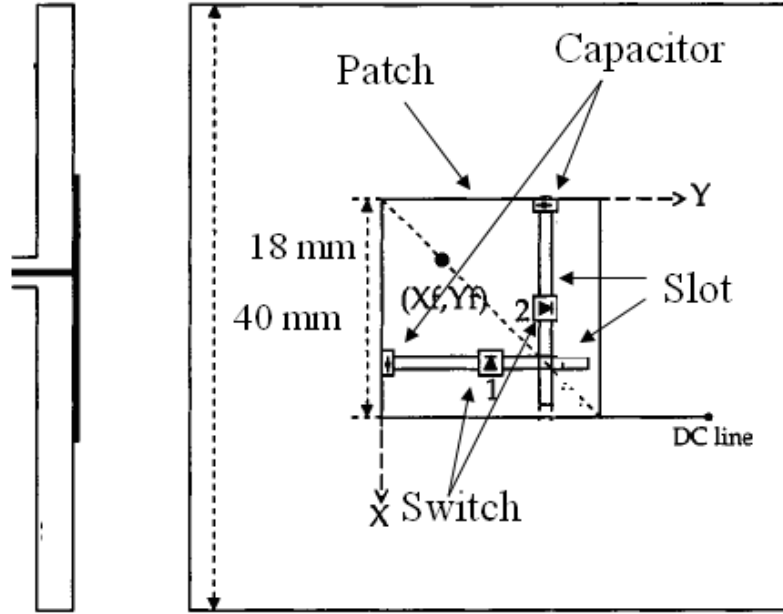
Fig. 2.7 Geometry of a patch antenna with switchable slots for RHCP/LHCP) diversity [5]

The second example is a circular coplanar-waveguide (CPW)-fed microstrip antenna [6] with polarization reconfigurable features. The circular-patch antenna is excited by a diagonal slot and the CPW open end, as shown in Fig. 2.8(a). The two sets of symmetrical coupling diagonal slots, incorporating two pairs of pin diodes, have ±45° inclination to the CPW open end and, as shown in Fig. 2.8(b). A dc-bias voltage is supplied through a divided ground plane, as shown in Fig. 2.8(a) and large capacitors are built over the slits by stacking copper strips and adhesive tapes (upper layer on Fig. 2.8a). By switching on a pair of diodes while the other is OFF, the antenna can switch between the RHCP and LHCP states. The measured axial ratio (AR) shown in ref. [6], occurs at the same frequency (5.8 GHz), is approximately 1.8% (AR < 3 dB).

(a)

(b)
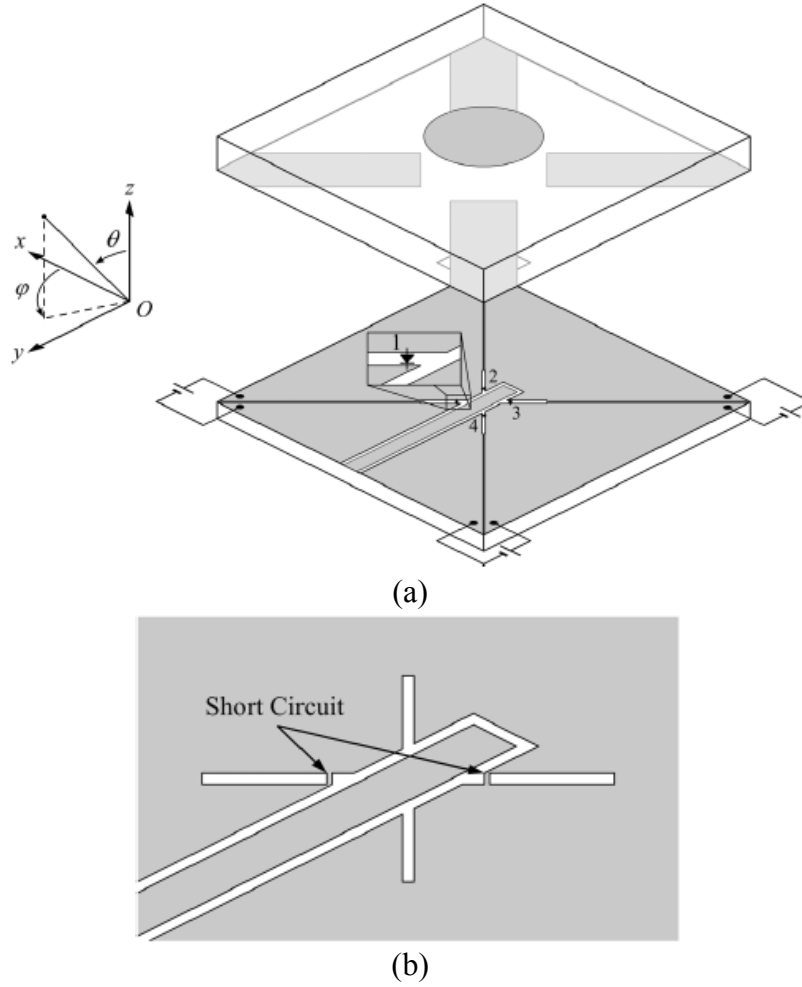
Fig. 2.8 (a) Circularly polarized reconfigurable structure; (b) Position of the ideal short circuit in the slots [6]

The last but not the least interesting example is a reconfigurable circularly-polarized (CP) microstrip array antenna with conical-beam radiation, which is described in ref. [7]. The antenna structure consists of four L-shaped patch antennas arranged in a square-ring formation and each of them is shorted to the ground plane through two groups of conducting walls, i.e. group A and group B. The shorting walls of group A and B are connected to the L-shaped patches through capacitors of 100 pF and pin diodes, respectively. For a simple DC bias network, a thin pin is used to connect the L-shaped patches and an isolated circular pad from the ground plane then the positive and negative of the battery are linked to the pad and ground plane, respectively, as shown in Fig. 2.9. As with a top-loaded monopole feed, two orthogonal resonant

modes, loop mode and monopole mode, can be excited simultaneously. However, with only group A of conducting walls, LHCP is obtained while incorporating two groups of conducting walls simultaneously, RHCP is obtained. Measured results show that the 3 dB axial ratio for LHCP is 1.6% with respect to the centre frequency of 2475 MHz and the RHCP operating bandwidth is 2% with respect to the centre frequency of 2895 MHz.
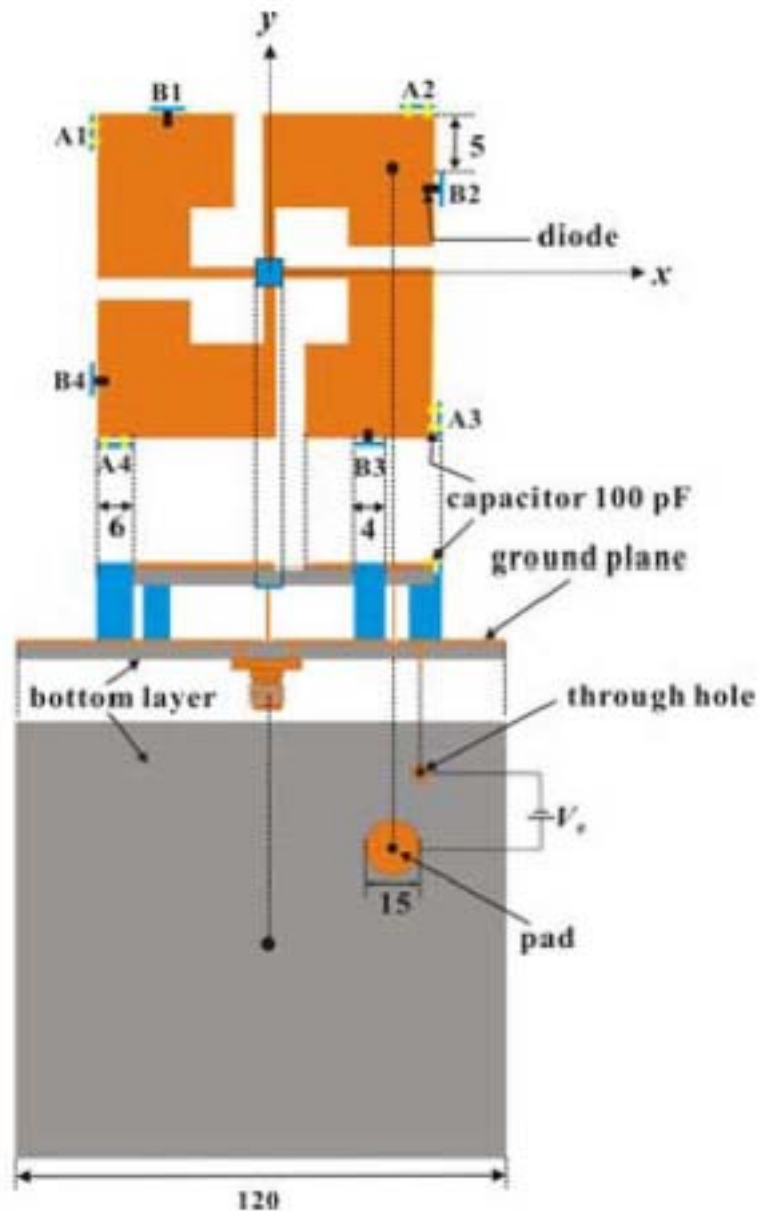
Fig. 2.9 Structure of a reconfigurable circularly-polarized microstrip array antennas [7]

2.1.1.3. Frequency Reconfigurable Antenna

Many papers discuss frequency reconfigurable antennas. The details of a number of them are summarised in Appendix A. The main techniques to achieve frequency reconfiguration are, a) selectively switching in or out parts of the antenna structure, or switching between different external matching circuits; b) adjusting the loading of the antenna externally, i.e. varactor diodes; c) changing the substrate characteristic, i.e. permittivity; and d) changing the antenna geometry by mechanical movement.

Switching or tuning within an antenna or in an external circuit can be achieved by means of PIN diodes, GaAs FETs (Gallium Arsenide Field-Effect Transistor), MEMS (Microelectromechanical Systems) devices or varactors [8, 9]. MEMS devices have the advantage of very low loss, but the disadvantages are high operating voltage, high cost and lower reliability than semiconductor devices [10]. GaAs FETs used in switching mode, with zero drain to source bias current, have low power consumption but poorer linearity and higher loss. PIN diodes can achieve low loss at low cost, but the disadvantage is that in the on state there is a forward bias dc current, which degrades the overall power efficiency. Varactor diodes have the advantage of providing continuous reactive tuning rather than switching, but suffer from poor linearity. Changing the substrate permittivity to shift the resonant frequency is another approach, but the cost may be problematic. Adjusting the resonant frequency by changing the antenna geometry using mechanical movement can provide lossless and ideal linearity. However, it needs mechanical adjustment and requires more time for switching between frequency operating bands.

2.1.1.3.1.   Reconfiguration by Switches

A significant number of reconfigurable antennas incorporating switches, both switching in or out parts of the antenna structure or switching between external matching circuits, have been summarised in Appendix A. Examples reviewed in this section are representative of that extensive literature.

Ref. [11] presents an antenna system consisting of two self-diplexing planar inverted F antennas (PIFAs) that are co-designed with an antenna interface module (AIM) that contains switches, filters, matching, and interconnects realised in conventional technologies. Diplexing is achieved by using two antennas, as shown in Fig. 2.10, i.e. one for the low-band group and anther for the high-band group. The co-design of two PIFAs with an antenna interface module (AIM), as shown in Fig. 2.11, allows a reconfigurable system with more optimal antenna matching to be achieved to cover a number of bands with reduced both dimensions and losses. By incorporating 8 switches which were connected to 8 different impedance matching circuits, 8 different operating bands were obtained, such as 0.824 to 0.849 GHz, 0.880 to 0.915 GHz, 0.925 to 0.960 GHz, 0.824 to 0.894 GHz, 1.710 to 1.785 GHz, 1.850 to 1.910 GHz, 1.850 to 1.990 GHz, and 1.920 to 2.170 GHz.
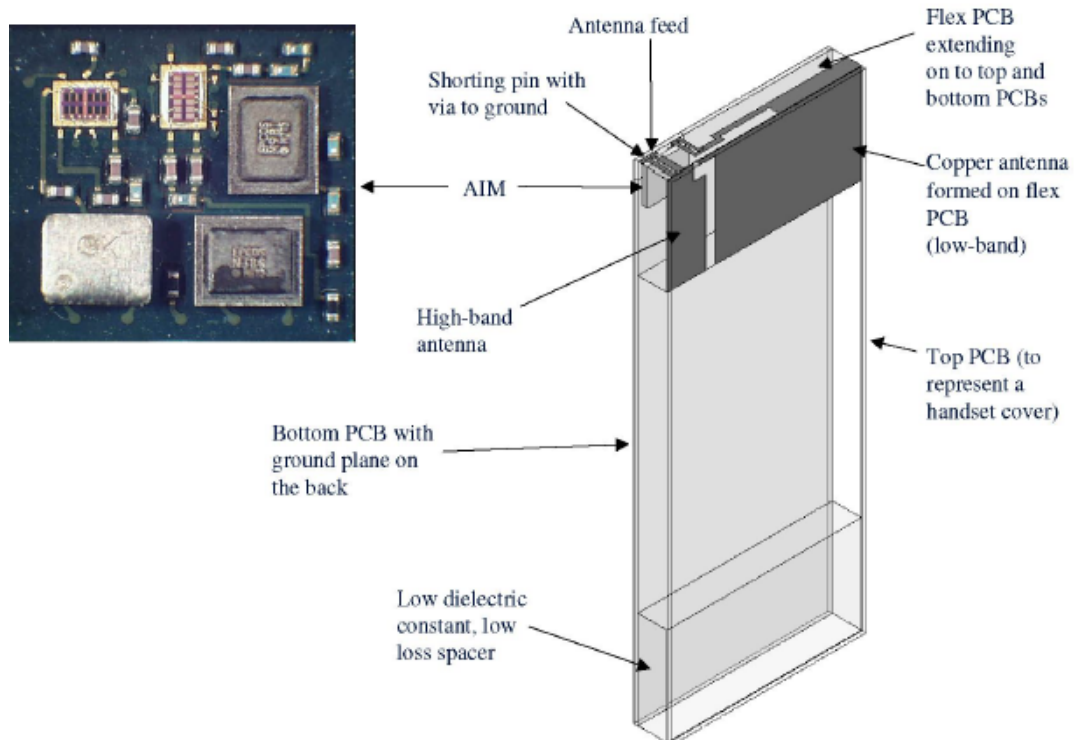
Fig. 2.10 Structure of a five-band, seven-mode reconfigurable antenna and antenna interface module [11]
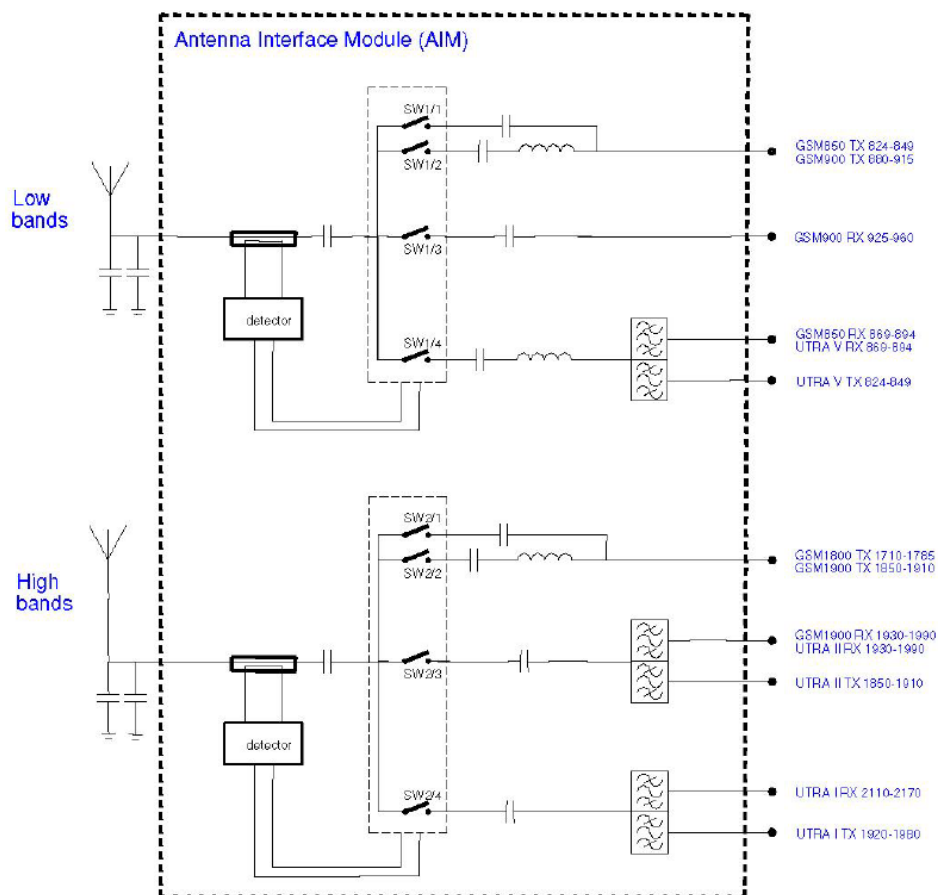
Fig. 2.11 Overall system schematic of the antenna interface module (AIM) [11]

Ref. [12] describes a single port chassis antenna, which incorporates 17 matching circuits to cover from 76 MHz to 2500 MHz and 5 matching circuits to cover from 470 MHz to 2500 MHz. Switches were used to connect different impedance matching circuits. Fig. 2.12 shows the antenna concept which consists of a coupling element to excite the entire PCB (Printed Circuit Board), i.e. chassis, of the mobile to act as antenna and a tuning network to optimize the coupling according to the requirements in the different frequency bands of the applications.
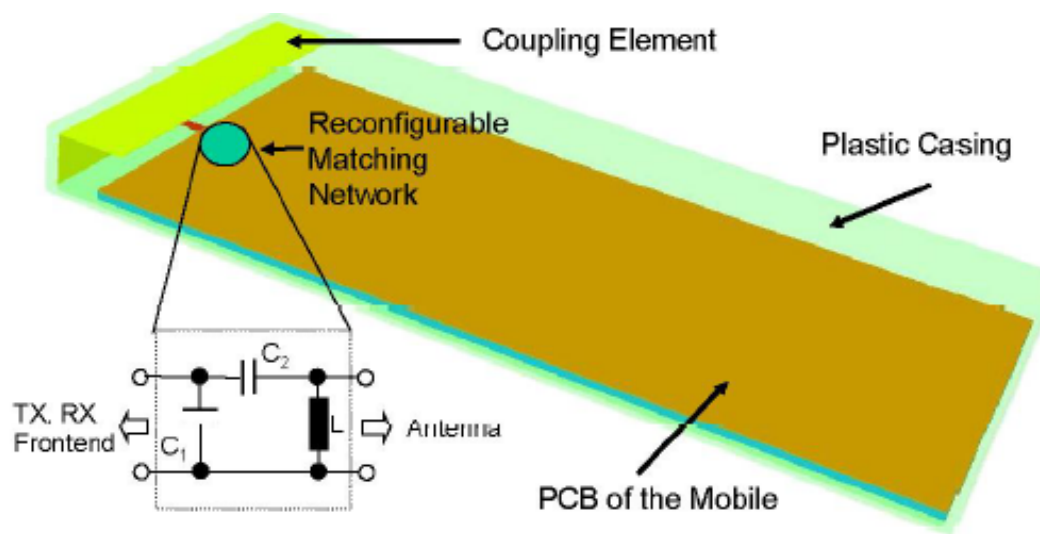
Fig. 2.12 Geometry of a single port chassis antenna [12]

A Vivaldi antenna, shown in Fig. 2.13, with a capability to operate in wideband or narrowband operations is presented in ref. [13]. Four pairs of switchable ring slots were introduced to change the wideband properties into narrower pass bands. A wideband operation was achieved when all ring slots are decoupled from the tapered slot, by short circuiting all the gaps to provide a smooth flow of induced current along the tapered profile. To obtain the narrowband mode, ring slots in lowermost, middle and uppermost positions were coupled or decoupled. In wideband mode, the antenna covered from 1 to 3.2 GHz. In narrowband mode, three sub bands, low band 1.1 GHz, mid band 2.25 GHz and high band 3.1 GHz, were achieved.
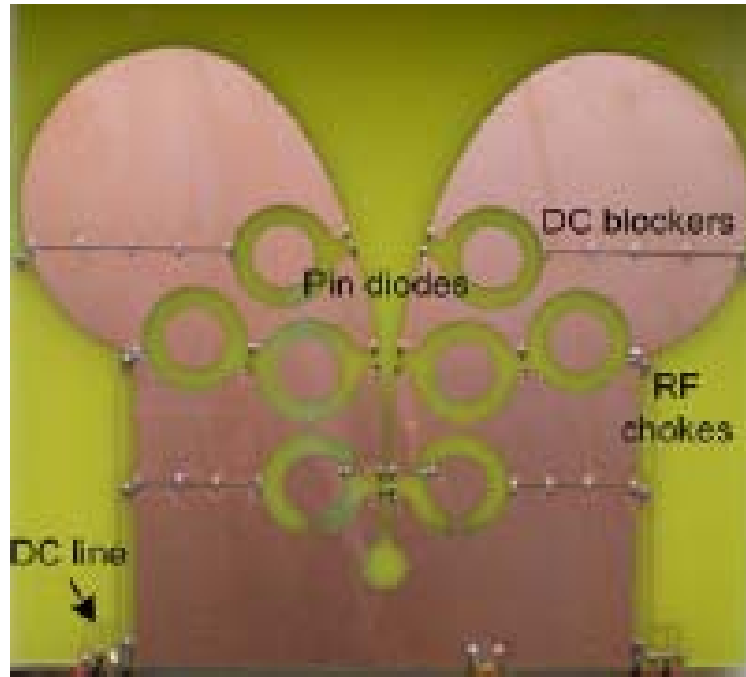
Fig. 2.13 A Vivaldi antenna incorporating four pairs of switchable ring slots [13]

A reconfigurable printed dipole antenna is presented in ref. [14]. Six ideal switches on each dipole arm, as shown in Fig. 2.14, were used to obtain seven frequency bands, such as 0.9 GHz, 1.05 GHz, 1.205 GHz, 1.46 GHz, 1.75 GHz, 2.05 GHz and 2.77 GHz, with approximate values of return loss from 16 dB to 31 dB. Fig. 2.14 shows the harmonic trap which is used to eliminate the higher order modes. The radiation patterns for those resonant frequencies in E-plane, described in ref. [14], show that nulls occur at the higher frequency bands. The authors in ref. [14] believe the degradation in the radiation patterns is due to the tapered ground plane.

(a)   (b)
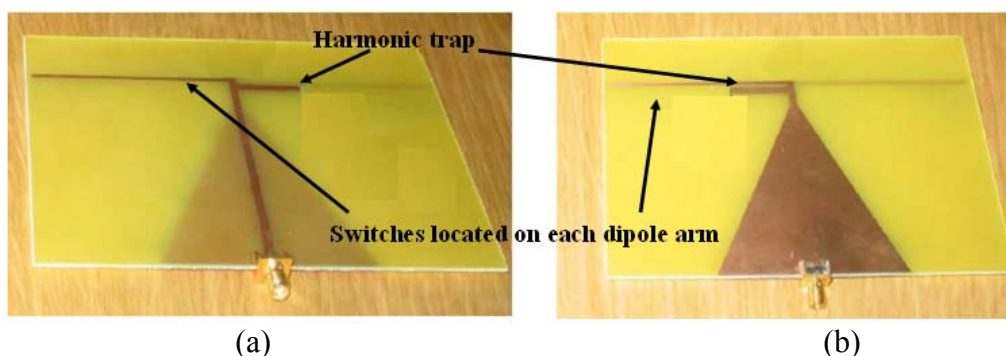
Fig. 2.14 Printed dipole antenna with harmonic trap, a) topside, b) backside [14]

2.1.1.3.2.   Reconfiguration by Varactor Diodes

Many papers discussed reconfigurable antennas incorporating varactor diodes and most of them have been summarised in Appendix A.

Ref. [15] presents a two-port chassis-antenna to cover the DVB-H band (470 to 702 MHz) and EGSM-900 (880 to 960 MHz) simultaneously. The tunable DVB-H antenna is mounted on a 110mm×50mm printed circuit board. The antenna for the EGSM band is located on the side of PCB and opposite to the antenna for the DVB-H band, as shown in Fig. 2.15. The DVB-H band is achieved by an external matching circuit, consists of an anti-series varactor pair in series with an inductor. A filter is added to the matching circuit to block EGSM TX to the DVB-H antenna.
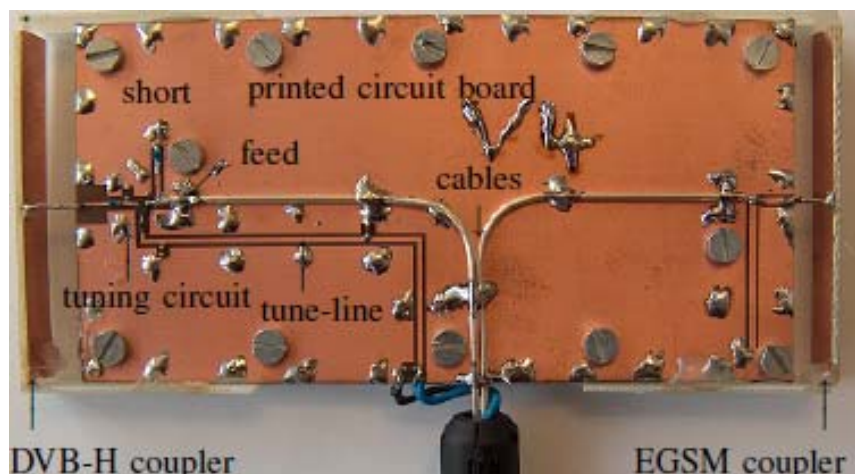
Fig. 2.15 Structure of two port chassis-antenna, tunable DVB-H antenna together with an EGSM antenna [15]

A design of low profile reconfigurable microstrip patch antenna is presented in ref. [16]. The antenna, with a total size of $50×50×1.57$ mm^3, consists of four sub-patches connected to one feed line, as shown in Fig. 2.8. Each sub-patch generates a single band. When the antenna is not biased, the resonant frequencies for the antenna are 0.92 GHz, 1.7 GHz, 1.95 GHz, 2.4 GHz and 2.9 GHz, respectively. By placing a

variable capacitor at the input of the sub-patches, the frequency for the best match can be tuned over a wide range from 0.92 to 2.98 GHz. Fig. 2.17 shows the radiation patterns for E and H planes when all switches set to be 0V at the fundamental frequencies.
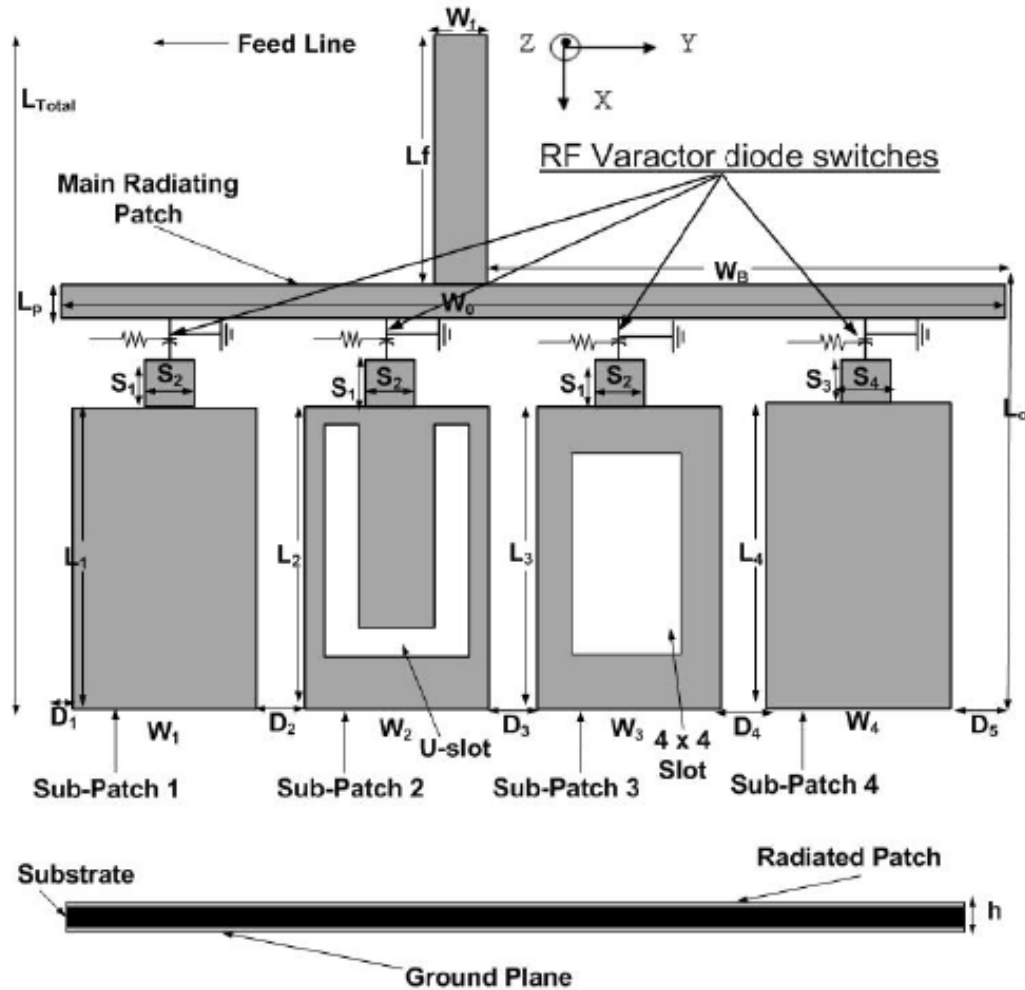
Fig. 2.16 Structure of a reconfigurable microstrip patch antenna, which consists of four sub-patches connected to one feed line [16]
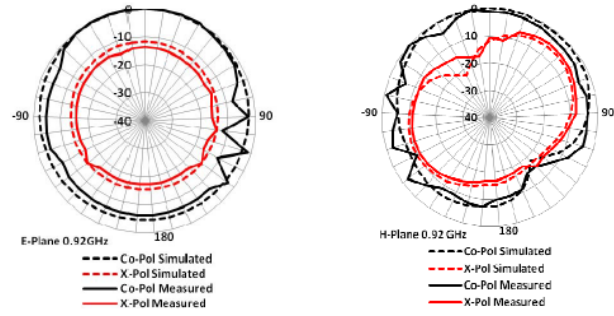
(a) 0.92 GHz
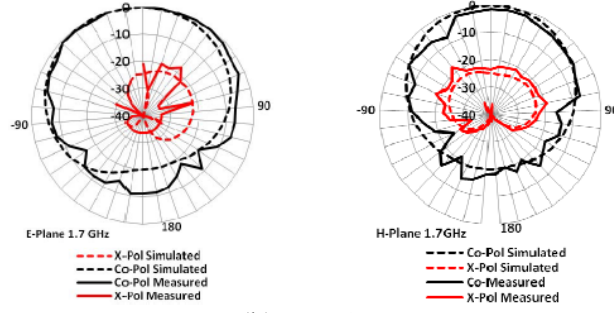
(b) 1.7 GHz
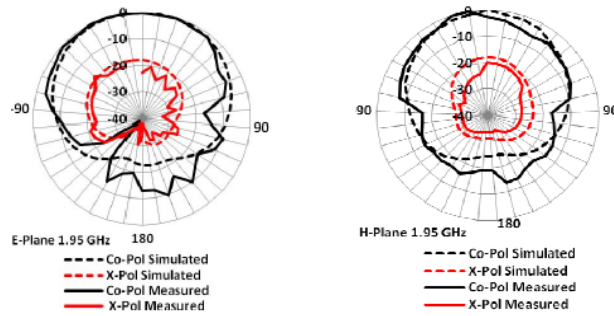
(c) 1.95 GHz
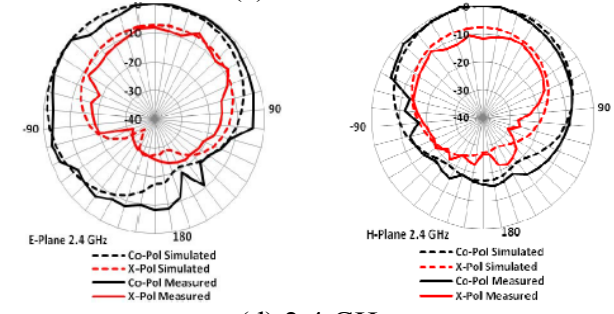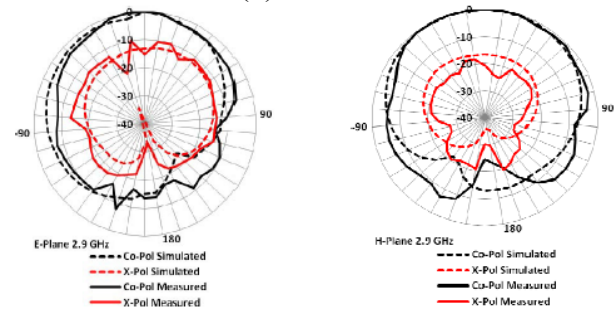
(d) 2.4 GHz

(e) 2.9 GHz

Fig. 2.17 Radiation patterns for E and H plane when all switches set to be 0V at (a) 0.92 GHz; (b) 1.7 GHz; (c) 1.95 GHz; (d) 2.4 GHz and (e) 2.9 GHz [16]

A printed loop-monopole wide frequency tunable reconfigurable antenna is presented in ref. [17]. The antenna consists of a tunable monopole and an adjustable loop antenna, as shown in Fig. 2.18. The loop section controls the tuning of an upper frequency band by using a bank of RF switches while the monopole part contributes to the tuning of the lower band by using an LC (varactor)-tank resonating tuner. Although the whole size of the PCB has not been provided in ref. [17], the size of the antenna element is 41×13 mm^2. The proposed antenna can operate for a tuning range from 700 MHz to 6 GHz with at least 6 dB return loss. Ref. [17] shows the antenna has an omni-directional pattern at 900 MHz with 1.19 dB gain. However, nulls occur at higher frequencies, such as 2.2 GHz, with 4.9 dB gain.
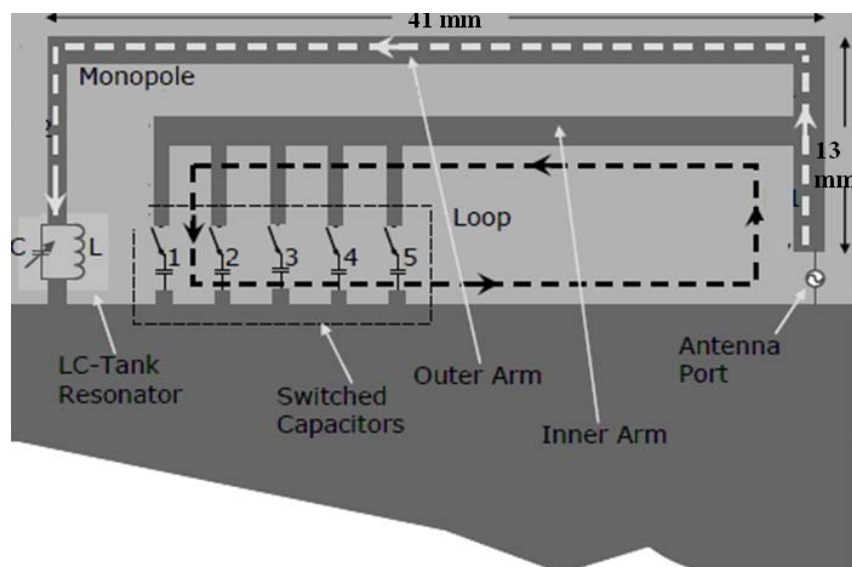
Fig. 2.18 A layout diagram of the printed loop-monopole wide frequency tunable reconfigurable antenna [17]

A frequency tunable coplanar waveguide (CPW)-fed coplanar strip (CPS) dipole antenna using varactors is presented in ref. [18]. A wide band coplanar waveguide-to-coplanar strip balun is used to transform the unbalanced CPW feed line to balanced CPS feed line for the dipole antenna, as shown in Fig. 2.19. The whole length of the dipole is 30 mm. However, the size of substrate is not shown. Two varactors were

integrated with CPS dipoles to form integrated antennas. Ref. [18] shows that the CPS dipole antenna has two distinct operating frequencies of 2.065 GHz and 3.955 GHz. The frequencies can be electrically tuned by varying the varactor bias voltages. The tuning range of the two operating bands was from 2.065 to 2.365 GHz and from 3.505 to 3.955 GHz, respectively. The radiation patterns for both E and H planes show low cross-polarization and low side lobes.
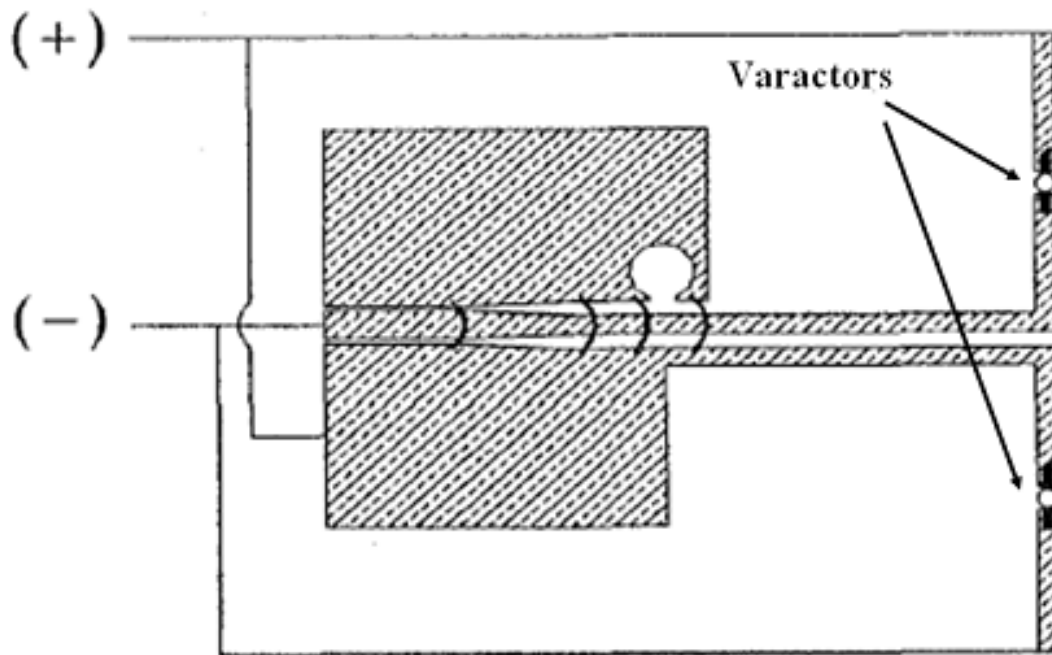
Fig. 2.19 Structure of frequency tunable CPW-fed CPS dipole antenna using varactors [18]

2.1.1.3.3. Reconfiguration by Changing Substrate Characteristic

Ref. [19] proposes the use of a liquid crystal substrate for a patch antenna whose frequency can be tuned by changing the biasing voltage across the substrate, shown in Fig. 2.20. The simulations showed that by varying the biasing voltage from 0 V through 11 V, the operating frequency of the circular patch antenna can be varied from 1.08 GHz through 2.35 GHz. Neither gain nor radiation pattern is discussed in ref. [19].
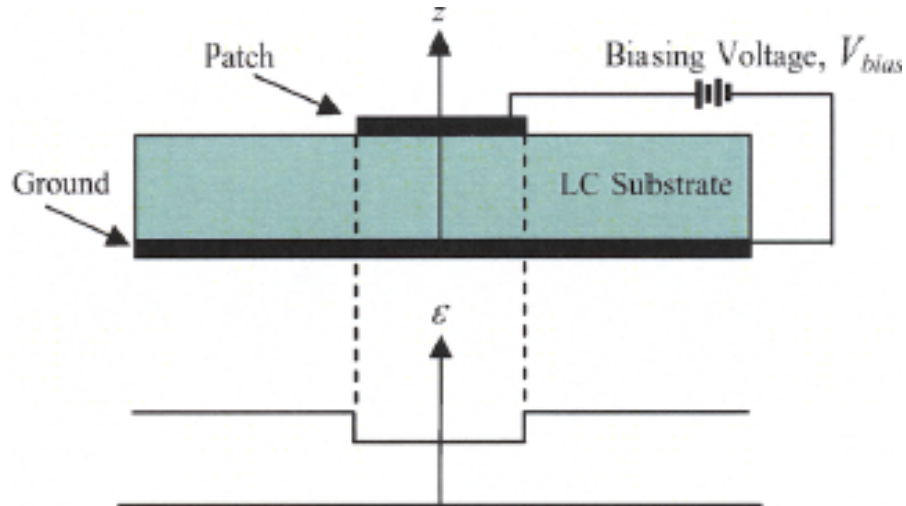
Fig. 2.20 A typical profile of the permittivity for a patch antenna with an LC substrate and a bias voltage. [19]

Ref. [20] presents a microstrip antenna on a ferrite substrate whose resonant frequency can be tuned by varying the DC magnetic bias field applied to the ferrite. The geometry and co-ordinate system are shown in Fig. 2.21. The size of the substrate is not shown, but the size of the patch is 14×18 mm^2. A permanent magnet is used on the ground plane side of the substrate with adjustable spacers to control the strength of the bias. The magnetic bias can be achieved along one of three possible principal axes. The resonant frequency of the unbiased antenna is 4.6 GHz. For the x- and z- biased directions, the resonant frequency increases from 4.6 to 5.5 GHz while the resonant frequency decreases from 4.6 to 2.8 GHz for the y-bias direction with at least 10 dB return loss. Ref. [20] shows that co-polarised patterns are similar to those of a patch element and the back lobe radiation appearing in the results is caused by the small ground plane of the substrate.
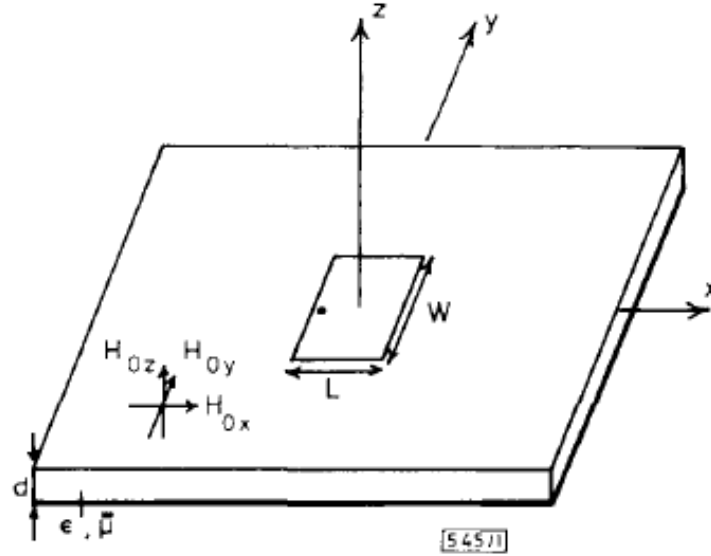
Fig. 2.21 Geometry and co-ordinate system for a rectangular microstrip antenna on a ferrite substrate [20]

2.1.1.3.4. Reconfiguration by Mechanical Movement

Ref. [21] presents an antenna scheme suitable for cognitive radio (CR) applications. A UWB sensing antenna and a frequency reconfigurable communicating antenna are incorporated together into the same antenna substrate, as shown in Fig. 2.22. The antenna is printed on a 70×50 mm^2 substrate. The UWB antenna searches for available spectrum holes while the reconfigurable antenna simultaneously tunes its frequency to that frequency determined by the sensing antenna. Tunability was achieved by a rotational motion of a series of antenna patches, as shown in Fig. 2.23. The sensing antenna can cover from 2 to 10 GHz. Fig. 2.24 shows the return loss for the five different patches. It is clear that each patch on the rotating section resonates at a different band and the five patches cover from 2 to 10 GHz. The radiation patterns, for both the sensing antenna and all the different stages of the rotating section, are not quite omni-directional and become worse at higher frequencies.

Fig. 2.22 The fabricated prototype combined with a UWB sensing antenna and a frequency reconfigurable communicating antenna. [21]
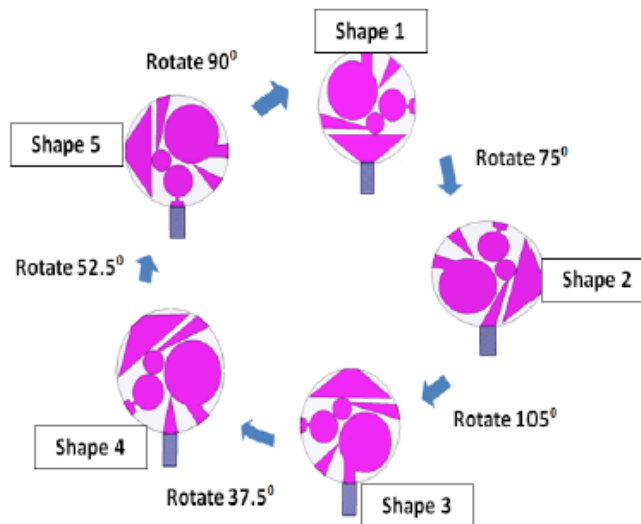
Fig. 2.23 Antenna reconfigurability process [21]
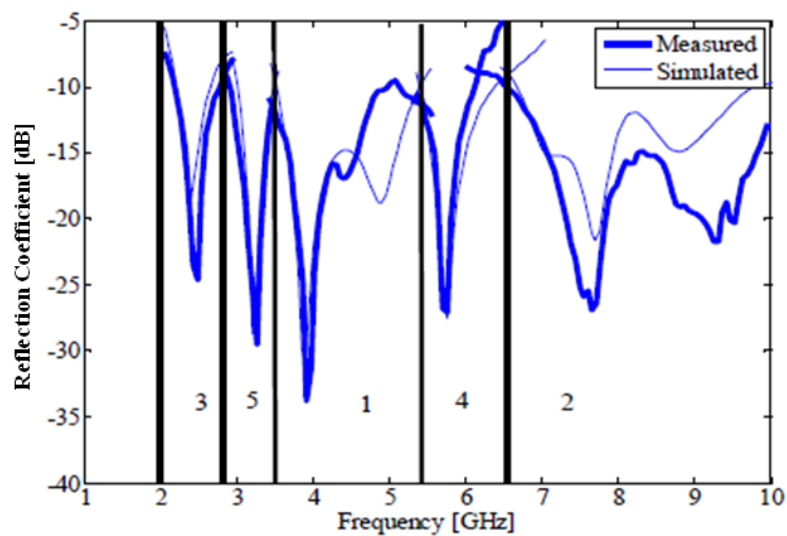
Fig. 2.24 A comparison between the measured and simulated reflection coefficient for the reconfigurable antenna with different shapes shown in Fig. 2.23 [21]

2.1.1.3.5. Summary of Frequency Reconfigurable Antenna

The summary in Appendix A shows that there were many antenna designs available for handset application in the open literature. However, in those literatures only the antenna in ref. [12] can cover from 470 MHz up to 2450 MHz. There is no antenna with dual-band simultaneous operation which can continuously cover from DVB (470 MHz) to Wifi (2450 MHz) Bands. Ref. [12] describes a single port chassis antenna, which has the widest covering range. The antenna incorporates 17 matching circuits to cover from 76 MHz to 2500 MHz and 5 matching circuits to cover from 470 MHz to 2500 MHz. However, there are two disadvantages. Firstly the large number of switches will introduce significant losses and secondly the antenna is limited to one band at a time and is thus not suitable for terminals which require more than one service access.

2.1.2. MIMO Antenna

Designing a MIMO antenna that is able to access a very large number of multiple wireless communication standards is a formidable challenge for the mobile terminal designer, who is already short of space in which to locate the antennas. Several papers discuss MIMO antennas [22-33]. Both isolation and correlation coefficient between antennas are important features. In general, lower isolation will result in lower correlation. Isolation higher than 10 dB or correlation below about 0.4 will lead to useful capacity increases in MIMO systems. The techniques to achieve low correlation are:

1.   design the antennas with different radiation patterns [22-24];

2.   apply a decoupling network between antennas [25-28];

3.   use EBG substrates to reduce the mutual coupling among the antennas [29-30];

4.   etch the ground plane between two antennas [31-32];

5.   introduce a parasitic element along the ground plane to achieve high isolation (i.e. a T-shaped shorted strip along the ground plane in [33].

2.1.2.1. Techniques of Reducing Coupling

2.1.2.1.1. Design with Different Radiation Patterns

Ref. [22] presents a combination of a monopole with dense meandering end and a PIFA with a shorted parasitic branch. The size of the prototype is $100 \times 43 \times 9$ mm^3. The main antenna is a monopole with one of the branches forming a patch with dense meandering end, which is placed at the bottom end of the prototype, as shown in Fig. 2.25. The diversity antenna is a PIFA with a shorted parasitic branch, which is located at the other end of the prototype. Simulation shows each of the antennas covers the bands of 869-894 MHz, 1805-2170 MHz with 6 dB return loss. The isolation is above 3 dB and 10 dB at lower and higher bands, respectively. The values of mean effective gain, at free space, for both antennas, are between -6 to -8 dBi at the lower band and -4 to -8 dBi at higher band. Ref. [22] describes the magnitude radiation patterns of the main and diversity antenna at 0.88 GHz in both free space and user's hand, respectively. The results show that the user hand alters the radiation characteristics of the two antennas, creating more difference between their magnitude patterns than in free space. It leads to the correlation, between the two antennas, dropping from 0.51 (in free space) to 0.34 (in user's hand).
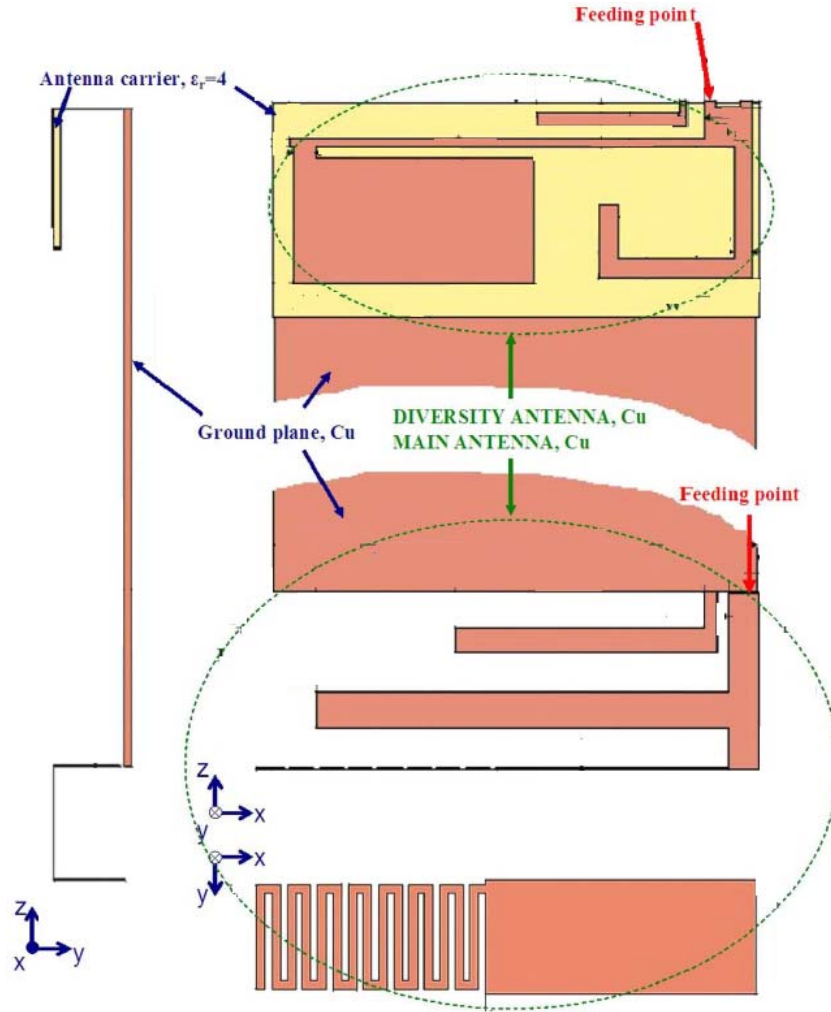
Fig. 2.25 Structure of a monopole with dense meandering end and a PIFA with a shorted parasitic branch [22]

A LTE MIMO system, which combines an adjustable antenna with several matching circuits and a passive antenna which is loaded with a ceramic branch and incorporates a matching circuit, is shown in Fig. 2.26 [23]. By incorporating different matching circuits, the MIMO antennas can cover LTE bands 12, 13, 14 and 17 (698-798 MHz) as well as band 7 (2500-2690 MHz), GM850 (824-894 MHz), EGSM900 (880-960 MHz), PCN (1710-1880 MHz), PCS (1850-1990 MHz) and UMTS (1920-2170 MHz) with return loss above 6 dB and isolation above 10 dB. The values of total efficiency for both antennas are least -4.2 dB at low band (700 – 960 MHz), at least -3.4 dB at mid band (1730 – 2170 MHz), and at least -3.5 dB at high band (2520 – 2680 MHz).
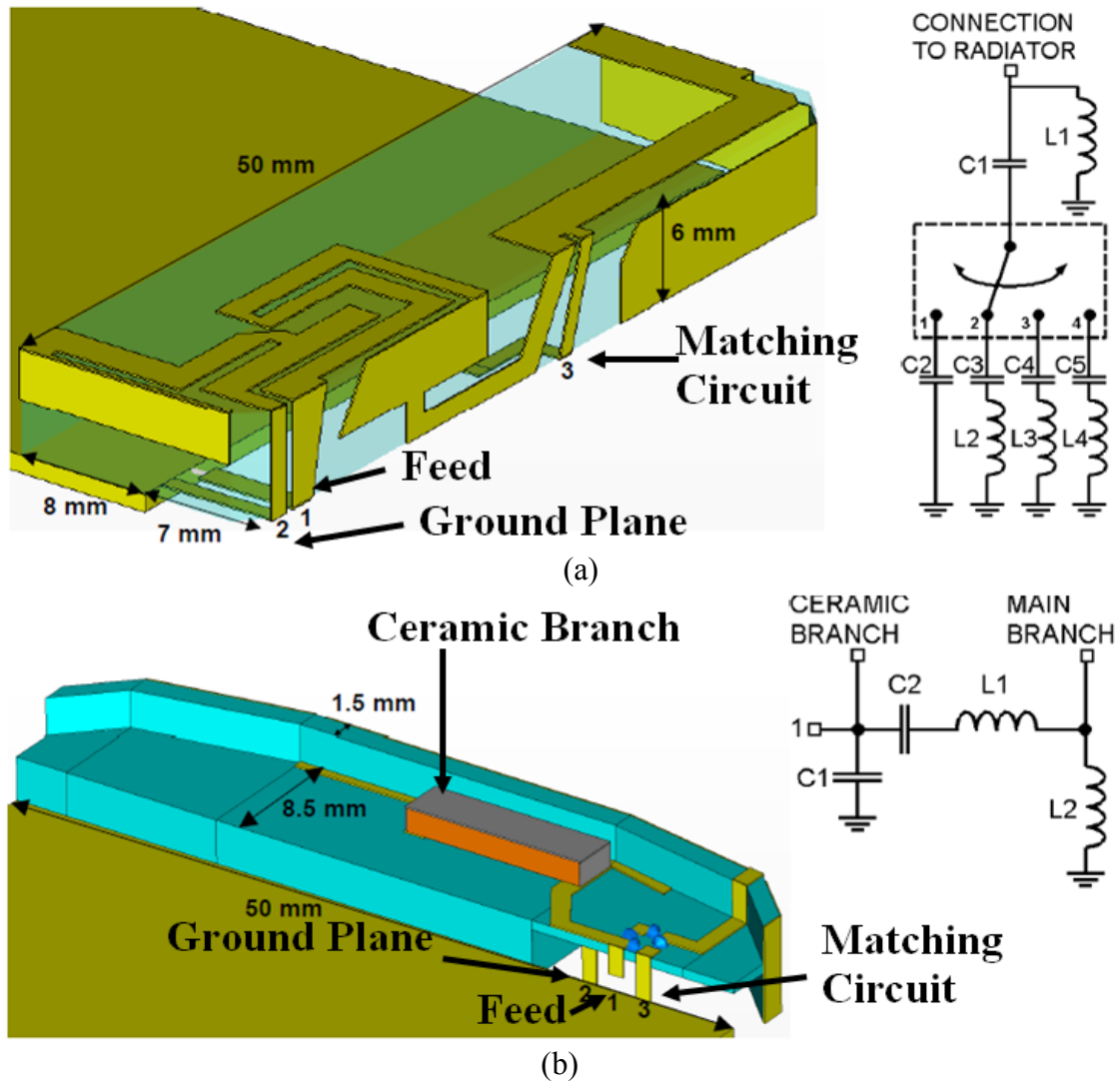
Fig. 2.26 A LTE MIMO system is combined with two antennas, i.e. a) adjustable antenna with matching circuits; and b) passive antenna loaded with ceramic branch and incorporating a matching circuit. [23]

Fig. 2.27 shows an internal handset antenna array [24] with main and auxiliary antennas for MIMO operation to cover LTE bands 704-787 and 2300-2690 MHz with return loss above 6 dB and isolation above 10 dB.
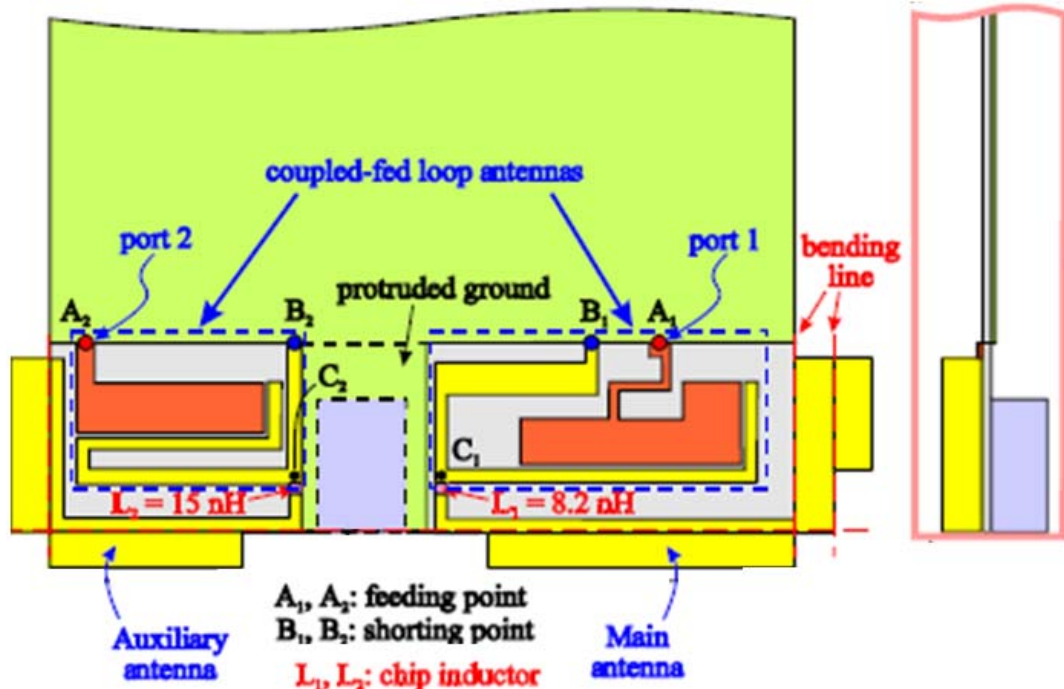
Fig. 2.27 Geometry of the internal handset antenna array [24]

2.1.2.1.2. Decoupling Network

Ref. [25] demonstrates a MIMO system using two PIFAs positioned on the top corner of a PCB, incorporating a neutralisation link between the feeding strips (shown in Fig. 2.28), it is possible to achieve the mutual coupling below -18 dB at the resonant frequency of 1.96 GHz. It is an improvement of 10 dB relative to the reference structure without the neutralisation link. From the radiation pattern point of view, the $E_\emptyset$ patterns are not affected by the introduction of the neutralised line, but the E_θ patterns have changed. Ref. [25] concludes that strong currents, flowing in the neutralisation link and perpendicular to the main currents flowing on the PCB and the PIFAs, are responsible for the different shape amount of the E_θ patterns. There is also a small increase in the measured maximum gain in the xz-plane, 0.7 dBi, due to the improved isolation.
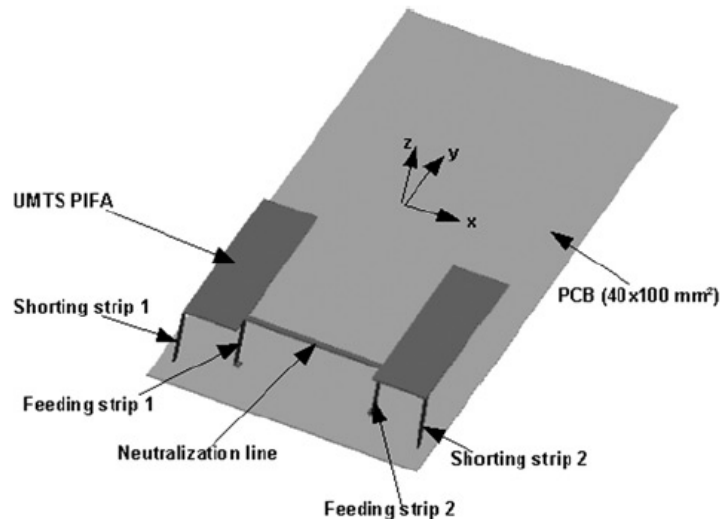
Fig. 2.28 3D view of the two PIFAs structure with the neutralisation link between the feeding strips. [25]

A decoupling technique, using the circuit approach, for improving the isolation for between two closely spaced antennas is shown in Fig. 2.29 [26]. Two examples are given, namely printed monopole antennas and miniaturized monopole antennas, respectively. The decoupling network is comprised of a shunt capacitor between the two ports and a simple L-section matching network on each port. With the decoupling network, the isolations is greatly improved from 3 dB to more than 20 dB at the centre frequency at around 2.45 GHz while the input return losses remained better than 10 dB.
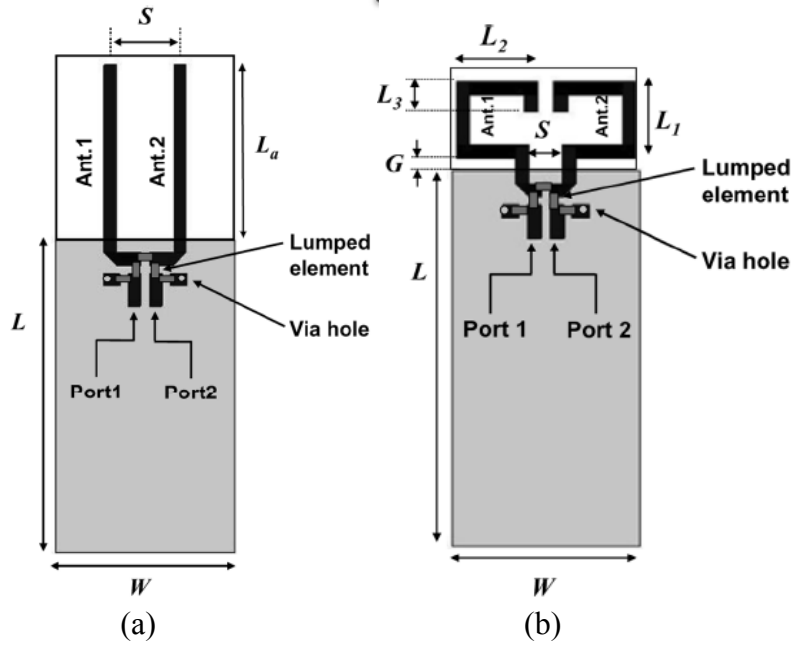
Fig. 2.29 The configuration of the two closely spaced antennas, (a) printed monopole antennas and (b) miniaturized monopole antennas [26]

A dual band MIMO antenna [27] is shown in Fig. 2.30 for operation in the 2.4 GHz and 5.2 GHz WLAN bands. By using a chip inductor between the two antennas, it is possible to have the isolation of about 20 dB at the lower band and over 18 dB at the upper band.
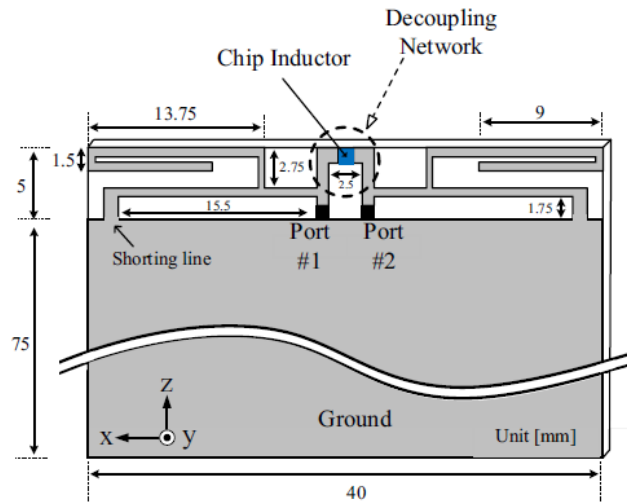
Fig. 2.30 Geometry of MIMO antenna with chip inductor in the middle [27]

Ref. [28] describes a MIMO antenna incorporating a decoupling network, which consists of two transmission lines, a shunt reactive components and quarter-wavelength jointed shorting structure, as shown in Fig. 2.31. The isolation is improved from 6 dB to more than 15 dB in the LTE band 13 (i.e. 770 MHz), while the input return losses remain better than 6 dB.

(a)   (b)
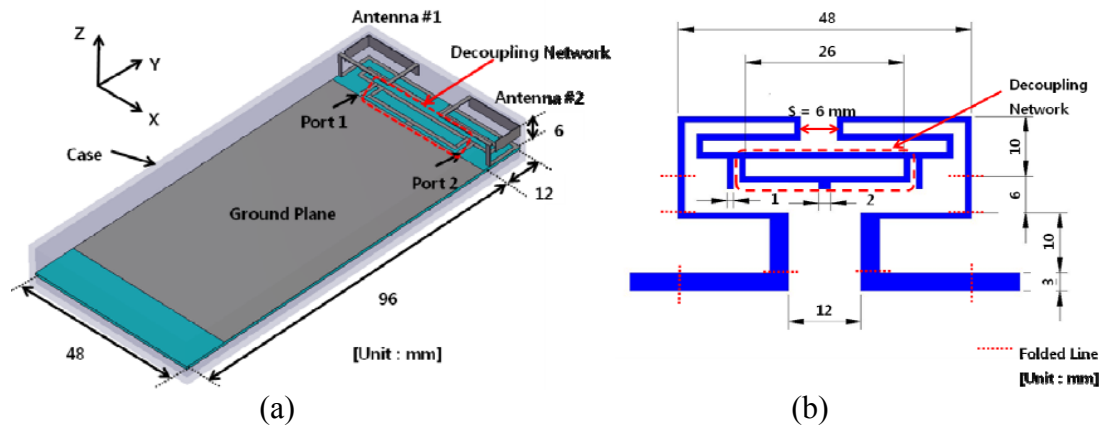
Fig. 2.31 Geometry of (a) MIMO antenna with (b) decoupling network [28]

2.1.2.1.3. EBG Structure

Four columns of fork-like EBG patches are inserted between the E-plane coupled antennas to reduce the mutual coupling, as shown in Fig. 2.32 [29]. When the EBG structure is employed, a 6.51 dB mutual coupling reduction is achieved at 5.2 GHz.

(a)   (b)
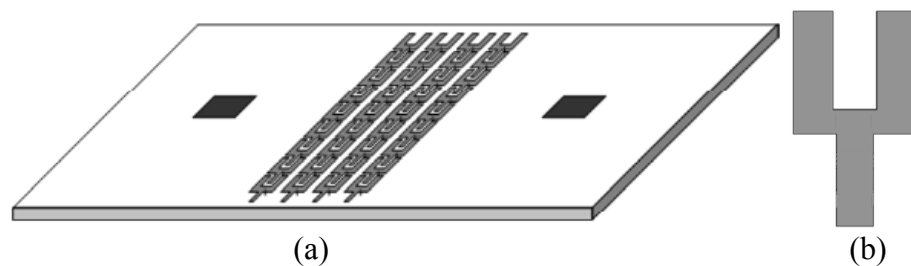
Fig. 2.32 (a) Microstrip antennas separated by the fork-like EBG structure for a low mutual coupling. Four columns EBG patches are used; (b) a fork-like EBG structure [29]

A mushroom-like EBG structure is implemented in the design of microstrip antenna arrays to reduce the strong mutual coupling is shown in Fig. 2.33 [30]. With the mushroom-like EBG structure, it is possible to improve the isolation from 16.15 to 25.03 dB at the resonant frequency, 5.86 GHz.

(a)   (b)
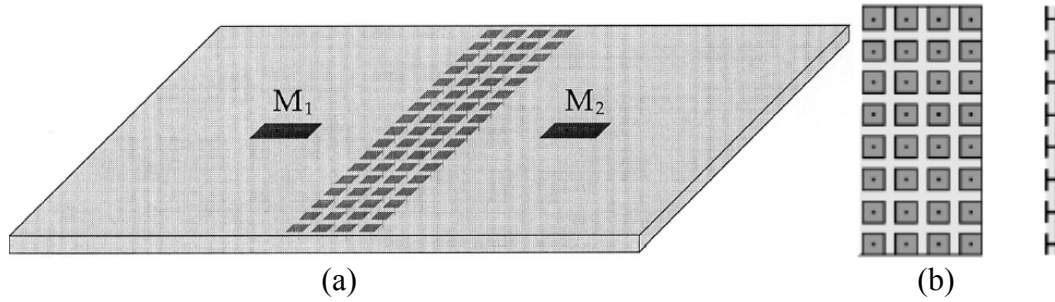
Fig. 2.33 (a) Microstrip antennas separated by the mushroom-like EBG structure for a low mutual coupling. Four columns EBG patches are used; (b) a mushroom-like EBG structure [30]

2.1.2.1.4. Ground Plane Slots

Ref. [31] introduces a dual-feed planar PIFA. Two isolated feeding ports are using one common radiating plate. The main technique introduced is to etch the ground plane under the radiating plate, as shown in Fig. 2.34, to reduce the mutual coupling. Simulation shows both branches of the antenna have a -10 dB bandwidth from 2.35 to 2.55 GHz with isolation better than 9 dB.
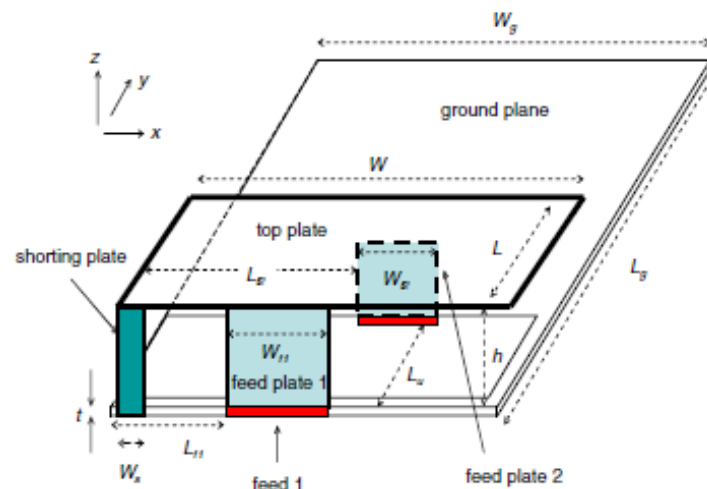
Fig. 2.34 Geometry of dual-feed PIFA for MIMO applications [31]

A MIMO antenna with two closed PIFAs incorporating a slit on the ground plane between two antennas is shown in Fig. 2.35 [32]. The isolation is improved by 12 dB at 2.53 GHz.
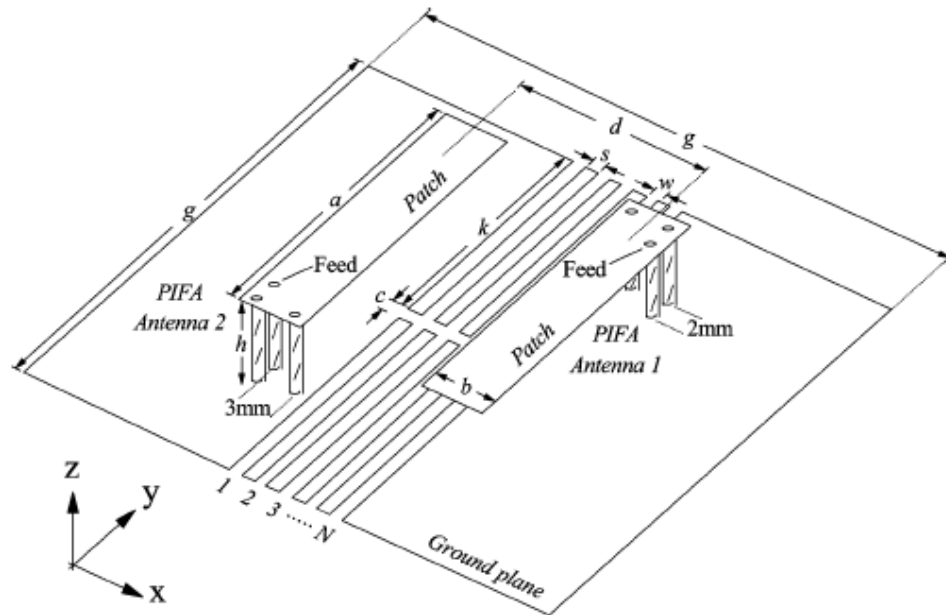
Fig. 2.35 Geometry of two closely-packed PIFAs with slotted ground plane structure [32]

2.1.2.1.5. Parasitic Elements

Ref. [33] presents a MIMO system using three EMC chip antennas in a PDA phone (as shown in Fig. 2.36) to generate a wide bandwidth covering WLAN (i.e. 2.4 GHz). By introducing a T-shaped shorted strip along the side edge of the system ground plane to modify the surface-current distributions on the ground plane, it is possible to achieve the isolation above 20 dB.

Fig. 2.36 (a) Configuration of the three-antenna MIMO system with a T-shaped shorted strip; (b) detailed dimensions of the metal pattern of the EMC chip antenna unfolded into a planar structure in the proposed MIMO system. [33]

2.1.2.2. Summary of MIMO Antennas

In conclusion, only the antennas proposed in refs. [23-24] can provide multi-band MIMO operation for small terminals. These two antennas in [23-24] have limited frequency range and are therefore not suitable for cognitive radio which might require

a frequency agile MIMO antenna, with wide tuning range, for spectrum sensing and data transmission at the same time [34].

2.1.3. Wideband Antennas with Fixed Band-Rejection

Several designs have been proposed for planar printed UWB antennas incorporating a fixed notch-band [35-44]. The most widely used methods involve inserting slots into the radiating elements or the ground plane [35-42]. C shaped [35], U shaped [35-36], L shaped [37], ring slot [38], CPW slot [39], meandered grounded stubs [40], and dual-gap open-loop slot [41] have been demonstrated. Another popular method is to use a resonator on the other side of the substrate, such as split ring resonators (SRRs) [42], square ring resonator [43], or a dual-gap open-loop resonator [41]. Parasitic elements have also been used to achieve band rejection behaviour. For example, Nikolaou et al. used L shaped resonators on either side of the radiating element [44]. These designs are now described in detail.

In ref. [35], CPW-fed compact elliptical monopole UWB antennas, having a U-shaped slot and a C-shaped slot, shown in Fig. 2.37 respectively, are introduced. The band rejection characteristic is caused by the presence of an approximately $\lambda/2$ slot at 5.8 GHz. The C-shaped slot resulted in a frequency notch band with significantly increased bandwidth compared to U-shaped slot. The values of gain suppression were 10 dB and 5 dB for U-shaped and C-shaped slots, respectively.

Fig. 2.37 CPW-fed compact elliptical monopole UWB antennas integrated a U-shaped slot and a C-shaped slot, respectively [35]

A CPW-fed UWB antenna with dual band-notched characteristics is proposed in ref. [36]. By etching two symmetrical rectangle slots in the ground plane nearby the feed line, a notched band at 5.5 GHz is obtained. The other notched band at 3.5 GHz is implemented by slotting a rectangle split ring slot in the radiator, as shown in Fig. 2.38. The gain suppression for those two notch bands were 7 dB and 9 dB, respectively. However, inserting slots on ground plane will reduce space and it will be concerned if in the case system designers want to place components on the ground plane.
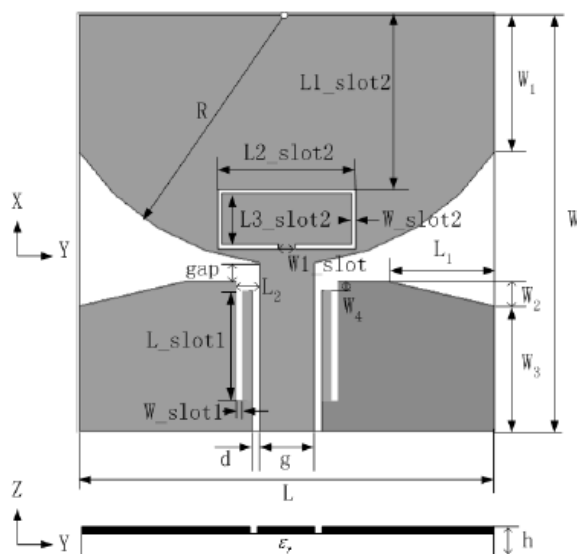
Fig. 2.38 A CPW-fed UWB antenna with dual band-notched characteristics [36]

An UWB antenna with a narrow frequency notch is presented in ref. [37]. The frequency notch at 5.65 GHz is introduced by two slots near the coplanar waveguide feeding the patch, as shown in Fig. 2.39. Performance on gain suppression for this antenna is not provided in ref. [37]. This proposed antenna has the same concerns about space of ground plane as the one in ref. [36]
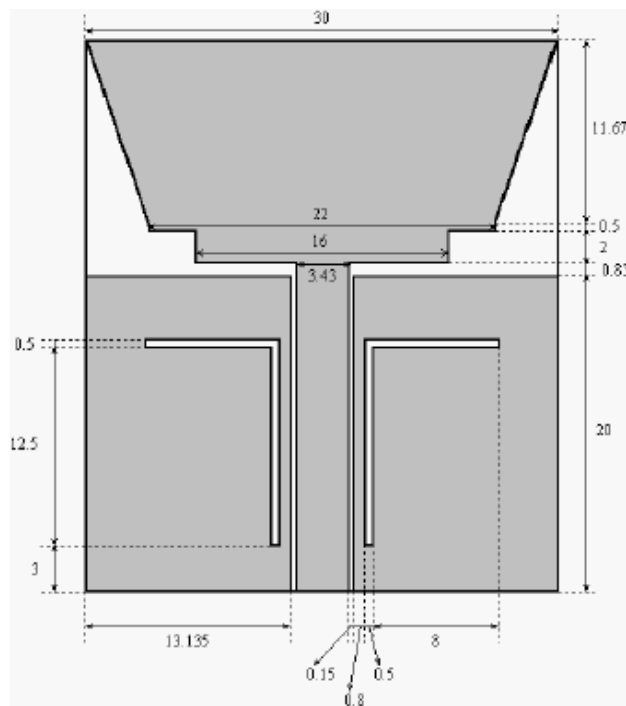
Fig. 2.39 An UWB antenna incorporating two slots [37]

Ref. [38] introduces a planar circular patch monopole UWB antenna with multiple etched ring slots on the patch, as shown in Fig. 2.40. The results showed that the antenna covers an ultra wide frequency band of 2.1-10.5 GHz (defined by VSWR<2) of 2.23-2.45, 2.36-3.48 and 5.54-5.88 GHz, respectively. The values of gain suppression for those three notch band were 8 dB, 4 dB, and 8 dB, respectively.
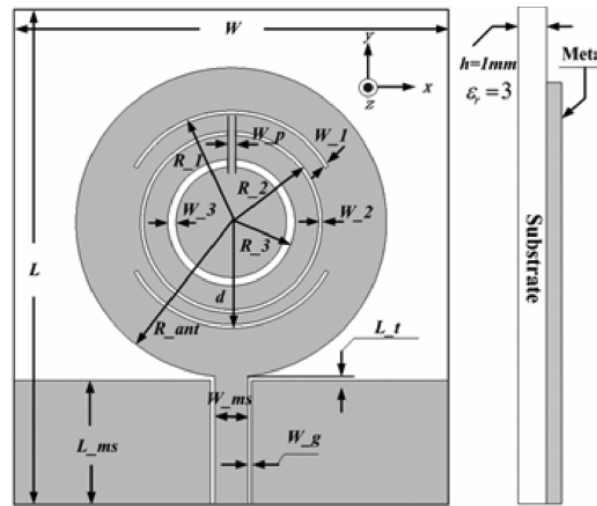
Fig. 2.40 A planar circular patch monopole UWB antenna with multiple etched ring slots on the patch [38]

A compact UWB monopole antenna [39] with a dual-band notched characteristic is shown in Fig. 2.41. The antenna consists of a semi-circular radiator and a dual-coplanar-waveguide (CPW) resonator, has two notched bands at the center frequencies of 3.5 and 5.5 GHz in the UWB region, with gain suppression of 8 dB and 7 dB, respectively.

(a)   (b)
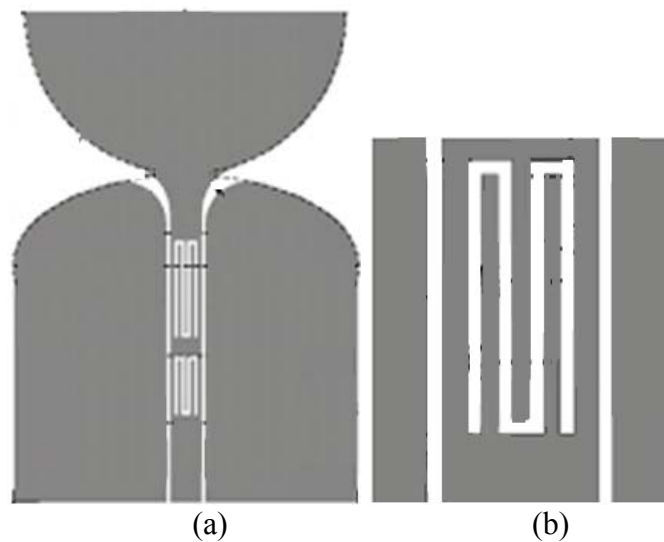
Fig. 2.41 A compact UWB monopole antenna with a dual-coplanar-waveguide resonator [39], a) layout of the antenna; b) layout of CPW resonator

The use of meandered grounded stubs in a dual band-notched planar-monopole antenna is shown in Fig. 2.42 [40]. The results showed that the two sets of dual-band notches were at the lower WLAN band (5.15-5.35 GHz) and higher WLAN band (5.725-5.825 GHz) with gain suppression of 9 dB and 4 dB, respectively.
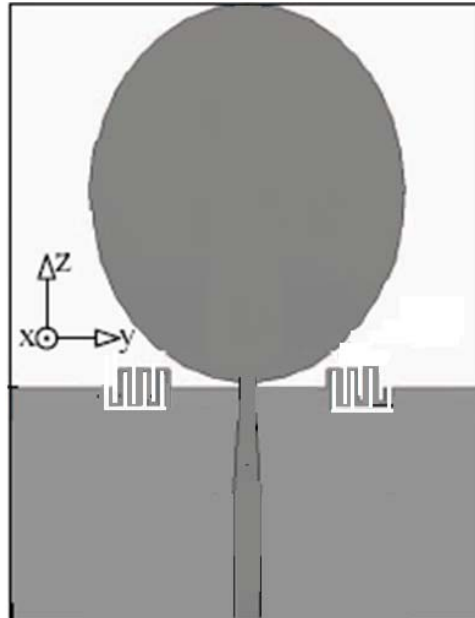
Fig. 2.42 an UWB antenna incorporating two meandered grounded stubs [40]

Two UWB antennas incorporated an open-loop resonator, which was printed onto the reverse side of the substrate material, and a dual-gap open-loop resonator, which was cut into the disk monopole, respectively, are presented in ref. [41], and are shown in Fig. 2.43. By printing the open-loop resonator onto the back of the substrate, it has an 11 dB gain suppression at 5.244 GHz. In the dual-gap open-loop resonator etched into the disk monopole, the notch band was centred at 4.13 GHz with 5.8 dB gain suppression.
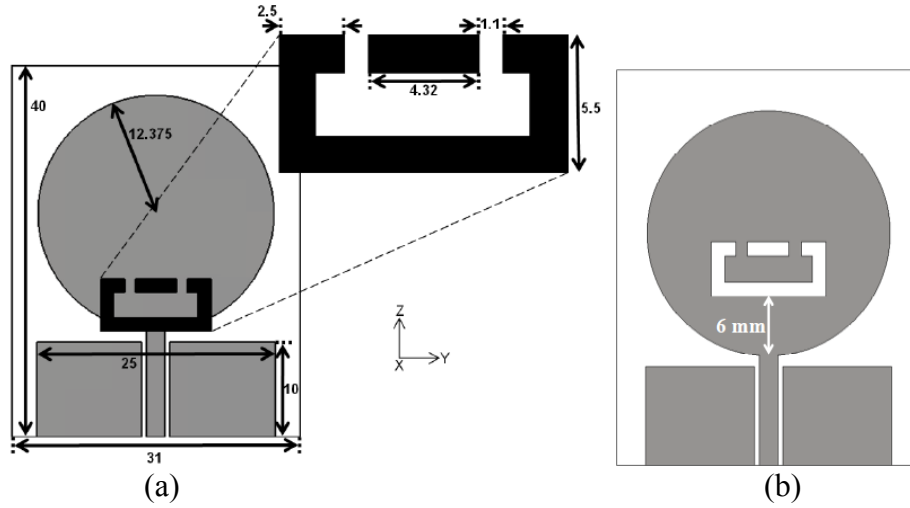
Fig. 2.43 (a) structure of the UWB antenna with an open-loop resonator; (b) a UWB antenna incorporating a dual-gap open-loop resonator cut into the disk monopole [41]

In ref. [42], a CPW fed UWB planar monopole antenna was proposed as shown in Fig. 2.44 (a). By embedding a split ring resonator (SRR) array, as shown in Fig. 2.44 (b), at the region between antenna and ground plane a notch band at around 5.5 GHz with gain suppression of 14 dB is obtained.
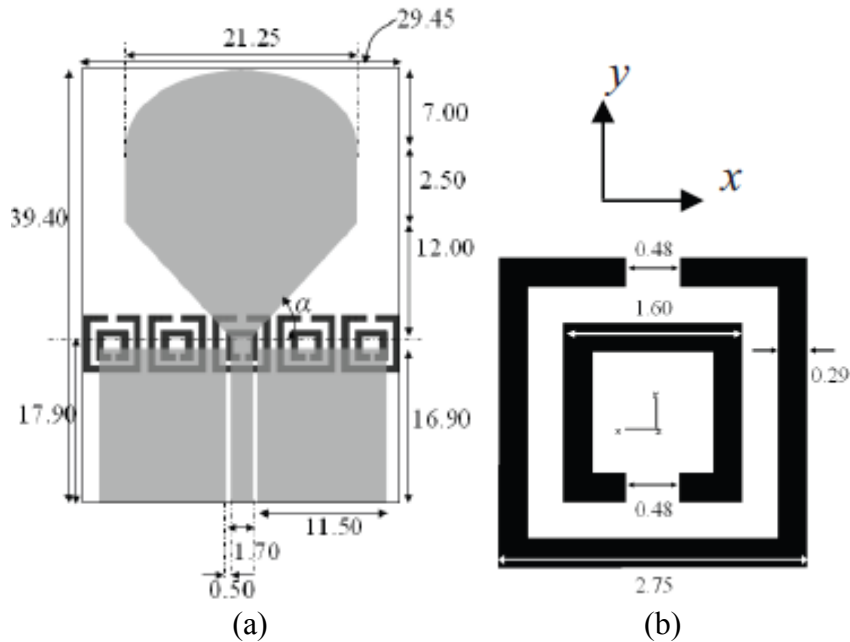
Fig. 2.44 (a) Illustration of the UWB band notched antenna with the SRR array at the back of the substrate; (b) Close up view of the SRR element with dimensions [42]

An UWB microstrip slot antenna with a square ring resonator embedded in the tuning stub was proposed in ref. [43], as shown in Fig. 2.45. The results showed the band-notched frequency is at 5.5 GHz with peak gain suppression of about 18 dB.
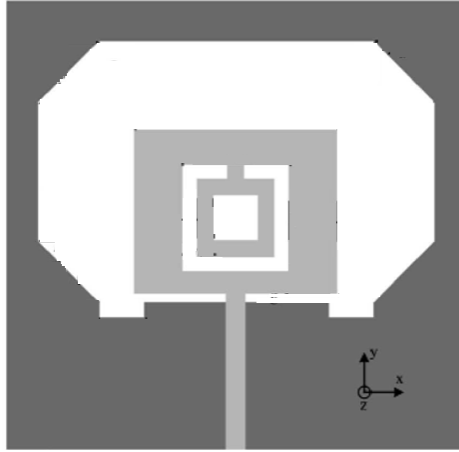
Fig. 2.45 an UWB microstrip slot antenna with a square ring resonator embedded in the tuning stub [43]

A CPW-fed compact elliptical monopole UWB antenna [44] with two resonating inverted L-shaped stubs that are connected to the elliptical radiator is shown in Fig. 2.46. The notch band centre frequency is at 5.5 GHz with 5 dB of gain suppression.
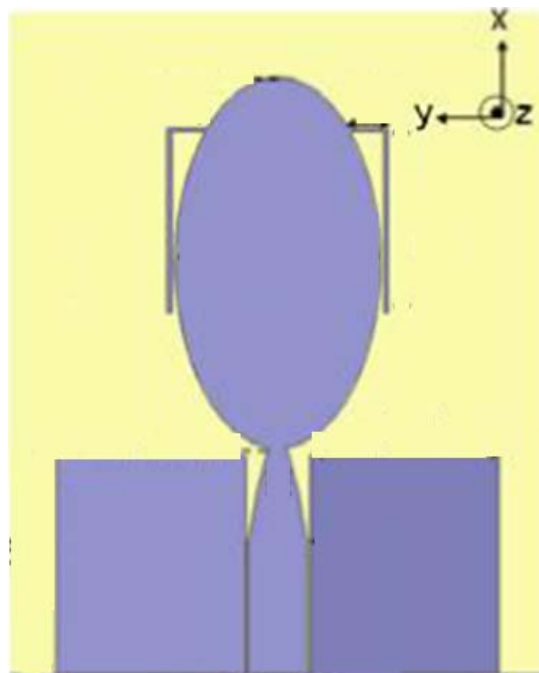
Fig. 2.46 a CPW-fed compact elliptical monopole UWB antenna incorporating two resonating inverted L-shaped stubs [44]

In conclusion, Lui et al. [43], described an UWB slot antenna incorporating a square ring resonator, which provides about 18 dB of peak gain suppression, and claimed it to be the best gain suppression currently available in literature. However, many of the proposed solutions suffer from at least one of the following limitations: 1) poor rejection at the notch frequency, 2) poor omni-directional radiation pattern at frequencies within the operating band, and are thus not suitable for IEEE 802.22 applications [45].

2.1.4. Wideband Antennas with Tunable Notched Band Frequency

In the previous section, wideband antennas with fixed band-rejection have been reviewed. It is clear that the notch band frequencies can only be changed by modifying the length of slots prior to manufacture. Several designs have been proposed for planar printed UWB antennas incorporating a tunable notch-band [46-49].

Ref. [46] presents a planar monopole with an etched square ring slot to create band rejection. The monopole is perpendicular to the ground plane, as shown in Figure 2.47. A varactor diode is used to obtain a tunable band rejection capability from $5.2 - 5.8$ GHz. The gain suppression is around 8 dB.
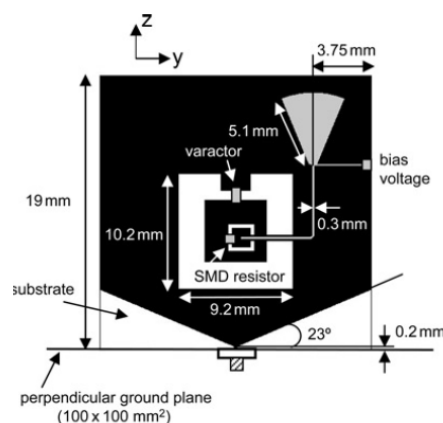
Fig. 2.47 Planar wideband monopole perpendicular to ground plane [46]

A planar monopole [47] using two slots to demonstrate dual band notches is shown in Fig. 2.48. One capacitor is used in each slot to tune the corresponding band notch in the demonstration. However, the capacitor can be replaced by a varactor diode. When incorporating two capacitors with value of 0.1 pF, it provided about 8 dB of gain suppression, at 3.5 GHz and 4.8 GHz, respectively.
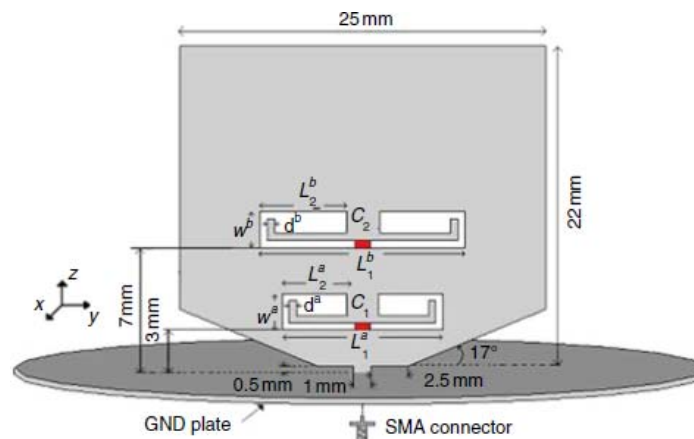
Fig. 2.48 Planar monopole with two slots [47]

In [48], a short circuited quarter wavelength stub with a varactor is applied to a wideband planar monopole as shown in Fig. 2.49. A tuning range from 4.6 – 6.5 GHz was achieved using two varactors.
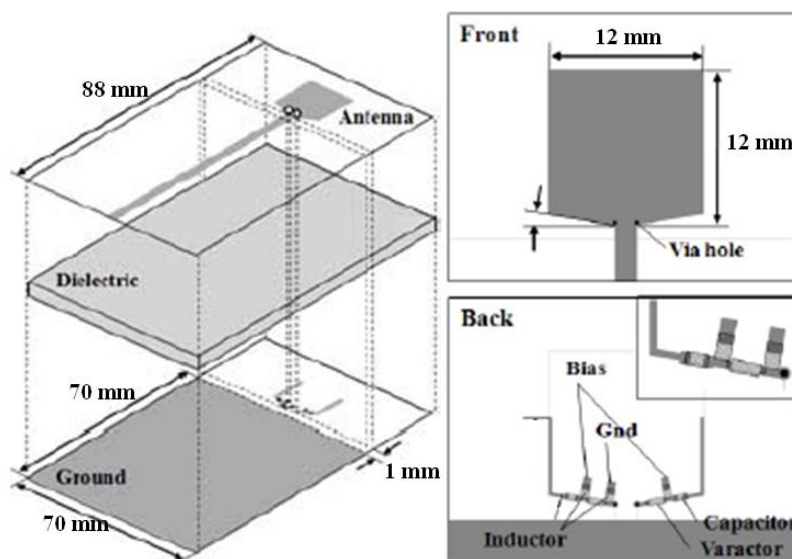
Fig. 2.49 Planar monopole with short circuited microstrip stub [48]

A reconfigurable Vivaldi antenna incorporating an L shaped microstrip resonator is shown in Fig. 2.50 [49]. By locating two series varactors on the resonator, measured results showed that the tuning range was 4.0 – 4.45 GHz with gain suppression at the stop band centre from 13 dB to 6 dBi.

| (a) | (b) |
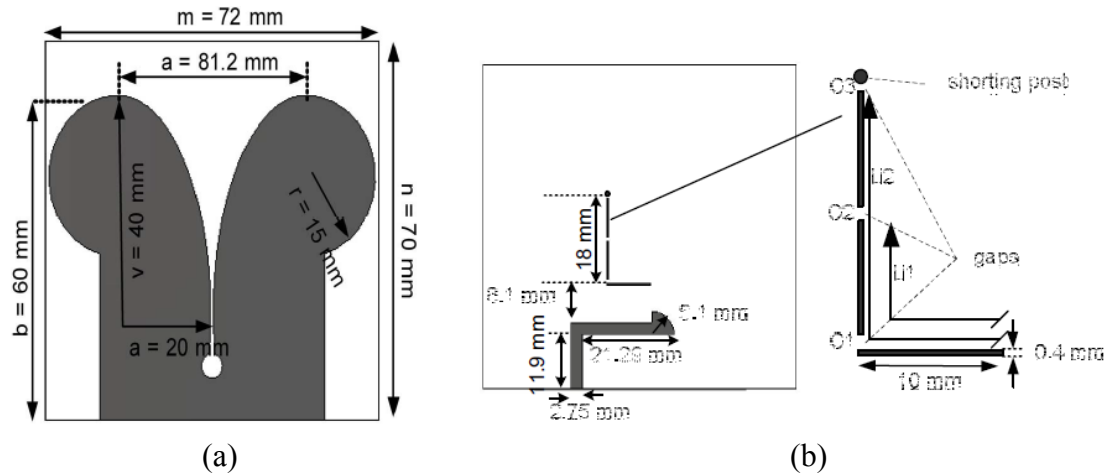
Fig. 2.50 Reconfigurable Vivaldi antenna (a) front view; (b) rear view showing microstrip feed and resonator. [49]

In conclusion, those designs in refs. [46-49] provided wide tuning range and good gain suppression. However, planar UWB antennas do not offer stable omni-directional patterns within the operating frequency band, especially at high frequencies (i.e. 10 GHz). This makes them not preferable for IEEE 802.22 [45], rural area network applications, which require both Tx/Rx antenna and sensing antenna with omni-directional pattern, as mentioned earlier.

2.2.   Summary

From this background study, several conclusions can be drawn. In the field of reconfigurable antennas, it shows that there were many reconfigurable antenna designs available for current and future small terminal applications in the literature. However, there is no antenna with dual-band operations simultaneously to

continuously cover from DVB (470 MHz) to Wifi (2450 MHz) bands. Most of the designs were limited to either only single service access or narrow tuning range. In order to be able to access a very large number of multiple wireless communication standards with increased channel capacity, several MIMO antennas have been proposed to achieve low correlation using different techniques. Only two proposed antennas, [23 and 24], can provide multi-band MIMO operation for small terminals. However, those two antennas, in refs. [23 and 24], have limited frequency range and are not suitable for cognitive radio, which might require a frequency agile MIMO antenna, with wide tuning range, for spectrum sensing and data transmission at the same time [34]. In the field of wideband antennas with band-rejection behaviour, most of them were with fixed notched band frequency and only a few can provide tunable band-rejection. However, none of them can provide omni-directional radiation pattern at high frequencies within the operating band. Addressing the above issues and investigating good antennas for small mobile terminals for current and future applications are the main objective of this PhD study.

References:

[1]   C. A. Balanis, Antenna Theory, 3rd edition, Analysis and Design, John Wiley & Sons, Inc, 2005, pp. 283-295.

[2]   S. Lim and H. Ling, "Design of electrically small, pattern reconfigurable Yagi antenna", *Electronics Letters,* Vol. 43, No. 24, 22nd Nov. 2007, pp. 3-4

[3]   W. S. Kang, J. A. Park, and Y. J. Yoon, "Simple reconfigurable antenna with radiation pattern", *Electronics Letters,* Vol. 44, No. 3, 31st Jan. 2008, pp. 182-183

[4]   Z. P. Wang, P. S. Hall, J. Kelly and P. Gardner, "TEM horn circular array for wide band pattern notch reconfigurable antenna system", *LAPC 2010, Loughborough Antennas & Propagation Conference, 2010, 8-9 Nov. 2010, Loughborough, UK, pp. 365-367*

[5]   F. Yang, and Y. Rahmat-Samii, "A reconfigurable patch antenna using switchable slots for circular polarization diversity", *IEEE Microwave and Wireless Components Letters,* Vol. 12, No. 3, March, 2002, pp. 96-98

[6]   H. Aissat, L. Cirio, M. Grzeskowiak, J. – M. Laheurte, and O. Picon, "Reconfigurable circularly polarized antenna for short-range communication systems", *IEEE Transactions on Microwave Theory and Techniques,* Vol. 54, No. 6, June, 2006, pp. 2856-2863

[7]   J. – S. Row, and M. – C. Chen, "Reconfigurable circularly-polarized patch antenna with conical beam", *IEEE Transactions on Antennas and Propagation,* Vol. 58, No. 8, Aug. 2010, pp. 2753-2757

[8]   Y. Yashchyshyn, "Reconfigurable antennas by RF switches technology", *in Perspective Technologies and Methods in MEMS Design, 2009. MEMSTECH 2009, 5th International Conference*, 2009, pp. 155-157

[9]   P. Gardner, M. R. Hamid, P. S. Hall, J. Kelly, F. Ghanem, and E. Ebrahimi, "Reconfigurable antennas for cognitive radioL requirements and potential design approaches", *in Wideband, Multiband Antennas and Arrays for Defence or Civil Applications, 2008 Institution of Engineering and Technology Seminar on, 2008*, pp. 89-94

[10]   G. M. Rebeiz and J. B. Muldavin, "RF MEMS switches and switch circuits", *Microwave Magazine, IEEE*, vol. 2, 2001, pp. 59-71

[11] K. R. Boyle, P. G. Steeneken, Z. Liu, Y. Sun, A. Simin, T. Huang, E. Spits, O, Kuijken, T. Roedle, and F. Van Straten, "Reconfigurable antennas for SDR and cognitive radio", *Antennas and Propag., 2007, EuCAP 2007, The Second European Conference* on 11-16 Nov. 2007, pp. 1-6.

[12] D. Manteuffel, M. Arnold, "Considerations for reconfigurable multi-standard antennas for mobile terminals", Antenna Technology: Small Antennas and Novel Metamaterials, 2008, iWAT 2008. International Workshop in 2008, pp. 231-234

[13] M. R. Hamid, P. S. Hall, P. Gardner, and F. Ghanem, "Frequency reconfigurable Vivaldi antenna", *Antennas and Propagation (EuCAP), 2010 Proceedings of the Fourth European Conference in 2010*, pp. 1-4

[14] A. Mirhamali, P. S. Hall, and M. Soleimani, "Wideband reconfigurable printed dipole antenna with harmonic trap", *Antenna Technology Small Antennas and Novel Metamaterials, 2006, IEEE International Workshop in* 2006, pp. 188-191

[15] L. Huang, and P. Russer, "Tunable antenna design procedure and harmonics suppression methods of the tunable DVB-H antenna for mobile applications", *Wireless Technologies, 2007 European Conference* on 8-10 Oct. 2007, pp. 304-307.

[16] H. F. Abutarboush, R. Nilavalan, K. M. Nasr, H. S. Al-Raweshidy and D. Budimir, "Widely tunable multiband reconfigurable patch antenna for wireless applications", *Antennas and Propagation (EuCAP), 2010 Proceedings of the Fourth European Conference in 2010,* pp.1-3

[17] M. G. S. Hossain, and T. Yamagajo, "Reconfigurable printed antenna for a wideband tuning", *Antennas and Propagation (EuCAP), 2010 Proceedings of the Fourth European Conference in 2010*, pp. 1-4

[18] A. T. Kolsrud, Ming-Yi Li, and K. Chang, "Frequency tunable CPW-fed CPS dipole antenna using varactors", *Antennas and Propagation Society International Symposium, 1998, IEEE,* Vol. 1, 1998, pp. 308-311

[19] R. Bose, and A. Sinha, "Tunable patch antenna using a liquid crystal substrate", *Radar Conference, 2008, RADAR '08, IEEE,* 26-30 May 2008, pp. 1-6.

[20] D. M. Pozar, and V. Sanchez, "Magnetic tuning of a microstrip antenna on a ferrite substrate", *Electronics Letters,* Vol. 24, Issue 12, 9th June 1988, pp. 729-731

[21] Y. Tawk, J. Costantine, and C. G. Christodoulou, "A rotatable reconfigurable antenna for cognitive radio applications", *Radio and Wireless Symposium (RWS), 2011 IEEE*, pp. 158-161

[22] V. Plicanic, B. K. Lau, A. Derneryd and Z. Ying, "Actual diversity performance of a multiband diversity antenna with hand and head effect", *IEEE Trans. Antennas Propagat.,* Vol. 57, May, 2009, pp. 1547-1556

[23] R. Kuonanoja, "Low correlation handset antenna configuration for LTE MIMO applications", *Antennas and Propagation Society International Symposium (APSURSI), 2010 IEEE*, pp. 1-4

[24] T. Kang, K. Wong, and M. Tu, "Internal handset antenna array for LTE/WWAN and LTE MIMO Operations", *European Conference on Antenna and Propagation, 2011, 5th EuCAP 2011* on 11-15 April, 2011, Rome, Italy.

[25] A. Diallo, C. Luxey, P. Le Thuc, R. Staraj and G. Kossiavas, "Enhanced two-antenna structures for universal mobile telecommunications system diversity terminals", *Microwaves, Antennas & Propagation, IET,* Vol. 2, Issue 1, 2008, pp. 93-101

[26] Shin-Chang Chen, Yu-Shin Wang, and Shyh-Jong Chung, "A decoupling technique for increasing the port isolation between two strongly coupled antennas", *Antennas and Propagation, IEEE Transactions on* Vol. 56, Issue 12, 2008, pp. 3650-3658

[27] Juman Kim, Minseok Han, Changho Lee, and Jaehoon Choi, "Dual band mimo antenna using a decoupling network for WLAN application", *Advanced Communication Technology (ICACT), 2011 13th International Conference,* 2011, pp. 624-627

[28] Min-Seok Han and Jaehoon Choi, "MIMO antenna using a decoupling network for next generation mobile application", *Communications and information Technology, 2009, ISCIT 2009, 9th International Symposium*, 2009, pp. 568-571

[29] L. Yang, M. Fan, F. Chen, J. She, and Z. Feng, "A novel compact electromagnetic-bandgap (EBG) structure and its applications for microwave circuits", *Microwave Theory and Techniques, IEEE Transactions on* Vol. 53, Issue 1, 2005, pp. 183-190

[30] Y. Fan, and Y. Rahmat-Samii, "Microstrip antennas integrated with electromagnetic band-gap (EBG) structures a low mutual coupling design for array applications", *Antennas and Propagation, IEEE Transactions on* Vol. 51, Issue 10, Part 2, 2003, pp. 2936-2946

[31] H. T. Chattha, Y. Huang, X. Zhu, and Y. Lu, "Dual-feed PIFA diversity antenna for wireless applications", *Electronics Letters,* Vol. 46, Issue 3, 2010, pp. 189-190

[32] Chi-Yuk Chiu, Chi-Ho Cheng, R. D. Murch, and C. R. Rowell, "Reduction of mutual coupling between closely-packed antenna elements", *Antennas and Propagation, IEEE Transactions on* Vol. 55, Issue 6, Part 2, 2007, pp. 1732-1738

[33] K. L. Wong, C. H. Chang, B. Chen, and S. Yang, "Three-antenna MIMO system for WLAN operation in a PDA phone", *Microwave Opt. Technol, Lett.,* Vol. 48, Jul. 2006, pp. 1238-1242

[34] W. Lee, and D.-H. Cho, "Enhanced spectrum sensing scheme in cognitive radio systems with MIMO antennae", *IEEE Transactions on Vehicular Technology,* Vol. 60, Issue 3, March 2011, pp 1072-1085.

[35] S. Nikolaou, B. Kim, Y. –S. Kim, J. Papapolymerou, and M. M. Tentzeris, "CPW-fed Ultra Wideband (UWB) Monopoles with Band rejection Characteristic on Ultra Thin Organic Substrate," *Proceedings of APMC 2006,* CD-Rom: FROF-26, Dec. 12-15, 2006.

[36] Z-A. Zheng, and Q-X. Chu, "A CPW-fed ultrawideband antenna with dual notched bands", *Ultra-Wideband, 2009, ICUWB 2009, IEEE International Conference on 2009,* pp. 645-648.

[37] E. Pancera, D. Modotto, A. Locatelli, F. M. Pigozzo, and C. De Angelis, "Novel design of UWB antenna with band – notch capability," *Wireless Technologies, 2007 European Conference on 2007,* pp. 48-50.

[38] Y. Zhang, W. Hong, C. Yu, Z-Q. Kuai, Y-D. Don, and J-Y. Zhou, "Planar ultrawideband antennas with multiple notched bands based on etched slots on

the patch and/or split ring resonators on the feed line," *IEEE Trans. Antennas and Propag.,* vol. 56, issue 9, 2008, pp. 3063-3068.

[39]   Y. F. Weng, W. S. Cheung, and T. I. Yuk, "Ultrawideband antenna using CPW resonators for dual-band notched characteristic," *Wireless Communications & Signal Processing, 2009, WCSP 2009, International Conference on 2009*, pp. 1-4.

[40]   Y. F. Weng, W. J. Lu, S. W. Cheung, and T. I. Yuk, "UWB antenna with single or dual band-notched characteristic for WLAN band using meandered ground stubs," *Antennas & Propagation Conference, 2009, LAPC 2009, Loughborough, U.K.* 2009, pp. 757-760.

[41]   J. Kelly, P. S. Hall, and P. Gardner, "Planar band-notched UWB antenna," *Antennas and Propagation, 2009, EuCap 2009, 3rd European Conference on 2009*, pp. 1636-1639.

[42]   R. Ghatak, R. Debnath, D. R. Poddar, P. K. Mishra, and S. Chaudhuri, "A CPW fed planar monopole band notched UWB antenna with embedded split ring resonators*," Antennas & Propagation Conference, 2009, LAPC 2009, Loughborough, U.K.* 2009, pp. 645-647.

[43]   W-J. Lui, C-H. Cheng, and H-B. Zhu, "Improved frequency notched ultrawideband slot antenna using square ring resonator*," IEEE Antennas and Propag.*, vol. 55, issue 9, 2007, pp. 2445-2450.

[44]   S. Nikolaou, A. Amadjikpe, J. Papapolymerou, and M. M. Tentzeris, "Compact Ultra Wideband (UWB) Elliptical Monopole with Potentially Reconfigurable Band Rejection Characteristic," *Proceedings of APMC 2007*, pp. 1-4.

[45] IEEE 802.22 Wireless Regional Area Networks - Enabling rural broadband wireless access using cognitive radio technology, IEEE 802.22-10/0073r03, 2010-06-15.

[46] E. Antonino-Daviu, M. Cabedo-Fabres, M. Ferrando-Bataller, and A. Vila-Jimenez. "Active UWB antenna with tunable band-notched behaviour," *Electronics Letters*, vol. 43, Issue 18, 2007, pp. 959-960.

[47] B. Rahmati and H. R. Hassani, "Wideband planar plate monopole antenna with dual tunable notch", *Electronics Letters*, vol. 46, issue 7, 2010, pp. 480-481.

[48] Won-Seok Jeong, Sang-Yun Lee, Won-Gyu Lim, Ho Lim, and Jong-Won Yu, "Tunable band-notched Ultra Wideband (UWB) planar monopole antennas using varactor", *Microwave Conference, 2008. EuMC 2008. 38th European*, 2008, pp. 266-268.

[49] M. R. Hamid, P. Gardner, P. S. Hall, and F. Ghanem, "Reconfigurable Vivaldi antenna with tunable stop bands", *Antenna Technology (iWAT), 2011 International Workshop in 2011*, pp. 54-57.

CHAPTER III

CHASSIS-ANTENNA

This chapter presents a novel two-port reconfigurable chassis antenna for use in current and future mobile wireless communication systems. The antenna uses a pair of coupling elements to excite resonant modes within the handset chassis. The elements are capacitively coupled to the chassis, are located in close proximity to each other, and are fed via two separate ports. Using a number of external matching circuits including switches and varactor diodes, the antenna can operate in either a narrowband or wideband mode. When operating in the narrow band mode, the antenna can provide one band to cover from 462 to 2522 MHz while the other band can cover from 1606 to over 3000 MHz simultaneously using a combination of switching and electronic tuning. However, the total tuning range is depended on the capacitance range of varactor diodes. Studies showed that the selection of a frequency in port 1 will restrict choice in port 2, and vice versa. In the wideband mode, the antenna can operate in one of six different wideband modes in the range of 470 to 2918 MHz.

All of the simulations presented in this chapter were performed using the transient solver in CST Microwave Studio$^{®}$. The s2p file representing the antenna response was used as a starting point for designing the matching networks. Microwave Office, from Applied Wave Research, was then used to adjust the value of each component to optimise the return loss performance of the antenna. The equivalent circuit simulations were performed using Advanced Design System.

The original concept for this two-port chassis-antenna is from Dr. Peter Song, who was a Research Fellow in School of Electronic, Electrical and Computer Engineering, University of Birmingham. This concept has been filed for a patent, [1].

3.1. Antenna Design

The antenna is shown in Fig. 3.1 and incorporates a pair of non-resonant coupling elements [1-7]. These are used to excite various resonant modes within the handset chassis. In this kind of resonant antenna-chassis combination (analysed in Ref [8]), the coupling elements are typically located at the end of the handset chassis, enabling the whole length of the chassis to be used as a radiating element. In this case, port 1 is connected to the large coupling element and port 2 is connected to the small one. The large element primarily excites modes within the lowermost band of frequencies, while the small element primarily excites modes with at the uppermost band of frequencies. The vertical portions of the two elements are separated from one another by a small gap, denoted as g_m. This gap helps to determine the amount of mutual coupling between these elements. In order to achieve effective coupling coefficient between each element and the handset chassis, the high frequency element needs to be sandwiched between the low frequency element and the chassis, as shown in Fig. 3.1. The feed line for the large element is positioned off-centre and is fixed to the top edge of the element. This arrangement offers two advantages. Firstly, the non-symmetrical currents which are generated within the handset chassis support a larger number of resonant modes. Secondly, the offset allows the higher frequency element (small element as shown in Fig. 3.1) to have more space since the feed pin of the large element has been offset. This means that the resonant frequency of the small element can be shifted lower, therefore bringing the resonant frequency separation of the two

elements closer. This enables opportunities for the smaller element to act as a parasitic hence optimising the bandwidth of the antenna system dynamically. Each coupling element is connected to a separate matching circuit or set of matching circuits, as shown in Fig. 3.2, denoted by M_1^N, M_2^N, M_1^W and M_2^W. Matching circuits M_1^N and M_2^N are used to obtain narrowband operation and by using M_1^W and M_2^W, wideband operation is obtained. Port 1 is connected to the large coupling element and port 2 is connected to the smaller one. The antenna has a ground plane size of 100×40 mm^2 and the coupling elements also occupy a very small space of $40\times5\times4$ mm^3. The gap between the coupling elements and the ground plane is 3 mm, which gives an overall size of $108\times40\times4$ mm^3, which is the typical size of a smart phone. The prototype antenna is shown in Fig. 3.1(c). It was fabricated from a microwave substrate material, Taconic TLY-3-0450-C5, which has a permittivity of 2.33, a thickness of 1.143 mm, and a metal thickness of 0.01778 mm. The coupling elements are copper with thickness of 0.5 mm and are supported with Rohacell^{TM}, which has a dielectric constant of 1.08 within the chosen frequency bands. It should be noted that the Taconic substrate is used purely as a carrier and the design is fully compatible with conventional metal stamp technology.

(a)

(b)   (c)

(d)
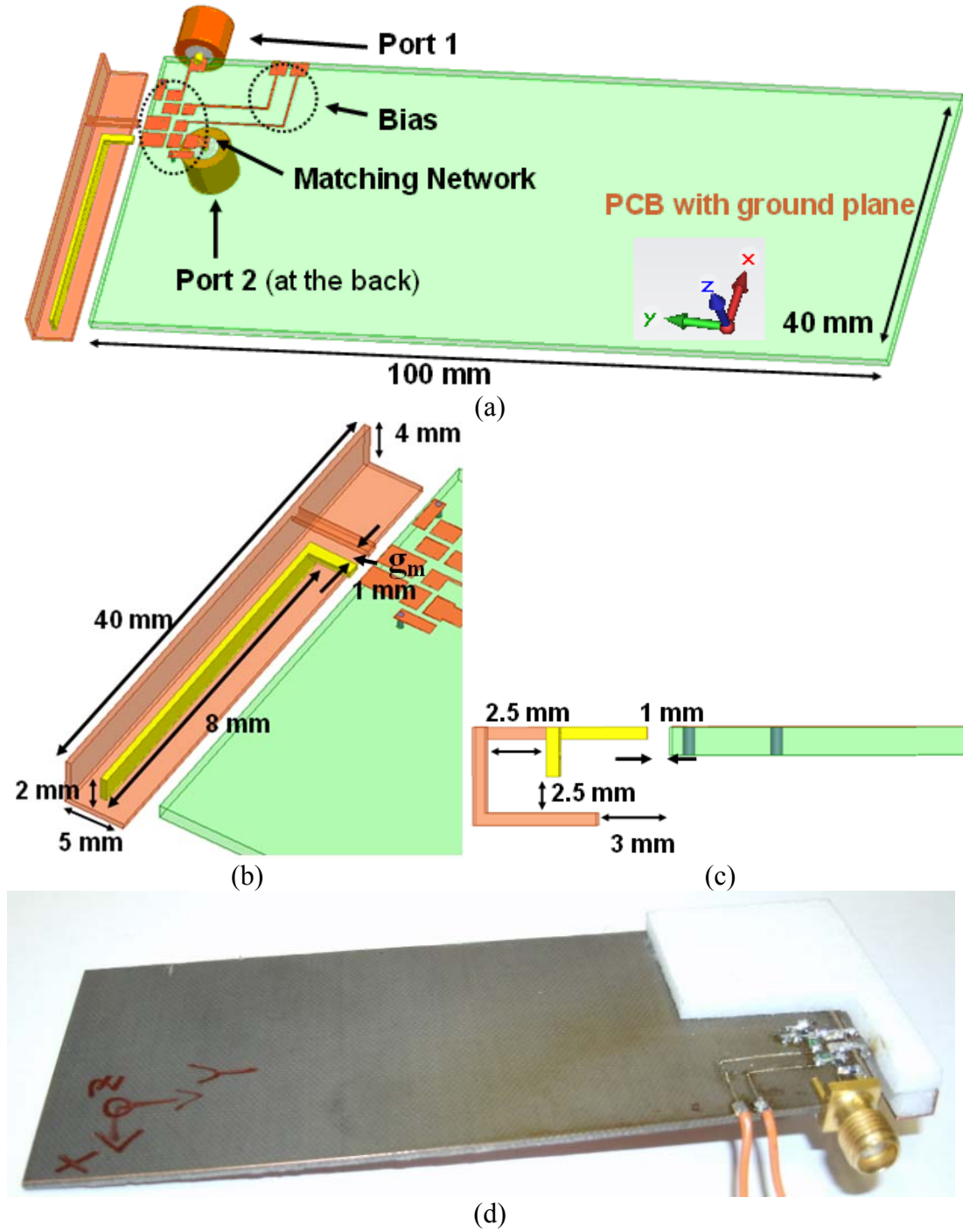
Fig. 3.1 (a) The structure of the reconfigurable handset chassis antenna; (b) the antenna elements; (c) side view of the antenna elements; (d) Top view of the completed fabricated antenna with matching circuit integrated
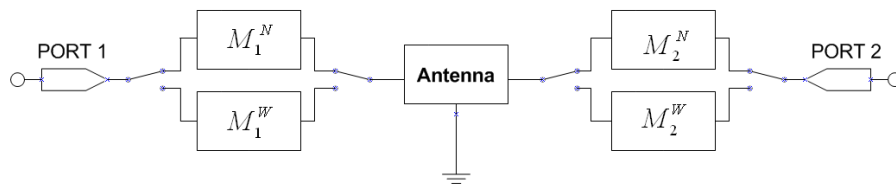
Fig. 3.2 Antenna system configuration

3.2. Narrowband Mode

3.2.1. Matching Circuit Design

In the narrowband mode, each coupling element is connected to a separate matching circuit and port, as shown in Fig. 3.2, but in this case port 1 has two narrow band matching circuits, selected by switches and port 2 has a single circuit. The matching circuit design procedure can be referred to Appendix B. The circuits are detailed in Table 1, and comprise a varactor diode and two fixed inductors. Matching circuits M_1^{N0} and M_1^{N1} on port 1, are used to obtain two "modes" of operation (denoted mode 0 and mode 1). When operating in mode 0, port 1 can cover the GSM, GPS, UMTS and WLAN bands while port 2 can cover the UMTS and WLAN bands. The switches were not included in either simulation or measurement, but the effect of switch loss is discussed later. When operating in mode 1, port 1 can cover the DVB-H and the GSM bands.

Names	Circuit Types & Values
M_1^{N0}	12.77 nH 3.39 nH
M_1^{N1}	59.06 nH 3.47 nH
M_2^{N0}	3.86 nH 2.4 nH
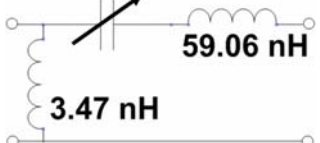
Table 3.1 Details of narrowband matching circuit of Fig. 3.2.

3.2.2. Simulations

3.2.2.1 Mode 0 in Simulation

As noted earlier, simulations were performed with CST Microwave Studio$^{®}$ and Microwave Office, from Applied Wave Research. Fixed capacitors were used to represent the varactors. No components parasitics were used in the simulations, which will result in slightly less loss and frequency shift in the simulations compared to the measurements in the next section. For M_1^{N0} and M_1^{N1}, capacitor C_1 was varied from 0.2 pF to 8 pF and for M_2^{N0} capacitor C_2 varied in value from 0.2 pF to 6 pF. Although higher upper values could have been used they give little extra tuning range. The range of capacitance for each varactor was optimized to achieve maximum tuning range. In practical, the full capacitance range might be impractical or expensive. However, it shows the antenna can potentially cover such wide frequency ranges.

When operating in mode 0, the antenna incorporates matching circuits, M_1^{N0} and M_2^{N0}, as shown in Table 3.1. Fig. 3.3(a) shows the resonant frequencies with reflection coefficient and instantaneous bandwidth at 6 dB while varying C_1 (which is located in matching circuit M_1^{N0}) from 0.2 pF to 8 pF and C_2 is fixed at 6 pF. With the selected range of capacitance, it is able to move the resonant frequency, looking into port 1, from 800 MHz to 2430 MHz while maintaining a return loss above 6 dB. Fig. 3.3(b) shows the resonant frequencies with reflection coefficient and instantaneous bandwidth at 6 dB while varying C_2 from 0.2 pF to 6 pF while C_1 is fixed at 8 pF. In this way it is possible to move the resonant frequency from 1680 MHz to 2860 MHz. The simulated S_{21} curve in Fig. 3.4 shows that there is a high degree of coupling between the two ports (i.e. over -7 dB) when C_1 is varied from 1.5 pF to 0.4 pF. This

occurs because the operating frequencies of two elements are tuned to coincide with each other. However, this mode of operation is unlikely unless Rx diversity application is desired, for example at UMTS2100. One of the best ways to address the high correlation coefficient is a decoupling network, which is beyond the goal of this work and is suggested for future work. The simulated resonant frequencies with reflection coefficient and instantaneous bandwidth at 6 dB for the narrowband mode 0 are shown in Tables 3.2 and 3.3.
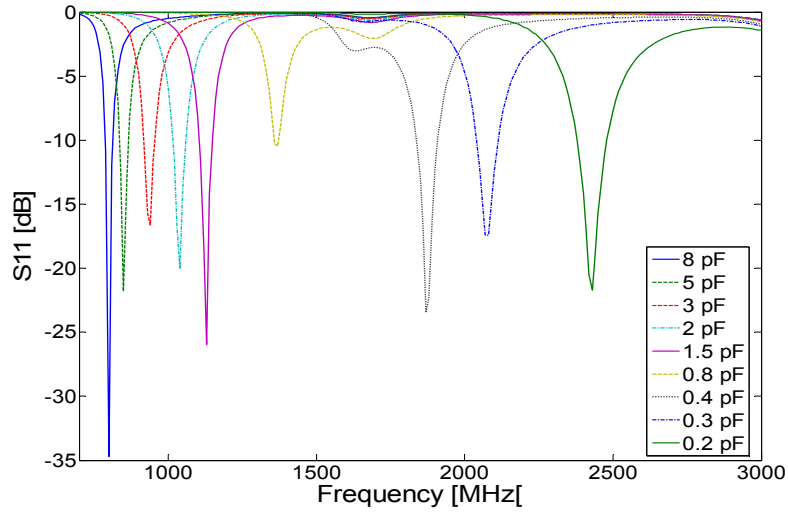
(a)
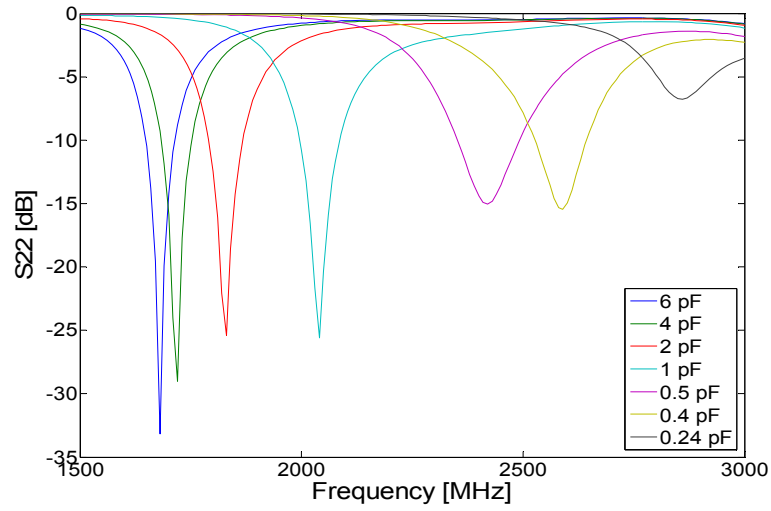
(b)

Fig. 3.3 Simulated reflection Coefficient for mode 0, (a) port 1 for large radiator, C_1 varied from 0.2 to 8 pF while C_2 fixed at 6 pF; (b) port 2 for small radiator, C_1 fixed at 8 pF while C_2 varied from 0.2 pF to 6 pF
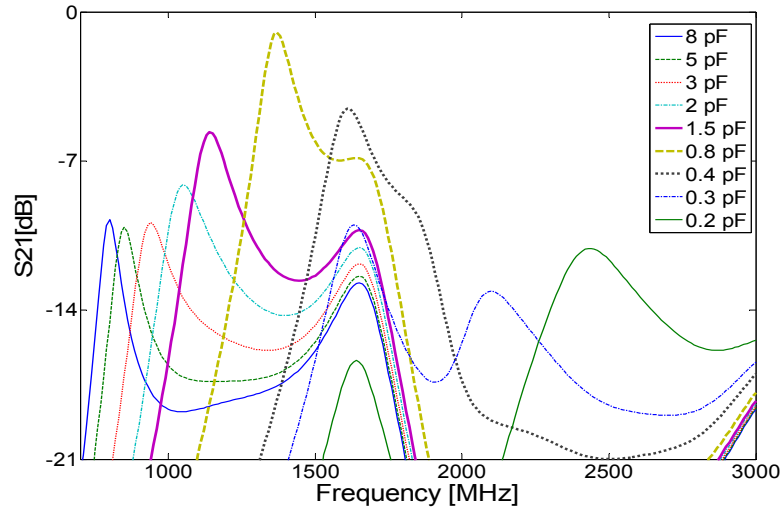
Fig. 3.4 Simulated S21 of mode 0 for port 1 with C_1 varied from 0.2 to 8 pF while C_2 fixed at 6 pF

	Capacitor (pF)	Freq. (MHz)	Refl. Coeff. (dB)	Bandwidth@ 6 dB (MHz)
	8	800	-34.52	43
	5	850	-21.78	52
Mode 0	3	940	-16.63	66
for	2	1040	-20.05	76
Port 1	1.5	1130	-25.95	74
Large	0.8	1370	-10.47	55
element	0.4	1870	-23.47	128
	0.3	2080	-17.42	134
	0.2	2430	-21.73	177

Table 3.2 Simulated Reflection Coefficient of mode 0 for port 1 with C_1 varied from 0.2 to 8 pF while C_2 fixed at 6 pF

	Capacitor (pF)	Freq. (MHz)	Refl. Coeff. (dB)	Bandwidth@ 6 dB (MHz)
	6	1680	-33.19	115
Mode 0	4	1720	-29.02	120
for	2	1830	-25.41	134
Port 2	1	2040	-25.60	160
Small	0.5	2420	-15.05	259
element	0.4	2590	-15.46	225
	0.24	2860	-6.77	69

Table 3.3 Simulated Reflection Coefficient of mode 0 for port 2 with C_1 fixed at 8 pF while C_2 varied from 0.2 pF to 6 pF

3.2.2.2 Mode 1 in Simulation

When operating in narrowband mode 1, the antenna incorporates a pair of matching circuits, M_1^{N1} and M_2^{N0}, as shown in Table 3.1. Fig. 3.5 shows simulation results for an antenna operating in narrowband mode 1. When C_1 is varied from 0.2 pF to 8 pF while C_2 is fixed at 6 pF, the resonant frequency, associated with port 1, shifts from 470 MHz to 1410 MHz. The return loss remains better than 6 dB throughout the tuning range. The simulated resonant frequencies with reflection coefficient and instantaneous bandwidth at 6 dB for the narrowband mode 1 are shown in Table 3.4.
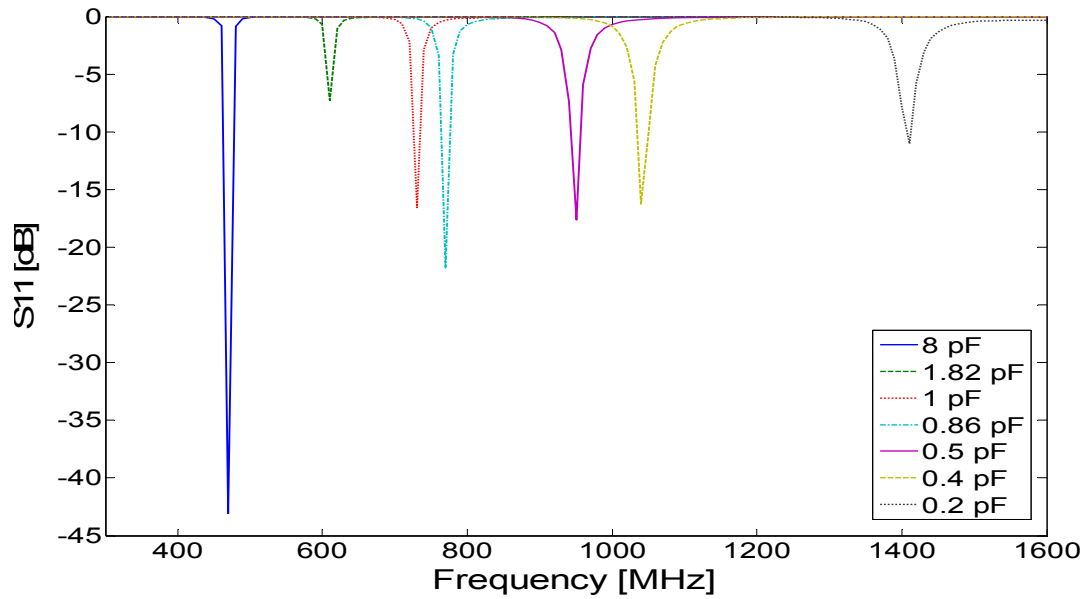
Fig. 3.5 Simulated S parameter of mode 1 for port 1 for large radiator, C1 varied from 0.2 to 8 pF while C2 fixed at 6 pF

	Capacitor (pF)	Freq. (MHz)	Refl. Coeff. (dB)	Bandwidth@ 6 dB (MHz)
	8	470	-43.06	17.4
Mode 1	1.82	610	-7.26	3.9
for	1	730	-16.54	25.0
Port 1	0.86	770	-21.78	17.0
Large	0.5	950	-17.60	22.9
element	0.4	1040	-16.24	26.6
	0.2	1410	-11.03	23.9

Table 3.4 Details of port 1 in mode 1 with C_1 varied from 0.2 to 8 pF while C_2 fixed at 6 pF

3.2.2.3 Summary for Modes 0 and 1 in Simulation

Dual band capability has been shown in this section. The simulations show that the narrowest instantaneous bandwidth is at 610 MHz, which is only 3.9 MHz, 0.64%. It can be increased somewhat by optimizing the matching circuit, but there is a trade off between the gain and the bandwidth. The maximum bandwidth, at 2420 MHz, is about 10.7%. The effect of the resonant frequencies with different values of capacitors, for both mode 0 and 1, was summarised in Fig. 3.6.
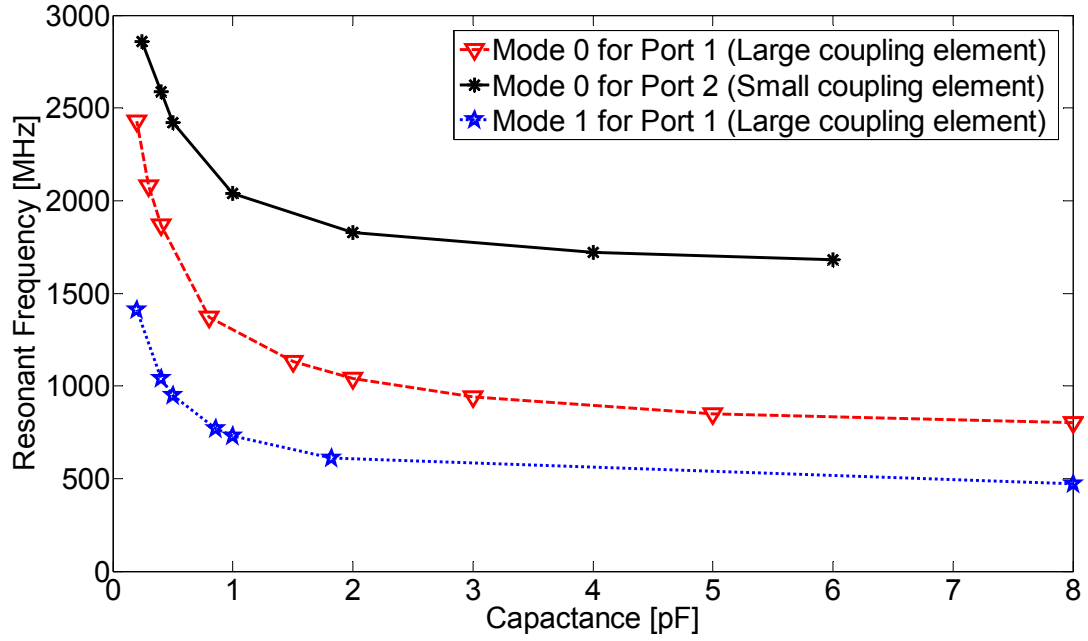
Fig. 3.6 Simulated resonant frequencies when the capacitors vary from 0.2 pF to 8 pF. (for port 1 in mode 0, the C_1 varied from 0.2 to 8 pF while C_2 fixed at 6 pF; for port 2 in mode 0, the C_2 varied from 0.2 to 6 pF while C_1 fixed at 8 pF; for port 1 in mode 1, the C_1 varied from 0.2 to 8 pF while C_2 fixed at 6 pF)

Table 3.5 shows the simulated frequencies, for each port of the chassis-antenna, with at least 6 dB of return loss, in the narrowband mode of operation under different conditions. It can be seen that the proposed antenna can provide dual band capability, wide tuning range with the frequencies fully controlled. However, the selection of a frequency in port 1 will restrict choice in port 2, and vice versa. The widest tuning range for port 1 is from 462 to 2522 MHz while from 1606 to over 3000 MHz for port 2, as shown in Table 3.5. Therefore, the antenna could potentially provide the wide tuning range from 462 MHz to over 3000 MHz when using the capacitors with range from 0.2 pF to 8 pF.

		Port 2 Cap fixed at 0.2 pF	894	2507
	Port 2	Large element left open circuit	1613	2742
		Port 1 Cap fixed at 8 pF	1625	2895
		Port 1 Cap fixed at 0.2 pF	1606	Over 3000
Mode 1	Port 1	Small element left open circuit	543	1480
		Port 2 Cap fixed at 6 pF	462	1419
		Port 2 Cap fixed at 0.2 pF	540	1476
	Port 2	Large element left open circuit	1613	2742
		Port 1 Cap fixed at 8 pF	1617	2789
		Port 1 Cap fixed at 0.2 pF	1625	2790

Table 3.5 Simulated frequencies of the chassis-antenna, with at least 6 dB of return loss, in narrowband mode of operation under different conditions

3.2.3. Measurements

During the measurement, both ports were operating simultaneously. In the demonstrator antennas, varactor diodes MV31009-150A, from Microsemi[®] were used. The capacitance of those varactors can be varied from 0.95 pF to 21.98 pF using a bias voltage from 15 V to 0 V. A dc bias line with a +ve voltage, incorporating a 10 k Ω resistor for decoupling was attached to the anode of each varactor. The –ve voltage is supplied from the inner conductor of the SMA connector by using a bias-tee, ZX85-12G-S+, from Mini-Circuits[®].

3.2.3.1 Comparison between Simulation and Measurement

Fig. 3.7 shows the comparison of simulation and measurement results. Full equivalent circuits from the vendors' library, were used for the components, although these were not available for the varactors. The resonant frequencies, obtained through simulation and measurement, differ by at most 60 MHz for port 1, and 79.5 MHz for port 2. The different s2p files of the fixed capacitors used in simulation and the varactors used in

measurement, along with the effect of manufacturing tolerances, helps to explain the slight discrepancies described above.
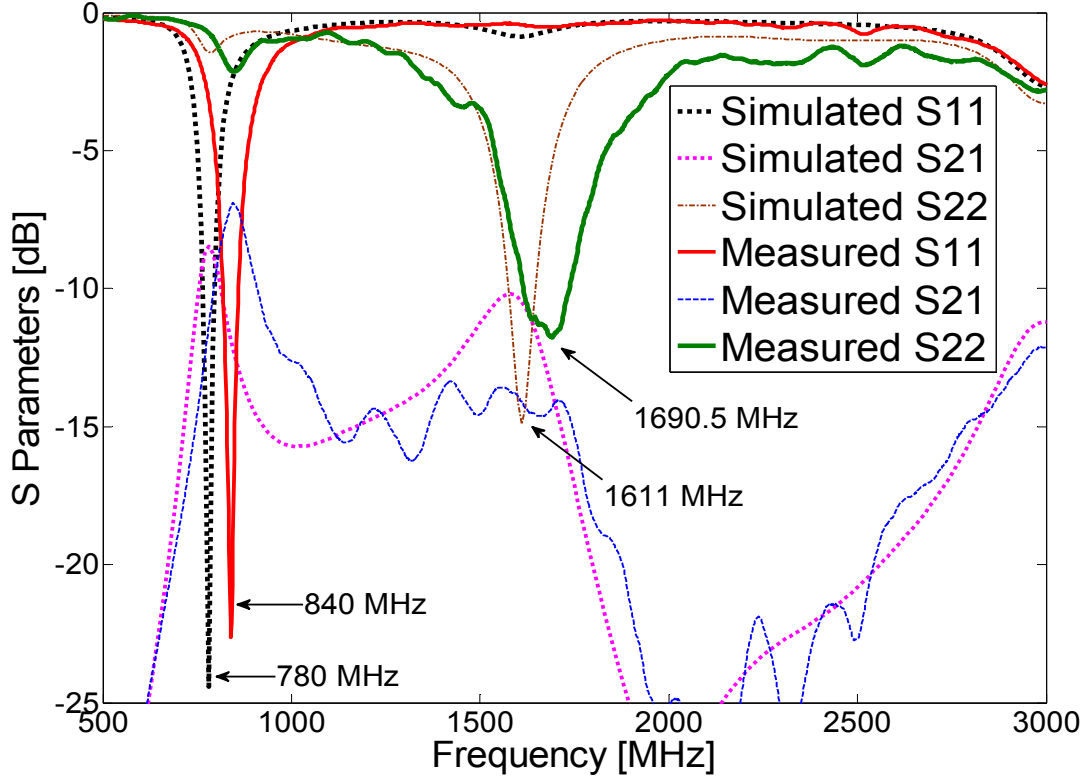
Fig. 3.7 Comparison of simulation (i.e. port 1 with fixed 8.2 pF capacitor and port 2 with fixed 6 pF capacitor) and measurement results (i.e. port 1 with varactor with voltage 1.2 V and port 2 with varactor with voltage 2 v)

3.2.3.2 Mode 0 in Measurement

Fig. 3.8 shows measured results. Fig. 3.8(a) illustrates the effect of varying the voltage applied to varactor 1 (which is located in matching circuit M_1^{N0}) from 1.2 V to 15 V, with the voltage applied to varactor 2 fixed at 2 V. The resonant frequency varies from 840 to 1306 MHz. It is likely that the frequency tuning range could be increased, if the capacitance tuning range of the varactor was wider. Fig. 3.8(b) shows the effect of varying the voltage applied to varactor 2 from 2 V to 15 V while that applied to varactor 1 was fixed at 1.2 V. The resonant frequency varies from 1657 to 2173 MHz. When the two resonant frequencies are close to one other, there will be

strong coupling between the two ports. Fig. 3.8(a) shows that the peak S_{21} varies from

-7.1 to -4.08 dB. However, when the voltage applied to varactor 2 was increased to 15

V, the S_{21} for port 1 is below -10 dB, as shown in Fig. 3.8(c). High isolation (i.e.

below -10 dB) occurs within the tuning range of 1657 to 2173 MHz for varactor 2

voltage from 2 V to 15 V while the voltage applied to varactor 1 was fixed at 1.2 V as

shown in Fig. 3.8(b).
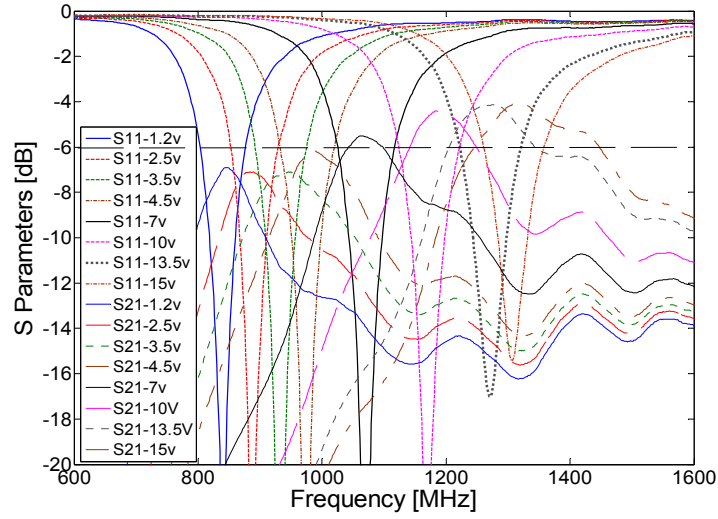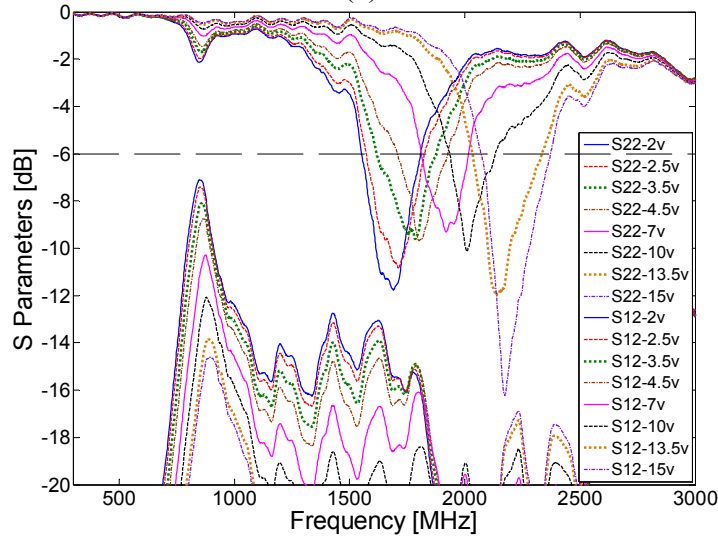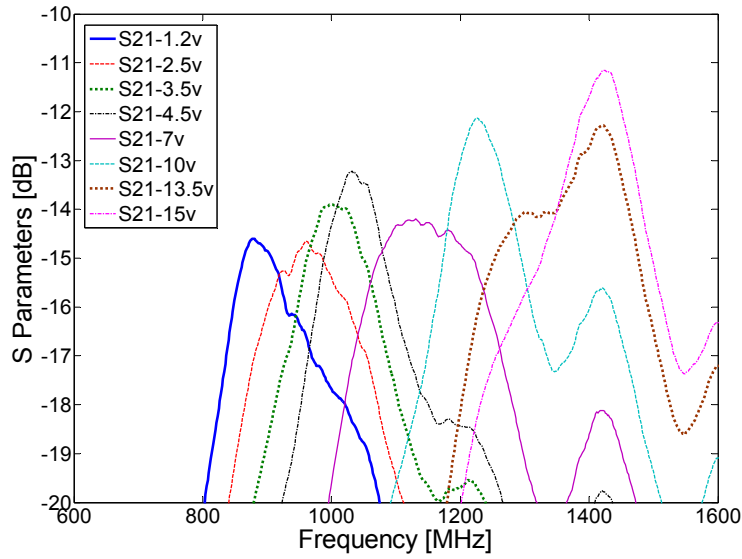
Fig. 3.8 Measured S parameter of mode 0 for (a) port 1 with varactor 1 varied from 1.2 V to 15 V while varactor 2 fixed at 2 V; (b) port 2 with varactor 2 varied from 2 V to 15 V while varactor 1 fixed at 1.2 V; (c) port 1 with varactor 1 varied from 1.2 V to 15 V while varactor 2 fixed at 15 V

3.2.3.3 Mode 1 in Measurement

Fig. 3.9(a) shows the measurement results for mode 1 obtained when varying the voltages applied to varactor 1 from 1.2 V to 15 V while that applied to varactor 2 was fixed at 2 V. This shifts the resonant frequency from 485 to 734 MHz. Fig. 3.9(b) shows the effect of varying the voltage applied to varactor 2 from 2 V to 15 V while that applied to varactor 1 was fixed at 1.2 V. The resonant frequency varies from 1671 to 2181 MHz. The coupling between the two ports remained below -10 dB throughout the tuning range in both cases.

(a)

(b)
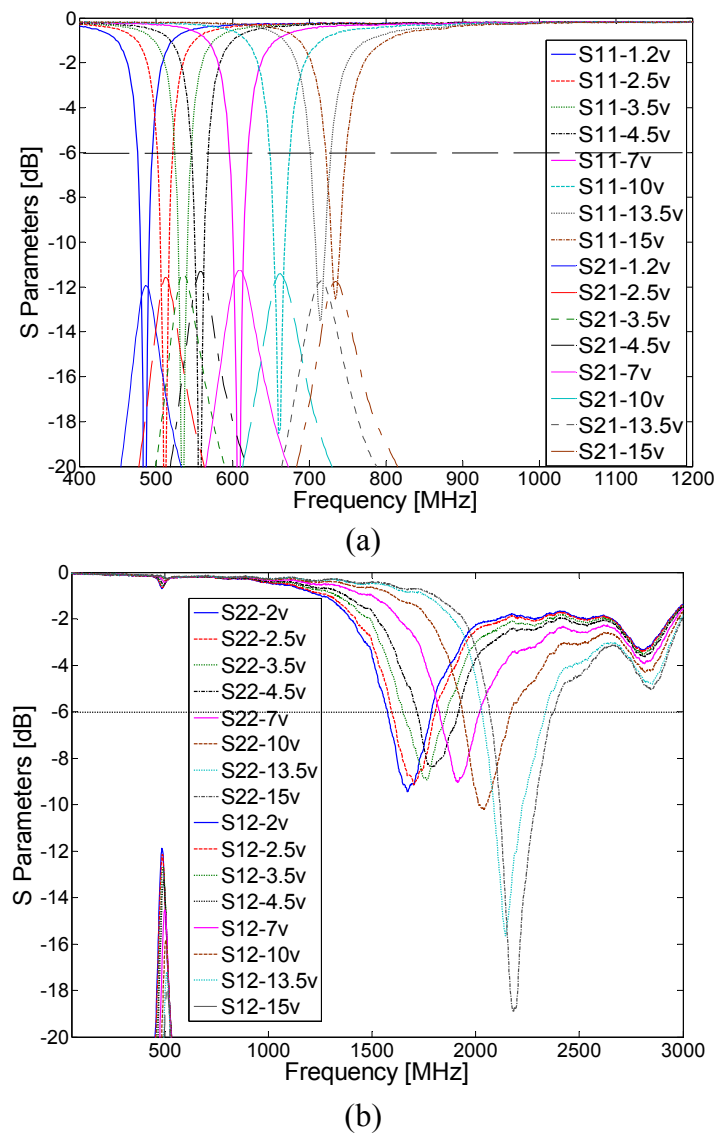
Fig. 3.9 Measured S parameter of mode 1 for (a) port 1 with varactor 1 varied from 1.2 V to 15 V while varactor 2 fixed at 2 V; (b) port 2 with varactor 2 varied from 2 V to 15 V while varactor 1 fixed at 1.2 V

3.2.3.4 Limitations

Figs. 3.8(a) and (b) show that the band from 1306 to 1657 MHz is not covered by the antenna within the capacitance tuning range of the varactor. Figs. 3.9(a) and (b) show the band not covered is from 734 to 1671 MHz. This problem can be solved by either using a varactor with lower capacitance limit or by using additional matching circuits. Studies showed that the selection of a frequency in port 1 will restrict choice in port 2, and vice versa, as mentioned in section 3.2.2 Simulations. For example, whilst the voltage applied to varactor was varied from 2 V to 15 V, the resonant frequency for port 1, with the voltage applied to varactor 1 fixed at 1.2 V, shifted from 840 to 872 MHz.

3.2.4. Radiation Patterns

Fig. 3.10 shows the measured radiation patterns at 470 MHz (port 1 at mode 1), 923 MHz (port 1 at mode 0), 1895 MHz (port 2 at mode 1) and 2109 MHz (port 2 at mode 0) for the antenna operating in the narrow band mode. In the figure, the E_θ and E_Φ are shown in Z-Y and Z-X plane respectively. Radiation of the chassis-antenna in free space for low frequency is close to omni-directional in the Z-X plane (i.e. $\Phi=90^o$), especially at 470 MHz and 923 MHz as shown in Fig. 3.10 (c). However, Fig. 3.10 (d) shows that at higher frequencies, i.e. 1895 MHz and 2109 MHz, gain is slightly reduced at about–Z and +X directions, which is due to the bias cables effect. Results show that there is no significant nulls in Z-X plane and suggest that this type of chassis-antenna is a good candidate for mobile phone application.
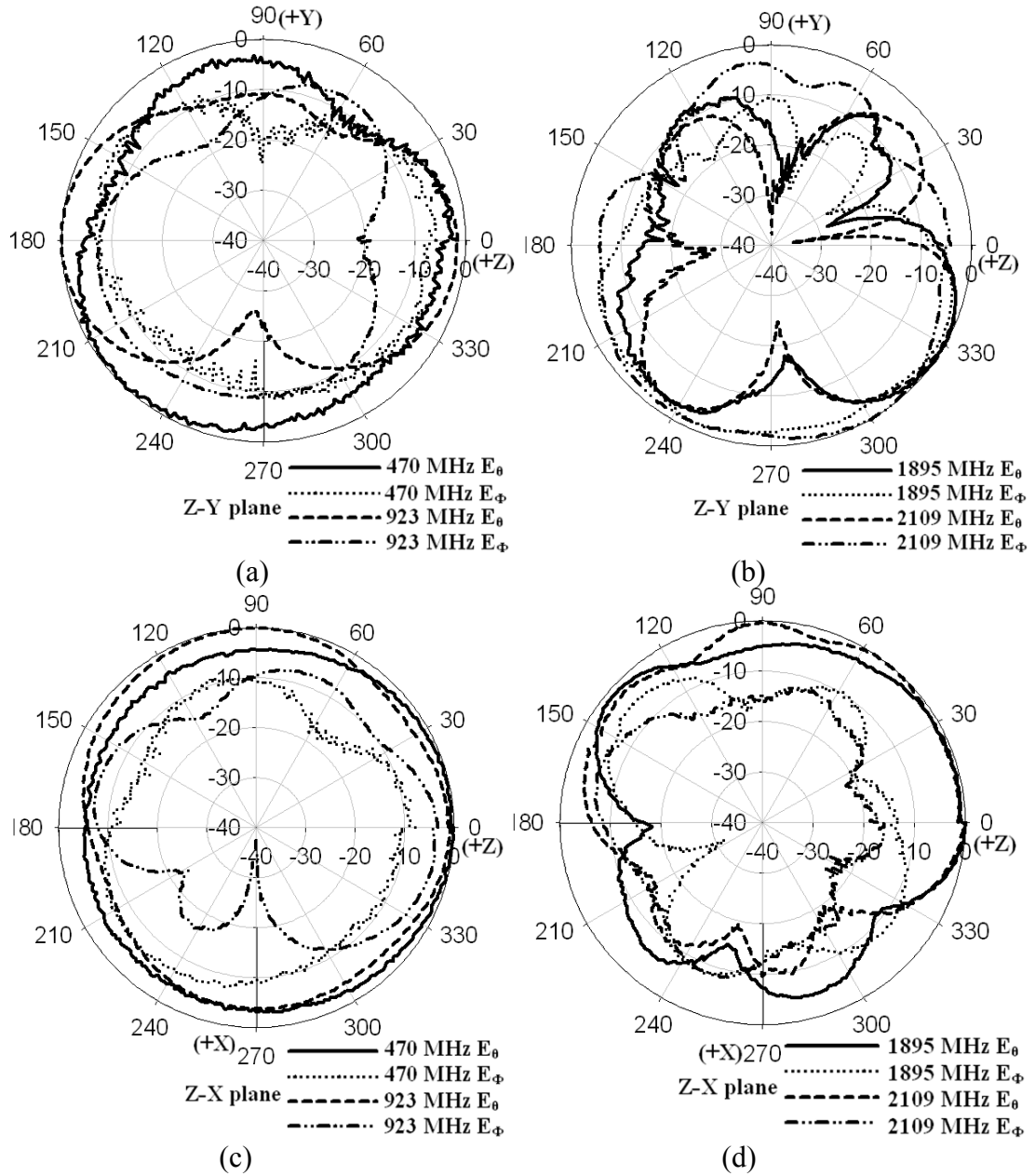
Fig. 3.10 Measured radiation patterns for (a) Z-Y plane at 470 MHz and 923 MHz; (b) Z-Y plane at 1895 MHz and 2109 MHz; (c) Z-X plane at 470 MHz and 923

3.2.5. Current Distributions

For this type of chassis-antenna, the current distribution is sinusoidal and similar to dipole-type antenna. Figs. 3.11 (a) to (d) show the simulated current distributions for the chassis-antenna at 470 MHz, 923 MHz, 1895 MHz and 2109 MHz, respectively. It is clear that for each resonant frequency, the current is mainly distributed on the

coupling elements and the edge of the ground plane with a null at the bottom end of the ground plane. However, for higher frequency, i.e. 1895 MHz and 2109 MHz, there is strong current which is distributed along the lower edge of ground plane with a null of current in the middle of the ground plane, as shown in Figs. 3.11 (c) and (d).

(a)   (b)

(c)   (d)
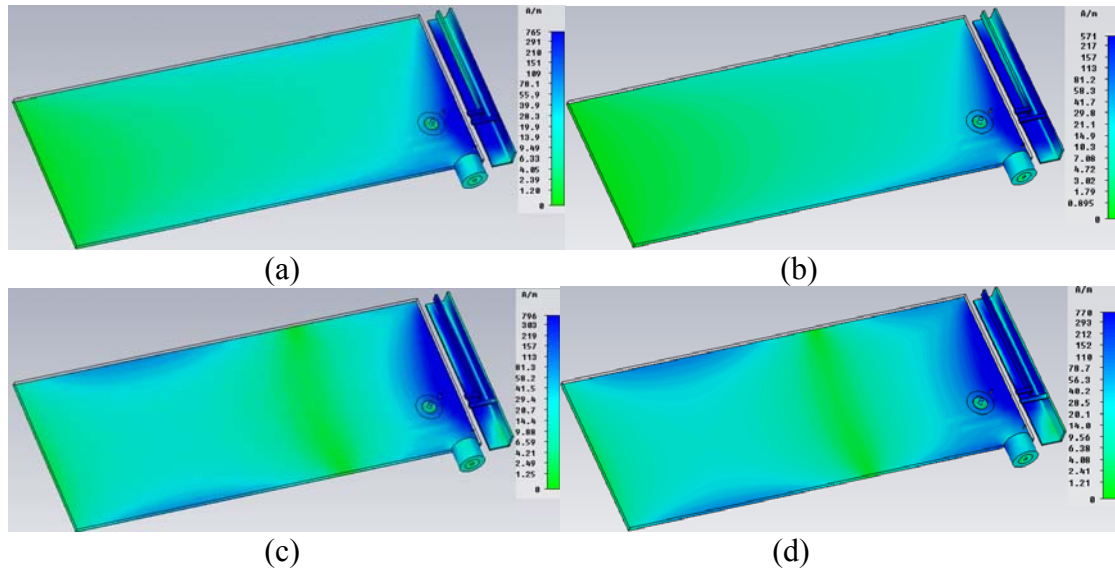
Fig. 3.11 Simulated current distribution at (a) 470 MHz; (b) 923 MHz; (c) 1895 MHz and (d) 2109 MHz.

3.2.6. Gain and Efficiency

Table 3.6 gives the measured realized gain and simulated radiation efficiency, total efficiency and realized gain for the antenna when operating in the narrowband mode, at a selection of different frequencies. These antennas were designed to operate at 470 MHz (port 1 at mode 1), 923 MHz (port 1 at mode 0), 1895 MHz (port 2 at mode 1) and 2109 MHz (port 2 at mode 0), respectively. The value of capacitor for each case was 11 pF, 4.3 pF, 1.5 pF and 0.8 pF, respectively. The radiation efficiency indicates the dielectric, metal and matching component loss. The total efficiency also includes the loss due to mismatch. It can be seen that the radiation efficiency is low at -8.91 dB at the lowest frequency, due to the antenna being electrically small, but increases at higher frequencies. This is reflected in the realized gain, and the measured value is

above 0.33 dBi above 923 MHz. The realized gain, obtained through simulation and measurement, differ up to 1.01 dB. The effect of different s2p files of the fixed capacitors used in simulation and the varactors used in measurement helps to explain the differences described above.

Port	Simulated				Measured
	Frequency [MHz]	Radiation Efficiency [dB]	Total Efficiency [dB]	Realized Gain [dBi]	Realized Gain [dBi]
1	470	-8.91	-10.25	-8.15	-7.26
2	1895	-0.79	-1.51	3.38	4.39
1	923	-0.91	-1.27	0.77	0.33
2	2109	-0.04	-0.11	4.64	4.26

Table 3.6 Simulated efficiency, simulated and measured realized gain for the chassis-antenna in narrowband mode of operation. (Simulated and measured realized gain were in the peak direction)

3.3. Wideband Mode

3.3.1. Matching Circuit Design

In the wideband mode, fixed matching circuits and switches are used, as shown in Fig. 3.12. The circuits are detailed in Table 3.7. When the circuits M_1^{W1} to M_1^{W4} are selected, the other port is left open circuit. When the circuit M_1^{W5} is selected, M_2^{W1} is used, and for M_1^{W6}, M_2^{W2} is used. The states related to M_1^{W1}, M_1^{W2} and M_1^{W3} correspond to Sub Bands 1, 2 and 3 respectively of the DVB-H band.
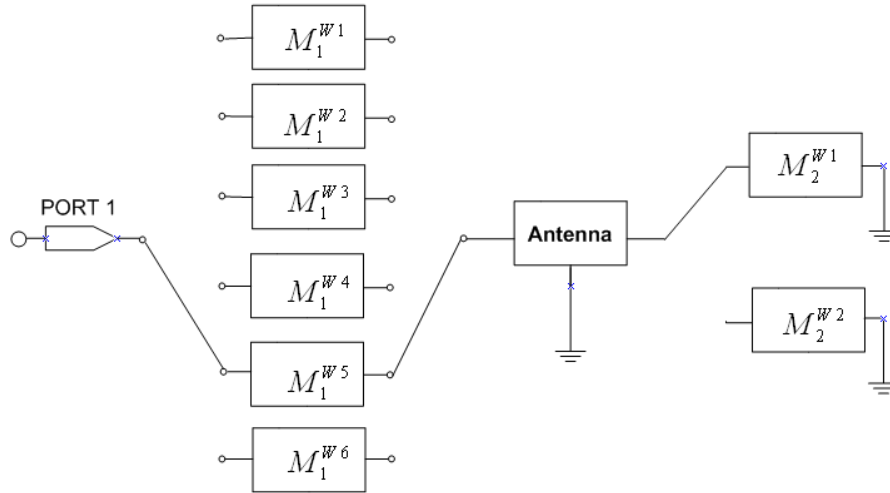
Fig. 3.12 High-level view of matching circuit in wideband mode (Switches are set for State 5)

Names	Circuit Types & Values
M_1^{W1}	0.95 pF, 100 nH, 54.85 nH, 11.48 nH
M_1^{W2}	1.02 pF, 67.52 nH, 36.66 nH, 11.71 nH
M_1^{W3}	1.57 pF, 21.09 nH, 19.97 nH, 10.39 nH
M_1^{W4}	6.74 nH, 4.586 nH, 4.71 pF
M_1^{W5}	10 pF, 3.88 pF, 2.27 nH
M_1^{W6}	1.39 nH, 5.18 nH, 0.33 pF
M_2^{W1}	11.9 nH
M_2^{W2}	0.57 pF

Table 3.7 Details of matching circuit required for each operating state in wideband mode

- 79 -

3.3.2. Simulation and Measurement Results

Six antennas, incorporating hard wired switches, were fabricated and measured. In the simulations full models of the matching components from the component vendor's library were used. In this study, the effect of using realistic microwave switches is not considered.

Figs. 3.13 and 3.14 show measured and simulated reflection coefficients. From Fig. 3.13, it can be seen that the measured reflection coefficient (solid line) for the three sub-bands (i.e. state 1, 2 and 3) are not always below -6 dB or -3 dB. Fortunately the reflection coefficient for a DVB-H antenna is not too critical rather it is the realized gain, presented in the next section, which must be met. The measured reflection coefficient, shown in Fig. 3.14, shows that the other three states have a close to 6 dB return loss bandwidth in the range from 853 MHz to 2860 MHz.

From Fig. 3.13, it can be seen that, the simulations had better reflection coefficient (dash line), at least 3 dB, through the three DVB-H sub-bands. Fig. 3.14 shows the simulated return loss (dash line) performance for the other three operating "States". In State 4, the antenna has 6 dB return loss bandwidth of the antenna has lower and upper cut-off frequencies of 827 MHz and 1529 MHz (i.e. a bandwidth of approximately 60%). In State 5, the bandwidth is close to 29% and ranges from 1527 MHz to 2046 MHz. In State 6, the antenna has 6 dB return loss bandwidth is approximately to 43% and ranges from 1888 MHz to 2918 MHz. In general agreement between measurement and simulation is not as good as in the narrowband mode, particularly at the lower frequencies. In the wideband mode, the resonant frequencies are dependent on the external matching circuit and sensitive to the value

of components, especially for low frequencies. Minimising the manufacture tolerance and improving the modelling structure would help to reduce discrepancy.
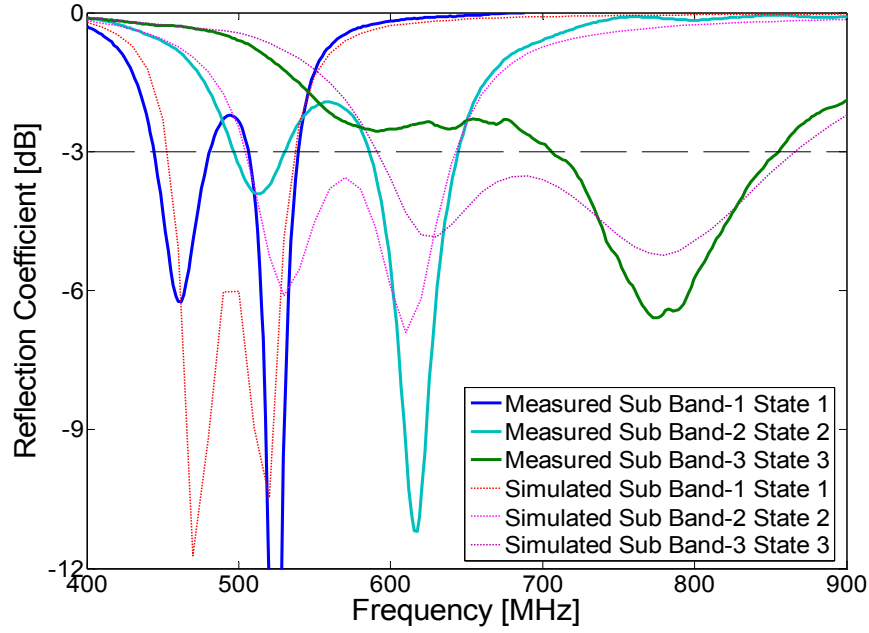
Fig. 3.13 Measured (solid line) and simulated (dash line) reflection coefficient for the DVB-H wideband operating mode. (Sub Band-1 State 1 $= M_1^{W1}$; Sub Band-2 State 2 $= M_1^{W2}$; Sub Band-3 State 3 $= M_1^{W3}$)
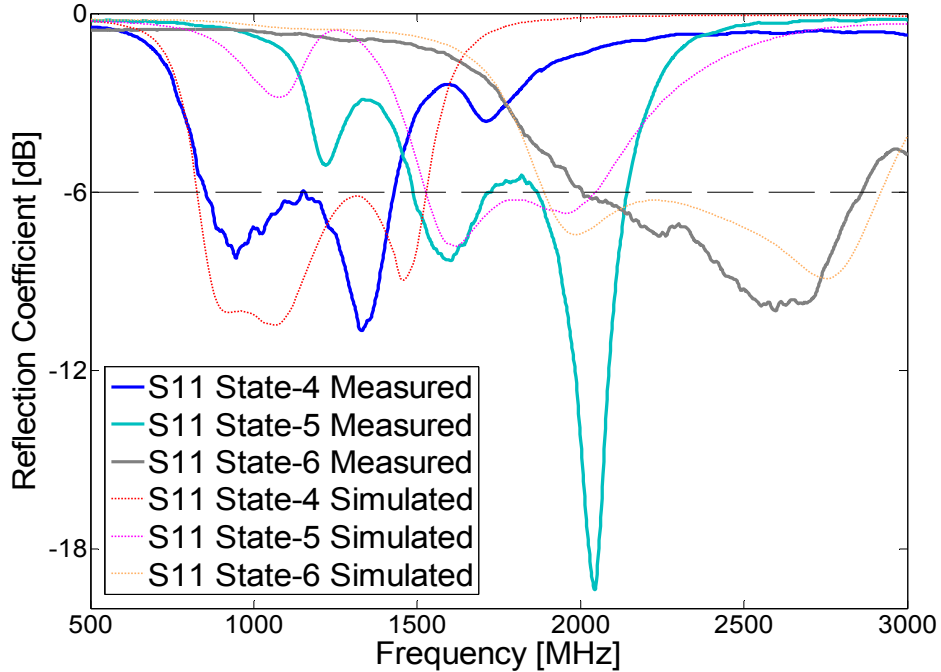
Fig. 3.14 Measured (solid line) and simulated (dash line) reflection coefficient for wideband operating states 4, 5 and 6 operation.

(State-4 $= M_1^{W4}$; State-5 $= M_1^{W5} + M_2^{W1}$; State-6 $= M_1^{W6} + M_2^{W2}$)

3.3.3. Radiation Patterns

Fig. 3.15 shows the measured radiation patterns at 470 MHz, 620 MHz, 730 MHz, 1120 MHz, 1800 MHz and 2475 MHz for the prototype antennas operating in the wideband mode. In the figure, the E_θ and E_Φ components are shown in Z-Y and Z-X plane respectively. It can be seen that the E_θ and E_Φ components for both 470 MHz and 1800 MHz, as shown in Fig. 3.15, have similar shape compared to the ones for 470 MHz and 1895 MHz in narrow band mode, as shown in Fig. 3.10. Results show that there is no significant nulls in Z-X plane within the operating frequencies and suggest that this type of chassis-antenna is a good candidate for mobile phone application.
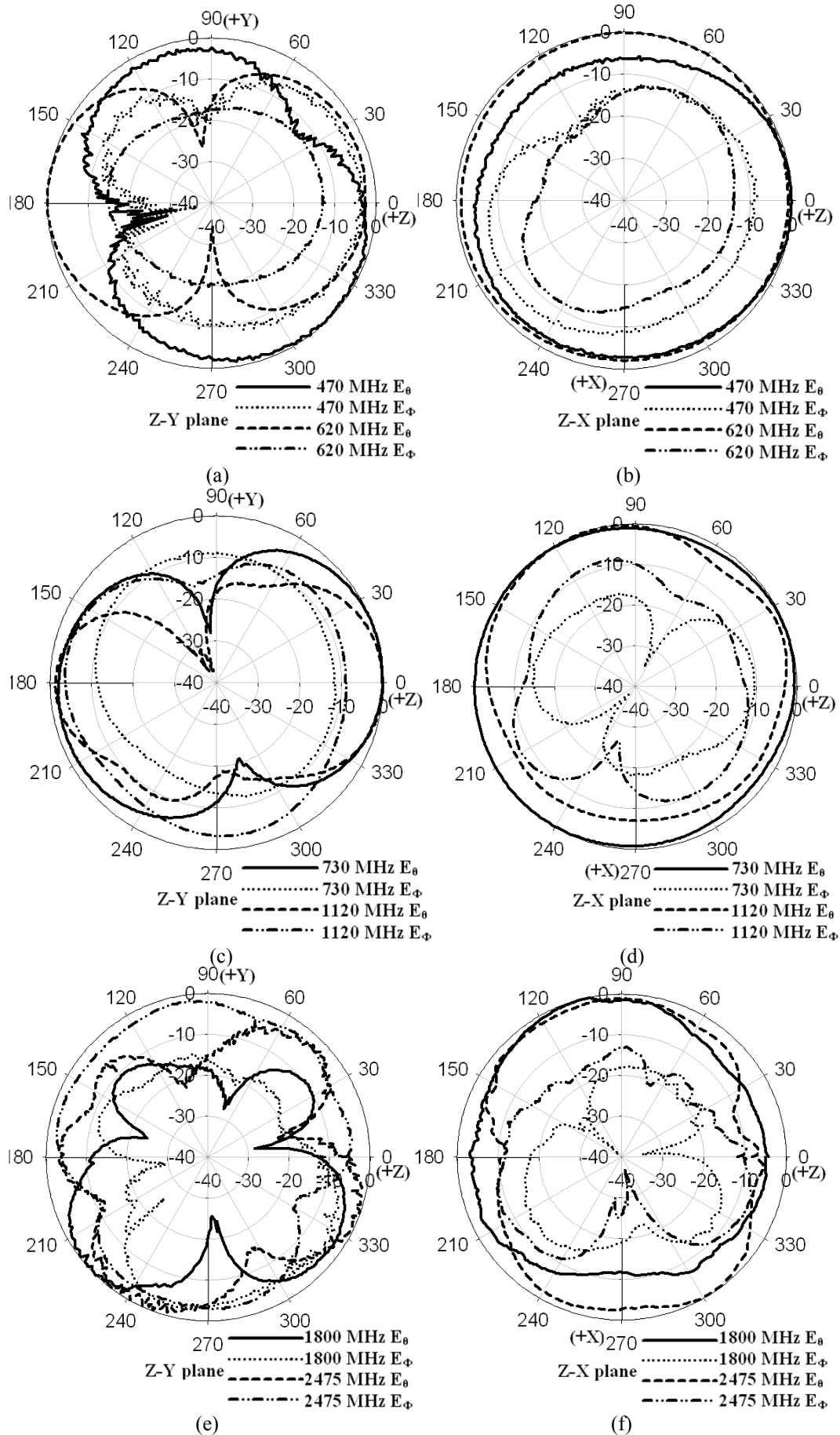
Fig. 3.15 Measured radiation patterns for (a) Z-Y plane at 470 MHz and 620 MHz; (b) Z-X plane at 470 MHz and 620 MHz; (c) Z-Y plane at 730 MHz and 1120 MHz; (d) Z-X plane at 730 MHz and 1120 MHz; (e) Z-Y plane at 1800 MHz and 2475 MHz; (f) Z-X plane at 1800 MHz and 2475 MHz

3.3.4. Gain and Efficiency

Fig. 3.16 shows the measured and simulated realized gain together with the specification for DVB-H. Measured results suggest that the realized gain is more than 1.5 dB (solid line) better than required. The realized gain depicted in Fig. 3.16 was measured in the –X direction, shown in Fig. 3.1. Although the measured realized gain for prototype met the specification of DVB-H, there are some differences between measurements and simulations. Particularly at around 610 MHz and 850 MHz, there is about 3 to 6 dB in difference. In order to minimise the discrepancy and achieve a better agreement, both reducing the manufacture tolerance and improving the modelling structure are needs.
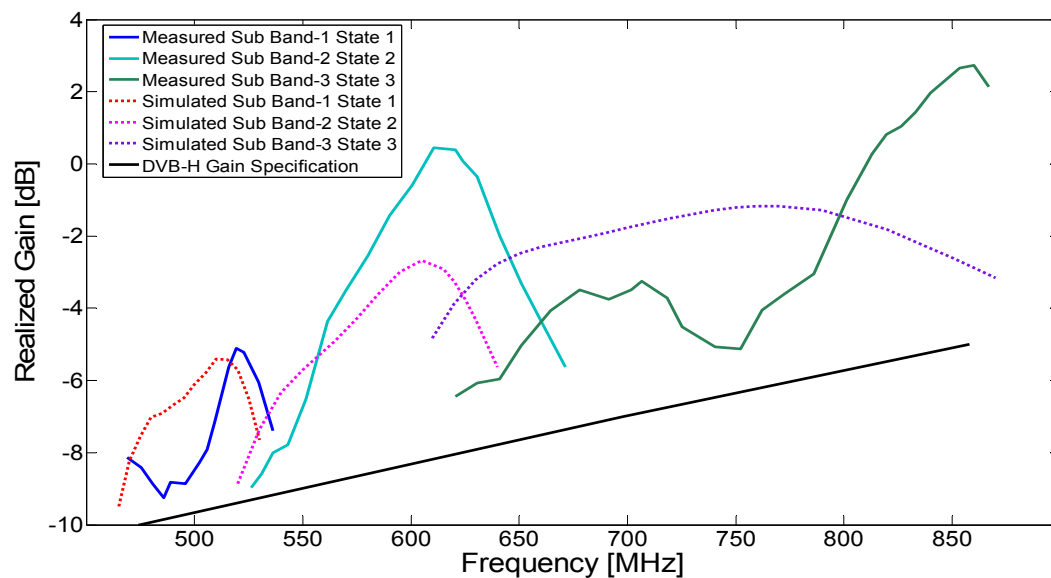
Fig. 3.16 Measured and simulated realized gain in wideband mode for DVB-H band, with realized gain specification [9]
(Both the measured and simulated realized gain were calculated in the –X direction)

Fig. 3.17 shows the measured and simulated realized gain under wideband operating states 4, 5 and 6. From Fig. 3.17, it is clear that the simulated realized gain (dash line) is above 0.20 dB from about 827 MHz to 2918 MHz. The realized gain (solid line)

shown in Fig. 3.17 for the prototype antenna, operating in State 2, was measured in the +Z direction while the other two were measured in the –X direction. In Fig. 3.17, the measured realized gain at around 1500 MHz is a bit lower than that predicted by simulation. This may be attributable to a miss-match around that frequency range which occurred due to manufacturing tolerances. Please note that the realized gain shown in Figs. 3.16 & 3.17 is calculated from the peak direction in the Z-X plane in CST.

Table 3.8 shows the simulated radiation efficiency and total efficiency for the chassis-antenna under wideband operating State 4, 5 and 6. Dielectric losses and components parasitics were considered in the simulation studies.
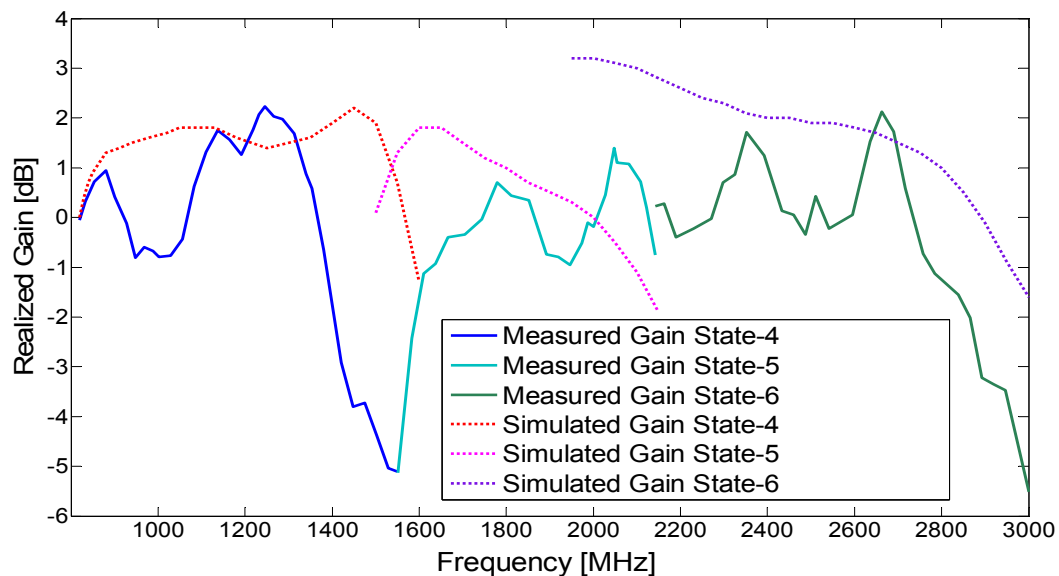
Fig. 3.17 Measured and simulated realized gain under wideband operating states 4, 5 and 6.
(Both the measured and simulated realized gain were calculated in the +Z direction for State 4 and in the –X direction for the others states)

Frequency [MHz]	Radiation Efficiency [dB]	Total Efficiency [dB]
830	-0.85	-1.99
900	-0.44	-0.87
1200	0.25	-1.05
1500	0.91	-1.66
1800	-0.29	-1.41
2150	-0.01	-1.15
2450	-0.15	-1.14
2800	-0.06	-0.75
2950	-0.27	-1.90

Table 3.8 Simulated radiation efficiency and total efficiency for the chassis-antenna under wideband operating states 4, 5 and 6

3.4. Switches and Varactor Diodes

The switches were not included in either simulation or measurement, as mentioned earlier. However, by the use of three switches (i.e. SP3T and 2×SP8T) the narrow band (two sub-circuits on port 1 and one on port 2) and wide band (six sub-circuits on port 1 and two on port 2) modes can be integrated, as shown in Fig. 3.18. For example, a single-pole three-throw (SP3T) switch from RFMD® (RF1131) would add 0.30 dB of insertion loss and a single-pole eight-throw (SP8T) switch (RF1480) would add 0.7 dB of insertion loss.

In the fabrication, varactor diodes MV31009-150A from Microsemi®, with capacitance range from 0.946 pF to 21.982 pF, were used. However, the varactor diodes with a lower capacitance limit are available from Microsemi®, though these were not available from this work. For example, diodes MV34002-150A have a range of 0.264 pF to 8.218 pF.
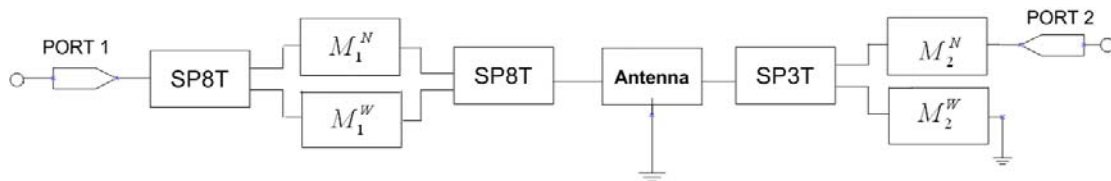
Fig. 3.18 Antenna system configuration with switches

3.5. Size of Chassis-Antenna Study

In order to examine how the size of the chassis-antenna affects the efficiency, a single port chassis-antenna is simulated with different length of ground plane (i.e. from 50 mm to 150 mm). The structure of antenna is shown in Fig. 3.19, which has a ground plane size of 100×40 mm^2 and the coupling element occupies a volumetric space of $40\times4\times7$ mm^3. The gain of chassis-antenna at 450 MHz, with ideal components and real components, are plotted together with the Harrington limit in Fig. 3.20. The first step is to simulate the antenna structure with different length of ground plane in CST Microwave Studio®. The s1p file representing the antenna response was used to optimise the matching network in Microwave Office, from Applied Wave Research. Note that same matching network as narrowband mode in the previous is used. From the Harrington-Chu limits, the maximum gain at 450 MHz for the antenna, with 40 mm width of ground plane and the length of ground plane changed from 50 mm to 150 mm, is from -2.07 dB to 3.10 dB, as shown in Fig. 3.20. The IEEE Gain of the antenna with different length (i.e. from 50 mm to 150 mm), incorporating matching circuit with ideal components (i.e. no parasitics), is a few dB below the Harrington limit (seen Fig. 3.20). It is shown that the Realized Gain of the antenna with ground size of 50×40 mm, incorporating matching circuit with real components (i.e. with parasitics loss), is very low at about -9.36 dB. Such low gain is due to the loss (i.e. heat dissipated) in the matching circuit. Fig. 3.20 shows that the efficiency increases with increasing size.
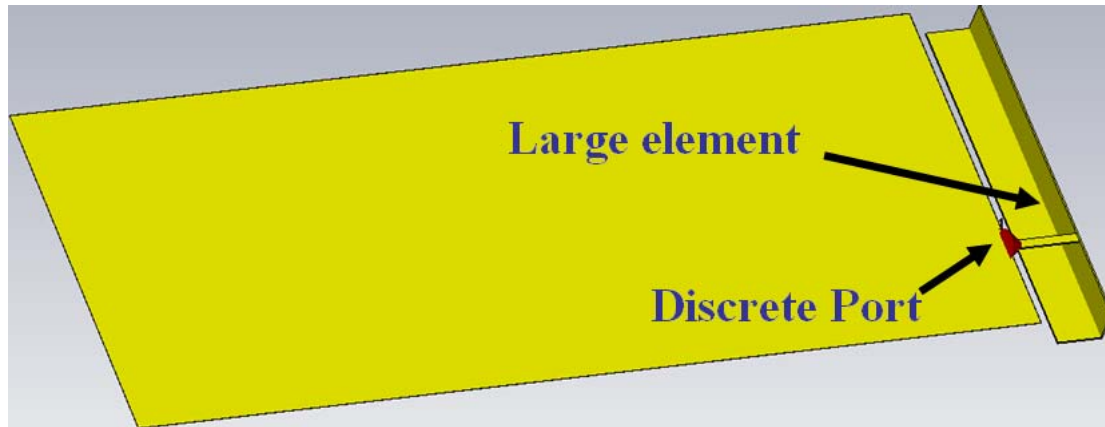
Fig. 3.19 The structure of single port chassis antenna with ground plane 100×40 mm^2
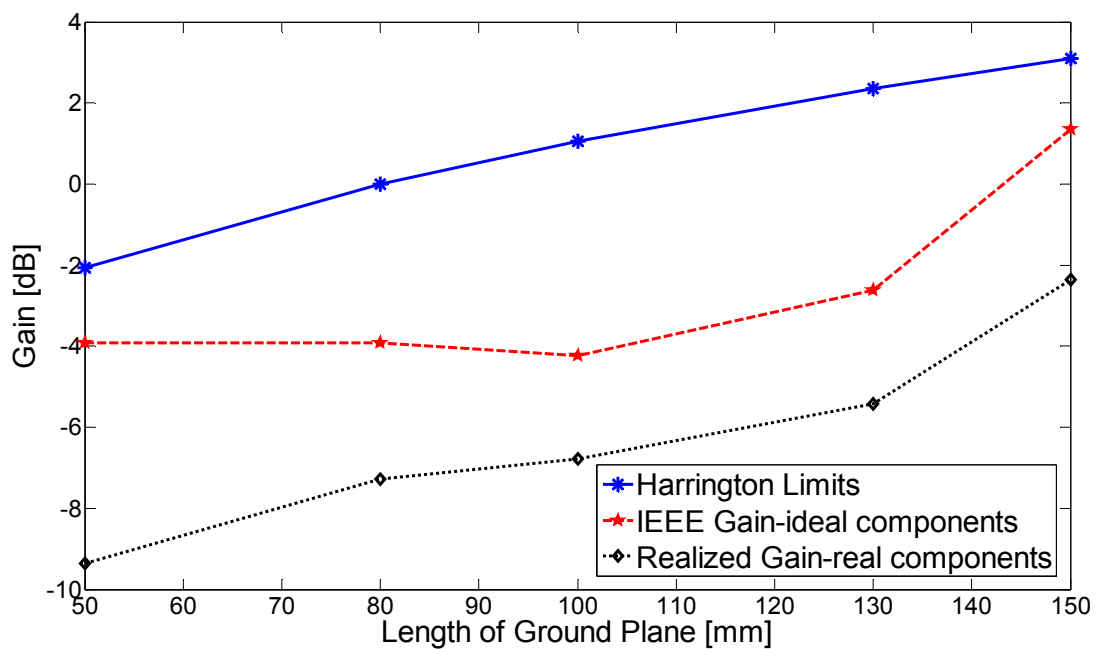
Fig. 3.20 Gain vs. length of ground plane

3.6. Components Comparison with/without Varactors

In the literature review section, it has been shown that the antenna from IMST [10], incorporating a number of matching circuits, has the potential to cover the frequency band from 470 MHz to 3000 MHz. In order to have a fair comparison, a single port chassis-antenna, as shown in Fig. 3.19, was simulated. Simulation shows that

operating from 470 MHz to 3000 MHz, two matching circuits, each circuit incorporating a varactor, are required. Table 3.9 shows the component count for the chassis-antenna in IMST and the single port chassis-antenna incorporating varactors. From Table 3.9, it can be seen that in order to cover DVB-H (470 – 862 MHz), GSM (824 – 960 MHz and 1710 – 1990 MHz), UMTS (1920 – 2170 MHz) and WLAN (2400 MHz), 19 components including 2 switches are needed for chassis-antenna incorporating 5 matching circuits. 8 components including 2 switches are needed for chassis-antenna incorporating two matching circuits (each matching circuit incorporates a single varactor diode). Fig. 3.21 shows that in order to cover from 470 MHz to 2760 MHz, 10 extra matching circuits are required for the IMST chassis-antenna, which will introduce a total of 45 components plus a number of switches, as shown in Table 3.10. However, by incorporating two matching circuits (i.e. two varactors), only 8 components are required. Thus, there is a trade-off to be made between the non-linearity and the number of components. It can be concluded that for wider band operation, more components are needed for the antenna only with matching circuits and switches, thus more cost and more space is need.
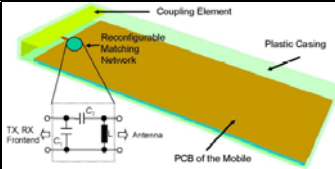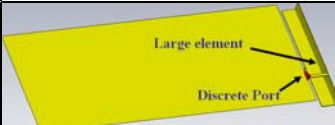
Cover DVB-H, GSM, UMTS and WLAN				
Antenna Structure	Ref	Number components of each matching circuits	Matching circuits to cover required bands	Total components (including 2 switches)
	10	3	5	19
	This Chapter	3	2	8

Table 3.9 Components count for the antennas to cover DVB-H (470 – 862 MHz), GSM (824 – 960 MHz and 1710 – 1990 MHz), UMTS (1920 – 2170 MHz) and WLAN (2400 MHz)
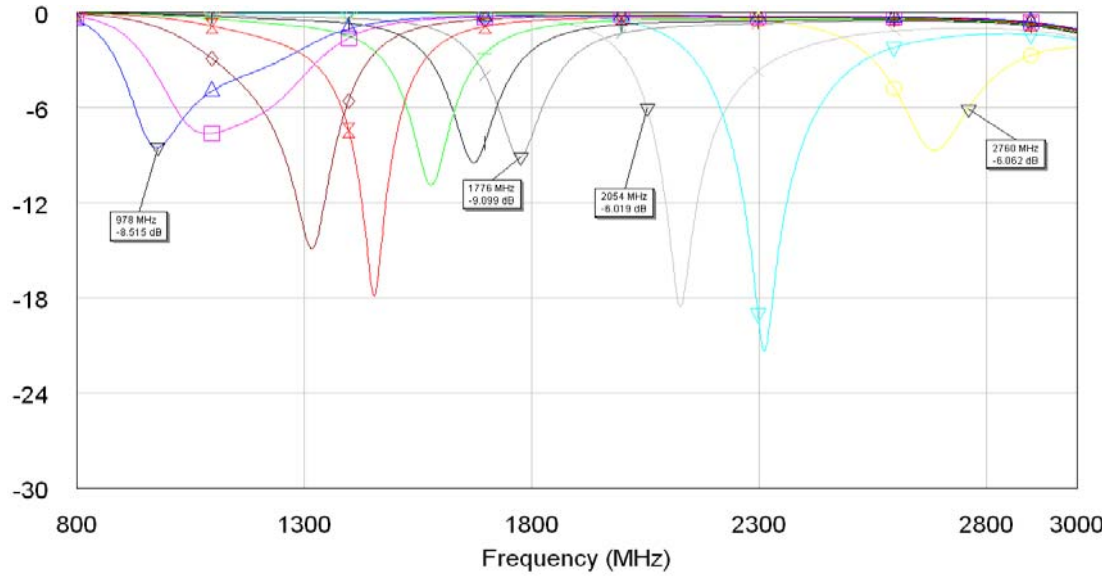
Fig. 3.21 Simulated reflection coefficient for the IMST chassis-antenna incorporating numbers of matching circuits to cover the rest bands from 470 MHz to 2760 MHz

Fully cover from 470 MHz to 2760 MHz				
Antenna Structure	Ref	Number components of each matching circuits	Matching circuits to cover required bands	Total components (including switches)
	10	3	5+10	45+switches
	This Chapter	3	2	8

Table 3.10 Components count for the antennas to cover from 470 MHz to 2760 MHz

3.7. Equivalent Circuit Modelling for Chassis-Antenna

3.7.1. Equivalent Circuit of Chassis-Antenna with One Port

The performance of a chassis-antenna incorporating a single coupling element has been carefully analysed in recent literature, [8]. This reference has thus been widely used as reference for chassis type antenna studies. Near the resonant frequency, it is well known that the impedance behaviour of an open-circuited or a short-circuited microstrip patch antenna (i.e. a PIFA) can be modelled as a parallel resonant circuit

[11-12]. For this reason, in Ref [8], the authors used a parallel resonator to represent the coupling element and a series resonator to represent the handset chassis. The equivalent circuit for a chassis-antenna must incorporate both a parallel and a series resonator. The reflection coefficient for the equivalent circuit proposed in Ref [8] agrees well with that of the antenna. However, when visualising the locus of the input impedance for the equivalent circuit on the Smith Chart, it was shown that it behaves differently from that of the antenna. In the chassis-antenna, the coupling elements are located at the edge as shown in Fig. 3.22, for this reason, it is found that the structure of the equivalent circuit should be modified as shown in Fig. 3.23. The locus of the input impedance for the new equivalent circuit [13], proposed here, agrees better with that of the chassis-antenna.
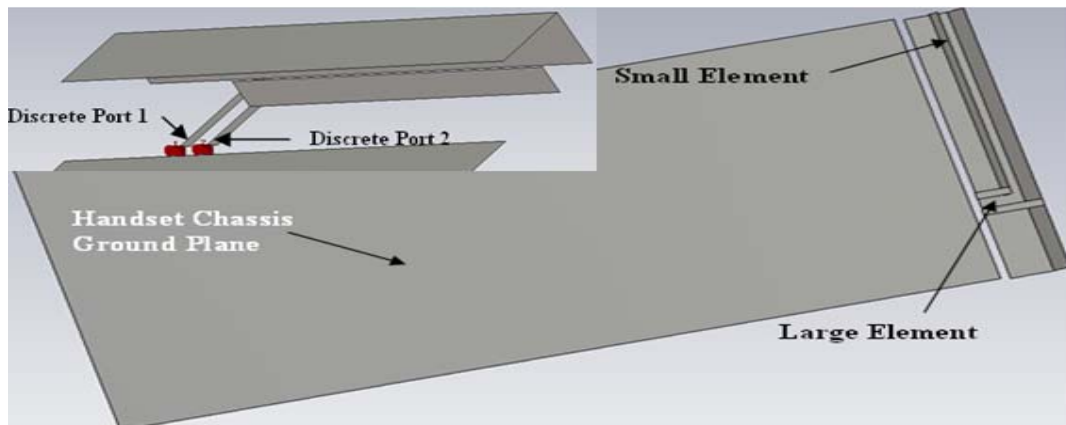
Fig. 3.22 The structure of the chassis-antenna with two coupling elements
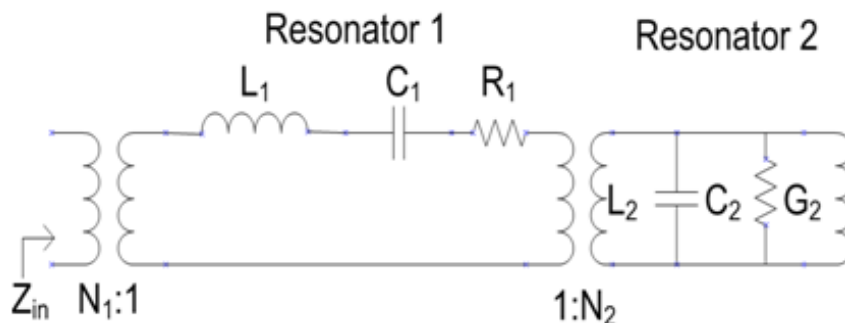
Fig. 3.23 New equivalent circuit model for the chassis-antenna with single coupling element (i.e. the structure example in Fig. 3.22 minus the small coupling element)

The first step in the process of deriving an improved equivalent circuit was to simulate a chassis antenna incorporating a single coupling element (i.e. the structure shown in Fig. 3.22 minus the small coupling element). The ground plane size was 100×40 mm^2 and the single coupling element occupies a volumetric space of $40 \times 4 \times 7$ mm^3. The new equivalent circuit, for this structure, is shown in Fig. 3.23. In this figure resonator 1 represents the coupling elements and resonator 2 represents the chassis. The input impedance Z_{in} of the circuit model in Fig. 3.23 is

$$Z_{in} = N_1^2 \left(R_1 + j\omega L_1 + \frac{1}{j\omega C_1} + \frac{1}{N_2^2 \left(G_2 + \frac{1}{j\omega L_2} + j\omega C_2 \right)} \right) \tag{3.1}$$

The first ideal transformer in the model represents the coupling between the feed line and the coupling element. The second transformer represents the coupling between the coupling element and the phone chassis. Both the coupling coefficients, i.e. N_1^2 and N_2^2, increase as the coupling gets stronger. Figs. 3.24 (a) and (b) show the return loss and the input impedance locus for a chassis-antenna incorporating one coupling element. These figures also shown the results obtained using the new equivalent circuit. The values of the components within each circuit were adjusted within the Advanced Design System (ADS) environment, in order to optimize the impedance behaviour. There is good agreement between the full-wave simulation results for the antenna and those derived using the equivalent circuit model. All of full-wave antenna simulations described in this paper were performed using the transient solver in CST Microwave Studio®. The circuit simulations were performed using Advanced Design Studio, as mentioned earlier.

(a)	(b)
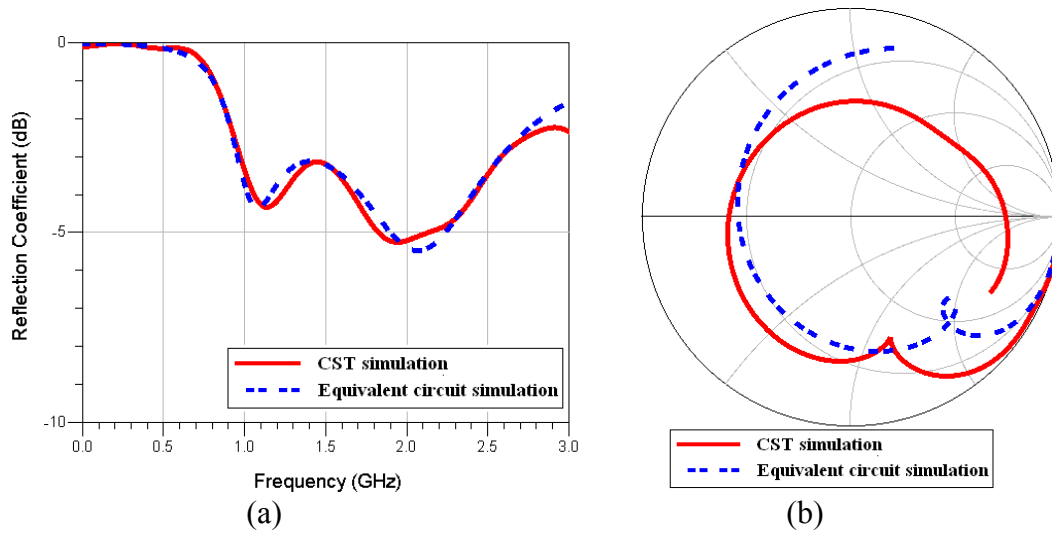
Fig. 3.24 Reflection coefficients for both the chassis-antenna with single element and the equivalent circuit model, as shown in Fig. 3.23, (a) in the Cartesian coordinate system and (b) on the Smith Chart

3.7.2. Equivalent Circuit of A Two-Port Chassis-Antenna

Fig. 3.22 shows a chassis-antenna incorporating a pair of coupling elements. The antenna has a ground plane size of 100×40 mm^2. The coupling elements occupy a very small volumetric space of $40 \times 4 \times 7$ mm^3, as mentioned earlier. The coupling element excites a resonant mode within the handset chassis, as mentioned in Ref [8]. For this reason it is possible to excite two separate resonant modes within the handset chassis by using a pair of coupling elements. If the two coupling elements are located on opposite sides of the handset chassis, as shown in Fig. 3.25, the circuit can simply be modelled as shown in Fig. 3.26 [13]. In this scenario the chassis resonators are seen to behave like a pair of parallel resonant circuits, having slightly different resonant frequencies. The result is a pair of resonances in the input impedance curves.
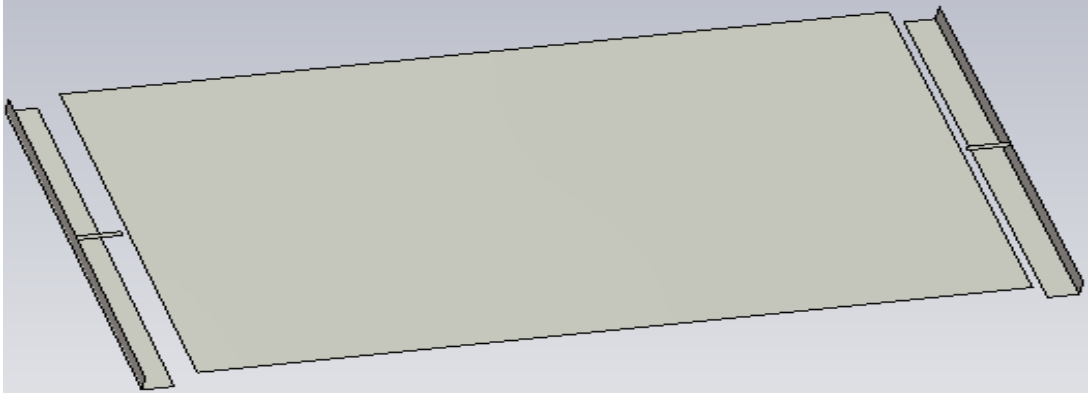
Fig. 3.25 Structure of the chassis-antenna with two elements on the opposite side of chassis
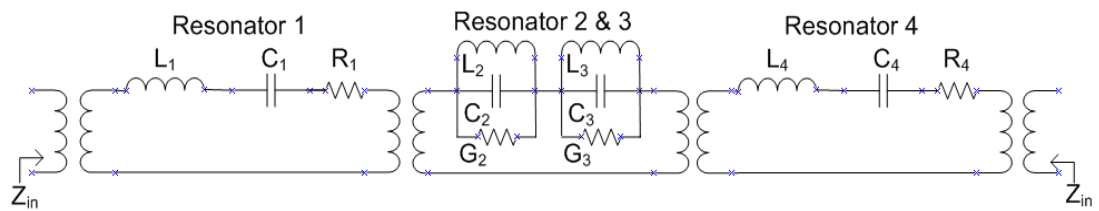
Fig. 3.26 Equivalent circuit model for the chassis-antenna with two elements on the opposite side of chassis, as shown in Fig. 3.25

However, when the two coupling elements are located close to one other, as shown in Fig. 3.22, there is strong coupling between them. Experiment results showed that such strong coupling was complex and cannot be represented by an ideal transformer. In order to represent the coupling between two elements, an impedance inverter, with $\pm 90°$ phase shift, is needed [14], as illustrated in Fig. 3.27.
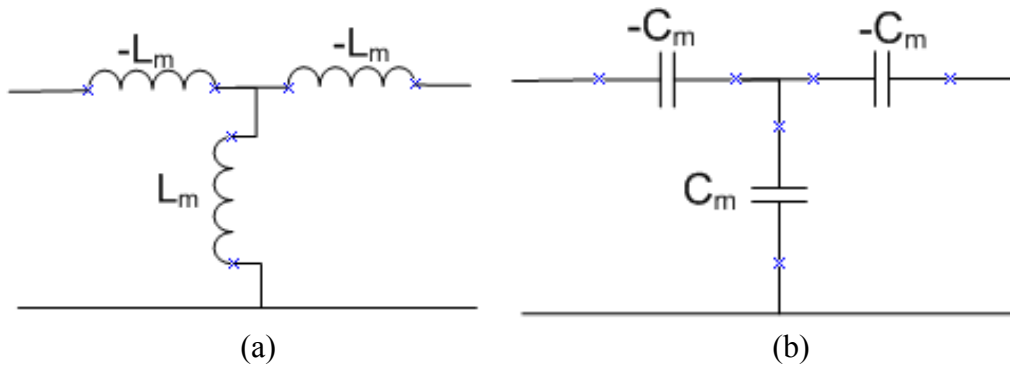
(a)   (b)
Fig. 3.27 An impedance inverter with lumped (a) inductors (L_m) or (b) capacitors (C_m)

In this case an impedance inverter incorporating lumped inductors has been selected to model the equivalent circuit, as shown in Fig. 3.28. In the dual-port chassis-antenna there is strong coupling between the two coupling elements. For this reason the radiation resistance of each element changes as current distribution changes. It is thus necessary to adjust all of the values of the components in the equivalent circuit for the coupling element in order to optimize the impedance behaviour. In Fig. 3.28, resonators 1 and 4 represent the two coupling elements. Resonators 2 and 3 represent resonant modes which are excited with in the handset chassis [4 and 13].
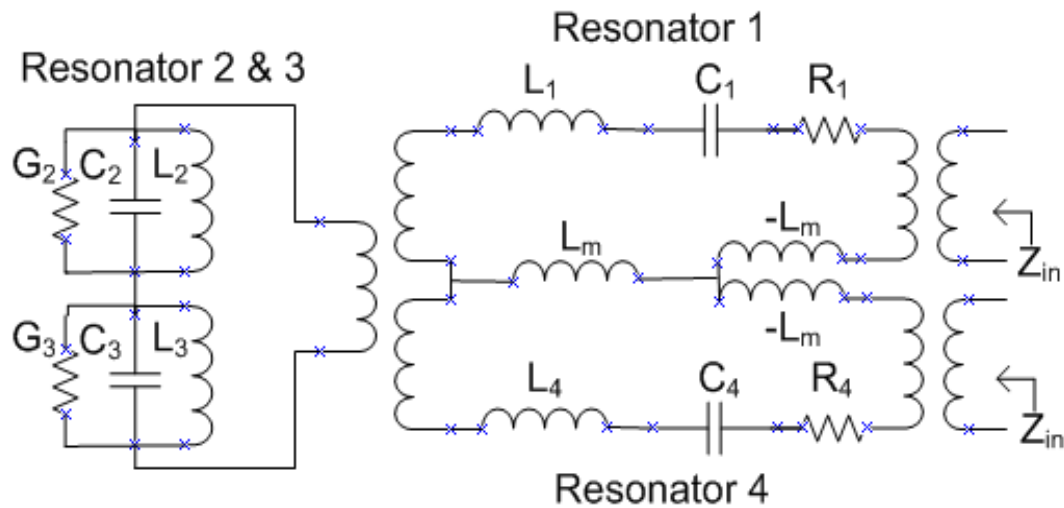
Fig. 3.28 Equivalent circuit model for chassis-antenna with two coupling elements on the same side of chassis

The simulation results obtained using the equivalent circuit are shown in Fig. 3.29. Fig. 3.29(a) shows the reflection coefficient of the larger coupling element which is excited by means of port 1. Fig. 3.29(b) shows the input impedance at port 1, on the Smith chart. Fig. 3.29(c) shows the reflection coefficient of the small coupling element which is excited by means of port 2. Fig. 3.29(d) shows the input impedance at port 2, on the Smith chart.
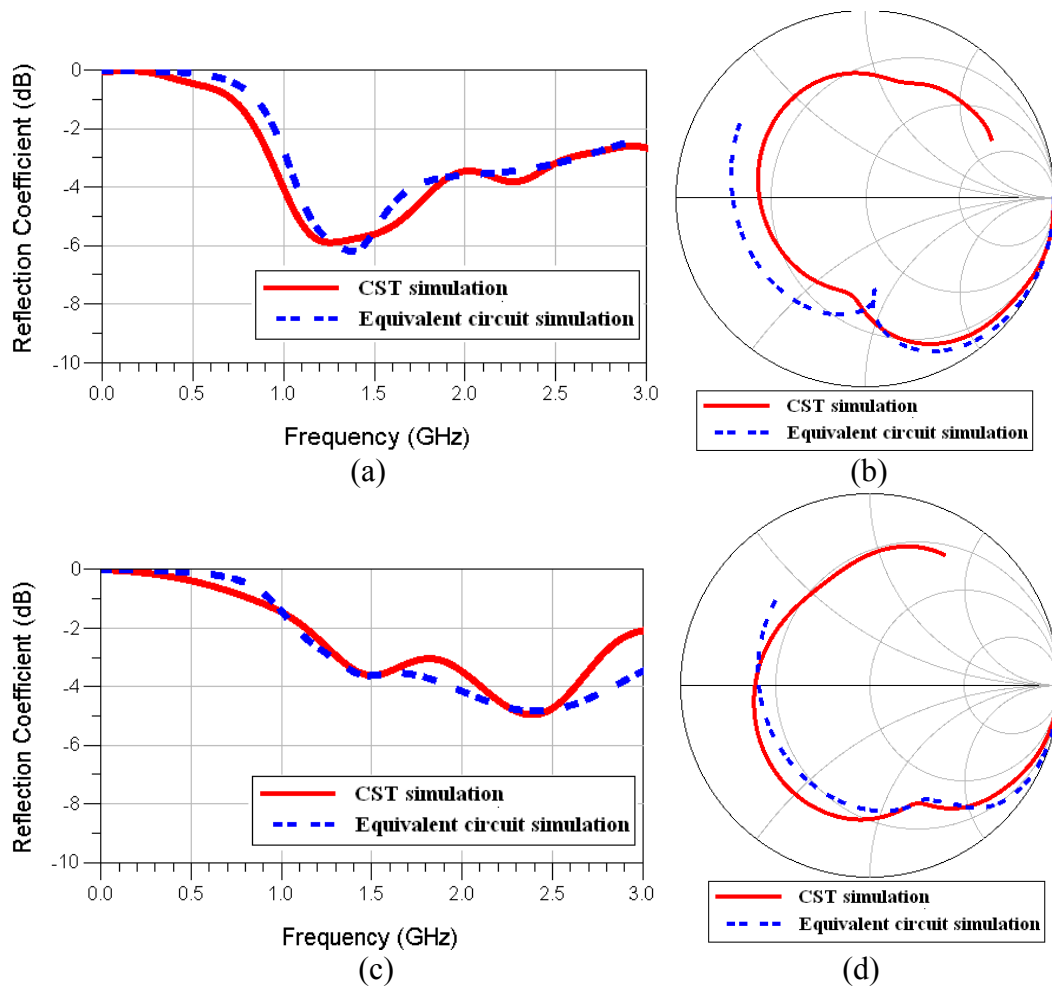
Fig. 3.29 Reflection coefficients for both the chassis-antenna with two coupling elements and the equivalent circuit model as shown in Fig. 3.28 respectively (a) for large antenna element which is excited by means of port 1 in the Cartesian coordinate system; (b) on the Smith Chart; (c) for small antenna element which is excited by means of port 2 in the Cartesian coordinate system; (d) the Smith Chart

An external matching circuit, shown in Fig. 3.30 was then connected to the equivalent circuit in order to model the matched antennas which were described earlier. Figs. 3.31 and Fig. 3.32 present the reflection coefficient and the impedance locus for each antenna element. The equivalent circuit results are compared with those obtained by applying a matching circuit to the simulation model for the antenna. Note that the large antenna element is excited by means of port 1, while the small antenna element is excited via port 2. Once again the values of the components within the matching circuit were optimized based on the antenna structure shown in Fig. 3.22. Fig. 3.31(a)

shows the return loss results for the larger antenna element (i.e. port 1). It is clear that the resonant frequency obtained using the equivalent circuit model differs by 11 MHz (and 1.4 dB) from that derived via full-wave simulation. In Fig. 3.31(b), the two curves almost perfectly overlap with each other on the Smith Chart. Fig. 3.32(a) shows the results for the small antenna element (i.e. port 2). Here the maximum deviation is 1.9 dB and 100 MHz. Although the results shown in Fig. 3.32 do not perfectly agree, they have quite similar impedance behaviour.
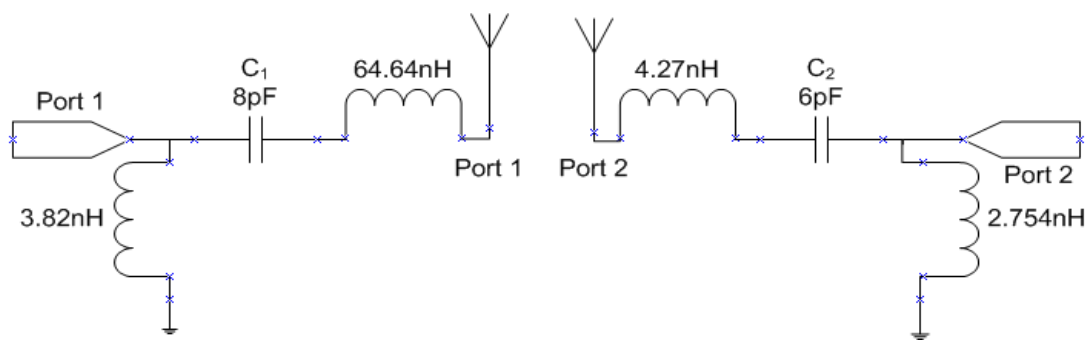
Fig. 3.30 The structure of L-network matching circuits

(a)   (b)
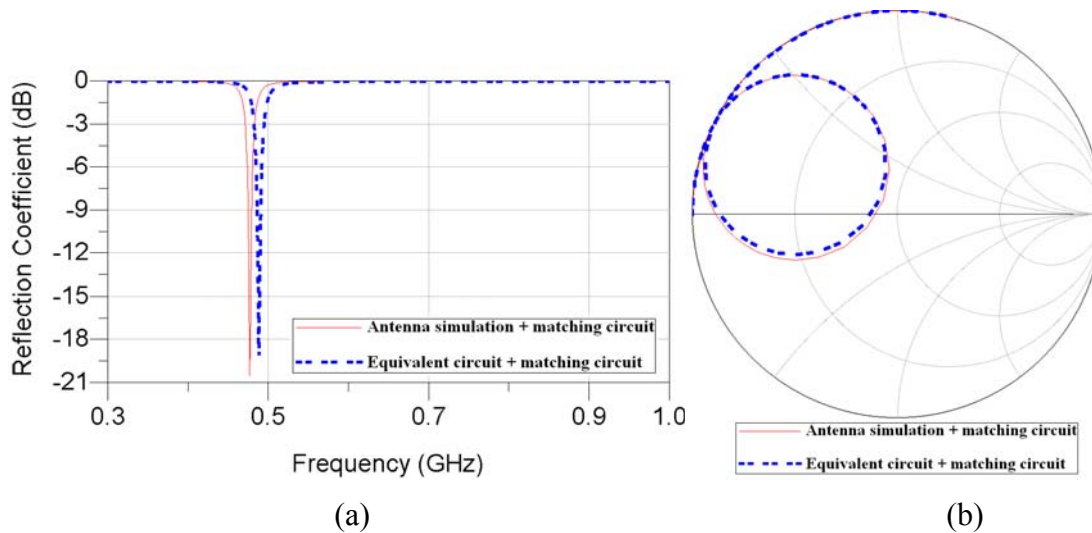
Fig. 3.31 Frequency responses of reflection coefficient obtained for the large antenna element which is excited by means of port 1 when the designed matching circuit as shown in Fig. 3.30 is connected either to the simulated antenna structure as shown in Fig. 3.22 (solid line), and to the equivalent circuit model as shown in Fig. 3.28 (dashed line) (a) in the Cartesian coordinate system; (b) on the Smith Chart
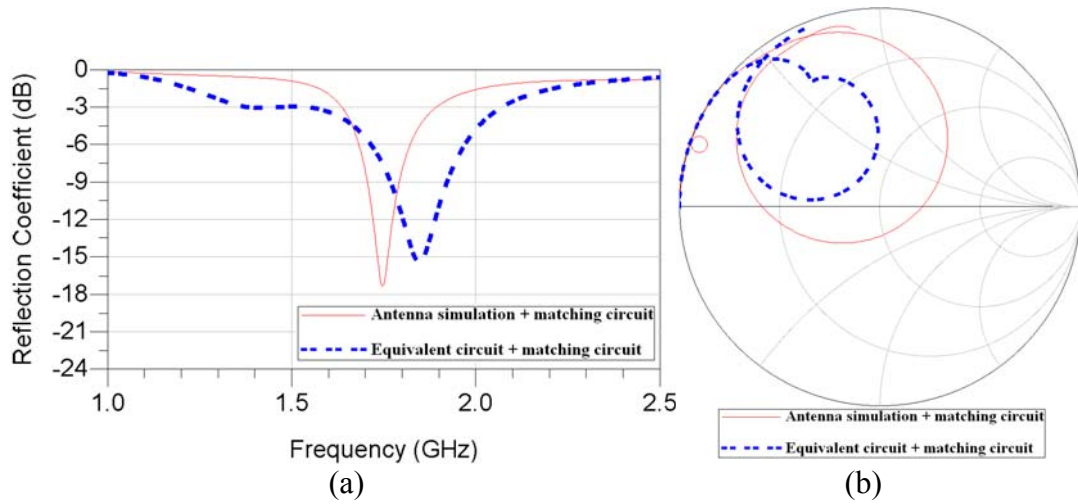
Fig. 3.32 Frequency responses of reflection coefficient obtained for the small antenna element which is excited by means of port 2 when the designed matching circuit as shown in Fig. 3.30 is connected either to the simulated antenna structure as shown in Fig. 3.22 (solid line), and to the equivalent circuit model as shown in Fig. 3.28 (dashed line) (a) in the Cartesian coordinate system; (b) on the Smith Chart

3.8.   Summary

This chapter describes the performance of a novel two port reconfigurable antenna, which can operate within a narrow band or wide band mode. In the narrowband mode, the antenna provides dual band operation with frequencies independently controlled at each port, as shown in the demonstration. Simulation shows that the antenna could potentially provide the wide tuning range from 462 MHz to over 3000 MHz when using the capacitors with range from 0.2 pF to 8 pF. However, the total tuning range of a prototype is depended on the capacitance range of varactor diodes. Studies showed that the selection of a frequency in port 1 will restrict choice in port 2, and vice versa. In the wideband mode, the antenna can operate in one of six different wideband modes in the range of 470 to 2918 MHz. Simulations using both CST and AWR show good agreement, except the DVB-H band. The measured realized gain for prototype within DVB-H met the specification, but there are some differences

between measurements and simulations. Particularly at around 610 MHz and 850 MHz, there is about 3 to 6 dB in difference. Although for a completed mobile terminal prototypes, a further optimisation is necessary; in order to minimise the discrepancy and achieve a better agreement between measurements and simulations in research's point of view, improving the modelling structure is needed. The antenna is potentially able to cover multiple wireless standards, such as the DVB-H, GSM, GPS, UMTS and WLAN bands. It has a total size of 108×40×4 mm^3, and is suitable to operate within hand held mobile devices such as mobile phones, laptops, and PDAs. The use of varactors and switches may lead to nonlinear effects, but these are beyond the scope of this research.

The size of single port chassis-antenna study shows that the efficiency is dependent on the size of the antenna. Small size of the antenna will lead to low efficiency, which is expected from Harrington-Chu limits.

The comparison the proposed antenna with the IMST antenna, which has potential to cover the similar frequency range (i.e. from 470 MHz to 2760 MHz) incorporating a large number of matching circuits and switches, shows that there is a trade-off to be made with the non-linear effects and the circuit components. For the chassis-antenna incorporates a matching circuit with a varactor, small amount of components is able to cover a wide frequency range. However, it will lead to poor linearity. If the antenna incorporating a large number of matching circuits and switches, it will lead to high cost and require more space.

The new equivalent circuit for the chassis-antenna, with a single coupling element, models the impedance of the antenna better than what was previously possible. For the chassis-antenna with two coupling elements, the equivalent circuit model becomes more complex and an impedance inverter has been used to represent the coupling between two closely separate coupling elements. The results for the proposed equivalent circuit are compared well with the antenna simulations and it provides useful insight into the operation of this chassis-antenna type combination. However, a further study needs to be continued in future to provide sufficient details to explain the coupling between the two close coupling elements.

References:

[1] C. T. P. Song, J. Kelly, and P. S. Hall, "Reconfigurable antenna", U.K. Patent application GB0918477.1. 2009.

[2] Z. H. Hu, C. T. P. Song, J. Kelly, P. S. Hall, and P. Gardner, "Wide tunable dual-band reconfigurable antenna", *Electron. Lett.*, vol. 22, Issue 22, Oct. 22 2009, pp. 1109-1110.

[3] C.T.P. Song, Z. H. Hu, J. Kelly, P. S. Hall, and, P. Gardner, "Wide Tunable Dual-Band Reconfigurable Antenna for Future Wireless Devices", *Loughborough Antenna and Propag. Conference*, Loughborough, UK, *LAPC* 2009, pp. 601-604

[4] Z. H. Hu, J. Kelly, C. T. P. Song, P. S. Hall, and P. Gardner, "A Novel Wide Tunable Dual-Band Reconfigurable Chassis-Antenna for Future Mobile Terminals", *European Conference on Antennas and Propagation 2010* on 12-16 April 2010, Barcelona, Spain.

[5]   Z. H. Hu, C. T. P. Song, J. Kelly, P. S. Hall, and P. Gardner, "A novel reconfigurable UWB chassis-antenna for future mobile terminals", *UK URSI Festival of Radio Science*, University of Birmingham, Tuesday, 15 December 2009

[6]   Z. H. Hu, C. T. P. Song, J. Kelly, P. S. Hall, and P. Gardner, "Novel Reconfigurable Dual-Port UWB Chassis-Antenna", Submitted to *2010 APS/URSI Symposium* on July 11-17, 2010, Toronto, Ontario, Canada.

[7]   Z. H. Hu, C. T. P. Song, J. Kelly, P. S. Hall, and P. Gardner, "Dual band reconfigurable chassis-antenna for small terminals", Submitted to *IEEE Antenna and Propagation Transaction*.

[8]   P. Vainikainen, J. Ollikainen, O. Kivekas, and K. Kelander, "Resonator-based analysis of the combination of mobile handset antenna and chassis", *IEEE Trans. Antennas and Propag.*, vol. 50, pp. 1433-1444, Oct. 2002.

[9]   EICTA: Mobile and Portable DVB-T Radio Access Interface Specification, version 1.0 8.3.2004.

[10]   D. Manteuffel, M. Arnold, "Considerations for reconfigurable multi-standard antennas for mobile terminals", *Antenna Technology: Small Antennas and Novel Metamaterials, 2008, iWAT 2008. International Workshop* in 2008, pp. 231-234

[11]   W. F. Richards, Y. T. Lo, and D. D. Harrison, "An improved theory for microstrip antennas and applications", *IEEE Transactions on Antennas and Propag.*, vol. AP-29, No.1, Jan. 1981, pp. 38-46.

[12]   T. Taga, *Analysis of planar inverted-F antennas and antenna design for portable radio equipment*, Chapter 5 in Analysis, Design, and Measurement of

Small and Low-Profile Antennas, K. Hirasawa and M. Haneishi, (Editors), Boston, 1992, Artech House, 270 p.

[13]   Z. H. Hu, J. Kelly, C. T. P. Song, P. S. Hall and P. Gardner, "Equivalent circuit modelling of chassis-antenna with two coupling elements", accepted by *2010 APS/URSI Symposium* on July 11-17, 2010, Toronto, Ontario, Canada.

[14]   G. Matthaei, L. Young, and E. M. T. Jones, *Microwave filters, impedance-matching networks, and coupling structures,* Mc Graw-Hill, New York, 1964, pp. 434-437.

CHAPTER IV

RECONFIGURABLE BALANCED ANTENNA AND ITS

MIMO APPLICATIONS

This chapter presents three wideband reconfigurable balanced antennas for use in current and future mobile wireless communication systems and considers its potential for reconfigurable MIMO applications. The balanced antenna is a simple dipole and using a single external matching circuit and a balun, the antenna can provide a wide tuning range.

However, the first two antennas studied experience high dissipation loss in the lumped elements in the circuit which leads to low efficiency. This problem can be solved either using low loss components (such as LTCC) or a bigger size of antenna element. Thus, a third antenna will be described. When combined with a two-port chassis-antenna, which has a wide tuning range, it becomes a reconfigurable MIMO antenna for small terminals with good isolation. To the best of my knowledge this is the first reconfigurable MIMO antenna with such a wide tuning range. This is an original concept and has been filed for two patents [1 and 2].

There are three main reasons for choosing a balanced antenna for this application:

1. It has low correlation with unbalanced antennas;

2. It has high isolation from the chassis, which reduces the user effect and the mobile terminal can be shaped quite freely;

3. Simple design with low cost.

All of the simulations presented in this chapter were performed using the transient solver in CST Microwave Studio®. The s-parameter file representing the antenna response was used as a starting point for designing the matching networks. Microwave Office was then used to adjust the value of each component to optimise the return loss performance of the antenna.

4.1. Antenna Configuration

The balanced antenna is a thin dipole. Fig. 4.1 illustrates the reconfigurable balanced antenna system configuration. It consists of a single external matching network and a balun. The matching network has two identical L-network matching circuits, which are connected to each leg, and then connected to an LC balun. Each L-network matching circuit incorporates a single varactor diode together with a bank of fixed inductors. To minimize the component count, the design of the matching network and the balun is co-optimized. The maximum capacitance for varactors was set to 10 pF, although higher upper values could have been used they give little extra tuning range. The range of capacitance for each varactor was optimized to achieve maximum tuning range. In practice, the full capacitance range might be impractical or expensive. However, it shows the antenna can potentially cover such wide frequency ranges.
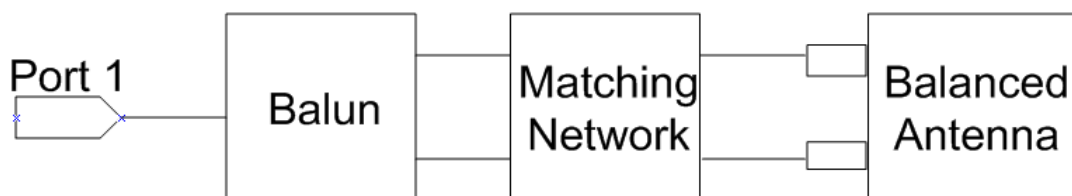
Fig. 4.1 Reconfigurable balanced antenna system configuration

4.2. Reconfigurable Balanced Antenna with Single Tunable Resonant Frequency

This section presents a small reconfigurable dipole (i.e. 40×14 mm^2), which enables a frequency tuning range from 700 MHz up to 2434 MHz with a 6 dB loss across the operating band with only 1 matching circuit [1]. For the DVB-H band or beyond 2500 MHz, additional matching circuits are required. Although it has high dissipated loss on the lumped elements in the circuit and low efficiency at low frequency such as 700 MHz, its size is suitable for MIMO applications in small terminals, for example, Watch Cell Phone.

4.2.1. Antenna Design and Structure

The balanced antenna, shown in Fig. 4.2, is 40 mm$\times$14 mm in size and has a total size of 110×40mm^2 and ground plane size of 100×40mm^2. The antenna was designed on a microwave substrate material, Taconic TLY-3-0450-C5, which has a permittivity of 2.33, loss tangent of 0.0009, a thickness of 1.143 mm, and metal thickness of 0.01778 mm. The dimensions of the balanced antenna are given in Table 4.1.
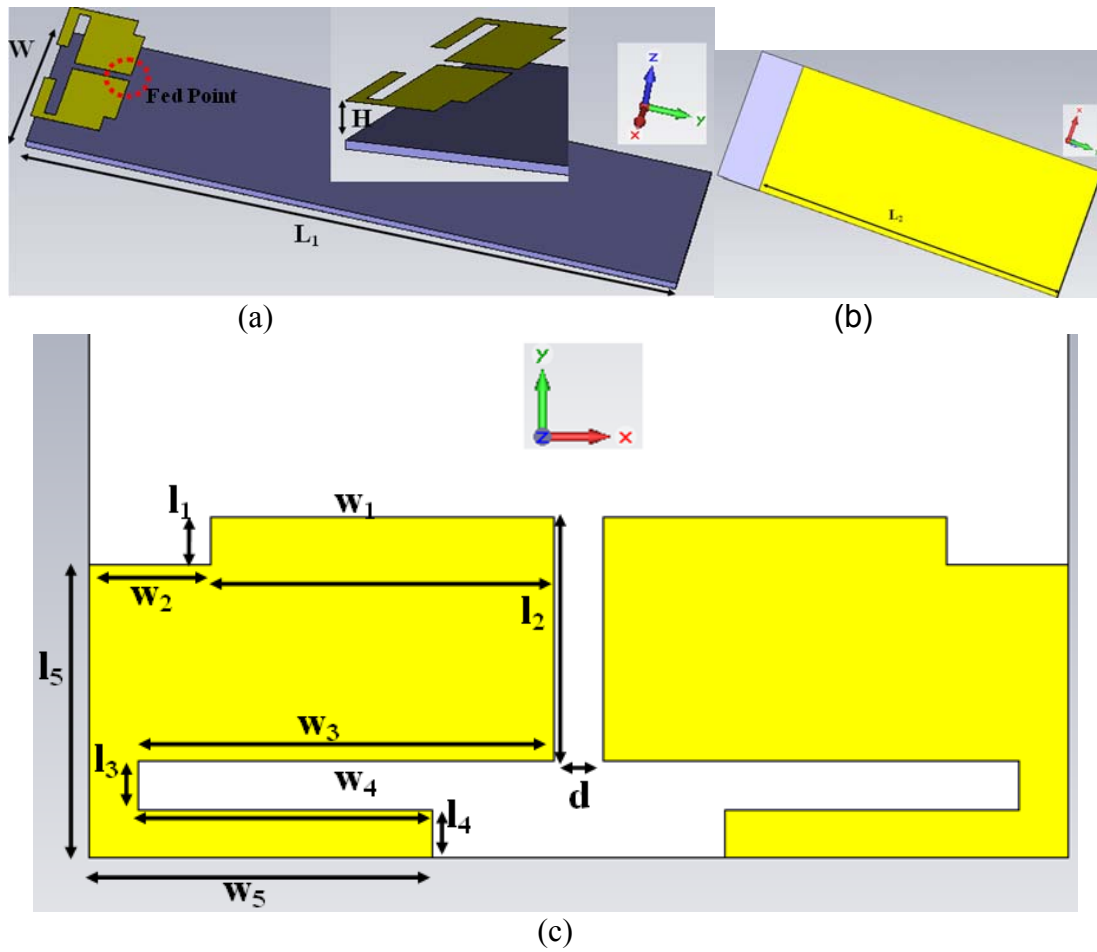
Fig. 4.2 The structure of balanced antenna with opening gap (a) front view; (b) back view; (c) overview of antenna element

H	5 mm	w_4	12mm
W	40 mm	w_5	14 mm
L_1	114 mm	l_1	2 mm
L_2	100 mm	l_2	10 mm
w_1	14 mm	l_3	2 mm
w_2	5 mm	l_4	2 mm
w_3	17 mm	l_5	12 mm

Table 4.1 Dimensions for the antenna shown in Fig. 4.2

4.2.2. Performance of the Antenna

The antenna system is shown in Fig. 4.1. By operating with the circuit schematic in Fig. 4.3, this antenna enables a frequency tuning range from 700 MHz up to 2434 MHz with a 6 dB return loss when the varactor, denoted as "C_1", is varied from 0.1 pF to 10 pF, as shown in Fig. 4.4. The other values of the circuit elements used in the matching circuit (ideal components, i.e. no parasitics) are shown in Fig. 4.3.
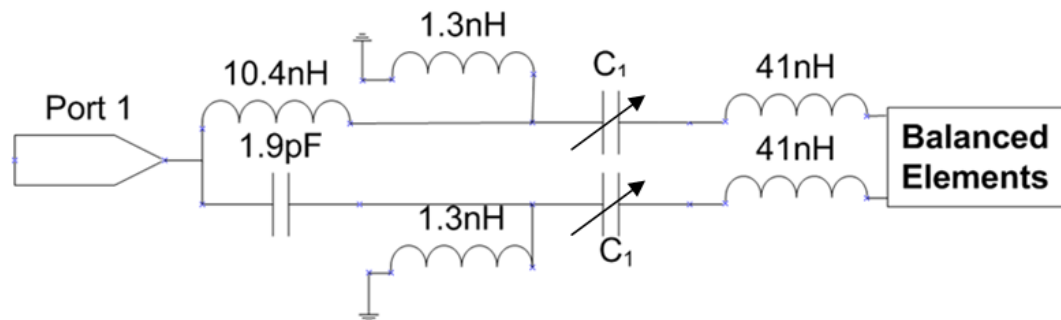
Fig. 4.3 The circuit schematic of balanced antenna as shown in Fig. 4.2
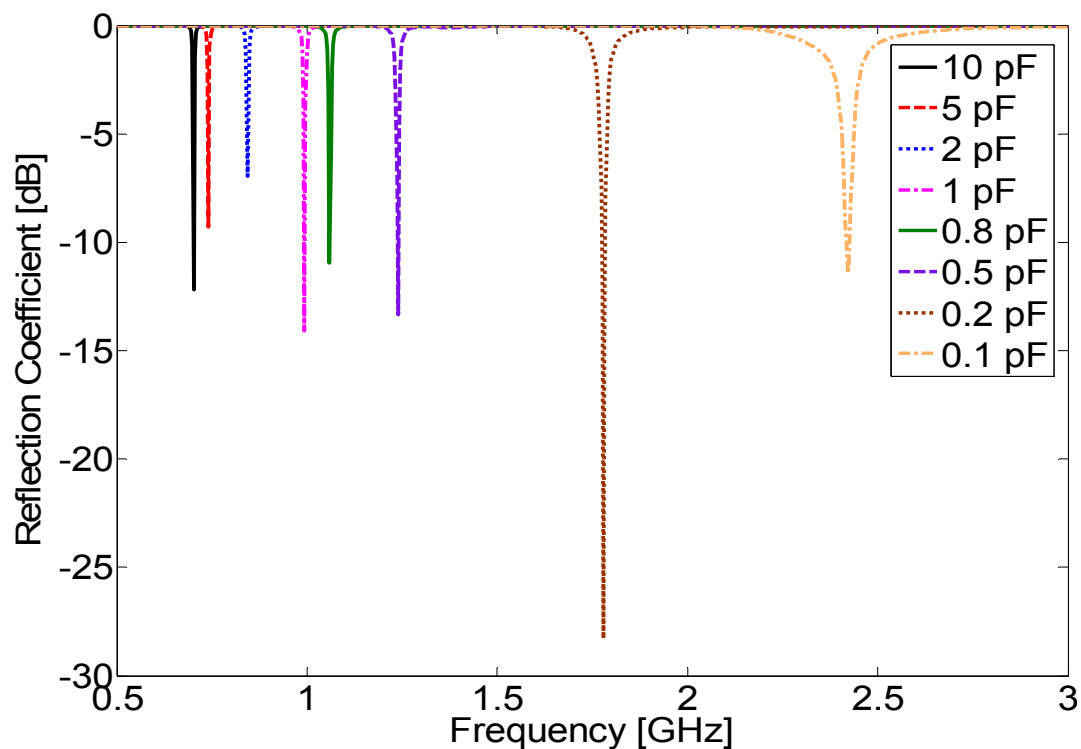
Fig. 4.4 Simulated resonant frequencies with reflection coefficient above 6 dB when the varactors C_1 vary from 10 pF to 0.1 pF.

Figs. 4.5 and 4.6 illustrate the current distribution and farfield plots for the small balanced antenna as shown in Fig. 4.2. Fig. 4.5 shows there is almost no current on the chassis. Thus the antenna is isolated from the chassis to reduce the user effect compared with conventional unbalanced antennas incorporating a chassis, such as PIFA, IFA, Monopole, Helix and etc. Due to the small effect of the chassis, it offers freedom in shaping of the mobile terminal.
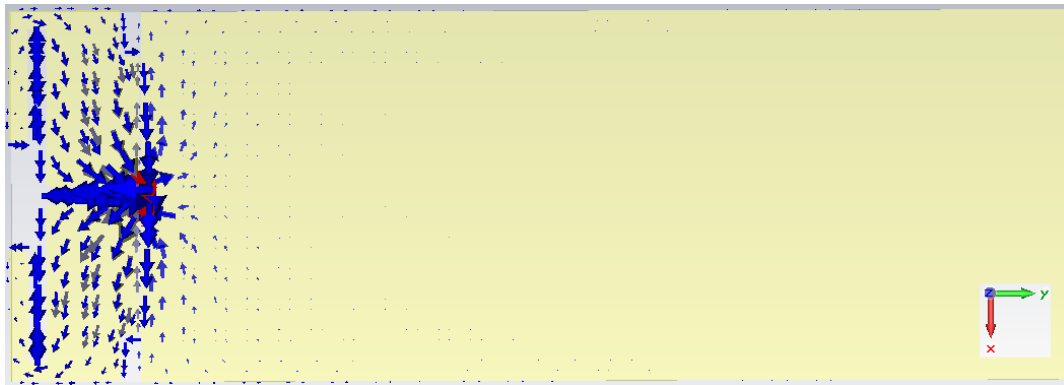
Fig. 4.5 Current distribution when driving the balanced antenna shown in Fig. 4.2

(a)   (b)
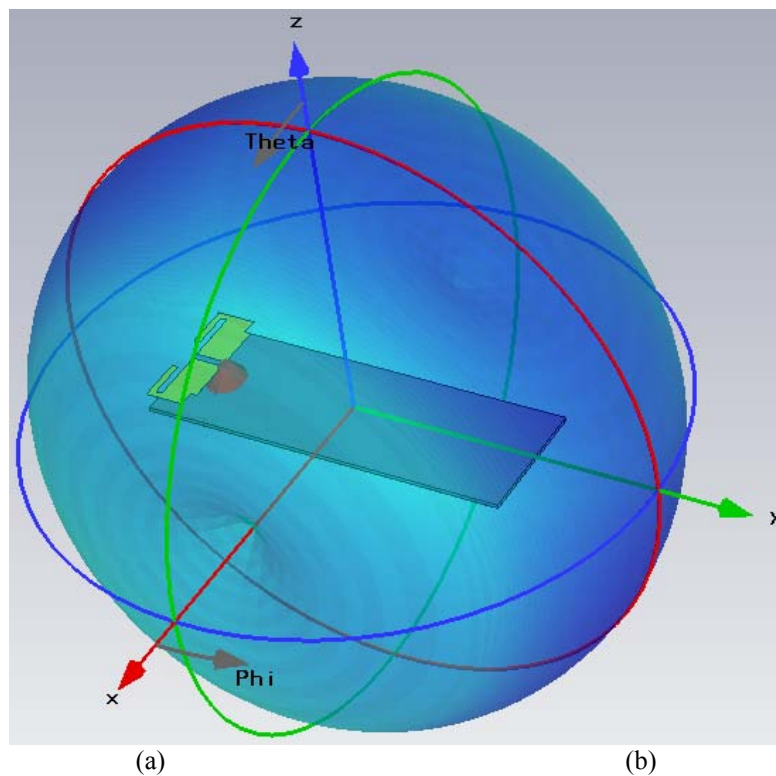
Fig. 4.6 Farfield for the small balanced antenna at 702 MHz

Table 4.2 shows the simulated radiation efficiency, total efficiency and realized gain for the balanced antenna for the ideal components (i.e. no parasitics loss) and real components (i.e. with parasitics loss), respectively. The small balanced antenna, incorporating ideal lumped elements, has high efficiency, i.e. -1.50 dB for total efficiency, as shown in Table 4.2. When incorporating real lumped elements, the total efficiency drops to -11.84 dB. It is found that such an efficiency drop is due to the electrically small size of the radiating element and dissipation loss in the components. Using low loss components (such as LTCC) or a bigger size of radiating element can eliminate this problem.

Circuit Components	Frequency (GHz)	Refl. Coeff. (dB)	Radiation Efficiency (dB)	Total Efficiency (dB)	Realized Gain (dB)
Ideal	**0.702**	**-12.1**	**-1.22**	**-1.50**	**0.39**
Real	**0.672**	**-18.4**	**-11.78**	**-11.84**	**-9.97**

Table 4.2 Simulated radiation efficiency, total efficiency and realized gain for the prototype shown in Fig. 4.2 when both C_1 were 10 pF

4.3. Reconfigurable Balanced Antenna (50mm) with Three Tunable Resonant Frequencies

This section presents a reconfigurable balanced antenna, consisting of L shaped dipole arms, is 50mm×40 mm in size, which enables three tunable resonant frequencies simultaneously to cover from 633 MHz to over 3000 MHz with a 6 dB loss with only 1 matching circuit [2-3]. For the DVB-H band, an additional matching circuit is required. However, the simulated prototype, with other supported material, shows there is some dissipated loss in the lumped elements and substrate and leading low efficiency at low frequency, i.e. -6.485 dB at 696 MHz. However, the exceptional

tuning range makes this antenna suitable for MIMO applications in small terminals when realised with lower loss supporting material.

4.3.1. Antenna Design and Structure

The balanced antenna, consisting of L shaped dipole arms, is 50 mm×40 mm in size with a 1 mm track width and has a total size of $110\times40mm^2$ and ground plane size of $100\times40mm^2$, as shown in Fig. 4.7. The antenna was designed on a microwave substrate material, Taconic TLY-3-0450-C5, which has a permittivity of 2.33, loss tangent of 0.0009, a thickness of 1.143 mm, and metal thickness of 0.01778 mm. The dimensions of the balanced antenna are given in Table 4.3.

(a)

(b)

(c)
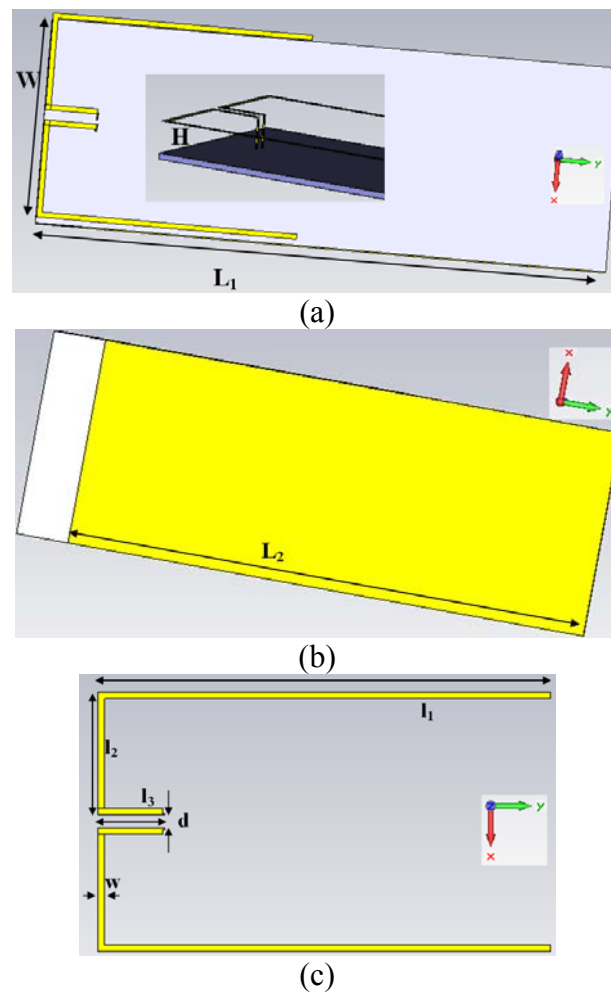
Fig. 4.7 The structure of balanced antenna with opening gap (a) front view; (b) back view; (c) overview of antenna element

H	5 mm	**L$_1$**	110 mm
W	40 mm	**L$_2$**	100 mm
l$_1$	50 mm	**l$_2$**	19 mm
l$_3$	10 mm	**d**	2 mm
w	1 mm	**-**	-

Table 4.3 Dimensions for the antenna shown in Fig. 4.7

4.3.2. Performance of the Antenna

The antenna circuit schematic is shown in Fig. 4.8. The antenna has three tunable resonant frequencies which simultaneously cover from 633 MHz to over 3000 MHz with a 6 dB loss with only 1 matching circuit, as shown in Fig. 4.9. By varying the varactors (capacitors), denoted as "C_1", from 10 pF to 0.1 pF it is possible to simultaneously tune the low-band resonant frequency from 648 MHz to 1616 MHz, the mid-band (from 1704 MHz to 2560 MHz) and the high-band (from 2280 MHz to over 3000 MHz) while maintaining a return loss above 6 dB, as shown in Fig. 4.10. The other values of the circuit elements used in the matching circuit without parasitics are shown in Fig. 4.8. For DVB-H band, some additional matching circuits are required.
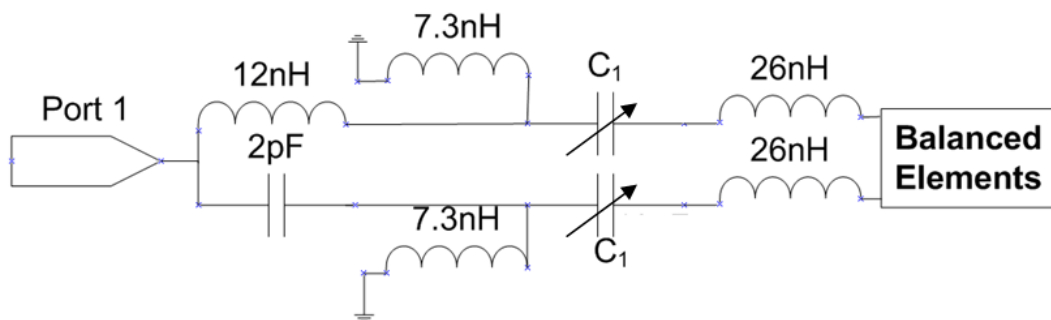
Fig. 4.8 The circuit schematic of balanced antenna as shown in Fig. 4.7
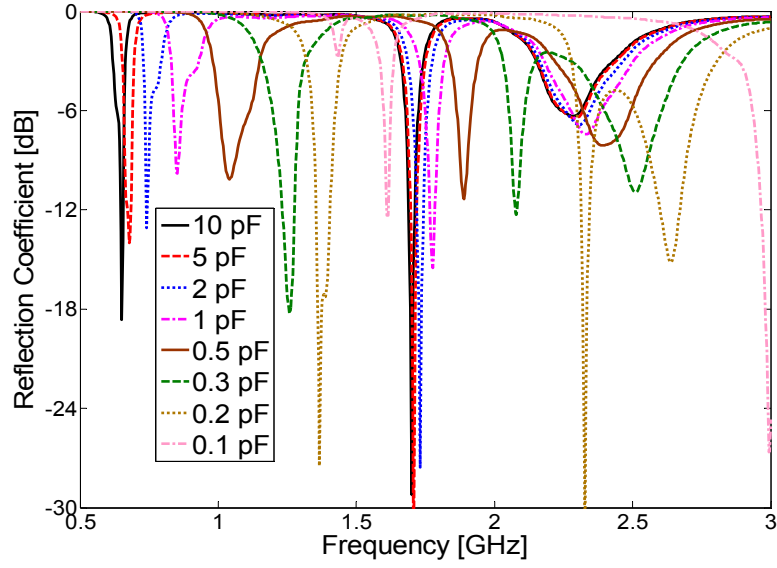
Fig. 4.9 Simulated resonant frequencies with return loss above 6 dB when the varactors C_1 vary from 10 pF to 0.1 pF.
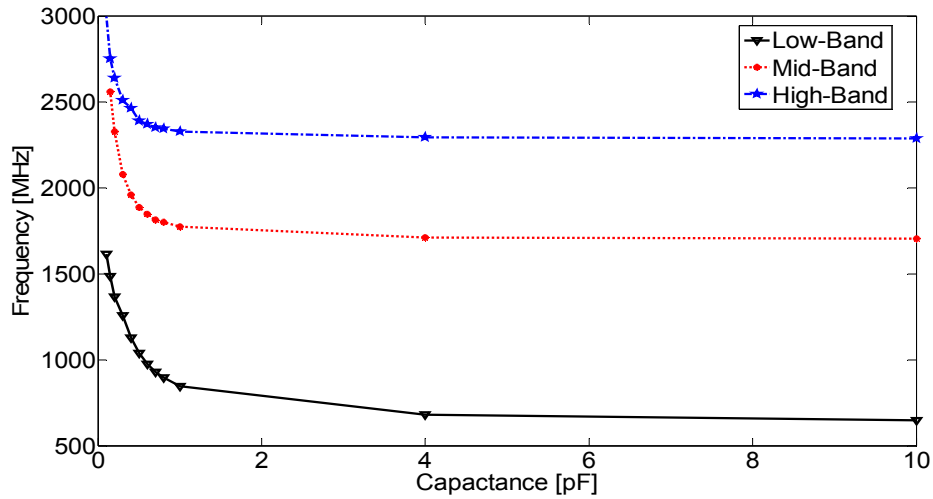
Fig. 4.10 Simulated resonant frequencies with return loss above 6 dB (for low-band, mid-band and high-band) when the varactors C_1 vary from 10 pF to 0.1 pF.

Table 4.4 shows the simulated radiation efficiency, total efficiency and realized gain for the balanced antennas as shown in Figs. 4.7 and 4.11, incorporating ideal components without parasitics and real components with parasitics, respectively. The balanced antenna, shown in Fig. 4.7, incorporating ideal lumped elements, has a high efficiency of at least -1 dB for total efficiency at 0.651 GHz, as shown in Table 4.4. When incorporating real components, the total efficiency drops to -3.80 dB at 0.693

GHz due to dissipated loss. However, when the balanced antenna, integrated with supported material, such as substrate (TLY-3-0450-C5) and Rocahell^{TM} with a dielectric constant of 1.08, shown in Fig. 4.11, the total efficiency at 0.696 GHz is only -6.49 dB, which is a bit lower than the industry requirement, which is at least -4.5 dB for the main TX & RX antenna and -5.5 dB for the 2nd RX antenna. Using lower loss support material or lower loss lumped elements (i.e. LTCC) would address this problem.

Circuit Components	Prototype	Bands	Frequency (GHz)	Refl. Coeff. (dB)	Radiation Efficiency (dB)	Total Efficiency (dB)	Realized Gain (dB)
Ideal	Fig. 4.7	Low	0.651	-16.1	-0.89	-0.10	1.15
		Mid	1.701	-25.6	-0.58	-0.60	3.38
		High	2.286	-6.0	-0.02	-1.28	3.12
Real	Fig. 4.7	Low	0.693	-10.9	-3.44	-3.80	-1.86
		Mid	1.692	-11.6	-1.20	-1.51	2.39
		High	2.268	-7.6	-0.48	-1.30	3.26
	Fig. 4.11	Low	0.696	-15.7	-6.37	-6.49	-4.93
		Mid	1.539	-12.9	-1.63	-1.86	1.73
		High	1.992	-22.6	-0.70	-0.72	4.51

Table 4.4 Simulated radiation efficiency, total efficiency and realized gain for the prototype shown in Figs. 4.7 and 4.11, respectively, when both C_1 were 10 pF.
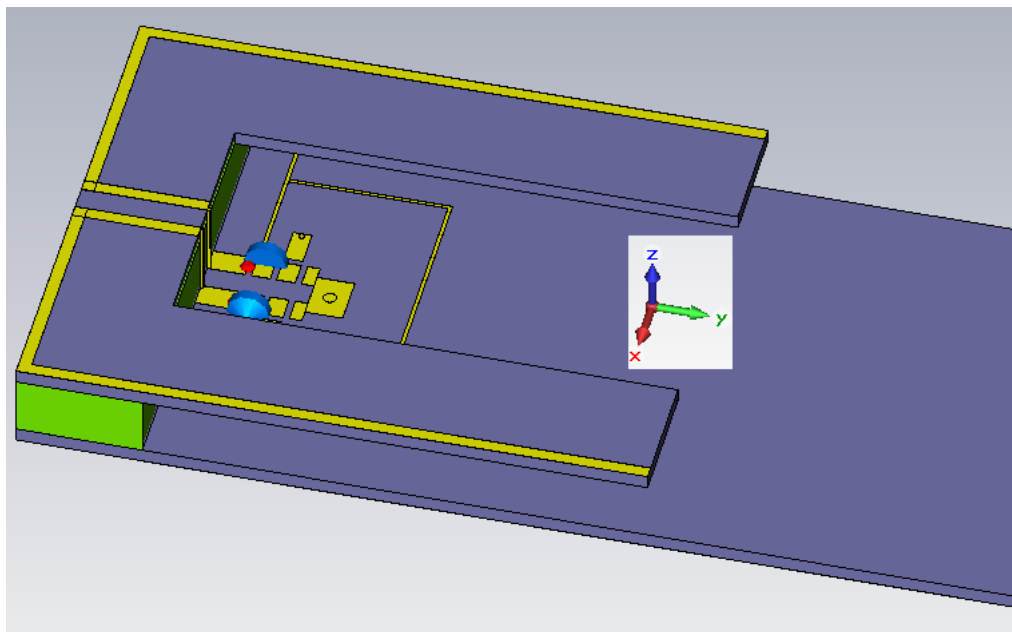
Fig. 4.11 The structure of prototype antenna with 50mm legs
(yellow – metal; blue – microwave substrate; green – Rocahell^{TM})

4.4. Reconfigurable Balanced Antenna (70mm) with Three Tunable Resonant Frequencies

This section presents a third reconfigurable balanced antenna to address the low efficiency problem. The balanced antenna is a simple thin dipole as in the 2nd structure. Using the same circuit structure, the antenna can provide three tunable resonant frequencies simultaneously to cover the low band (705 MHz to 951 MHz), mid-band (1692 MHz to 2457 MHz) and high-band (2862 to over 3000 MHz). This antenna, incorporating real components, provides at least -3.77 dB of total efficiency at 684 MHz [2-4].

4.4.1. Antenna Design and Structure

The balanced antenna, consisting of L shaped dipole arms, is 70 mm×40 mm in size with a 1 mm track width and has a total size of $110×40mm^2$ and ground plane size of $100×40mm^2$, as shown in Fig. 4.12. The antenna was designed on a microwave substrate material, Taconic TLY-3-0450-C5, which has a permittivity of 2.33, loss tangent of 0.0009, a thickness of 1.143 mm, and metal thickness of 0.01778 mm. The dimensions of the balanced antenna are given in Table 4.5.
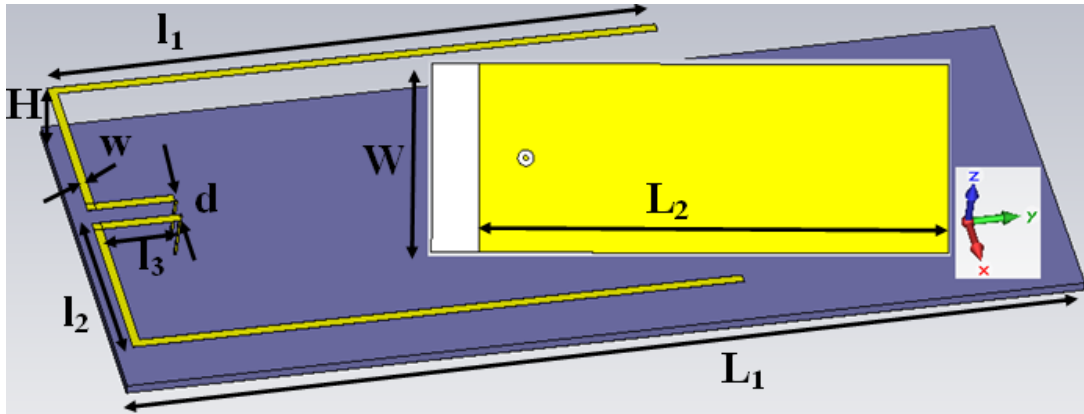
Fig. 4.12 The structure of balanced antenna (yellow-metal; blue-microwave substrate)

H	5 mm	L_1	110 mm
W	40 mm	L_2	100 mm
l_1	70 mm	l_2	19 mm
l_3	10 mm	d	2 mm
w	1 mm	-	-

Table 4.5 Dimensions for the antenna showed in Fig. 4.12

4.4.2. Performance of Antenna

The circuit schematic for the balanced antenna is shown in Fig. 4.13. Figs. 4.14 and 4.15 show the simulation results. Fig. 4.14 illustrates the effect of varying the capacitors C_1 from 10 pF to 0.28 pF. This moves the resonant frequencies simultaneously to cover the low-band from 705 MHz to 951 MHz, the mid-band from 1692 MHz to 2457 MHz and the high-band from 2826 MHz to over 3000 MHz, while maintaining a return loss above 6 dB, as shown in Figs. 4.15. The simulation results, using ideal components, show that this antenna has three bands behaviour. The low-band and mid-band can cover most of the existing cellular services, while the low-band can be tuned to cover LTE700, GSM850 and EGSM900, the mid-band can be tuned to cover PCN, GSM1800, GSM1900, PCS and UMTS.
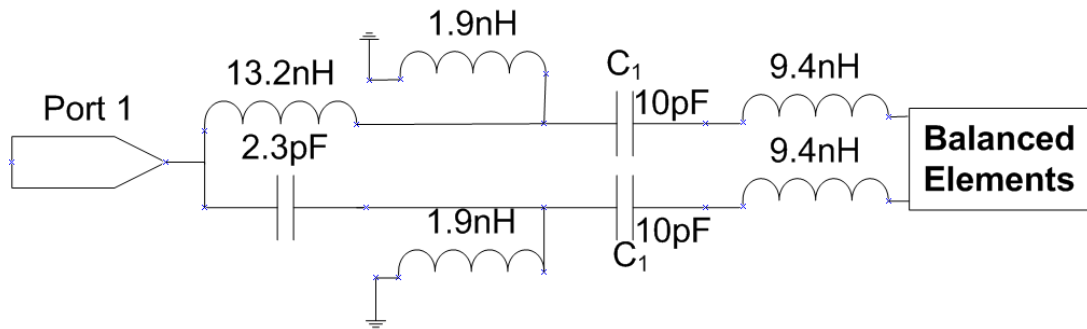
Fig. 4.13 The circuit schematic of balanced antenna shown in Fig. 4.12
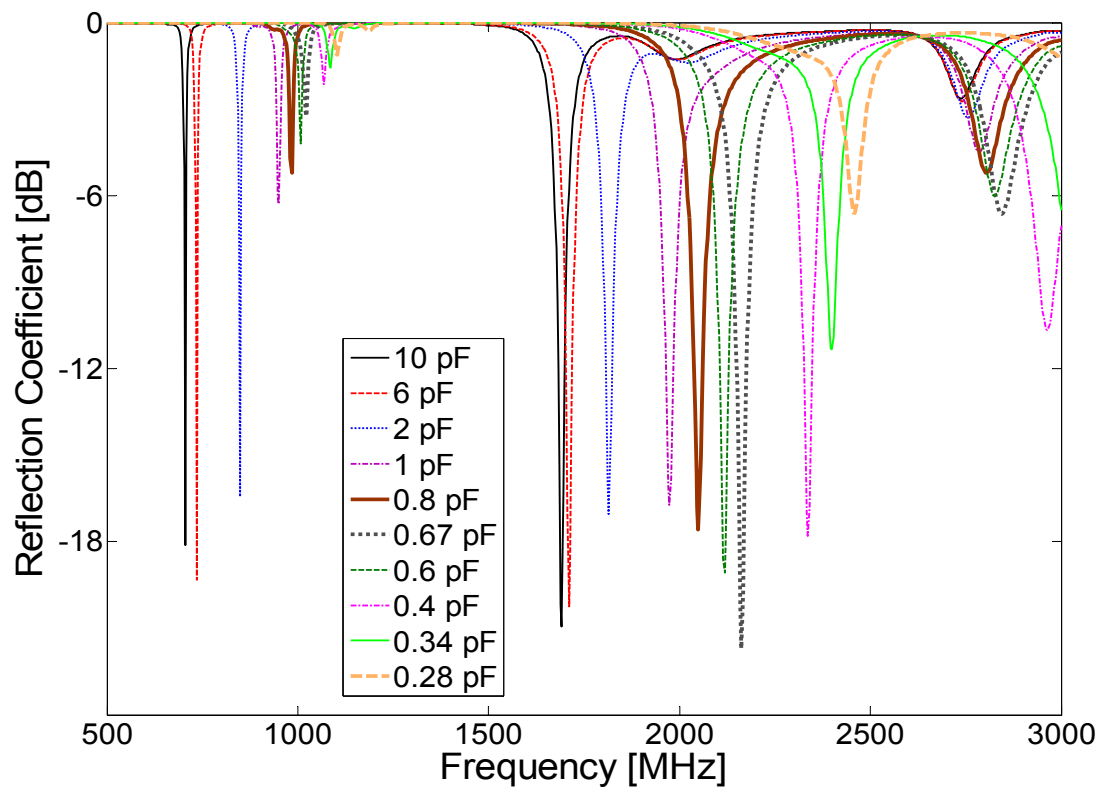
Fig. 4.14 Simulated reflection coefficient when the varactors vary from 10 pF to 0.28 pF.
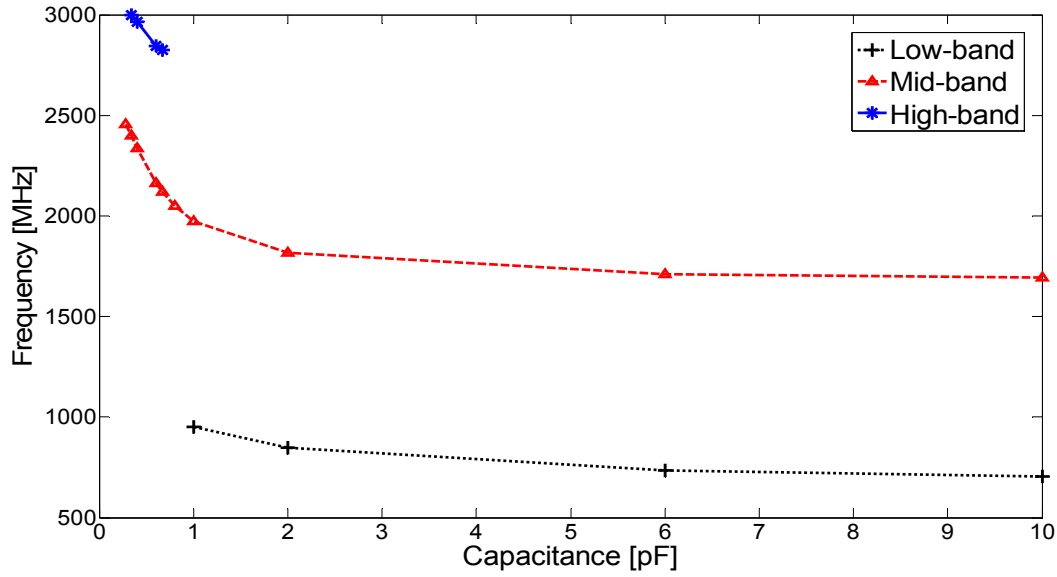
Fig. 4.15 Simulated resonant frequencies with return loss above 6 dB (for low-band, mid-band and high-band) when the varactors C_1 vary from 10 pF to 0.28 pF.

Table 4.6 shows the simulated radiation efficiency, total efficiency and realized gain for the balanced antennas as shown in Figs. 4.12 and 4.16, incorporating ideal components without parasitics and real components parasitics, respectively. The balanced antenna, shown in Fig. 4.12, incorporating ideal components, has a higher efficiency, at least -0.15 dB total efficiency at 0.705 GHz, as shown in Table 4.6. When incorporating real components, the total efficiency drops to -4.57 dB at 0.702 GHz due to dissipation. When the balanced antenna, integrated with supported material, such as substrate (TLY-3-0450-C5) and Rocahell[TM], as shown in Fig. 4.16, the total efficiency at 0.681 GHz is -3.964 dB, which meets the industry requirement. Using lower loss supported material or lower loss lumped elements (i.e. LTCC) would increase the efficiency.

Circuit Components	Prototype	Bands	Frequency (GHz)	Refl. Coeff. (dB)	Radiation Efficiency (dB)	Total Efficiency (dB)	Realized Gain (dB)
Ideal	Fig. 4.12	Low	0.705	-14.8	0	-0.15	1.13
		Mid	1.689	-19.5	-0.25	-0.30	4.61
		High	-	-	-	-	-
Real	Fig. 4.12	Low	0.702	-17.6	-4.50	-4.57	-3.28
		Mid	1.686	-21.5	-2.01	-2.04	2.90
		High	-	-	-	-	-
	Fig. 4.16	Low	0.681	-14.1	-3.79	-3.96	-2.75
		Mid	1.599	-22.3	-2.04	-2.07	2.71
		High	2.850	-17.5	-1.42	-1.50	5.90

Table 4.6 Simulated radiation efficiency, total efficiency and realized gain for the prototype shown in Figs. 4.12 and 4.16, respectively, when both C_1 were 10 pF.
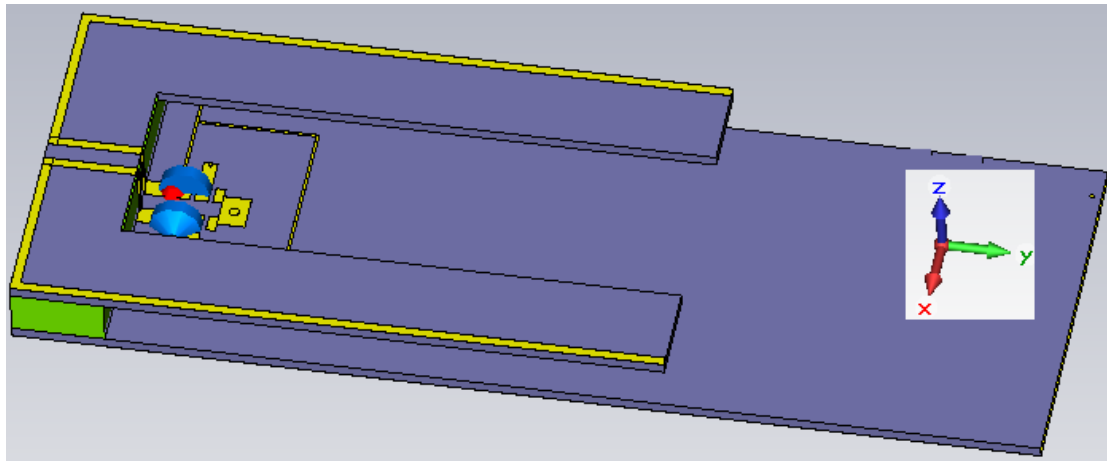
Fig. 4.16 The structure of prototype antenna with 70mm legs
(yellow – metal; blue – microwave substrate; green – Rocahell[TM])

4.5. Reconfigurable MIMO Antenna

4.5.1. MIMO Antenna Design and Structure

The proposed antenna shown in Fig. 4.17 consists of a balanced antenna element, which is described in the previous section, and a two-port chassis-antenna [5 and 6], which has been described in Chapter 3. The MIMO antenna has a total size of 118×40 mm^2 and ground plane size of 100×40 mm2. The coupling elements also occupy a small volume of 40×4×7 mm^3. Both antennas were fabricated on a microwave

substrate material, Taconic TLY-3-0450-C5, which has a permittivity of 2.33, loss tangent of 0.0009, a thickness of 1.143 mm, and metal thickness of 0.01778 mm. The substrate supporting the balanced antenna is much wider and longer than the antenna itself to provide mechanical support. The balanced antenna element and the coupling elements for the chassis antenna are supported with Rohacell^{TM}. The dimensions of the balanced antenna are given in Table 4.5.
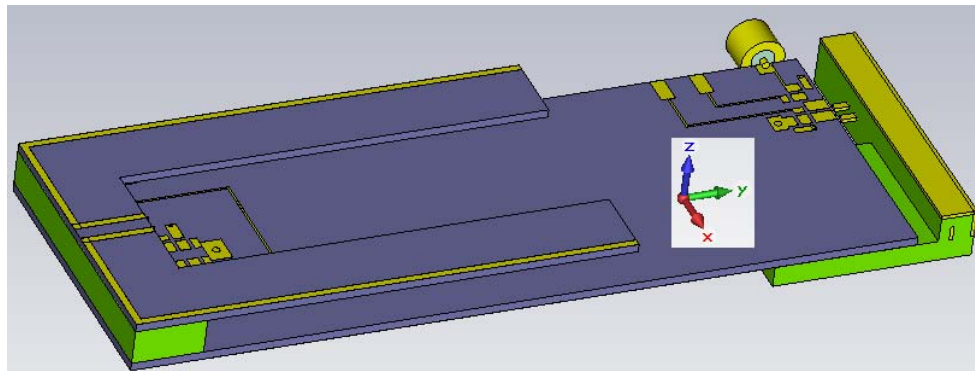
(a)
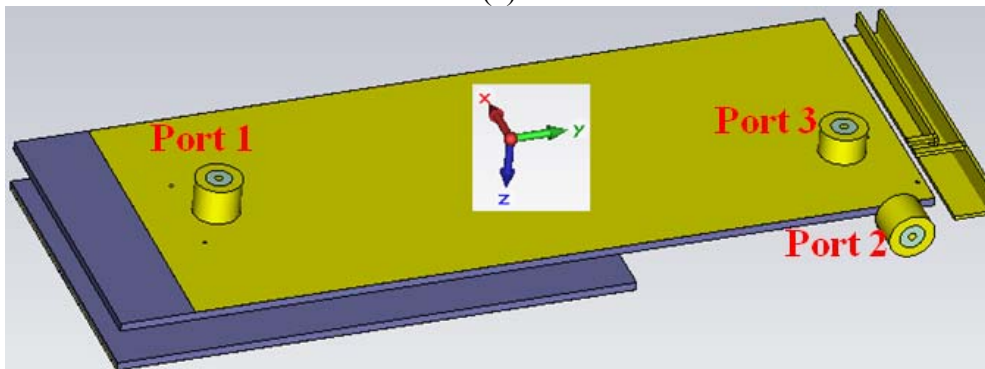
(b)
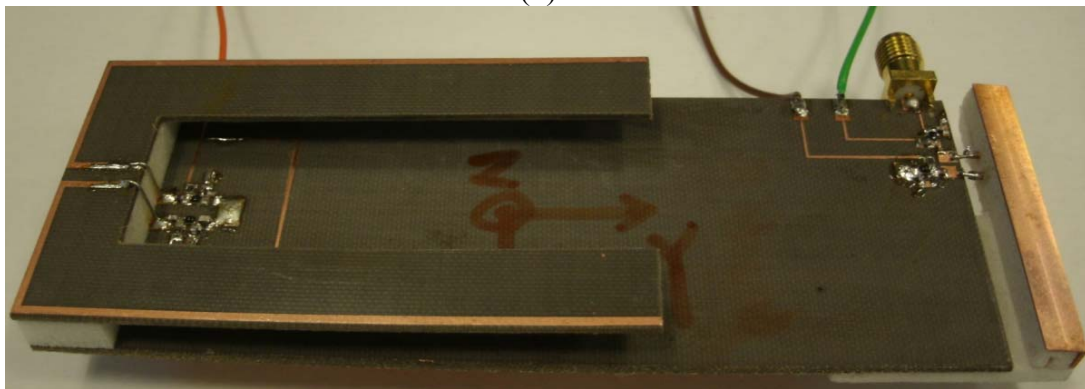
(c)

Fig. 4.17 The structure of MIMO antenna (a) front view; (b) back view; (c) fabricated prototype. (yellow – metal; blue – microwave substrate; green – Rohacell structural support)

4.5.2. Matching Circuits

As mentioned earlier, for the balanced antenna, two identical L-network matching circuits are connected to each leg, and then connected to an LC balun. For the chassis-antenna, an L-network matching circuit is connected to each of the coupling elements. The MIMO antenna was simulated in CST Microwave Studio®. The s4p file representing the frequency response of the antenna was then used to determine optimum component values in each matching circuit using Microwave Office, from Applied Wave Research. Each matching circuit incorporates a single varactor diode together with a bank of fixed inductors. The circuit schematics for the MIMO antenna are shown in Fig. 4.18.

In the demonstrator antenna, four varactor diodes (MV34003-150A) were used, with capacitance variable from 0.409 pF to 15.435 pF for an applied voltage of 15 V to 0 V. A dc bias line, incorporating a 10 k Ω resistor was attached to the anode of each varactor, to supply +ve voltage. A 10 k Ω resistor is used for damping any residual RF signals appearing on the dc line. The –ve voltage is supplied from the inner conductor of one of the SMA connectors by using a bias-tee (ZX85-122G-S+, from Mini-Circuits®).
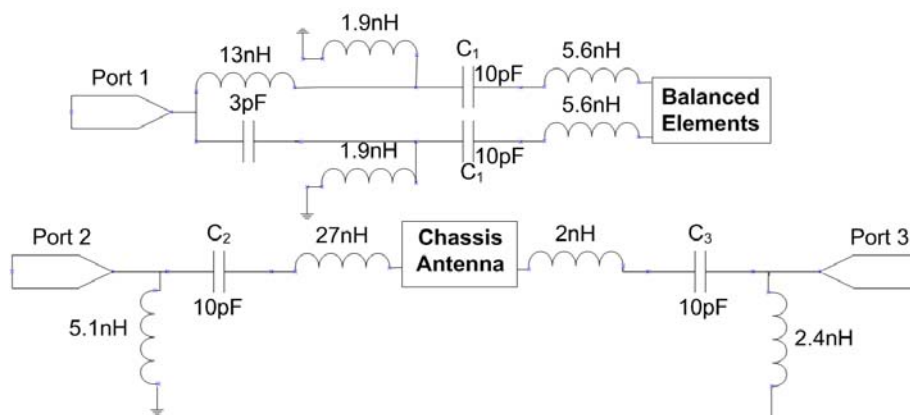
Fig. 4.18 The circuit schematics for the MIMO antenna of Fig. 4.17.

4.5.3. Results

Fig. 4.19 shows the measured reflection coefficient for the balanced antenna, which illustrates operation in the three simultaneous bands. Ports 2 and 3, of the chassis-antenna, were open circuit during the measurement. The varactors were varied from 0 V to 15 V. The resonant frequency varies from 646 MHz to 848 MHz for the low band, 1648 MHz to 2074 MHz for the mid-band and 2512 MHz to over 3000 MHz for high band, while maintaining a return loss above 6 dB. Table 4.7 shows the measured reflection coefficient for both ports of the chassis-antenna while the varactor voltages vary from 0 V to 15 V. During measurements on each port, the other two ports are left open circuit. Unlike the balanced antenna each port of the chassis antenna has a single resonance. The frequencies of each port vary from 597 MHz to 1124 MHz and 1586 MHz to 2332 MHz, respectively. Thus, the antenna provides MIMO operation from 646 MHz to 848 MHz and 1648 MHz to 2074 MHz. It is likely that the frequency tuning range could be increased, if the capacitance tuning range of the varactor was wider.
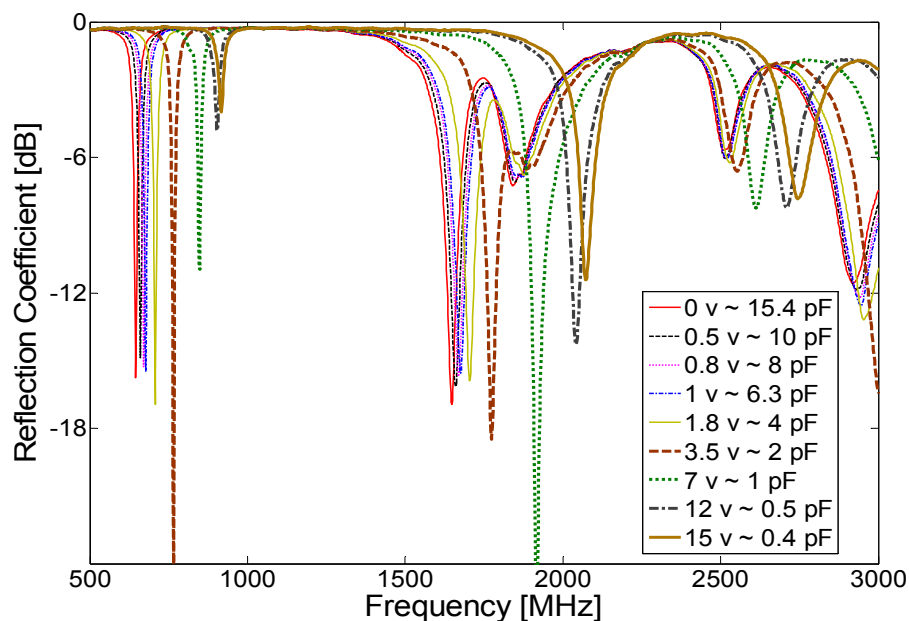
Fig. 4.19 Measured reflection coefficient for the balanced antenna when two varactors varied from 0 V to 15 V simultaneously

- 121 -

The instantaneous bandwidth at various frequencies for ports 2 and 3 are shown in Table 4.7. The bandwidth of port 1 for the same frequencies is also shown. The smallest of these thus represent the instantaneous MIMO bandwidth. It can be seen that port 2 gives a considerably narrower bandwidth than port 3. Table 4.7 shows that the minimum MIMO bandwidth is 14 MHz (at 771 MHz centre frequency) and the maximum MIMO bandwidth is 93 MHz (at 1812 MHz centre frequency).

Table 4.7 Measured reflection coefficient for the port 2&3 (chassis-antenna) with varactor varied from 0 V to 15 V, respectively

	Voltage (V)	Freq. (MHz)	Refl. Coeff. (dB)	Bandwidth@ 6 dB (MHz)	Bandwidth for Port 1 at same frequency (MHz)
Port 2	0	597	-19.72	39	-
	1	644	-21.30	42	17
	3.5	771	-32.71	34	14
	7	921	-18.32	44	-
	12	1075	-12.03	41	-
	15	1124	-10.62	35	-
Port 3	0	1586	-21.60	236	-
	1	1631	-25.97	289	73
	3.5	1812	-15.89	233	93
	7	2067	-18.41	224	61
	12	2300	-25.11	204	-
	15	2332	-23.91	189	-

Table 4.8 gives the measured S parameters for the MIMO antenna configuration. It is clear that isolation is good and at least 15 dB over all the bands. Please note that the capacity and efficiency would be considerably decreased by the poor isolation between the antennas. According to the LTE MIMO antenna specification from Sony Ericsson, at least 10 dB and 15 dB of isolation at low bands and high bands respectively are necessary for handset. For good MIMO operation, only port isolation is not sufficient and an investigation in a rich multipath environment on other parameters, i.e. correlation coefficient, power imbalanced, diversity gain, average

capacity increase, etc, is needed. However, this is beyond of the goal of this research

and would be suggested for future work.

Table 4.8 Measured S parameters for the MIMO antenna of Fig. 4.17
*applied voltage to the varactors of balanced antenna
[+]applied voltage to the varactors of chassis-antenna

Voltage (V)	Ports	Frequency (MHz)	S11 (dB)	S22 (dB)	S21 (dB)
0* & 1.3[+]	1 & 2	646	-16.85	-32.14	-20.15
1.72* & 2.53[+]	1 & 2	710	-16.25	-27.21	-17.17
6.85* & 5.6[+]	1 & 2	850	-10.85	-36.53	-18.25
0* & 1.1[+]	1 & 3	1645	-14.62	-25.36	-26.57
1.9* & 2.1[+]	1 & 3	1710	-16.01	-18.71	-25.40
12* & 6.4[+]	1 & 3	2050	-13.09	-14.54	-15.58

Tables 4.9 to 4.11 show the measured realized gain for the three ports of MIMO

antenna, shown in Fig. 4.17. The values of realized gain for those three ports were

also plotted in Fig. 4.20. The balanced antenna, used as 2nd RX antenna, the realized

gain meets the industry requirement (i.e. at least -4.5 dB for main TX & RX antenna

and -5.5 dB for 2nd RX antenna at free space). However, the chassis-antenna, used as

main TX & RX antenna, had minimum realized gain at low frequency, i.e. -6.4 dBi at

684 MHz. Such low gain was due to dissipation on the external matching of the

balanced antenna. Tables 4.10 and 4.11 shows that the effect of loss on the matching

circuits were less in mid and high frequencies. Studies and solution, focused on the

low gain of chassis-antenna, will be provided in the next section. The simulated

radiation efficiency, total efficiency and realized gain for the balanced antenna, while

the two capacitors are fixed at 10 pF and 3 pF, respectively, were shown in Table 4.12.

The results include the losses in the matching circuit, both loss in lumped components

and the strip line. The total efficiency for low bands is above -4 dB, for mid bands and

high bands it is above -3 dB. These values compare well with those for the chassis-

antenna reported in Ref. [6]. The realized gain of the chassis antenna is repeated in

Table 4.12 for comparison.

Table 4.9 Measured realized gain of port 1 of the MIMO antenna, shown in Fig. 4.17

	Balanced Antenna (Port 1)			
	Voltage (V)	Direction	Frequency (MHz)	Realized Gain (dBi)
Low Band	0	-Y	648	-2.4
	1.15	-Y	684	-4.1
	3.7	-Y	774	-1.1
	6	-Y	834	-0.6
	8	-Y	870	-2.4
	10	-Y	889	-2
	11	-Y	893	-2.9
	13	-Y	909	-4.9
	15	-Y	918	-5.1
Mid Band	0	-X	1605	1.3
	2.25	-X	1722	5.2
	5	-X	1832	5.4
	8	-X	1932	4.6
	10	-X	1989	3.6
	13	-X	2048	4.8
	15	-X	2062	4.7
High Band	0	+Z	2522	-0.6
	3	+Z	2553	-1.4
	5	+Z	2590	-2.8
	8	+Z	2646	-2.8
	0	+Z	2892	5.6
	2.75	+Z	2946	5.2

Table 4.10 Measured realized gain of port 2 of the MIMO antenna, shown in Fig. 4.17

Chassis-Antenna Large Element (Port 2)			
Voltage (V)	Direction	Frequency (MHz)	Realized Gain (dBi)
0	+X	583.5	-0.6
1	+X	597	-4.1
1.85	+X	684	-6.4
3	+X	745.5	-4
4	+X	772.5	-3.2
4.05	+X	774	-3.1
5	+X	813	-0.8
6	+X	880.5	-1.5
7	+X	907.5	-1.9
8	+X	921	-2.7
9	+X	975	-2.3
10	+X	1029	-2.5
11	+X	1042.5	-1.4
15	+X	1110	-3.4

Table 4.11 Measured realized gain of port 3 of the MIMO antenna, shown in Fig. 4.17

Chassis-Antenna Small Element (Port 3)			
Voltage (V)	Direction	Frequency (MHz)	Realized Gain (dBi)
0	+Z	1586	2.2
0.83	+Z	1605	2.7
3.5	+Z	1704	3.2
7	+Z	2096	1.7
12	+Z	2379	0.6

Fig. 4.20 Measured realized gain for three ports of the MIMO antenna, shown in Fig. 4.17

Table 4.12 radiation efficiency, total efficiency and realized gain for the prototype of Fig. 4.17

Balanced Antenna						Chassis-Antenna		
Capacitor For Balanced Antenna	Frequency (MHz)	Simulated Refl. Coe. (dB)	Simulated Rad. Effic. (dB)	Simulated Tot. Effic. (dB)	Simulated Rlzd. Gain (dB)	Measured Rlzd. Gain (dB)	Simulated Rlzd. Gain* (dB)	Simulated Rlzd. Gain+ (dB)	Measured Rlzd. Gain+ (dB)
10 pF	684	-17.93	-3.70	-3.77	-2.48	-4.1	-7.89	-7.89	-6.4
	1605	-22.21	-2.23	-2.25	2.56	1.3	4.37	4.37	2.7
	2892	-21.83	-1.48	-1.51	5.65	5.6	-	-	-
3 pF	774	-12.44	-2.70	-2.96	-1.92	-1.1	-4.73	-2.21	-3.1
	1722	-33.45	-1.89	-1.89	2.38	5.2	4.43	4.54	3.2
	2946	-26.83	-1.55	-1.56	5.10	5.2	-	-	-

* both antennas were operating at the same frequency
+ only chassis-antenna is in operation at that frequency while the capacitors for balanced antenna was fixed at 10 pF

4.5.4. Gain Improvement for Chassis-Antenna in MIMO Structure

As mentioned earlier, the total efficiency of the MIMO antenna should be at least -4.5 dB for main TX & RX antenna and -5.5 dB for 2nd RX antenna. Compared to that shown in ref. [6], the realized gain of the chassis antenna, when integrated with a balanced antenna, dropped at least 5 dB at low frequencies. One of the most

promising solutions to address this problem is to isolate the two matching circuits by

introducing slot in the ground plane, as shown in Fig. 4.21.
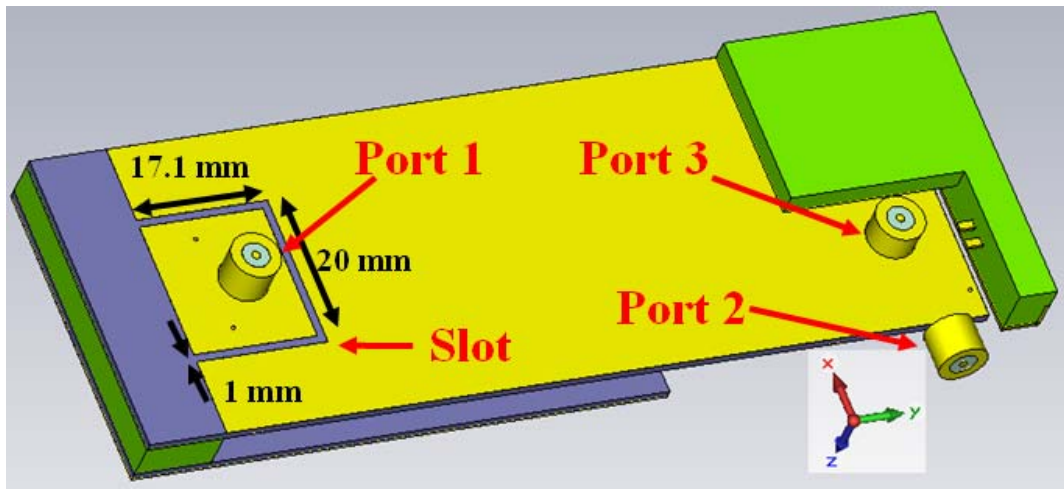
Fig. 4.21 The back view of MIMO antenna with slot line on ground plane (yellow – metal; blue – microwave substrate; green – Rohacell structural support)

Table 4.13 shows the simulated reflection coefficient, radiation efficiency, total

efficiency and realized gain for the MIMO antenna with a slot in the ground plane, as

shown in Fig. 4.21. It is clear that, the realized gain for the chassis-antenna has been

improved by 6.28 dB (79.6%) at 687 MHz, without affecting other parameters,

compared the one shown in Table 4.12.

Table 4.13 Simulated reflection coefficient, radiation efficiency, total efficiency and realized gain for the prototype of Fig. 4.21

| Capacitor For Balanced Antenna | Frequency (MHz) | Balanced Antenna | | | | Chassis-Antenna | | | | Simulated Isolation (dB) |
		Simulated Refl. Coe. (dB)	Simulated Rad. Effic. (dB)	Simulated Tot. Effic. (dB)	Simulated Rlzd. Gain (dB)	Simulated Refl. Coe. (dB)	Simulated Rad. Effic. (dB)	Simulated Tot. Effic. (dB)	Simulated Rlzd. Gain (dB)	
10 pF	**687**	-20.16	-3.34	-3.38	-2.10	-12.92	-3.36	-3.59	-1.61	-48.92
	1722	-12.64	-1.24	-1.70	1.80	-10.01	-0.45	-0.70	4.49	-28.99
	-	-	-	-	-	-	-	-	-	-

4.5.5. Current Distribution and Radiation Pattern

Table 4.12 shows that the MIMO antenna can provide high efficiency while maintaining high isolation between two antennas, i.e. -48.92 dB at 687 MHz and -28.99 dB at 1722 MHz. Such high isolation can be explained by analysing the current distribution and radiation pattern. Figs. 4.22 – 4.25 show the current distribution for each port at 687 MHz and 1722 MHz, respectively. Figs. 4.26 – 4.29 show the farfield plot for each port at 687 MHz and 1722 MHz, respectively. From Figs. 4.22 and 4.24, it is clear that the current were concentrated on the balanced antenna with much less on the chassis and the coupling elements. Conversely, the current were distributed on the whole structure for the chassis-antenna as the coupling elements are used to excite the resonant modes in the handset chassis, shown in Figs. 4.23 and 4.25. From those farfield plots shown in Figs. 4.26 – 4.29, it is clear that the maximum directivity for both antennas is different.
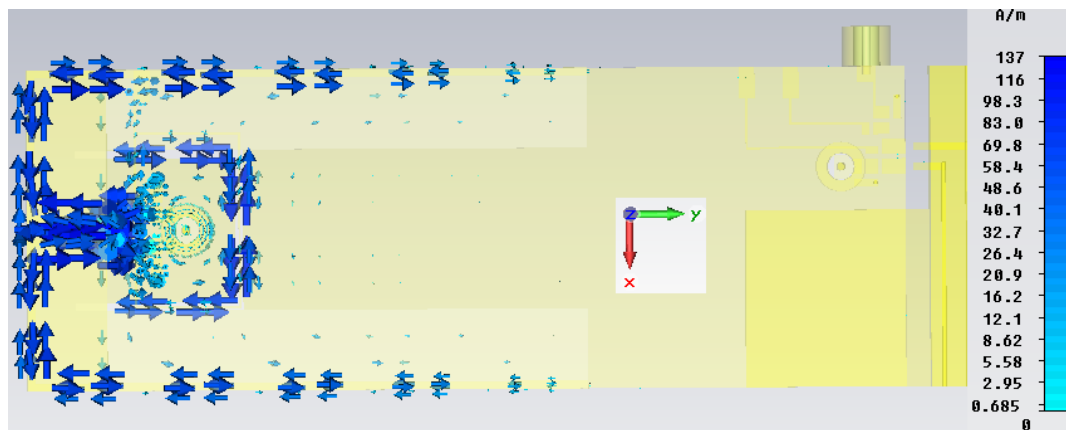
Fig. 4.22 Current distribution for port 1 (balanced antenna) of MIMO antenna at 687 MHz
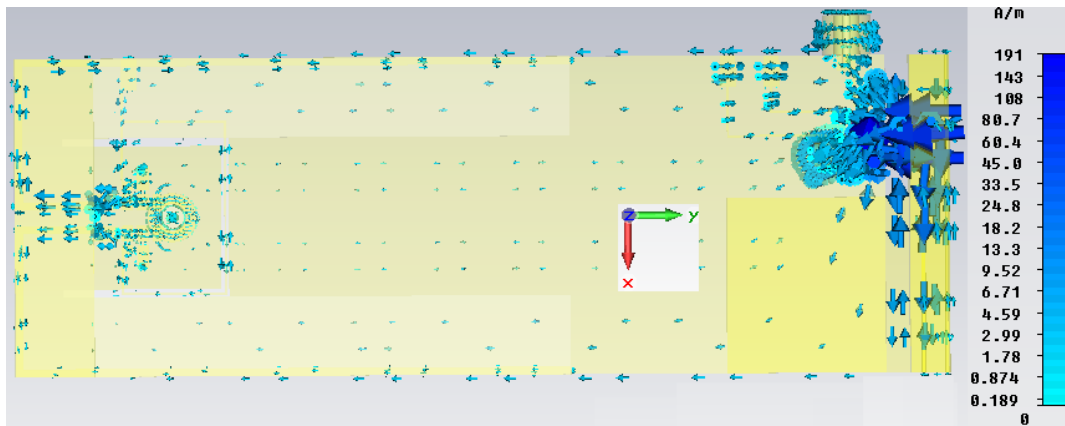
Fig. 4.23 Current distribution for port 2 (Chassis antenna) of MIMO antenna at 687 MHz
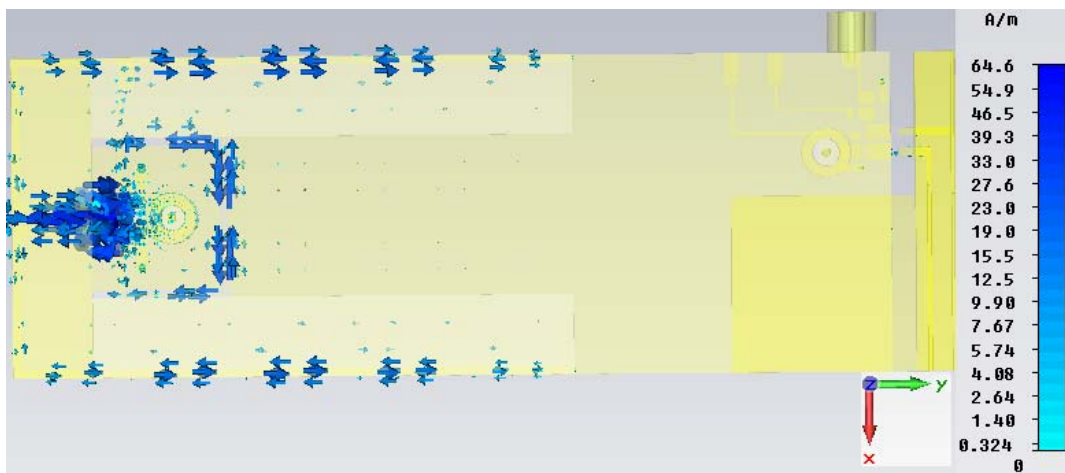
Fig. 4.24 Current distribution for port 1 (balanced antenna) of MIMO antenna at 1722 MHz
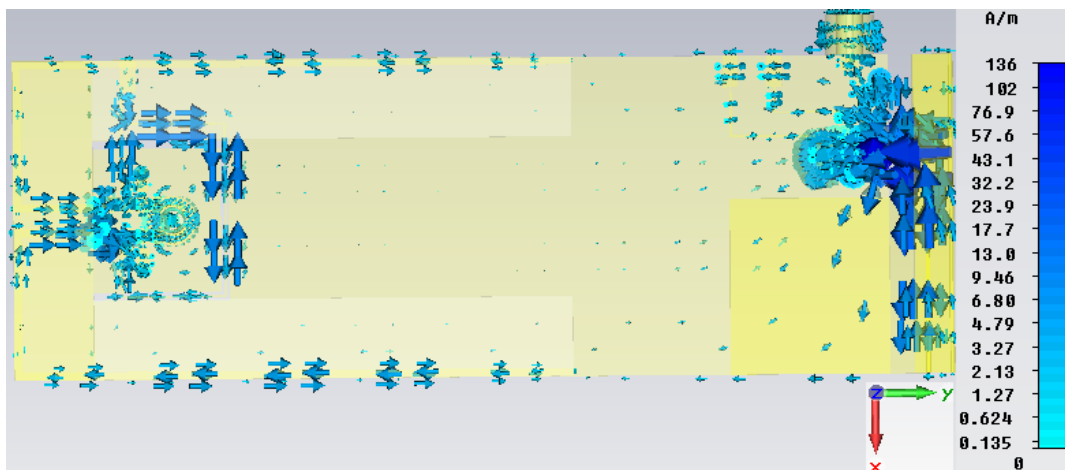
Fig. 4.25 Current distribution for port 3 (Chassis antenna) of MIMO antenna at 1722 MHz
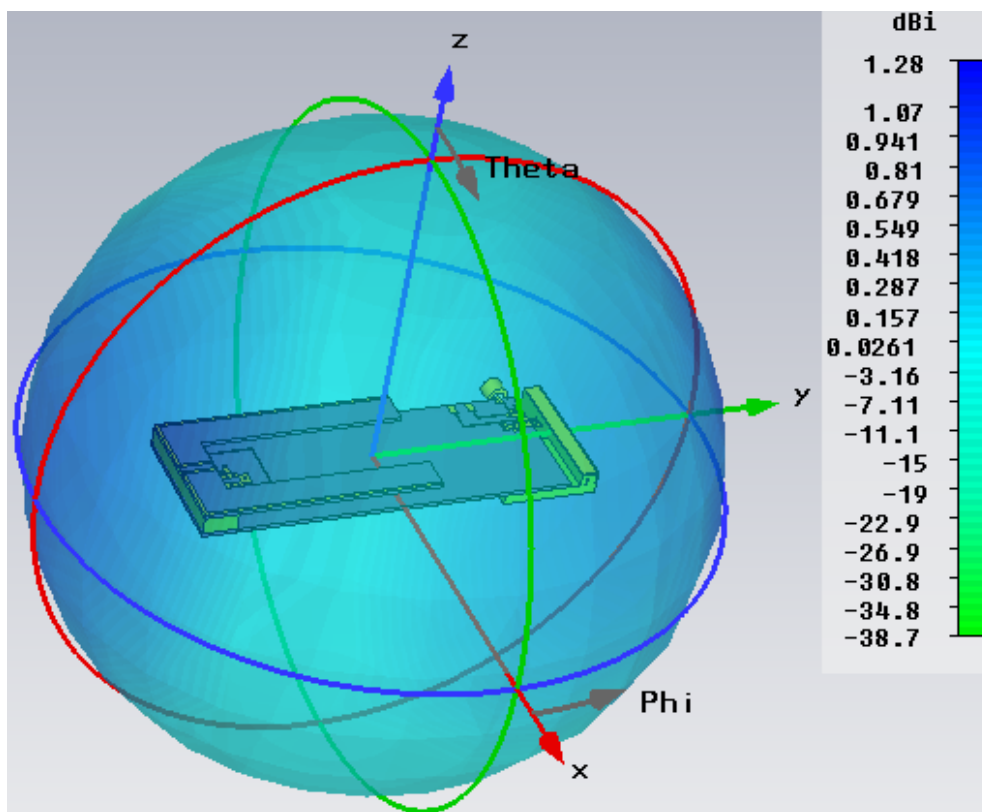
Fig. 4.26 Farfield plot for port 1 (balanced antenna) of MIMO antenna at 687 MHz
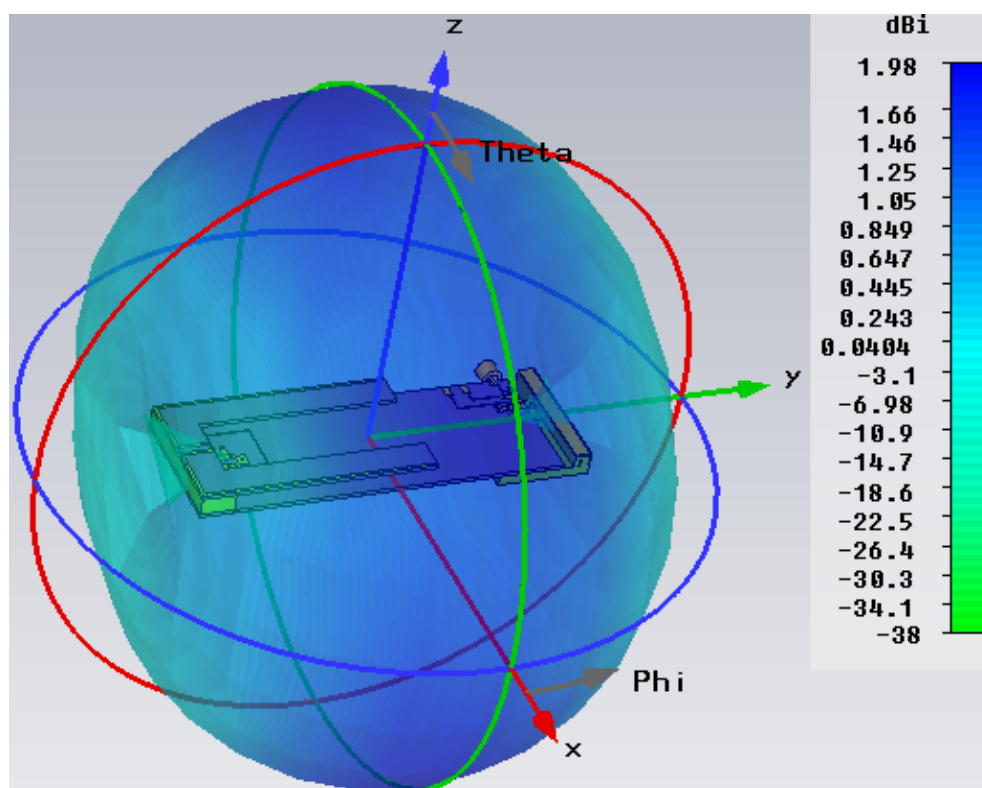
Fig. 4.27 Farfield plot for port 2 (balanced antenna) of MIMO antenna at 687 MHz
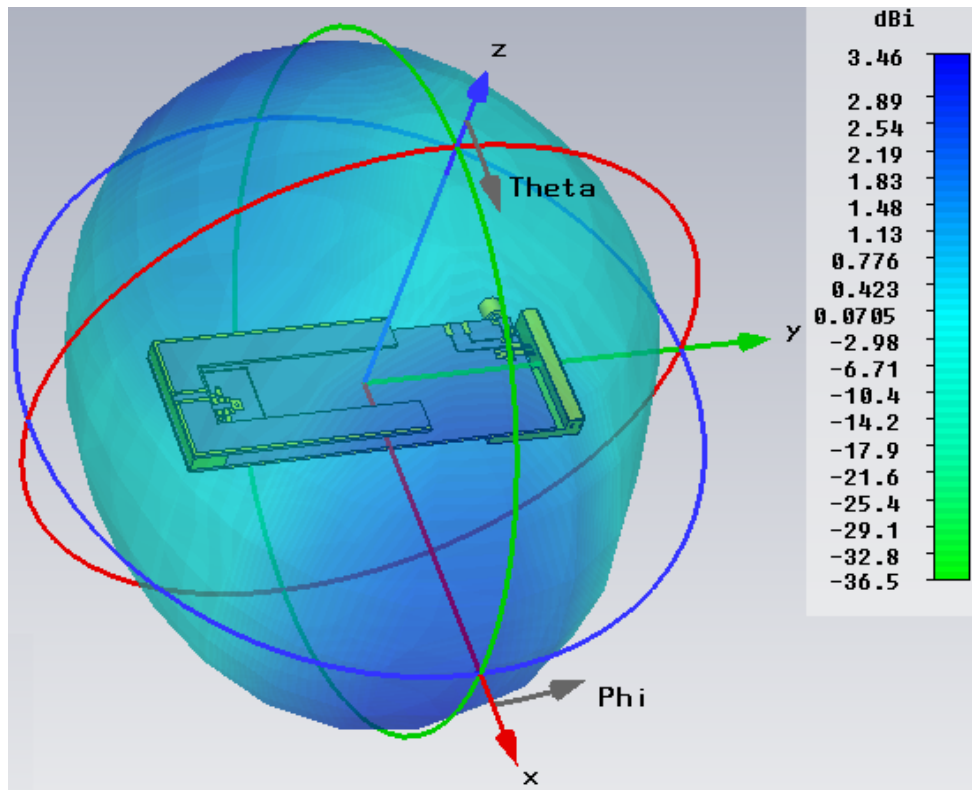
Fig. 4.28 Farfield plot for port 1 (balanced antenna) of MIMO antenna at 1722 MHz
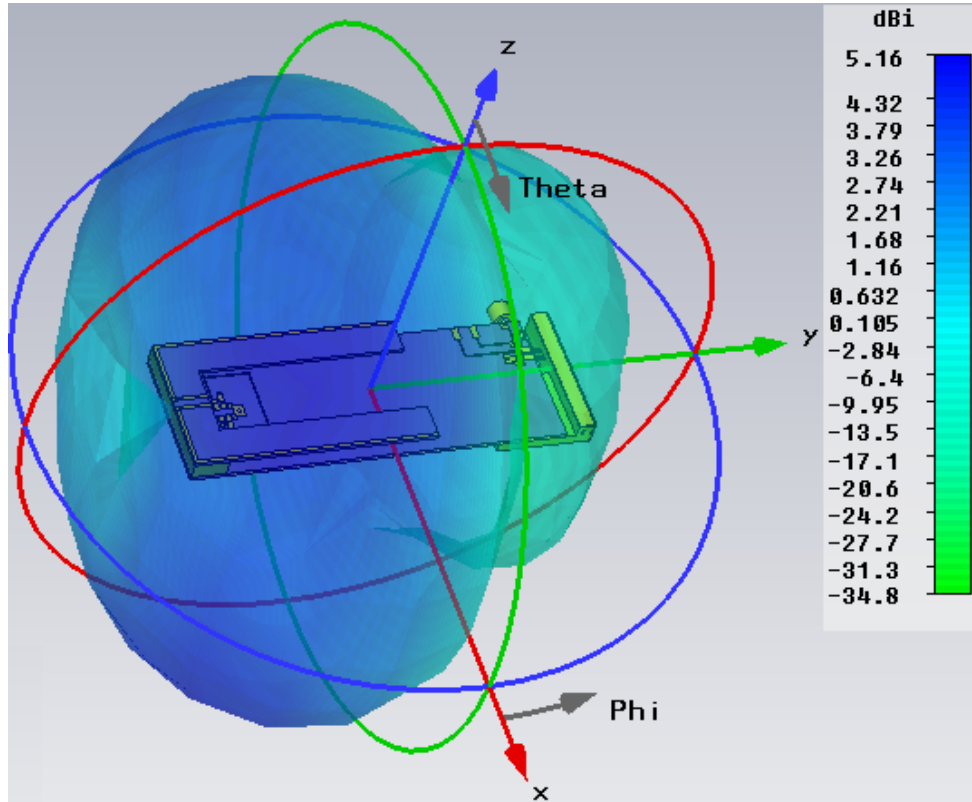
Fig. 4.29 Farfield plot for port 3 (balanced antenna) of MIMO antenna at 1722 MHz

4.6. Summary

This chapter presents three different structures of wideband reconfigurable balanced antennas for use in current and future mobile wireless communication systems and its potential for reconfigurable MIMO applications. To the best of our knowledge this is the first reconfigurable MIMO antenna with such a wide tuning range. Section 4.2 introduced a small dipole (i.e. 40×14 mm^2), which enables a frequency tuning range from 700 MHz up to 2434 MHz with a 6 dB loss across the operating band with only 1 matching circuit. Section 4.3 introduced a thin balanced loop with 50 mm length of each leg and 1 mm width, which enables three tunable resonant frequencies simultaneously to cover from 633 MHz to over 3000 MHz. However, the first two proposed antennas, shown in sections 4.2 and 4.3, experience high dissipated loss on the lumped elements in the circuit which leads to low efficiency. This problem can be solved either use low loss components (such as LTCC) or a bigger size of antenna element. Thus, the third antenna is proposed in section 4.4. The thin balanced dipole, with 70 mm length of each leg, can provide three tunable resonant frequencies simultaneously to cover the low band (705 MHz to 951 MHz), mid-band (1692 MHz to 2457 MHz) and high-band (2862 to over 3000 MHz), with good efficiency.

When the balanced antenna combined with a two-port chassis-antenna, which has a wide tuning range, it becomes a reconfigurable MIMO antenna for small terminals with good isolation. By inserting a slot into the ground plane, isolation is much improved. And this also improves the gain of chassis-antenna.

References

[1]   Z. H. Hu and P. S. Hall, "Reconfigurable Balanced Antenna", U.K Patent application GB1108456.3. 2011

[2]   Z. H. Hu and P. S. Hall, "Balanced Antenna System", U.K. Patent applicationGB1020202.6. 2010

[3]   Z. H. Hu, P. S. Hall, and P. Gardner, "Novel reconfigurable dipole-chassis antennas for small terminal MIMO applications", Accepted by *Electronics Letters*.

[4]   Z. H. Hu, P. S. Hall, P. Gardner, and Y. Nechayev, "Wide tunable balanced antenna for mobile terminals and its potential for MIMO applications", Accepted by *Loughborough Antenna & Propagation Conference 2011, LAPC 2011*.

[5]   C. T. P. Song, J. Kelly, and P. S. Hall, "Reconfigurable antenna", U.K. Patent application GB0918477.1. 2009.

[6]   Z. H. Hu, J. Kelly, C. T. P. Song, P. S. Hall, and P. Gardner, "Novel wide tunable dual-band reconfigurable chassis-antenna for future mobile terminals", *Antennas and Propagation (EuCAP), 2010 Proceedings of the Fourth European Conference on 2010.* pp. 1-5.

CHAPTER V

WIDEBAND CONICAL MONOPOLE ANTENNA WITH

FREQUENCY NOTCH-BAND BEHAVIOUR

This chapter presents conical monopole antennas incorporating different types of slots to achieve good band-rejection behaviour. Compared to the previous work reported in the literature, these conical monopole antennas provide omni-directional patterns throughout the operating band, even at high frequencies. The different shaped slots offer a choice of narrow or wide rejection band (i.e. high Q or low Q). Some of the designs provide significantly improved peak gain suppression in the vertical polarisation.

A new equivalent circuit model has been created for the wideband conical monopole antenna with frequency notch-band. It has been shown that the band-rejection can be improved by enhancing the antenna-slot coupling factor or by increasing the number of resonators. An analysis of the relationship between the quality (Q) factor and the coupling factor is also presented.

All of the simulations presented in this chapter were performed using the transient solver in CST Microwave Studio[®]. The equivalent circuit simulations were performed using Advanced Design System.

5.1. Wideband Conical Monopole Antenna with 2 C-Shaped Slots

This section presents a new elliptical cone monopole antenna with two C-shaped slots [1]. The monopole antenna is comprised of a conical section, mounted perpendicular to the centre of the ground plane. The band-notch is created by cutting two slots into the surface of the cone. One of the key strengths of the antenna is that it provides very high gain suppression (about 41.5 dB) to the vertical polarization at the notch-band frequency in four specific directions of the vertical polarizations and 11.3 dB of suppression in all directions.

5.1.1. Antenna Design and Structure

Fig. 5.1 illustrates the structure of the antenna. A prototype of the antenna has been machined from solid copper, as shown in Fig. 5.2. Details of the manufacturing process are given in Appendix G. A second, elliptical cone antenna without slots, named as "Reference Antenna", was also fabricated. Table 5.1 gives dimensions of the prototype. The 3-10 GHz, UWB, band has been chosen for the demonstrator for case of manufacture and straightforward comparison with the other numerous UWB notched antennas. However the concept may be useful for other frequencies bands and applications. This elliptical cone shaped antenna is inherently a wide band radiating element having an omni-directional radiation pattern [2], and is therefore will suited for use in wideband systems [3-4]. In this conical antenna the current is distributed evenly around the circumference, so that the slot can couple more strongly than other shapes, particularly planar types in which the current is concentrated along the edge. In addition, the bottom of an elliptical cone is larger than other shapes, such

as a V-shaped cone, which enables the slot to be located closer to the feed-point, to further enhance coupling. The elliptical cone antenna has three parameters, namely the height of the cone, the flare angle, and the distance between the base of the cone and the ground plane. By adjusting these parameters, it is possible to optimize the antenna's radiation pattern and input impedance [3].

(a)

(b)
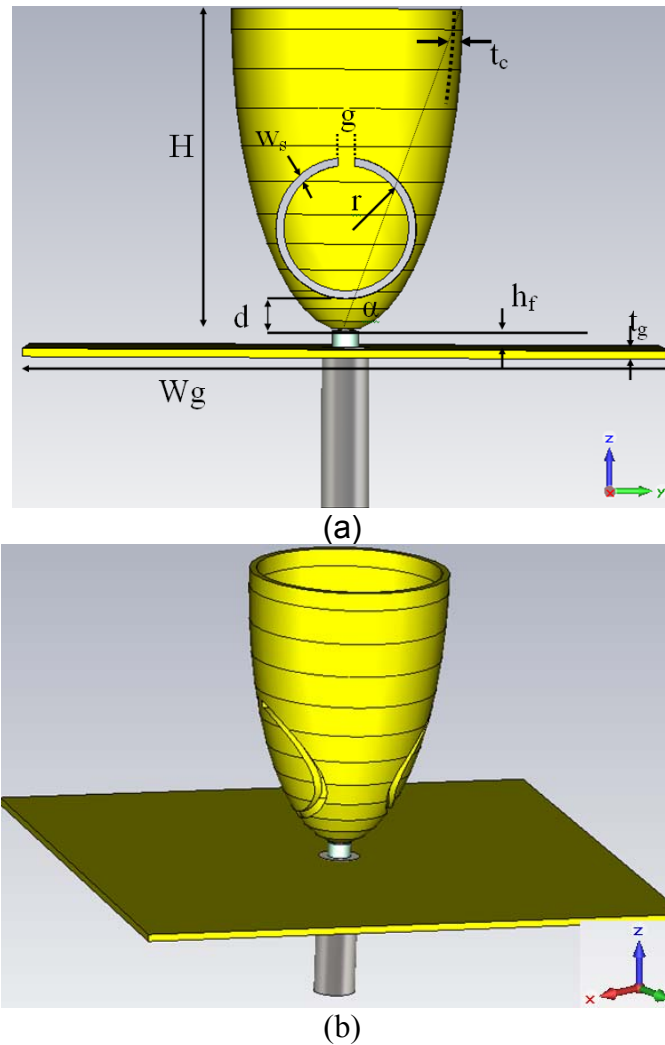
Fig. 5.1 (a) Structure of an elliptical cone antenna incorporating two C-shaped slots; (b) 3D view of the slotted antenna.

Table 5.1 Dimensions for wideband conical antenna with 2 C-shaped slots

H	20.0 mm	g	1.0 mm
w_s	0.5 mm	r	4.4 mm
d	2.0 mm	h_f	1.0 mm
Wg	40.0 mm	t_g	0.5 mm
α	80°	t_c	0.5 mm
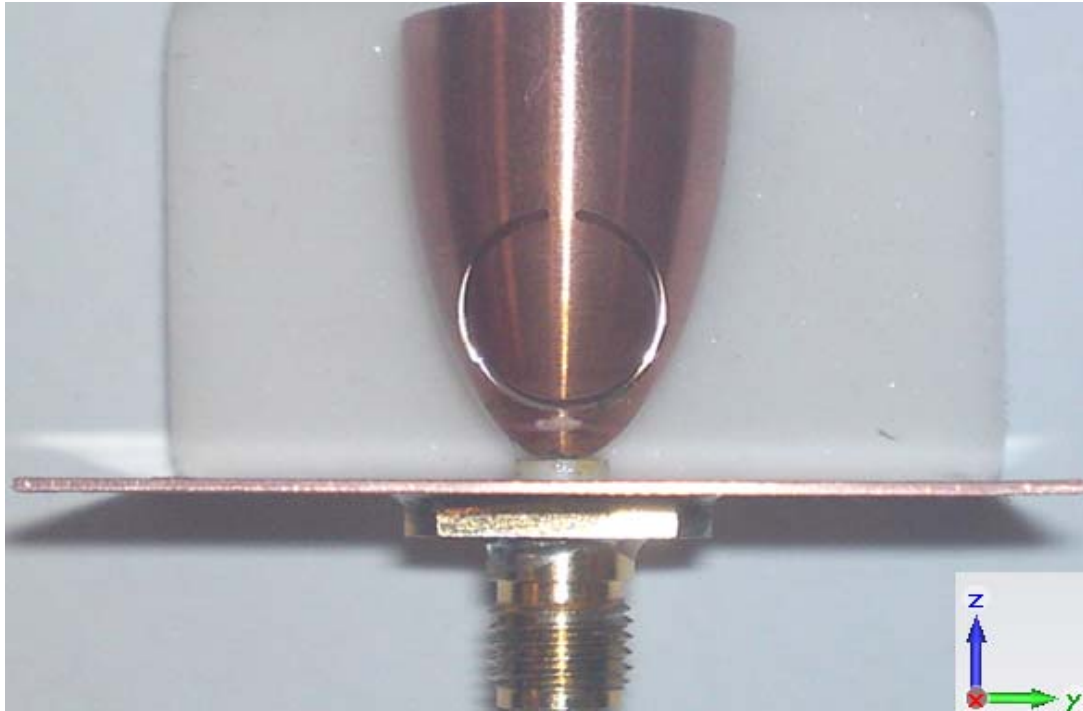
Fig. 5.2 Side view of the completed fabricated prototype.

5.1.2. Simulation and Measurement Results

5.1.2.1. Reflection Coefficient

Simulations were performed using the transient solver in CST Microwave Studio®. Fig. 5.3 shows the measured and simulated reflection coefficient curves for the slotted and reference antennas. In all cases the lowest reflection coefficient at about 10 GHz. For the simulated and measured antennas, the band notches are centred at 5.46 GHz and 5.42 GHz, where the return loss is 0.63 dB and 0.64 dB, respectively. The notch band has a 6 dB return loss bandwidth of 1107 MHz and 810 MHz, respectively. These correspond to quality factors of 4.93 and 6.70. The notch demonstrated here is illustrative of what might be used to suppress either the Hiperlan/2 bands in Europe (5.15-5.35 GHz, 5.470-5.725 GHz) or the IEEE 802.11a band in the U.S. (5.15-5.35 GHz, 5.735-5.825 GHz).

Fig. 5.3 Simulated and measured reflection coefficient for reference and slotted antennas of Fig. 5.1

5.1.2.2. Radiation Patterns

The measured E- and H- plane radiation patterns, for the reference antenna are presented in Fig. 5.4. These patterns were measured at 4 GHz, 8 GHz and 10 GHz. From Fig. 5.4, it is obvious that the elliptical cone antenna has a very stable omni-direction pattern even at high frequency, i.e. 10 GHz. Table 5.2 shows the values of the standard deviation from omni-directional, for the reference antenna, are 0.23 dB, 0.50 dB and 1.14 dB at 4 GHz, 8 GHz and 10 GHz, respectively.

Fig. 5.4 Measured normalised radiation patterns for the reference antenna at three different frequencies: (a) E-(zy-) plane, 4 GHz; (b) H- (xy-) plane, 4 GHz; (c) E-(zy-) plane, 8 GHz; (d) H- (xy-) plane, 8 GHz; (e) E- (zy-) plane, 10 GHz; (f) H-(xy-) plane, 10 GHz.

Frequency [GHz]	Standard deviation from Omni-directional (dB)
4	0.23
8	0.50
10	1.14

Table 5.2 Standard deviation in dB from omni-directional for the reference antenna at 4, 8 and 10 GHz

Fig. 5.5 shows simulated and measured radiation patterns for the antenna at 5.41 GHz in H-(xy) plane. There is a good agreement between the simulated and measured radiation patterns. The vertically polarized (co-polarisation or z directed) radiation pattern has two main lobes in the 0˚ and 180˚ positions with minor lobes in-between. The main lobes directions correspond to the centres of the C-shaped slots. There are also four nulls in the radiation pattern, which coincide with the directions of the sides of the slots. These nulls can be used to increase the gain suppression in the vertical polarization by placing them in the direction of known interfering signals. This would require mechanical rotation if the interference direction is dynamic, or appropriate mounting if the direction is fixed. For operation in a multipath environment, where interference may arrive at the antenna from multiple directions, suppression will be closer to the peak pattern levels. The frequency shown in the Fig. 5.5 is slightly different from the notch band centre frequency, because the nulls are quite sensitive to the frequency and the deepest nulls were slightly shifted away from the centre notch frequency.
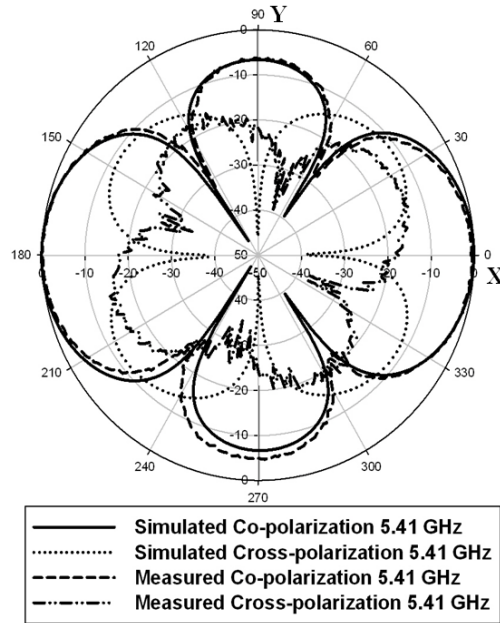
Fig. 5.5 Simulated and measured normalized radiation patterns in H-(xy-) plane for the elliptical cone antenna with two C-shaped slots.

The measured E-(zy) and H-(xy) planes patterns for other frequencies are presented in Fig. 5.6. It is shown that the proposed antenna has an omni-direction pattern in the vertical polarisation even at high frequencies such as 10 GHz. Table 5.3 shows the values of the standard deviation from omni-directional, for the slotted antenna, are 0.27 dB, 0.44 dB and 1.16 dB at 4 GHz, 8 GHz and 10 GHz, respectively. The large cross-polarisation, shown in Fig. 5.6, is due to relatively small square ground plane and can be reduced by a larger square ground plane or a circular ground. The reason for this is that the current return path for the antenna with the circular ground plane has the same length compared to the antenna with a square ground plane. Fig. 5.7 shows the pattern comparison between the slotted antennas incorporating a 40×40 mm2 square ground plane and a circular ground plane with 40 mm diameter at 10 GHz. It is clear that using a circular ground can reduce the cross-polarization by at least 10 dB.

- 141 -
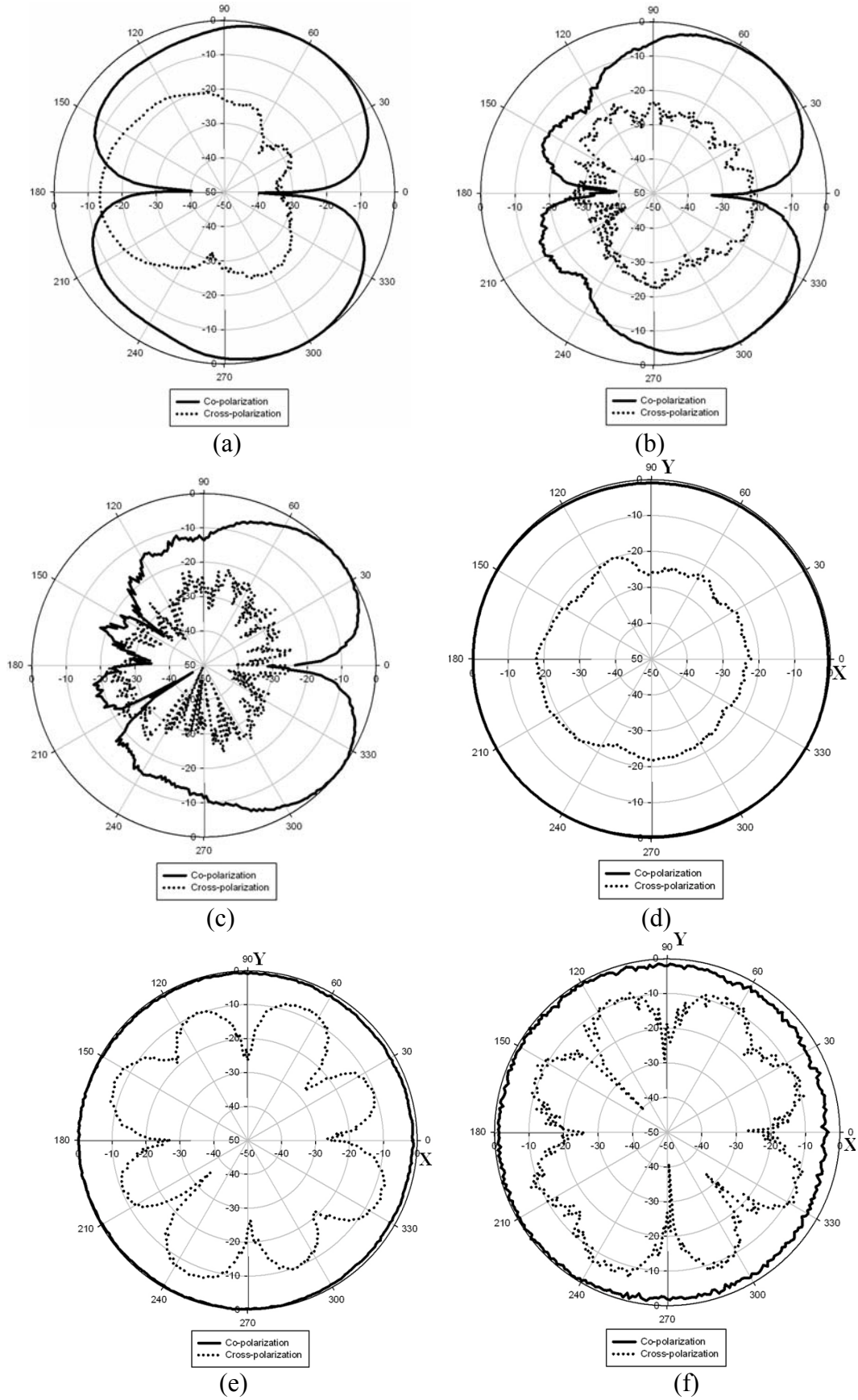
Fig. 5.6 Measured normalized radiation patterns for the elliptical cone antenna with two C-shaped slots at other three different frequencies: (a) E- (zy-) plane 4GHz; (b) E- (zy-) plane 8 GHz; (c) E- (zy-) plane 10 GHz; (d) H- (xy-) plane 4 GHz; (e) H- (xy-) plane 8 GHz; (f) H-(xy-) plane 10 GHz

Frequency [GHz]	Standard deviation from Omni-directional (dB)
4	0.27
8	0.44
10	1.16

Table 5.3 Standard deviation in dB from omni-directional for the elliptical cone antenna with two C-shaped slots at 4, 8 and 10 GHz
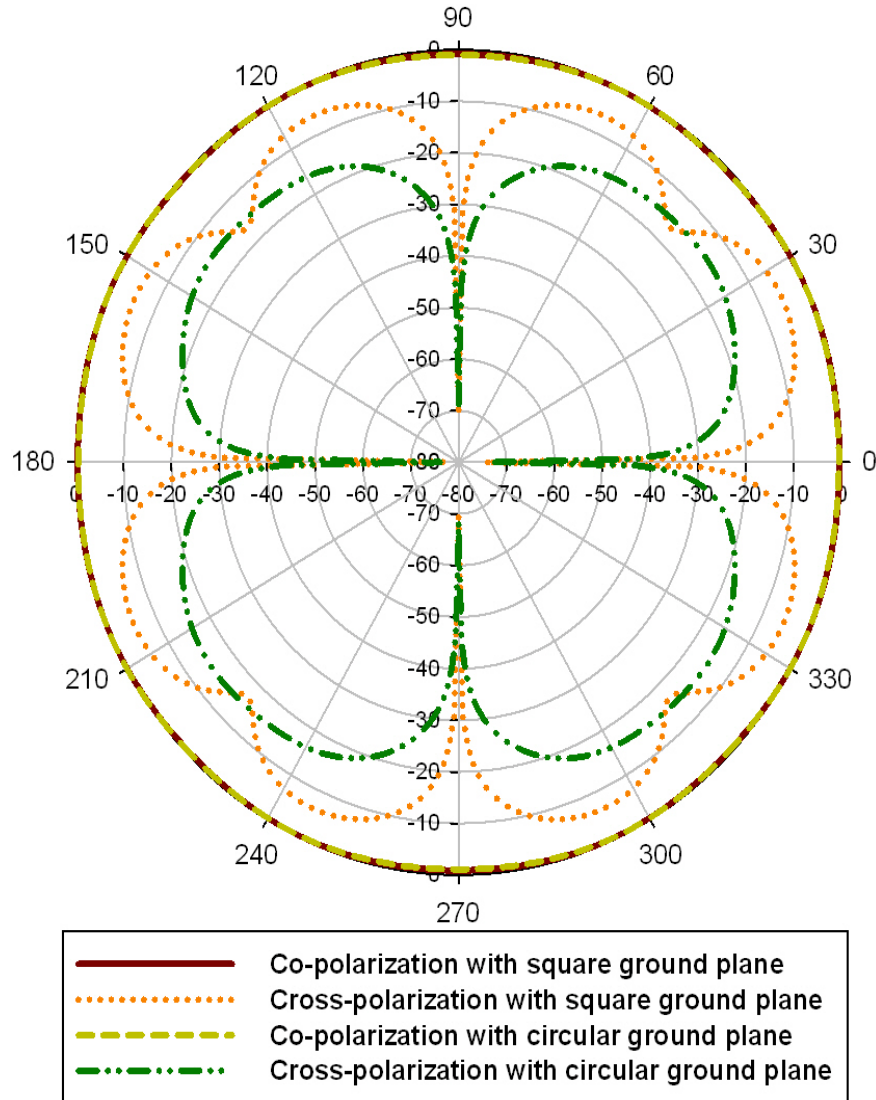
Fig. 5.7 Simulated normalized H- (xy-) plane radiation patterns for the slotted antenna at 10 GHz, incorporating a 40×40 mm^2 square ground plane and a circular ground plane with 40 mm diameter, respectively

5.1.2.3. Surface Current Analysis

Fig. 5.8 plots the average surface current distribution for the slotted antenna at two

different frequencies. The first frequency coincides with the centre of the notch-band

(5.456 GHz) and the second corresponds to the lowest reflection coefficient (10.784 GHz). In Fig. 5.8(a), it is clear that at the notch band centre frequency, the current is most heavily concentrated around the C-shaped slots. There is almost no current flow on the surface of the elliptical cone, as expected, compared to the current at the lowest reflection coefficient in Fig. 5.8(b). These surface currents are calculated directly from the magnetic fields in CST Microwave Studio®. Analysis of simplified equivalent current sources associated with the slot edge currents will be analysed in the next section.

(a)   (b)
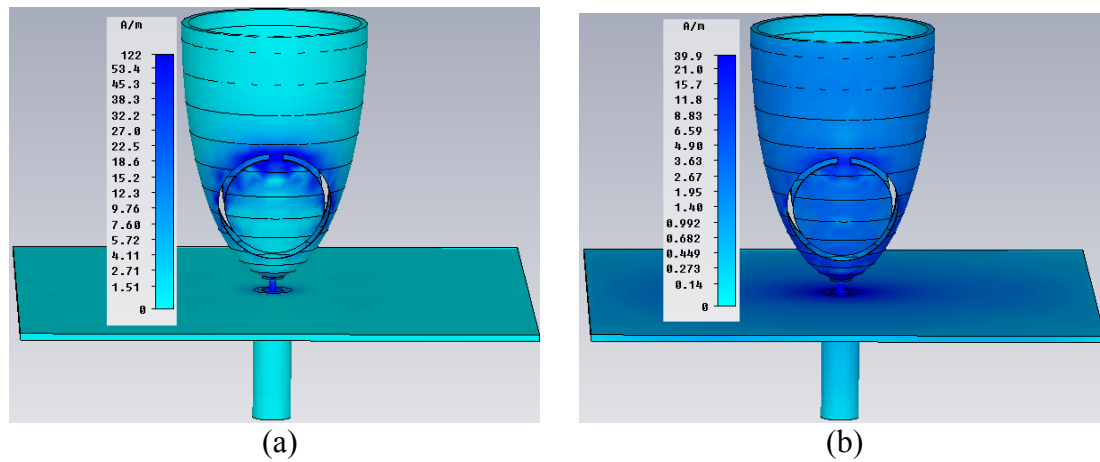
Fig. 5.8 Average surface current distribution for elliptical cone antenna with two C-shaped slots at (a) centre of the notch band 5.456 GHz; (b) lowest reflection coefficient 10.784 GHz.

5.1.2.4. Equivalent Current Sources Study

In extraction current sources, because we are interested in the vertically polarised patterns, vertical currents are of interest. Extraction of the surface currents on the antenna and ground plane, at 5.41 GHz, indicated that presence of strong currents on the top of the slots, and on the ground plane edges. Fig. 5.9 shows surface current on the antenna and the relative locations of these current concentrations. To enable a first order analysis of the likely radiation pattern of these current sources, it is assumed

that firstly there are strong vertical components of the currents at these locations, either across the metal bridge at the top of the C slots, or on the ground plane edge, and that secondly that the currents are of equal magnitude. A simple array analysis using the equation [5] as below:

$$AF = \sum_{n=1}^{N} I_{1n} \left[\sum^{M} I_{m1} e^{j(m-1)(kd_x \sin\theta \cos\phi + \beta_x)} \right] e^{j(n-1)(kd_y \sin\theta \sin\phi + \beta_y)} \qquad (5.1)$$

in which, m=2 and n=4 in the x and y directions with distances d_x=15mm and d_y=20mm. ϕ has a range from 0˚ to 360˚ and θ is fixed at 90˚. Both values of phase shift (i.e. β_x and β_y) are 0. This simple array analysis which assumes isotropic element patterns gives the radiation pattern shown in Fig. 5.10, compared to the simulated pattern in CST (Calculation details and Matlab code are given in Appendix C). Several conclusions can be drawn from this simplified analysis. Firstly the deep nulls at the notch frequency are due to the interaction of sources both on the cone and ground plane. This means that changes in the ground plane may affect the null depth, and in particular the use of the cone on a very large ground plane, such as a metallic vehicle might result in reduced null depth. For example, simulation shows when using a 80x80 mm^2 square ground plane, the current concentration on the ground plane is changed and getting smaller, as shown in Fig. 5.11. CST Array Tools, shown in Fig. 5.12 (details can be referred to Appendix C), has been used to analyse the current sources. Fig. 5.13 shows the simulated co-polarisation radiation pattern for the slotted antenna of Fig. 5.1 with 80 mm × 80 mm ground plane and the equivalent current sources as shown in Fig. 5.11. The simulation shows that the null depth is reduced by 18 dB compared to the one with size of 40x40 mm^2, as shown in Fig. 5.13. Secondly the application of this method to horizontally polarized patterns was not immediately successful, due, it is assumed to the more complex behaviour of the horizontally

oriented current sources. Additional simulations indicate that the nulls become

unstable or disappear if using more than two C-shaped slots or other shaped slots.
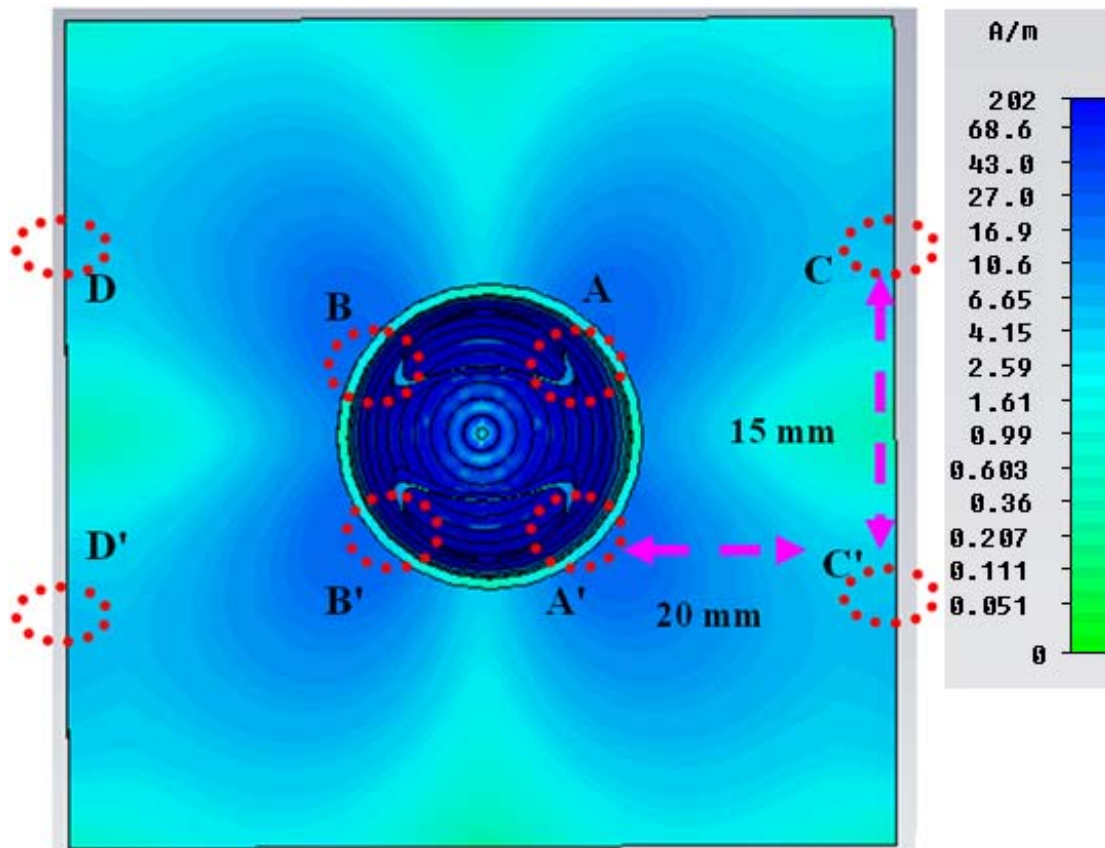
Fig. 5.9 Surface current plot and relative locations of current concentration on the cone and ground plane (ground plane size: 40 mm × 40 mm)
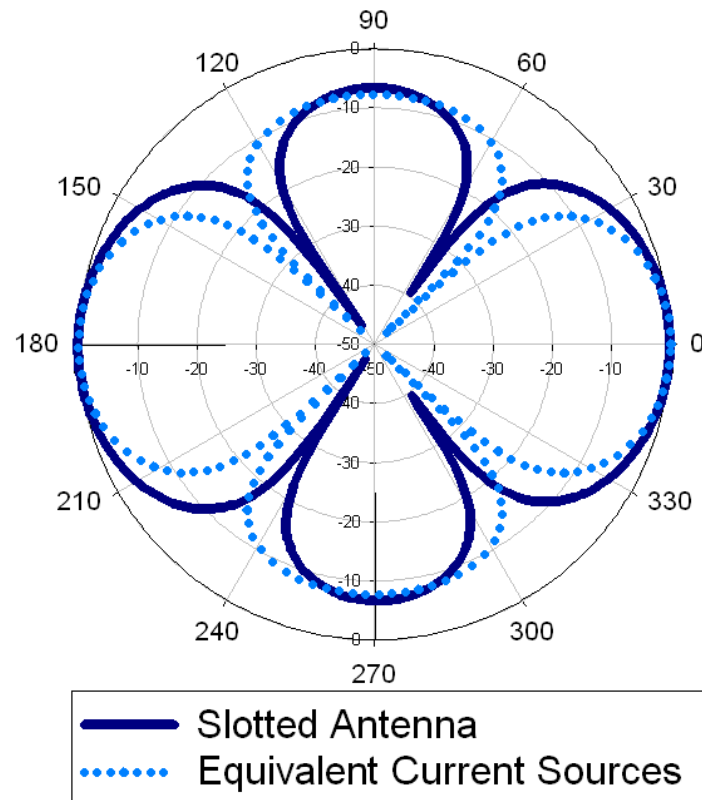
Fig. 5.10 Simulated co-polarisation radiation pattern for the slotted antenna of Fig. 5.1 and the equivalent current sources
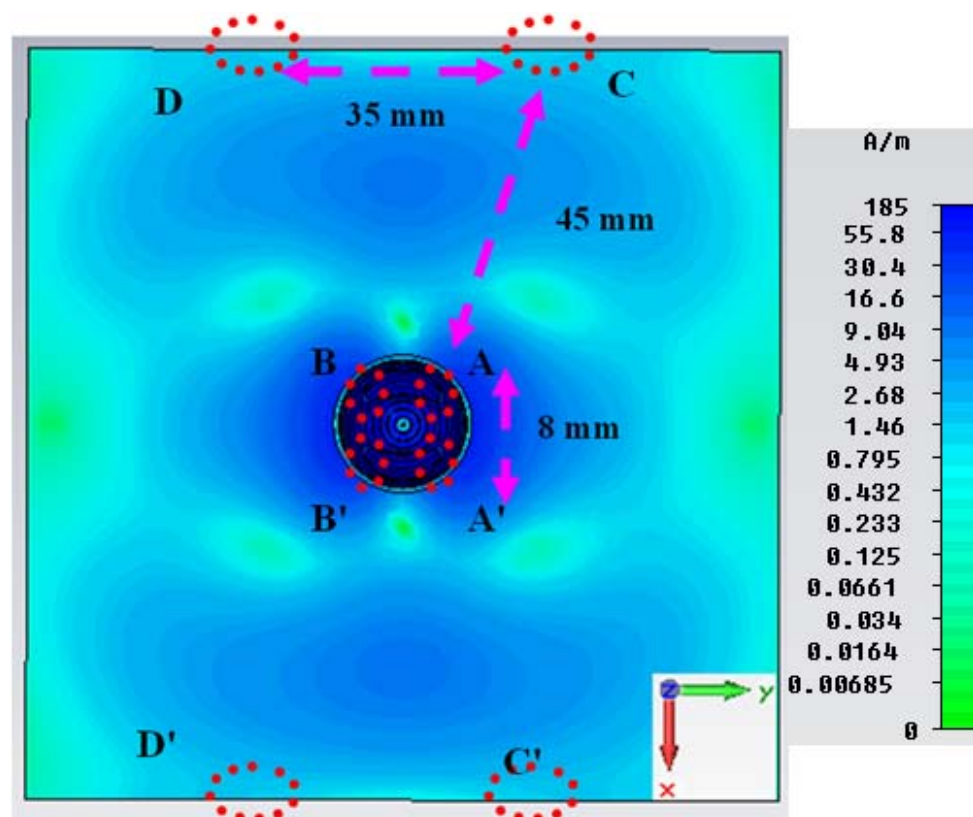
Fig. 5.11 Surface current plot and relative locations of current concentration on the cone and ground plane (ground plane size: 80 mm × 80 mm)

Fig. 5.12 CST Array Tool parameters setting
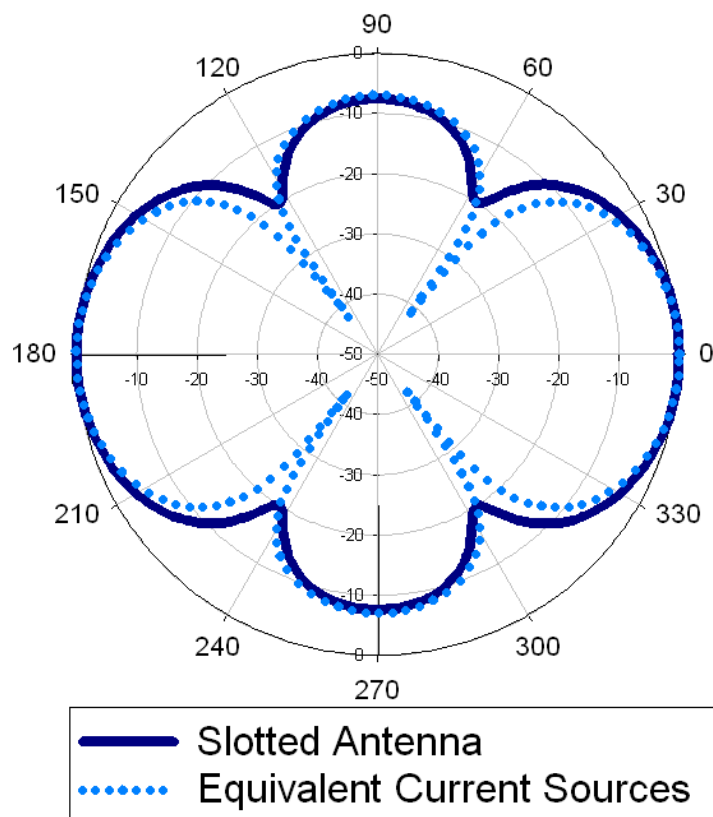
Fig. 5.13 Simulated co-polarisation radiation pattern for the slotted antenna of Fig. 5.1 with 80mm × 80mm ground plane and the equivalent current sources as shown in Fig. 5.11

5.1.2.5. Gain Suppression

Fig. 5.14 shows the simulated total efficiency for the reference and slotted antennas. Over the operating frequency band, the total efficiency for the reference antenna is greater than -0.7 dB. The lowest total efficiency for the slotted antenna is -12.6 dB at 5.43 GHz, which is close to the simulated notch centre frequency 5.46 GHz. Such low total efficiency shows that the slotted antenna can provide good average gain suppression for the notch band in all directions. Fig. 5.15 shows the measured power gain in dBi, in the azimuthal (xy-) plane, for the slotted and reference antenna. At the frequency of the band notch, the gain of the reference antenna is about 0.6 dBi. For a conventional monopole, a higher gain might be expected. Such a low gain is due to the small ground plane used and the fact that the maximum directivity is not in the H-(xy-) plane. In the direction of the main lobe, shown in Fig. 5.5, (+x, or $\phi = 0°$), the gain is reduced to -10.7 dBi, giving a gain suppression of 11.3 dB. In the direction of the lowest null (i.e. $\phi = 123°$), the vertically polarized gain is -40.9 dBi, giving 41.5 dB of gain suppression in that direction.
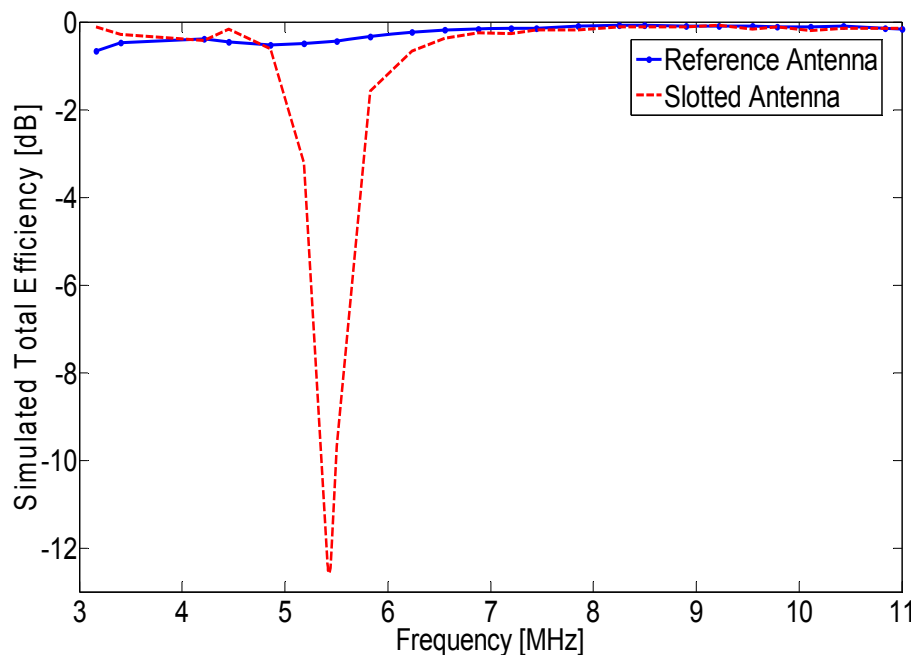
Fig. 5.14 Simulated total efficiency for the slotted and reference antennas
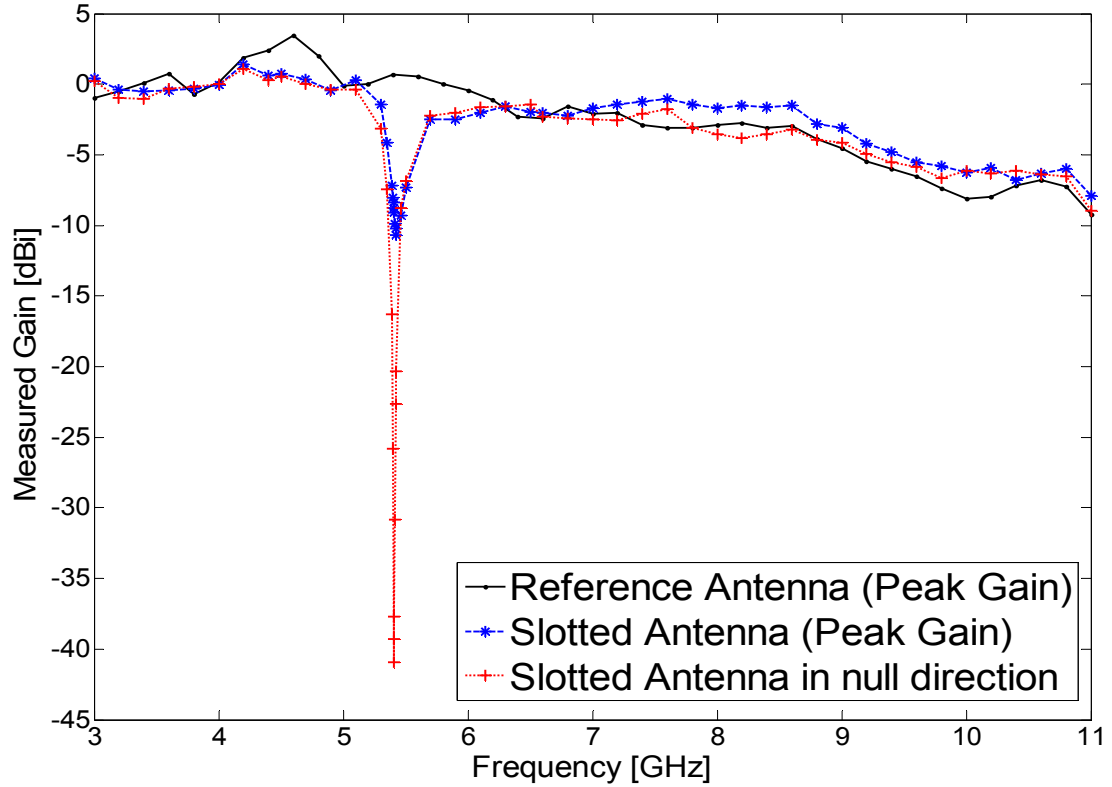
Fig. 5.15 Measured vertically polarized power gain for the slotted and reference antennas in H- (xy-) plane polarisation

5.1.3. Slot Design for Other Notch Frequencies

The slot is approximately half-a-wavelength long at the stop band frequency, and increasing the slot length will reduce the notch frequency. In order to establish whether the proposed antenna can provide good gain suppression at other frequencies, the relationship between the size of the slot and interference suppression has been studied.

To change the resonant frequency, the radius, r, of the slot is changed from 4.4 mm to r =3.0 and 5.2 mm and compared to the antenna in the previous section. Fig. 5.16 shows the simulated return loss for these cases. These slot sizes provide notch band centre frequencies of 4.46 GHz, 5.46 GHz and 8.04 GHz with return loss of -0.6 dB, -

0.6 dB and -2.1 dB at the notch resonant frequencies respectively for r = 5.2, 4.4 and 3.0 mm. The notch bands have a 3 dB return loss bandwidth of 854 MHz, 527 MHz and 240 MHz respectively. These values correspond to quality factors of 5.2, 10.4 and 33.5 respectively. In each case the length of the slot is approximately half-a-wavelength at the band-notch centre frequency. The larger the radius of the C-shaped slot, the lower the notch band centre frequency and larger the quality factor.
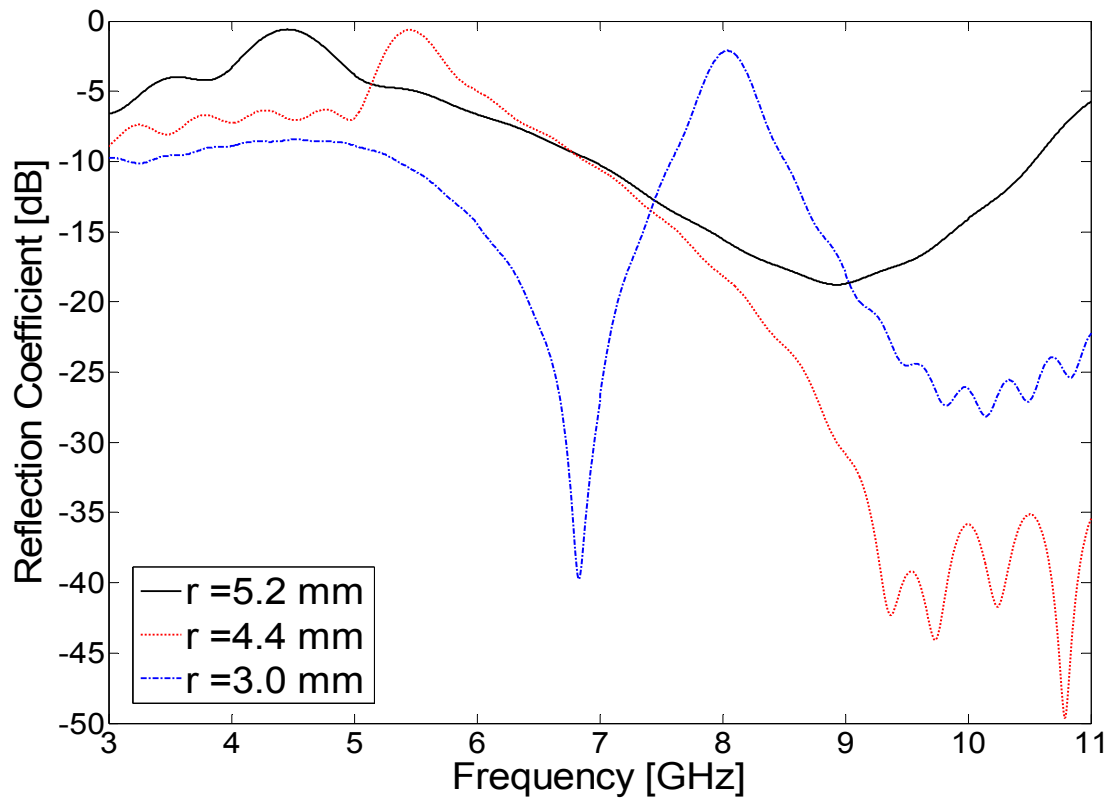
Fig. 5.16 Simulated return loss for the elliptical cone antenna with different radius of C-shaped slots, i.e. r =4.4 mm, r =5.2 mm, and r = 3.0 mm.

Fig. 5.17 shows the H- (xy-) plane co-polar radiation pattern for the antenna with different slot radii at their resonant frequencies, 4.46 GHz, 5.41 GHz and 8.02 GHz respectively. The frequencies shown in Fig. 5.17 are slightly different from the notch band centre frequencies shown in Fig. 5.16, because the nulls are quite sensitive to frequency and the deepest nulls were slightly shifted away from the centred notch frequency, as mentioned earlier. From Fig. 5.17, it is clear that the main lobes point in

the locations of two slots while the minor lobes occur between them. The figure also

shows how the slot size changes the depth of gain suppression. Although the nulls

disappear when r = 5.2 mm, due to the distance between current concentrations of

points A and B, in Fig. 7, is getting closer, there is a significant gain suppression

improvement, about 18 dB less gain, in the directions of the minor lobes (i.e.

$\phi = 90°$ and $\phi = 270°$). An adjustment to the shape of slot, i.e. elliptical shaped, may be

possible for maintaining the four nulls in H plane.
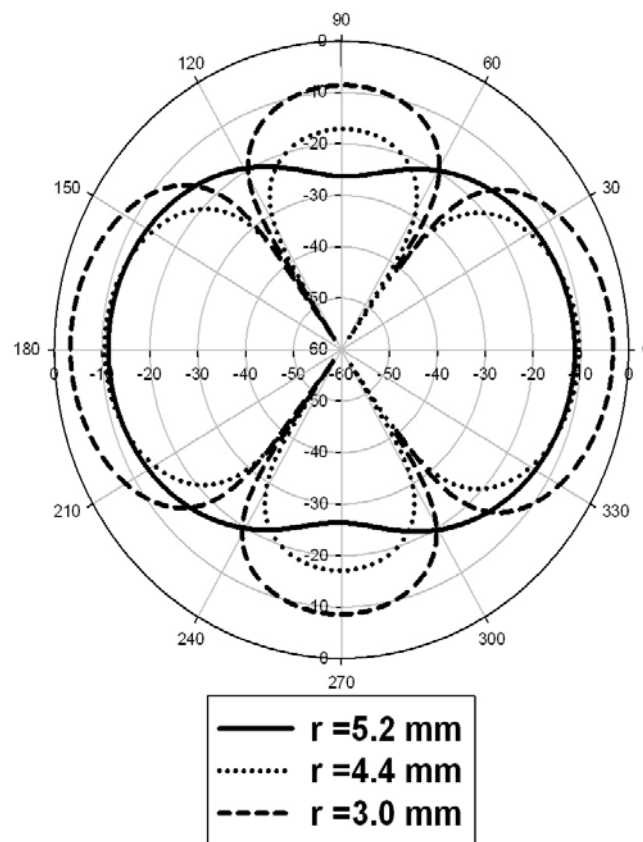
Fig. 5.17 Simulated co-polarisation radiation patterns in H- (xy-) plane for the elliptical cone antenna with different radius of C-shaped slots, i.e. r=5.2 mm at 4.456 GHz; r = 4.4 mm at 5.41 GHz; and r=3.0 mm at 8.018 GHz.

5.1.4. Antenna with Rotated C-Shaped Slots

In addition to rotation of the antenna, the notch band null directions can also be

moved by changing the inclination of the slots as shown in Fig. 5.18. Such an

inclination change could be implemented with switches located around the periphery of a continuous slot [6]. Whilst this has not been done here, simulations are used to demonstrate the effect. Fig. 5.18 shows the gap in the C-shaped slot inclined to an angle of Ω degrees. In all other respects these antennas are identical to that shown in Fig. 5.1(a). Six angles, 0˚, 30˚, 45˚, 60˚, 90˚ and 180˚ are simulated. Both slots are rotated in the same direction viewed from the front of each slot. Fig. 5.19 shows the simulated return loss curves for each case. The notch band centre frequencies for those antennas are 5.46 GHz, 5.55 GHz, 5.58 GHz, 5.58 GHz, 5.34 GHz and 4.38 GHz, respectively. Rotating the slot from just 0˚ to 90˚ alters the notch band centre frequency slightly, at most 2.2% shift. However, rotation by 180˚ gives a large shift and about 19.8% change.
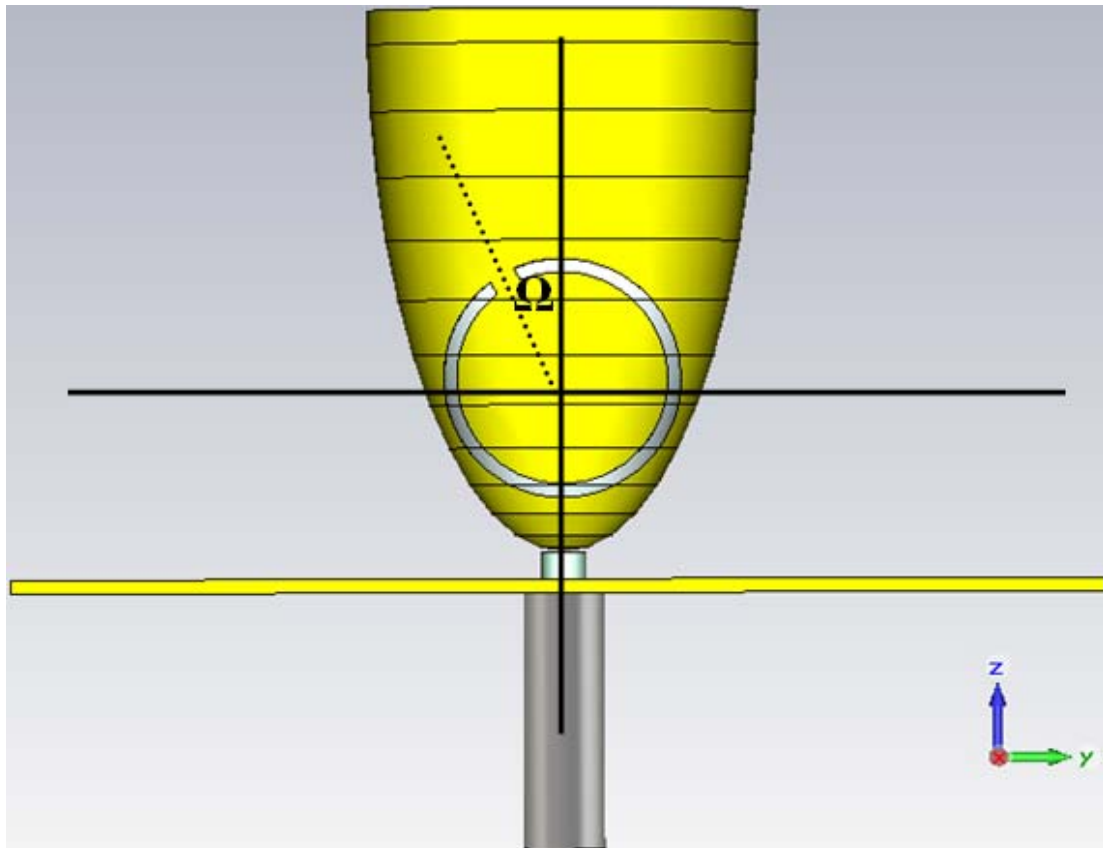
Fig. 5.18 The structure of the elliptical cone antenna with 2 C-shaped slots and the gap shifted with an angle of Ω.
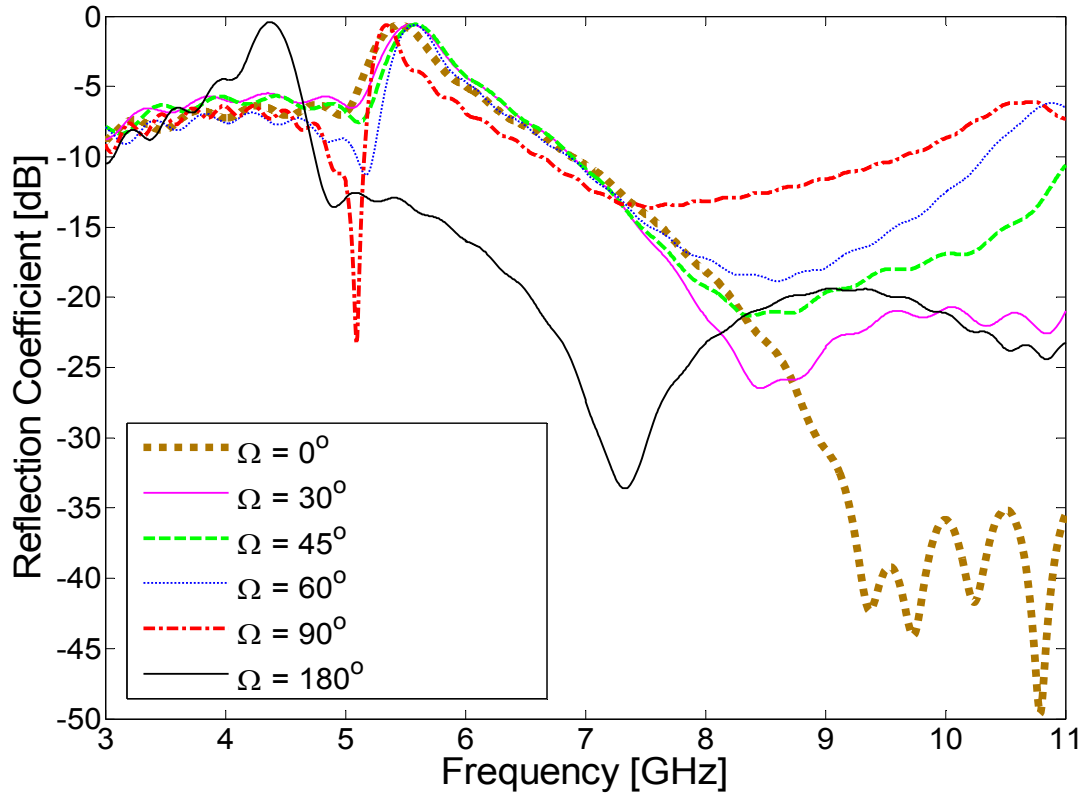
Fig. 5.19 Simulated return loss curve for the structure of the elliptical cone antenna with rotated 2 C-shaped slots as shown in Fig. 5.18.

Fig. 5.20 shows the simulated normalized radiation patterns in the H- (xy) plane for those antennas. From these results it is clear that rotating the C-shaped slot from 0° to 90°, rotates the direction of the radiation pattern nulls. When Ω is rotated from -90° to 90°, the first null can be rotated from 0° to 87°, as shown in Table 5.4. Thus, as there are four nulls in the pattern one can be placed anywhere in the range 0° to 360°. However, when the C-shaped slot is rotated to 180°, the pattern becomes almost omni-directional, as shown in Fig. 5.20.
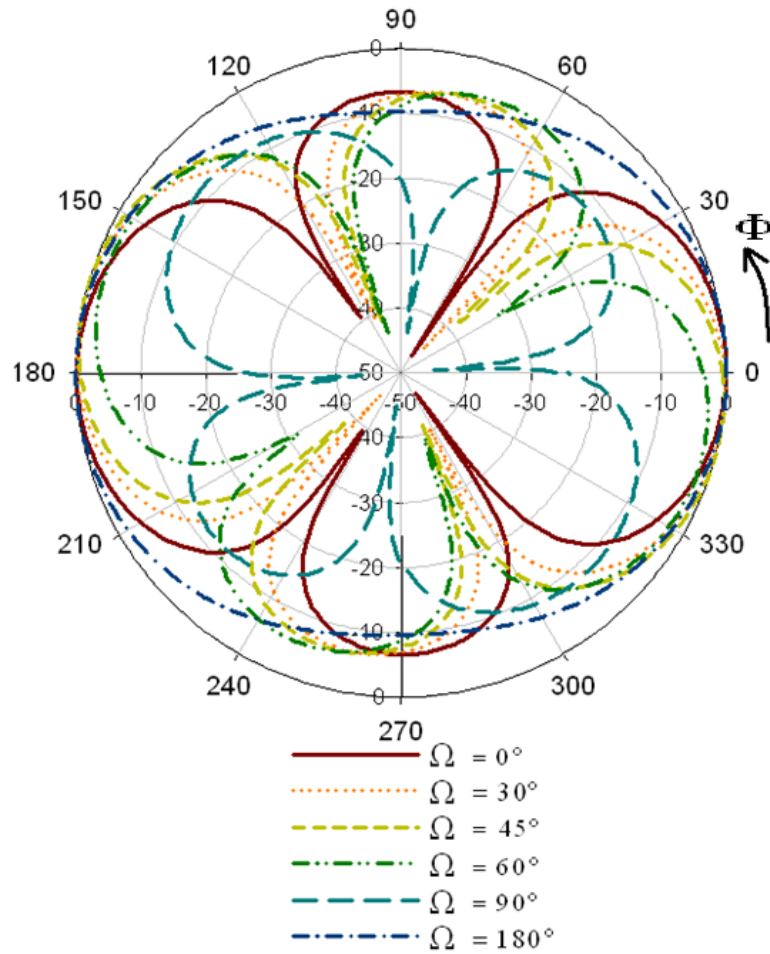
Fig. 5.20 Simulated normalized radiation patterns in H- (xy-) plane for the elliptical cone antenna with 2 C-shaped slots and the C-shaped slot rotates to different angular positions.

Rotation Angle Ω	-90°	-60°	-45°	-30°	0°	30°	45°	60°	90°
Null Angles Φ	87°	60°	49°	44°	34°	25°	20°	18°	0°

Table 5.4 The first null with angle Φ in the vertical polarisation vs. rotation angle Ω

5.2. Wideband Conical Antenna with 4 C-Shaped Slots

This section presents a wideband conical antenna with 4 C-shaped slots to achieve improved band-rejection behaviour with at least 28 dB of gain suppression [7]. The antenna also provides an omni-directional radiation pattern at frequencies within the operating band.

5.2.1. Antenna Design and Structure

Fig. 5.21 illustrates the structure of the antenna. The antenna dimensions are shown in Table 5.5. The close spacing (about 0.7 mm) between each C-shaped slot is significant as it ensures that the slots intercept as much of the current on the cone as possible. As seen in Fig. 5.21(a), the connector and attached cable were represented by an equivalent coax of length 10 mm, in the simulation.

(a)

(b)
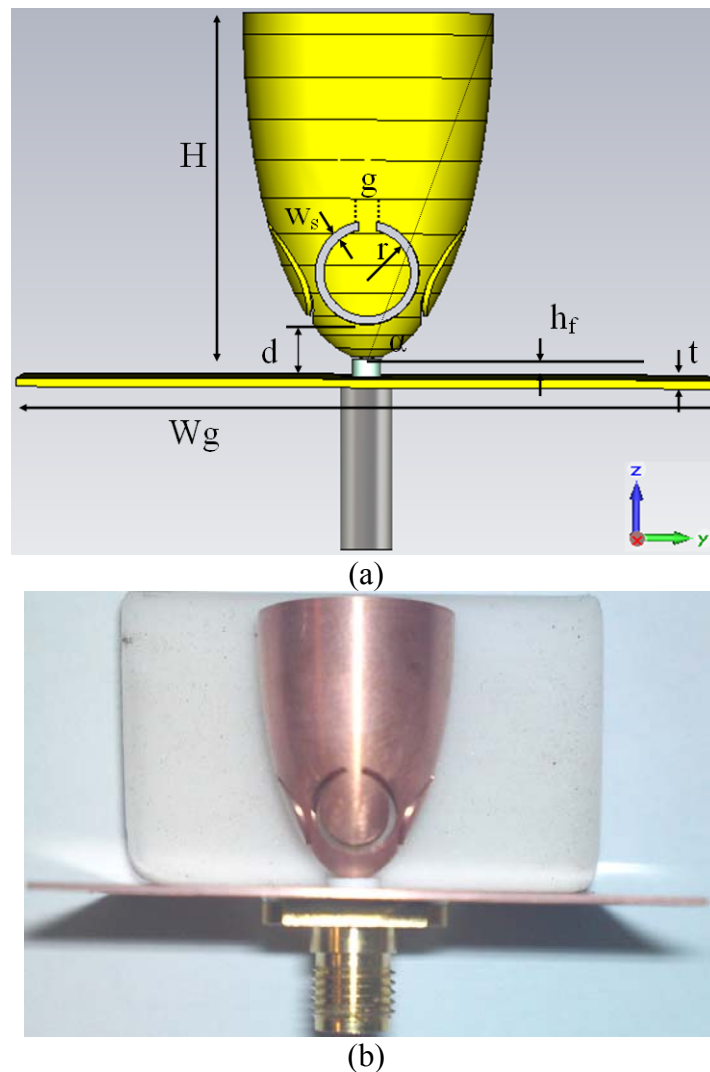
Fig. 5.21 (a) Structure of elliptical cone antenna incorporating four C-shaped slots; (b) side view of the fabricated prototype

H	20.0 mm	g	1.0 mm
w_s	0.5 mm	r	3.0 mm
d	2.0 mm	h_f	1.0 mm
Wg	40.0 mm	t	0.5 mm
α	80˚	-	-

Table 5.5 Dimensions for the antennas shown in Fig. 5.21

5.2.2. Simulation and Measurement Results

5.2.2.1. Reflection Coefficient

Fig. 5.22 shows simulated and measured return loss curves for the slotted and reference antenna. There is a frequency shift of 0.681 GHz between the location of the band notch obtained through simulation (8.024 GHz) and measurement (8.705 GHz). This slight discrepancy can be attributed to manufacturing tolerances. For these two cases the return loss at the band notch centre frequency is 0.10 and 0.31 dB, respectively. The notch band has a 6 dB return loss bandwidth of 1560 MHz for the prototype. This corresponds to a relatively low quality factor 5.58.
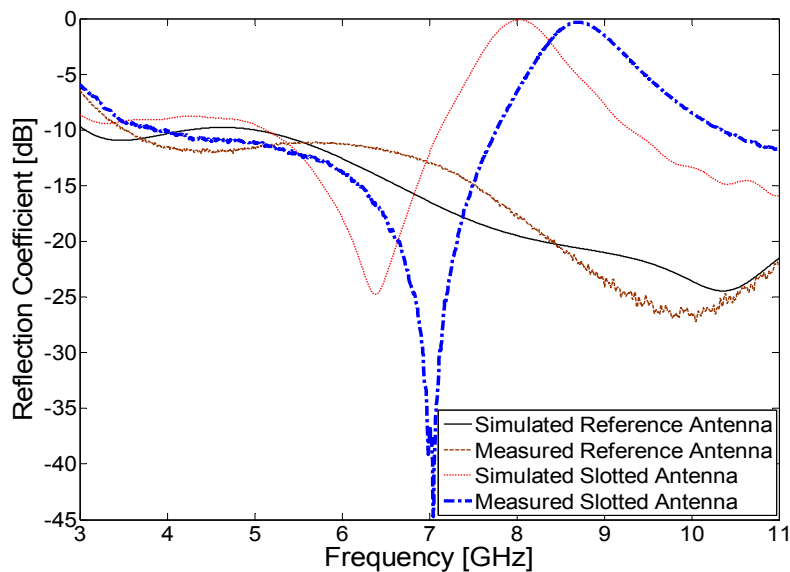
Fig. 5.22 Simulated and measured reflection coefficient for reference and slotted antennas (shown in Fig. 5.21)

5.2.2.2. Radiation Patterns

Fig. 5.23 illustrates the simulated and measured radiation patterns for the slotted antenna at 7.999 GHz and 8.669 GHz in H-(xy-) plane. The discrepancies on both simulated and measured radiation patterns are due to manufacturing tolerances. In the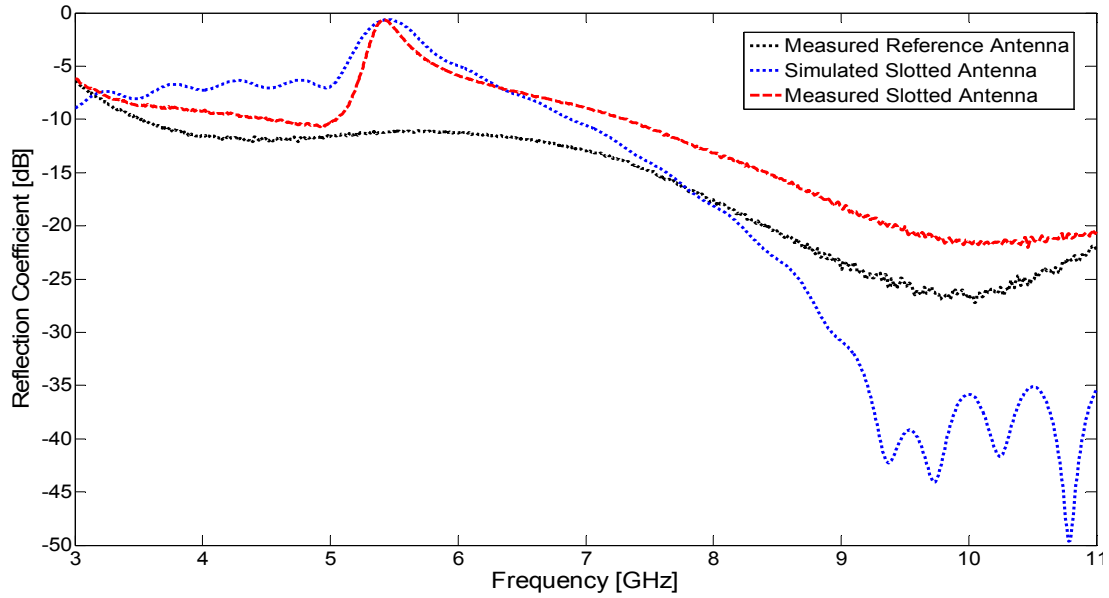 simulated radiation pattern, the pattern has eight lobes in the 0°, 47°, 91°, 135°, 182°, 225°, 271° and 317° positions. The lobes correspond to the locations of the C-shaped slots and also the gap between each slot. There are also eight nulls in the pattern, which coincide with the sides of the slots. These nulls can be used to increase the gain suppression by placing them in the direction of interfering signals. However, in the measurement, the fabricated slotted antenna only showed three nulls (shown in Fig. 5.23), that might be due to manufacturing tolerances. Those nulls in the patterns are can be explained in section 5.1.2.4, which explain the well-defined patterns are because the current sources from the slots and the ground plane.
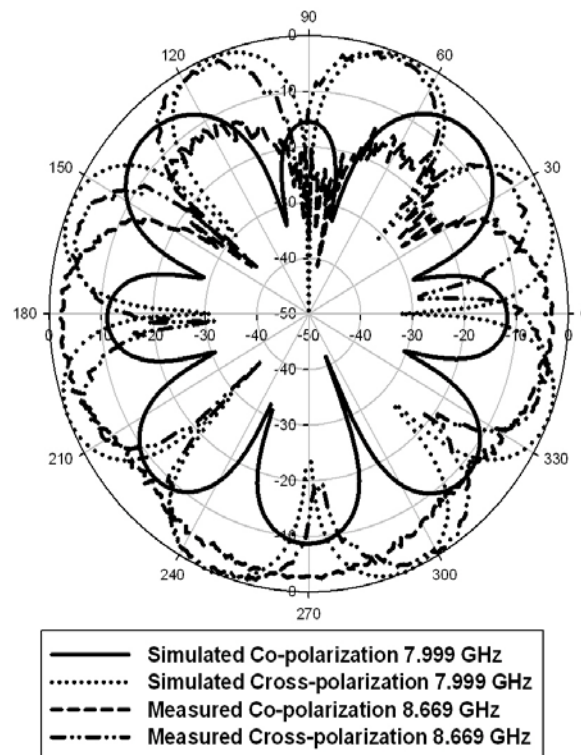
Fig. 5.23 Simulated and Measured normalized radiation patterns in H-(xy-) plane for the elliptical cone antenna with four C-shaped slots

Fig. 5.24 shows measured E-(zy) and H-(xy) plane radiation patterns for the slotted antenna at various different frequencies (i.e. 4 GHz, 8 GHz and 10 GHz). From Fig. 5.24, it is obvious that the elliptical cone antenna has a very stable omni-direction pattern even at high frequency, i.e. 10 GHz. Table 5.6 shows the values of the standard deviation from omni-directional, for the slotted antenna, are 0.16 dB, 0.49 dB and 0.63 dB at 4 GHz, 8 GHz and 10 GHz, respectively.
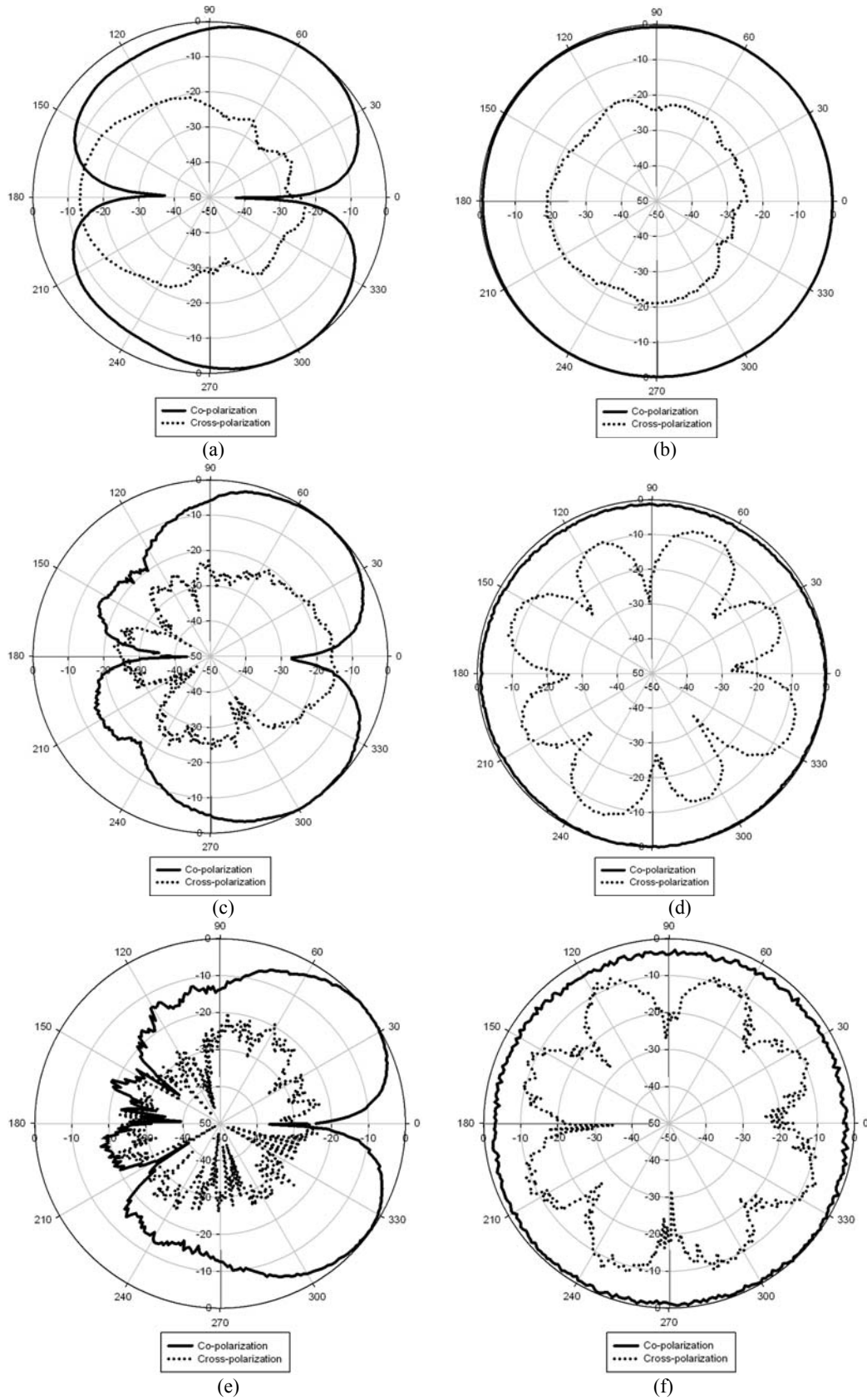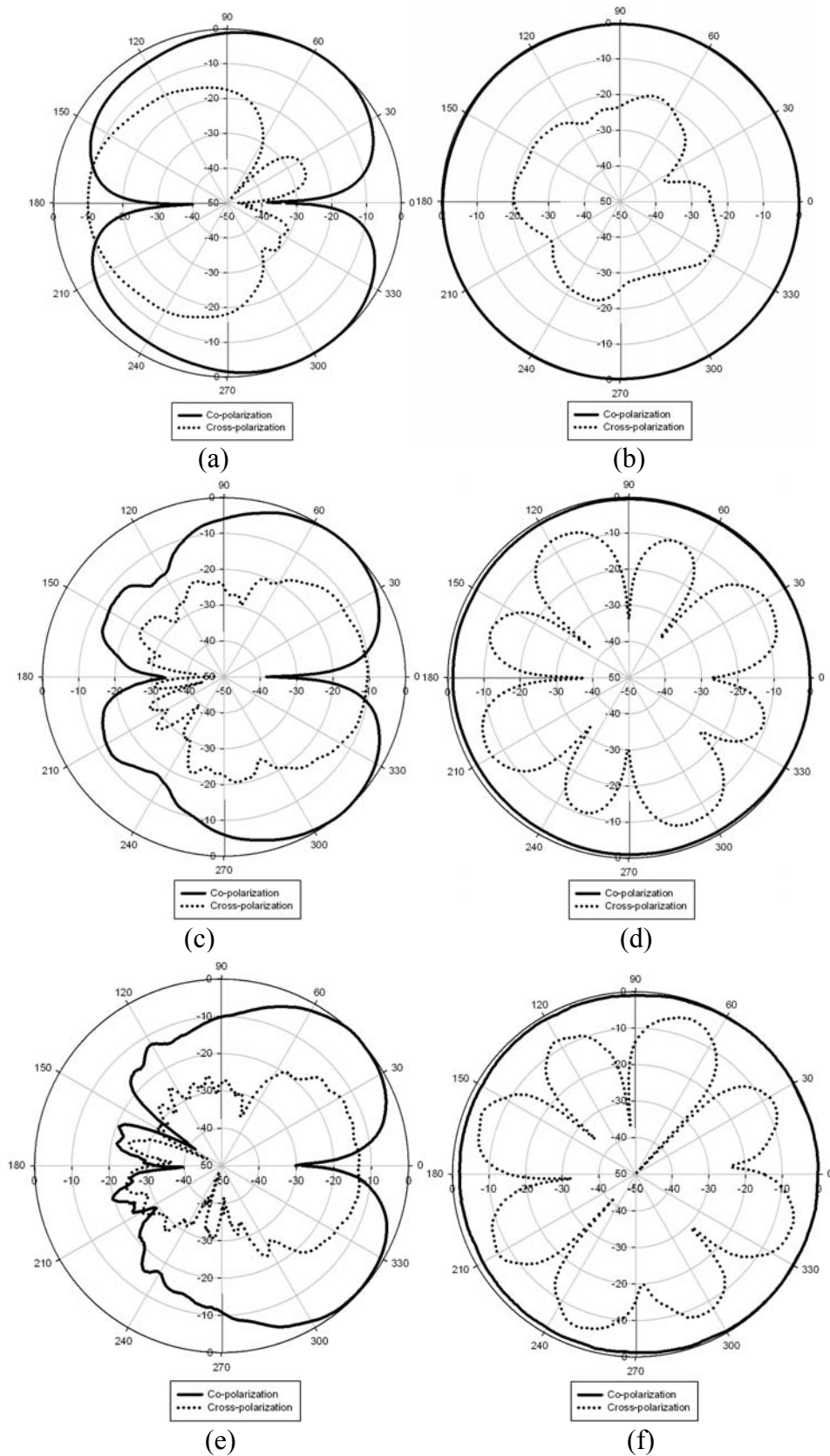
Fig. 5.24 Measured normalized radiation patterns for the elliptical cone antenna with 4 C-shaped slots at four different frequencies: (a) E- (zy-) plane, 4 GHz; (b) H- (xy-) plane, 4 GHz; (c) E- (zy-) plane, 8 GHz; (d) H- (xy-) plane, 8 GHz; (e) E- (zy-) plane, 10 GHz; (f) H- (xy-) plane, 10 GHz.

Frequency [GHz]	Standard deviation from Omni-directional (dB)
4	0.16
8	0.49
10	0.63

Table 5.6 Standard deviation in dB from omni-directional for the elliptical cone antenna with four C-shaped slots at 4, 8 and 10 GHz

5.2.2.3. Gain Suppression

Fig. 5.25 plots measured peak gain, in the azimuthal (xy) plane, for the slotted and reference antenna. In the operating frequency band, the total efficiency for the reference antenna is at least -0.09 dB. The lowest total efficiency for the slotted antenna is -28.30 dB at 8.020 GHz, which is close to the simulated notch centre frequency 8.024 GHz. Such low total efficiency shows that the slotted antenna can provide good average gain suppression for the notch band in all directions. At the frequency of the band notch, the gain of the reference antenna is about 3.45 dBi. The average value of the peak gain is about -2 dBi to -3 dBi over most of the operating band (from 1 dBi to -10 dBi). Please note that such a low gain is due to the small ground plane used and the fact that the maximum directivity is not in the H-(xy-) plane, as mentioned in the previous section. At the notched band in the direction of the main lobe of Fig. 5.23 (-x, or $\phi = 180°$), the antenna gain is reduced to -32.24 dBi. Compared to the peak gain of the reference antenna, the proposed antenna therefore has about 28.8 dB of gain suppression.
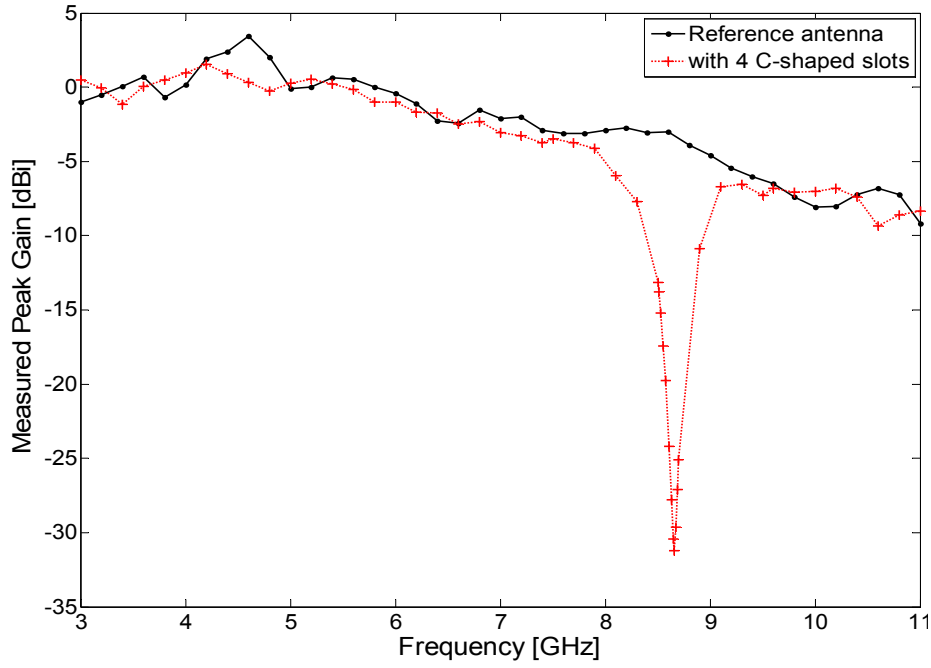
Fig. 5.25 Measured vertically polarized peak gain for the slotted and reference antennas

5.2.3. Effect of Flare Angle

5.2.3.1. Antenna Structure

The total length of the slot, as shown in Fig. 5.21(a) is approximately half-a-wavelength at the notch-band frequency. Increasing the slot length reduces the notch frequency. However, for the size shown in Fig. 5.21, the C-shaped slots will overlap if the slot length is increased any further. In this case increasing the slot size can be achieving by only increasing the antenna flare angle, which can avoid lowering the cut-off frequency below 3 GHz. Fig. 5.26 illustrates an elliptical cone antenna with four C-shaped slots, whose flare angle changes to 75˚. All other dimensions are shown in Table 5.7.
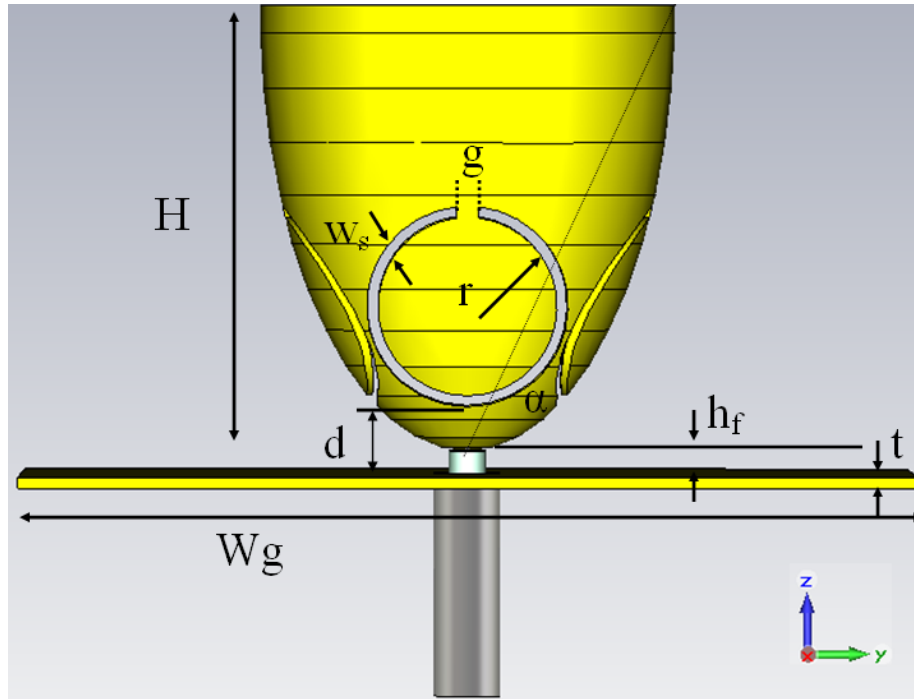
Fig. 5.26 The structure of elliptical cone antenna with four C-shaped slots with bigger flare angle (α = 75˚)

H	20.0 mm	g	1.0 mm
w_s	0.5 mm	r	4.5 mm
d	2.0 mm	h_f	1.0 mm
Wg	40.0 mm	t	0.5 mm
α	75˚	-	-

Table 5.7 Dimensions for the antennas shown in Fig. 5.26

5.2.3.2. Reflection Coefficient

Fig. 5.27 shows the simulated return loss curve for this antenna. The band notch is centred at 5.452 GHz, where the return loss is -0.40 dB. The notch band has a 6 dB return loss bandwidth of 1802 MHz. This corresponds to a quality factor of 3.22. The notch demonstrated here is illustrative of what might be used to suppress either the

HIPERLAN/2 bands in Europe (5.15-5.35 GHz, 5.470-5.725 GHz) or the IEEE 802.11a band in the U.S. (5.15-5.35 GHz, 5.735-5.825 GHz).
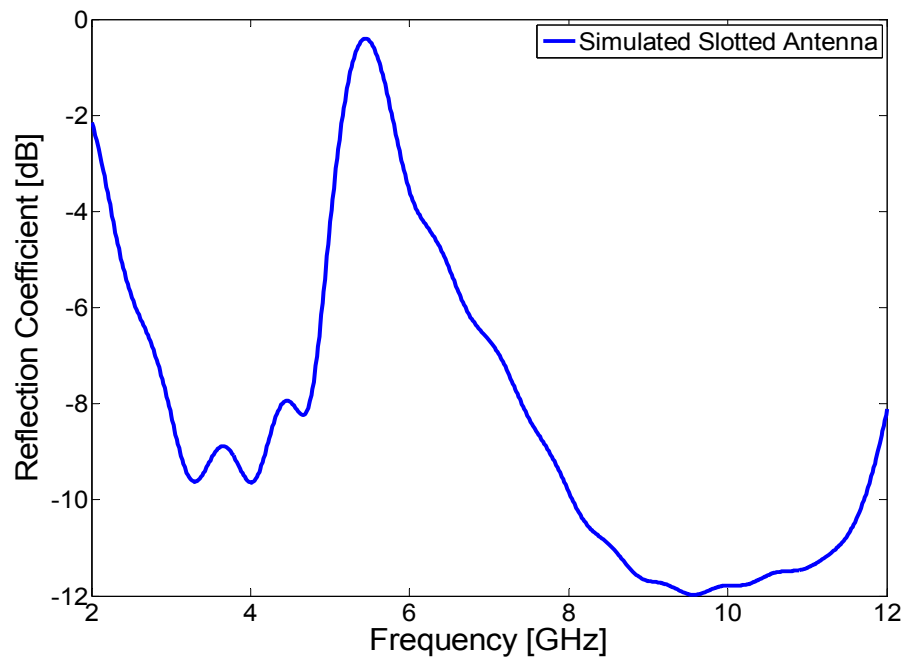
Fig. 5.27 Simulated return loss for the slotted antenna shown in Fig. 5.26

5.2.3.3. Gain Suppression

Fig. 5.28 plots simulated gain as a function of frequency for the band-notched antenna. At the centre of the notch band the antenna's gain is reduced to -22.55 dB. This confirms that the antenna provides a high level of rejection to signal at frequencies within the notch band.
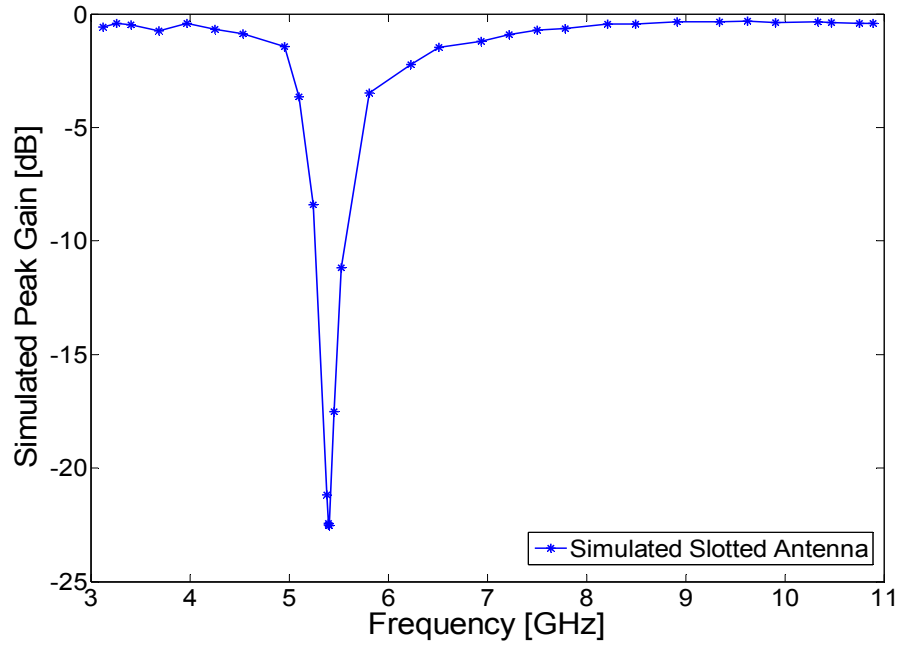
Fig. 5.28 Simulated peak gain for the slotted antenna shown in Fig. 5.26

5.3. Wideband Conical Antenna with 4 U-Shaped Slots

This section presents an elliptical cone antenna with four U-shaped slots [8]. One of the key strengths of this antenna is that it provides a high level of rejection, about 12.7 dB, at the notch-band centre frequency in peak direction, with a high quality factor of 34.5.

5.3.1. Antenna Design and Structure

Fig. 5.29 illustrates the structure of the antenna. The bandwidth of band-rejection is depending on the width of U-shaped slot (i.e. 2 mm in Fig. 5.29). Wider width will lead to lower quality factor.
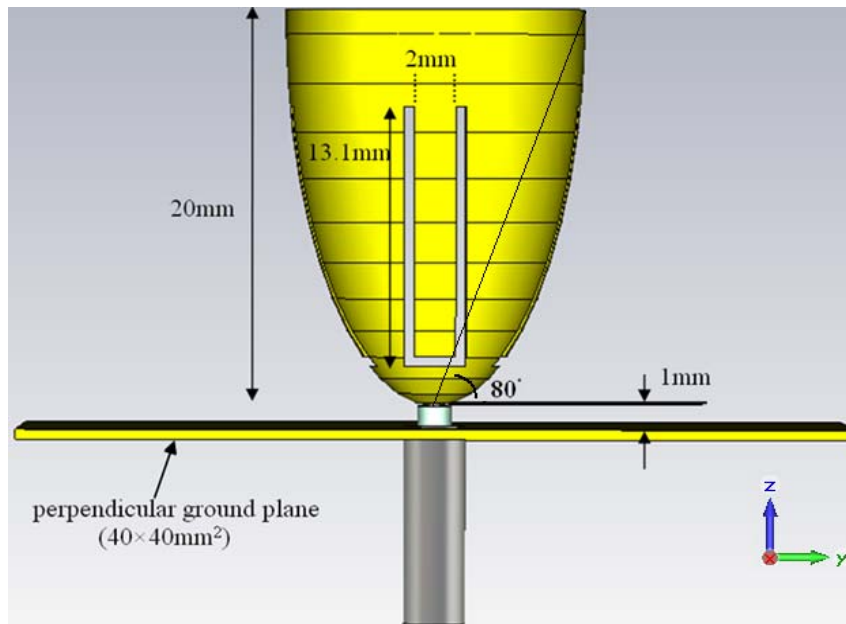
(a)
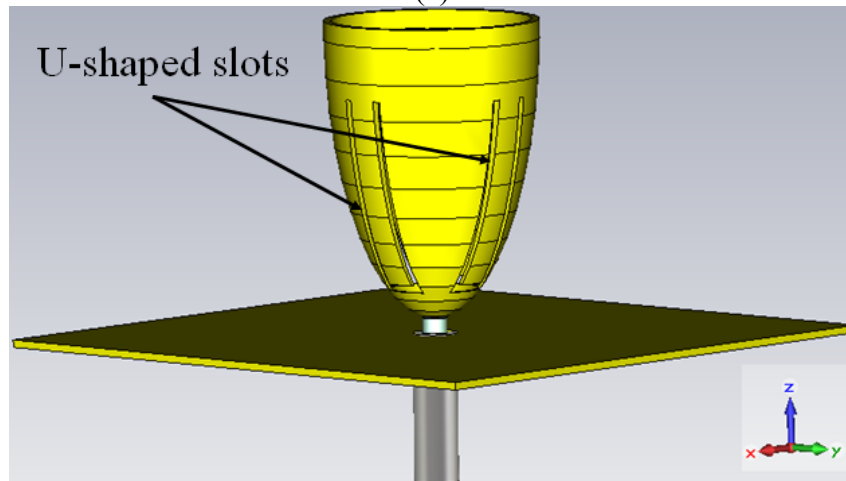
(b)
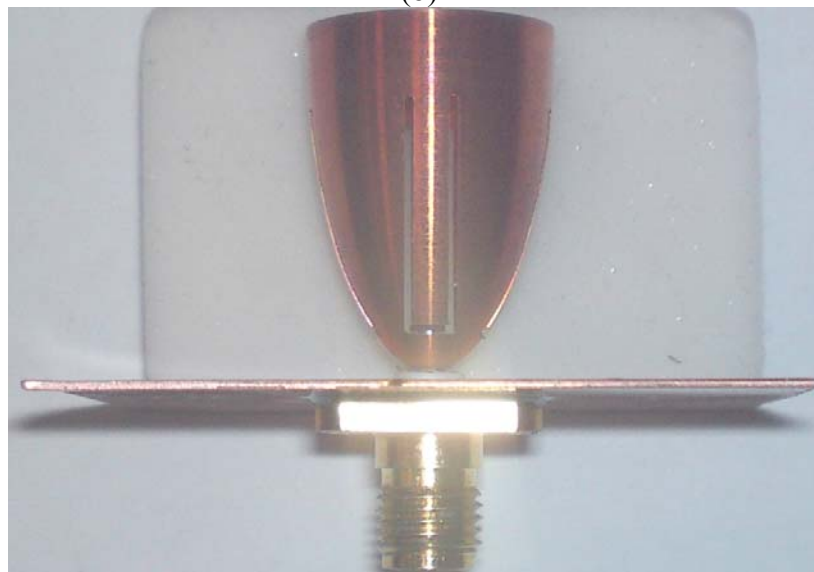
(c)

Fig. 5.29 (a) Structure of elliptical cone antenna incorporating four U-shaped slots;
(b) 3D view of the slotted antenna; (c) side view of the fabricated prototype

5.3.2. Simulation and Measurement Results

5.3.2.1. Reflection Coefficient

Fig. 5.30 shows the measured return loss for the slotted and reference antennas. The band notch is centred at 5.18 GHz. At this frequency the measured return loss was 1.3 dB. The total length of each U-shaped slot is approximately half-a-wavelength at the notch-band frequency. Increasing the slot length reduces the notch frequency. For the proposed antenna, the notch band has a 6 dB return loss bandwidth of 150 MHz. This corresponds to a relatively low quality factor 34.5, which is almost 5 times that of conical antenna with 2 C-shaped slots reported in section 5.1. Increasing the width of U-shaped slot reduces the quality factor at the notch-band frequency.
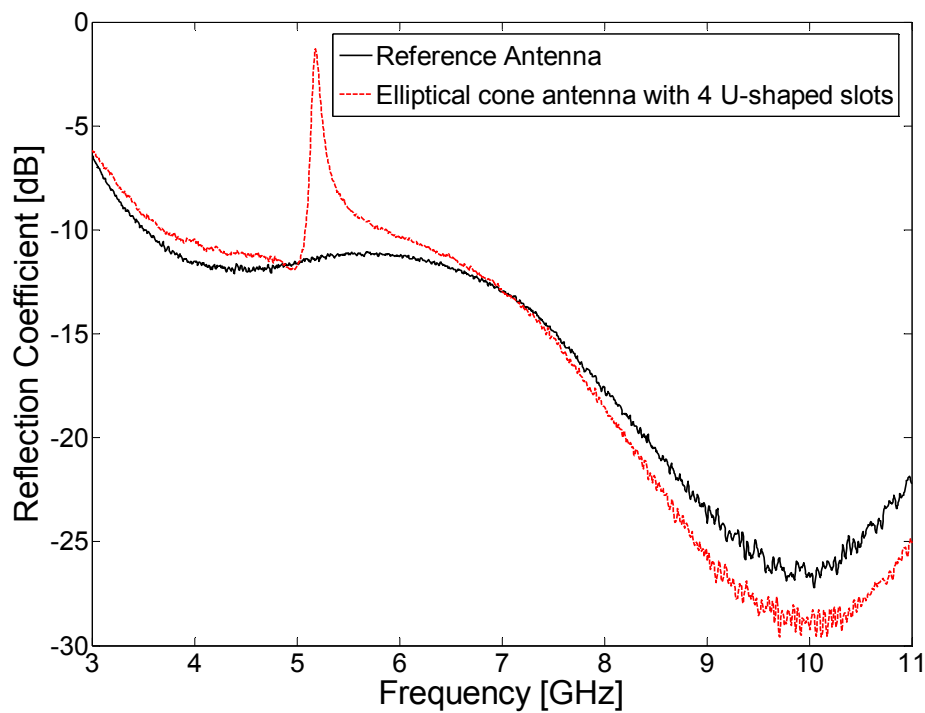
Fig. 5.30 Measured return loss for reference and slotted antennas (shown in Fig. 5.29)

5.3.2.2. Radiation Patterns

Fig. 5.31 illustrates the measured radiation patterns for the slotted antenna at 5.18 GHz in H-(xy-) plane.
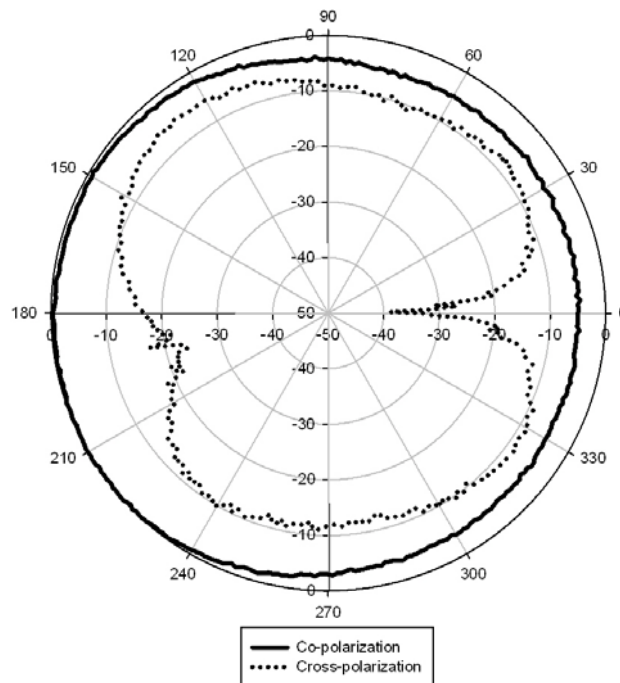
Fig. 5.31 Measured normalized H-(xy-) plane radiation patterns for the elliptical cone antenna with four U-shaped slots at 5.18 GHz

Fig. 5.32 shows the measured E-(i.e. zy-) and H-(i.e. xy-) plane radiation patterns for the slotted antenna. These patterns were measured at 4 GHz, 8 GHz and 10 GHz. From Fig. 5.32, it is clear that the elliptical cone antenna has a very stable omni-direction pattern even at high frequency, i.e. 10 GHz. Table 5.8 shows the values of the standard deviation from omni-directional, for the slotted antenna, are 0.23 dB, 0.24 dB and 0.56 dB at 4 GHz, 8 GHz and 10 GHz, respectively.
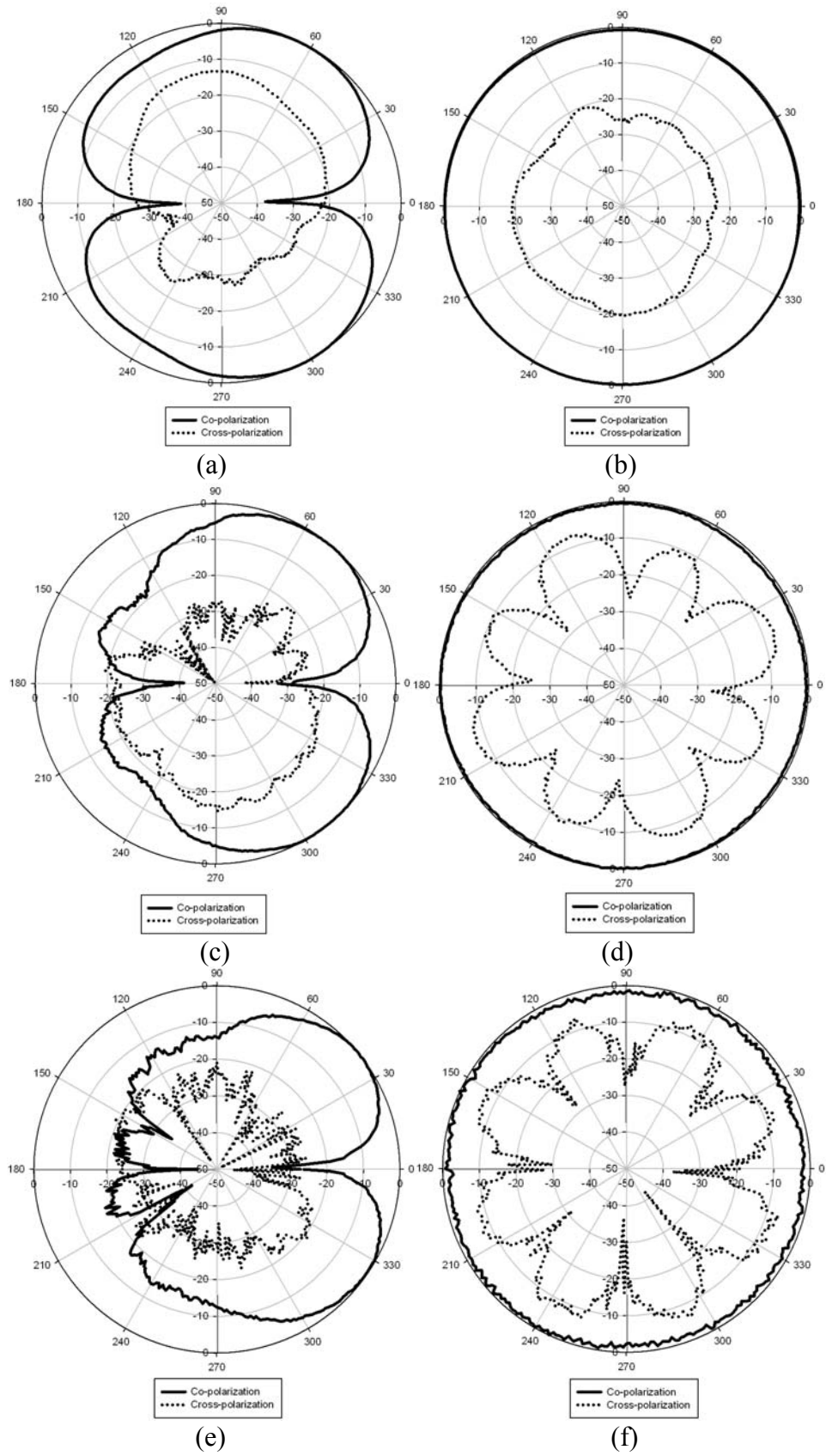
Fig. 5.32 Measured normalized radiation patterns for the elliptical cone antenna
with four U-shaped slots at four different frequencies: (a) E- (zy-) plane, 4 GHz;
(b) H- (xy-) plane, 4 GHz; (c) E- (zy-) plane, 8 GHz; (d) H- (xy-) plane, 8 GHz; (e)
E- (zy-) plane, 10 GHz; (f) H- (xy-) plane, 10 GHz.

Frequency [GHz]	Standard deviation from Omni-directional (dB)
4	0.23
8	0.24
10	0.56

Table 5.8 Standard deviation in dB from omni-directional for the elliptical cone antenna with four U-shaped slots at 4, 8 and 10 GHz

5.3.2.3. Gain Suppression

At the operating frequency band, the total efficiency for the reference antenna is at least -0.5 dB. The lowest total efficiency for the slotted antenna is -13.9 dB at 5.31 GHz, which is close to the simulated notch centre frequency 5.32 GHz. Such low total efficiency shows that the slotted antenna can provide good average gain suppression for the notch band in all directions. Fig. 5.33 plots measured peak gain, in the azimuthal (xy-) plane, for the slotted and reference antenna. At the frequency of the band notch, the gain of the reference antenna is about 0 dBi. Such a low gain is due to the small ground plane used and the fact that the maximum directivity is not in the H- (xy-) plane, At the notched band in the direction of the main lobe of Fig. 5.31 (-x, or $\phi = 209^o$), the antenna gain is reduced by -12.73 dBi compared to the peak gain of the reference antenna.
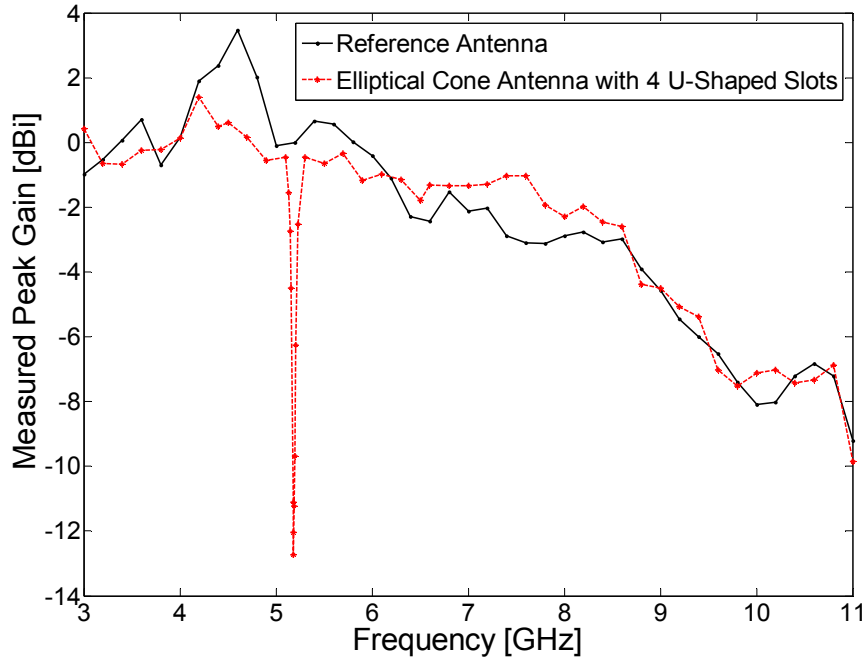
Fig. 5.33 Measured normalized radiation patterns in H- (xy-) plane for the elliptical cone antenna with four U-shaped slots

5.4.   Wideband Conical Antenna with 4 Tilted-U-Shaped and 4 U-C-Shaped Slots

In this section, two conical monopole antennas incorporating two different types of slots (i.e. 4 tilted-U-shaped and 4 U-C-shaped slots) are introduced to achieve improved band-rejection behaviour. Compared to previous work reported in the literature [1, 6, 7, and 8], the slotted antenna provides significantly improved peak gain suppression of up to 25 dB in the vertical polarisation. 4 tilted-U-shaped slot provides a relatively narrow rejection band (i.e. high Q) whilst the 4 U-C-shaped slot gives a relatively wide rejection band (i.e. low Q). The Band-notch frequency can be simply changed by modifying the slot length. They also yield omni-directional patterns at frequencies throughout the operating band.

5.4.1. Antenna Design and Structure

Fig. 5.34 illustrates the schematic diagram of the both antennas, i.e. elliptical cone antenna incorporating four tilted-shaped slots as shown in Figs. 5.34(a) and 3.34(b), elliptical cone antenna incorporating four U-C-shaped slots as shown in Figs. 5.34(c) and 3.34(d). Fig. 5.35 shows the side view of both prototypes. All of the prototype parameters for two types of slots are listed in Table 5.9 and Table 5.10, respectively. The reason of tilted-U-shaped slot is because it can enhance the coupling factor (the coupling between the resonators and antenna) compared with a standard vertical-U-shaped slot [8], and thus improving the band-rejection and maintain high-Q performance. The U-C-shaped slot can optimize the coupling to achieve high band-rejection while still easy to redesign for operation at a different frequency by just changing the upper length of the slot, compared to standard C-shaped slot [1, 6 and 7].
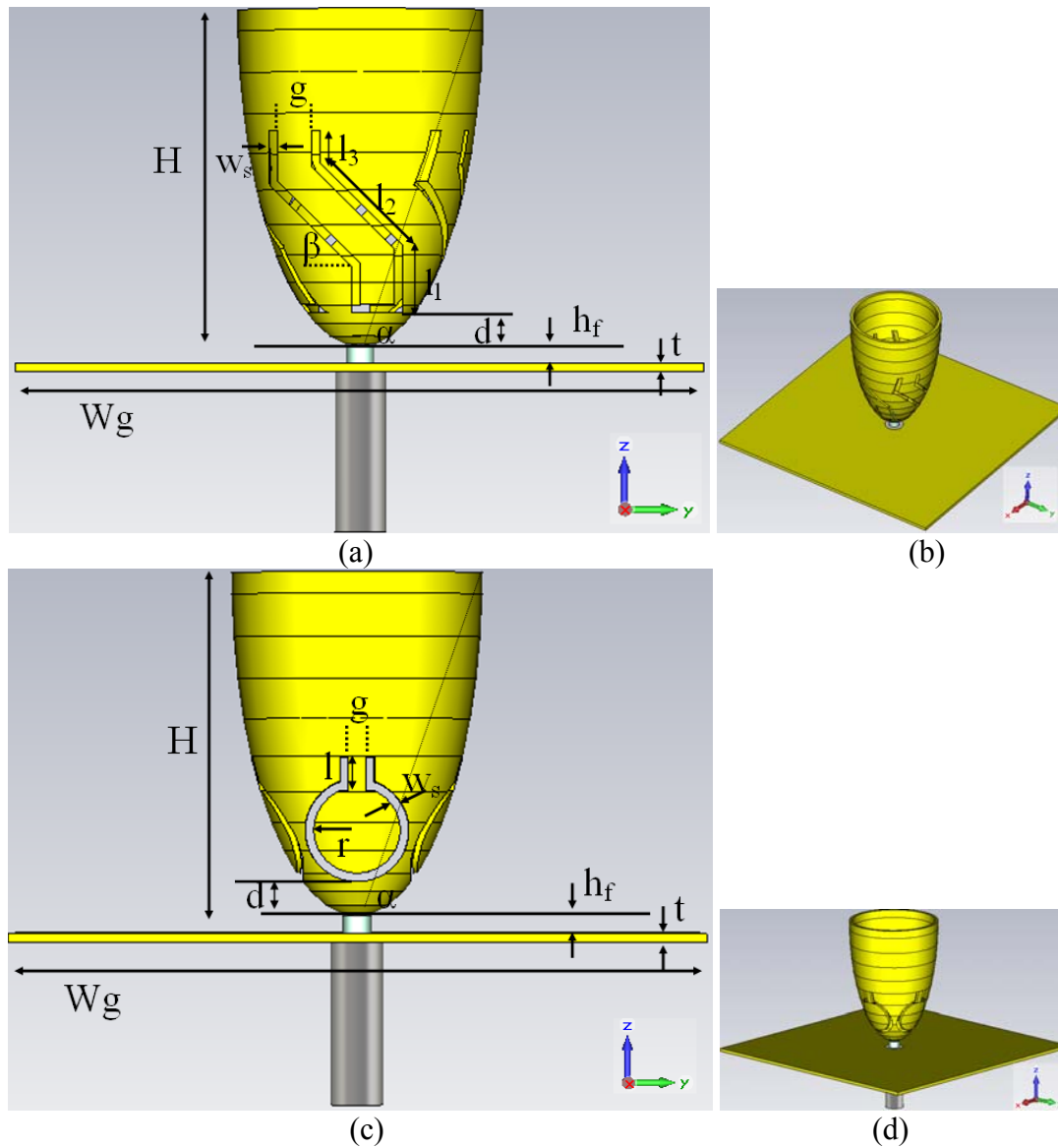
Fig. 5.34 (a) Structure of elliptical cone antenna incorporating four tilted-shaped slots; (b) 3D view of the slotted antenna; (c) Structure of elliptical cone antenna incorporating four U-C-shaped slots; (d) 3D view of the slotted antenna.

H	20.0 mm	g	2.0 mm
w_s	0.5 mm	β	45˚
d	2.0 mm	h_f	1.0 mm
Wg	40.0 mm	t	0.5 mm
α	80˚	l_1	4.0 mm
l_2	7.0 mm	l_3	2.2 mm

Table 5.9 Dimensions for the antennas shown in Fig. 5.34 (a)

H	20.0 mm	g	1.0 mm
w_s	0.5 mm	r	3.0 mm
d	2.0 mm	h_f	1.0 mm
Wg	40.0 mm	t	0.5 mm
α	80˚	l	2.0 mm

Table 5.10 Dimensions for the antennas shown in Fig. 5.34 (c)

(a)

(b)

Fig. 5.35 Side view of the completed fabricated prototype, (a) antenna with 4 tilted-U-shaped slots; (b) antenna with 4 U-C-shaped slots.

5.4.2. Simulation and Measurement Results

5.4.2.1. Reflection Coefficient

Three antennas were fabricated namely a reference antenna, an antenna with 4 tilted-U-shaped slots and an antenna with 4 U-C-shaped slots. Fig. 5.36 shows the measured reflection coefficient. The locations of the band notch obtained through measurement are 5.345 GHz and 7.405 GHz for the 4 tilted-U-shaped slots antenna and 4 U-C-shaped slots antenna, respectively. For these two cases the return loss at the band notch centre frequency is -0.87 dB and -0.46 dB, respectively. The slot is approximately half-a-wavelength long at this frequency, and increasing the slot length reduces the notch frequency, as expected. For the 4 tilted-U-shaped slots, the notch band has a 3 dB return loss bandwidth of 140 MHz. This corresponds to a quality factor of 38.18. By changing the dimension 'g' is possible to change the loaded Q factor. For the 4 U-C-shaped slots, the notch band has a 3 dB return loss bandwidth of 635 MHz. This corresponds to a quality factor of 11.66. The results show that the loaded Q of antenna with 4 U-C-shaped slots is reduced by 69.46%, compared to that with 4 tilted-U-shaped slots. However, the band-rejection is improved by 47.13%. There is a trade-off to be made between quality factor and band-rejection performance, which will be discussed in next section. The notch demonstrated here is illustrative of what might be used to suppress either the Hiperlan/2 bands in Europe (5.15-5.35 GHz, 5.470-5.725 GHz) or the IEEE 802.11a band in the U.S. (5.15-5.35 GHz, 5.735-5.825 GHz).
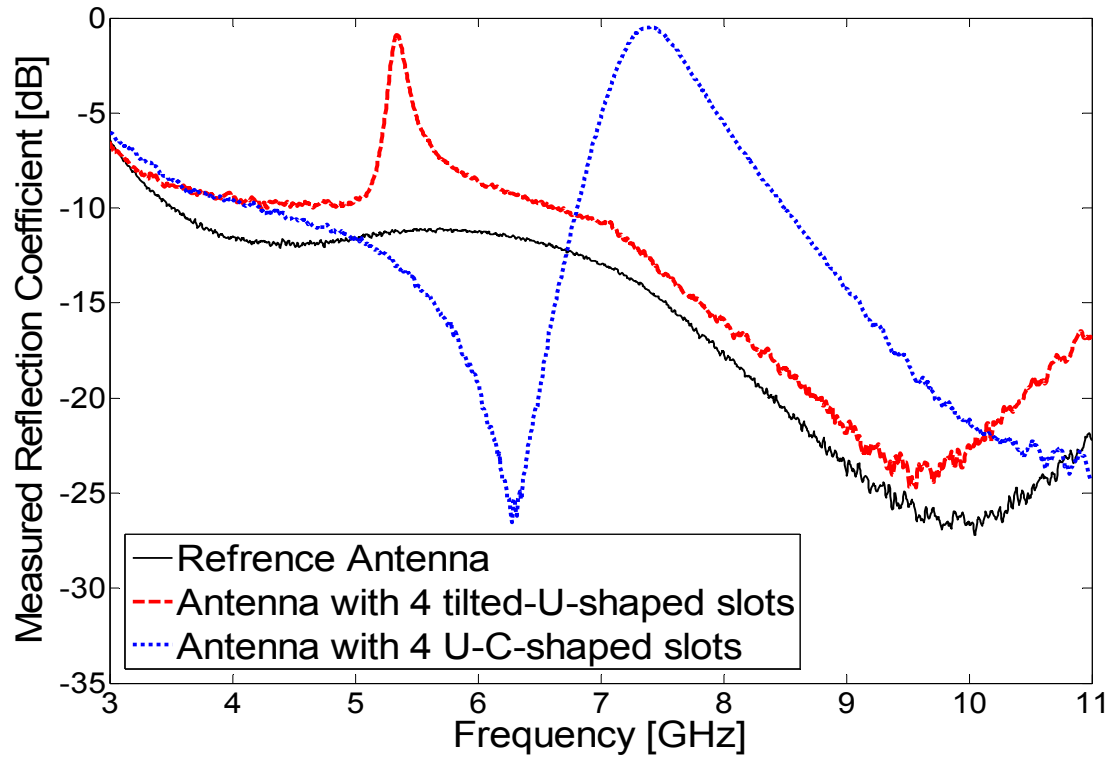
Fig. 5.36 Measured reflection coefficient for slotted and reference antennas (shown in Fig. 5.35)

5.4.2.2. Radiation Patterns

Fig. 5.37 (a) shows the measured radiation patterns for the slotted antennas at 5.345 GHz and 7.405 GHz in the H-(xy) plane, for elliptical cone antenna with 4 tilted-U-shaped slots and that with 4 U-C-shaped slots, respectively. The co-polarisation in the H-plane was measured when both the slot antenna and the reference antenna (i.e. Vivaldi) were placed vertically. The cross-polarisation in the H-plane was measured when the slot antenna was placed vertically while the reference antenna (i.e. Vivaldi) was placed horizontally. The measured co-polarisation patterns are almost omni-directional. Measurements show that the pattern maximum is directed at an angle of 299° and 109°, for the elliptical cone antenna with 4 tilted-U-shaped slots and that with 4 U-C-shaped slots respectively, as shown in Fig. 5.37(a). The measured H-(xy)

planes for both slots antenna at 10 GHz are presented in Fig. 5.37(b). It is clear that both proposed antennas have a very stable omni-direction pattern even at high frequencies. Table 5.11 shows the values of the standard deviation from omni-directional at 10 GHz, are 1.04 dB for the antenna with four tilted U-shaped slots and 0.87 dB for the antenna with four U-C-shaped slots, respectively. The large cross-polarisation, shown in Fig. 5.37, is due to relatively small square ground plane and can be reduced by adopting a larger square ground or a circular ground, as mentioned in section 5.1.2.2.

(a)

(b)
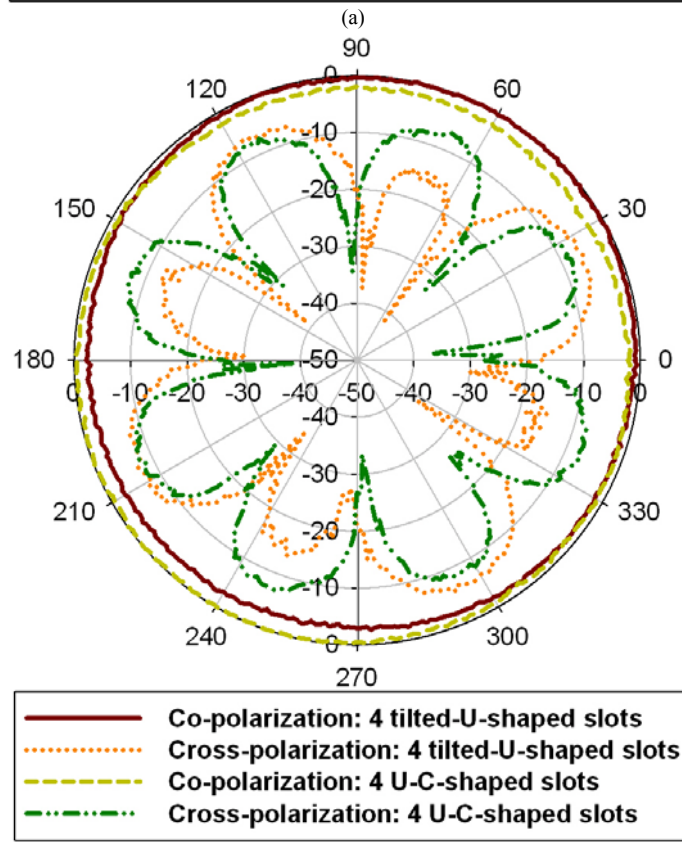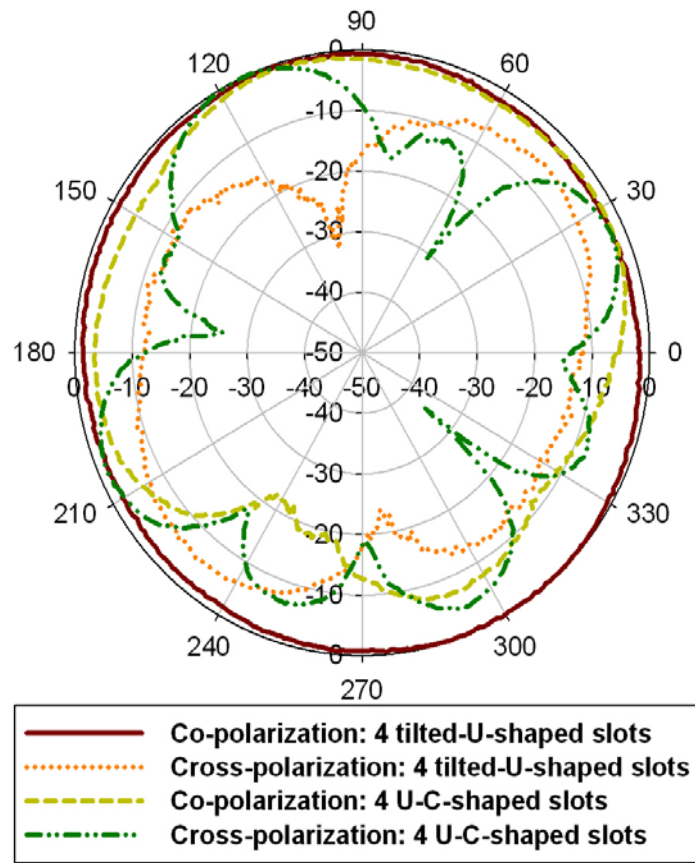
Fig. 5.37 Measured normalized radiation patterns in H- (xy-) plane for the elliptical cone antenna with four tilted-U-shaped slots and four U-C-shaped slots at (a) band notch frequency, 5.345 GHz and 7.405 GHz, respectively; (b) 10 GHz

Slot Type	Frequency [GHz]	Standard deviation from Omni-directional (dB)
Tilted U-Shaped	10	1.04
U-C-Shaped	10	0.87

Table 5.11 Standard deviation in dB from omni-directional for the elliptical cone antennas, with four tilted U-shaped and four U-C-shaped slots, at 10 GHz, respectively

5.4.2.3. Gain Suppression

At the operating frequency bands, for the tilted U-shaped and U-C-shaped slots, the total efficiencies for the reference antenna are at least -0.5 dB and -0.2 dB, respectively. The lowest total efficiencies for the slotted antennas are 15.62 dB at 5.313 GHz and -25.01 dB at 6.967 GHz, which is close to the simulated notch centre frequencies 5.32 GHz and 7 GHz, respectively. Such low total efficiency shows that the slotted antenna can provide good average gain suppression for the notch band in all directions. Fig. 5.38 shows the measured peak gain in dBi, in the azimuthal (xy) plane, for both slotted antennas and the reference antenna shown in Fig. 5.35. At the frequencies of the band notch of both slotted antennas (i.e. 4 tilted-U-shaped slots and 4 U-C-shaped slots), the gain of the reference antenna is about -0.64 dBi and -2.5 dBi, respectively. Such a low gain is due to the small ground plane used and the fact that the maximum directivity is not in the H-(xy-) plane. In the peak direction of H-(xy) plane shown in Fig. 5.37 ($\phi = 229°$ and $\phi = 109°$), the gains are reduced to -19.06 dBi and -27.5 dBi, giving a gain suppression of 19.7 dB and 25 dB, for both slotted antennas (i.e. 4 tilted-U-shaped slots and 4 U-C-shaped slots), respectively. This has been improved by 9.4% and 38.9% compared to the best antenna reported in the literature, which provided a peak gain suppression of 18 dB [9].
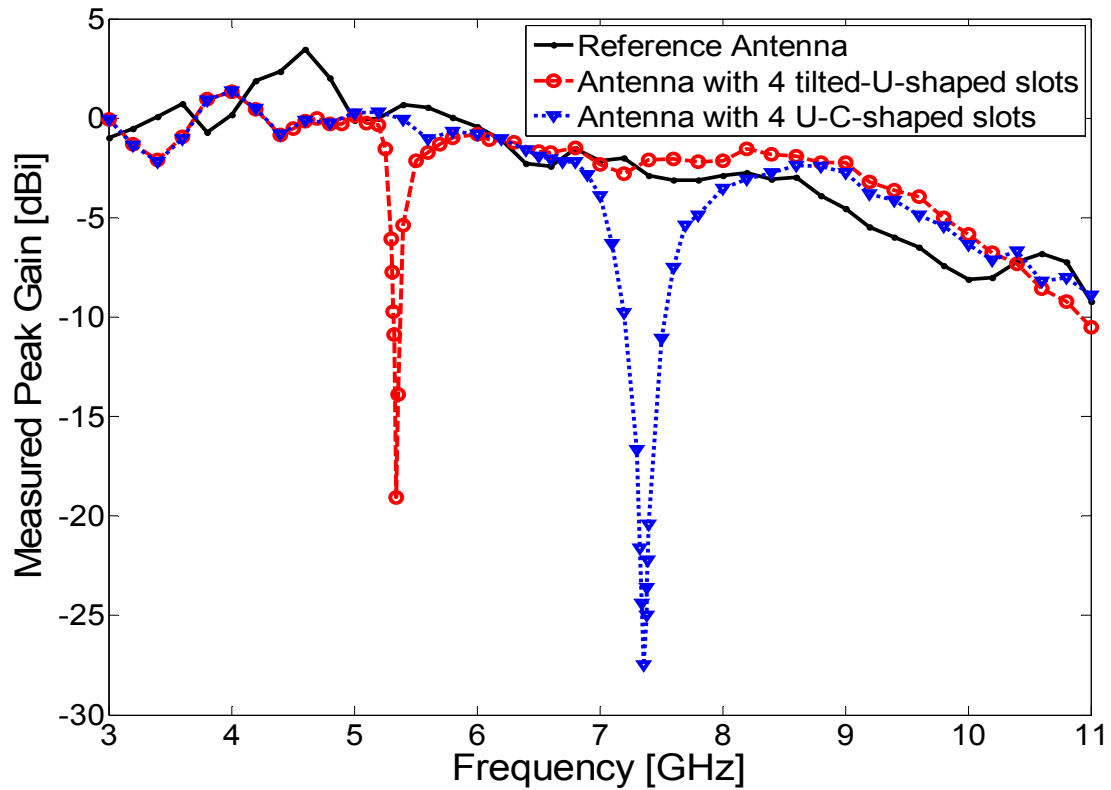
Fig. 5.38 Measured vertically polarized gain for the slotted and reference antennas shown in Fig. 5.35

5.4.2.4. Variation of the Slot Length

Fig. 5.39 illustrates the reflection coefficient for the tilted-U-shaped slotted antenna with five different lengths of the upper section of the slot, where are l_3 = 1.2 mm, 2.2 mm, 3.2 mm, 4.2 mm, and 5.2 mm, respectively. In all other respects these antennas are identical to that shown in Fig. 5.35(a). The notch band centre frequencies for those antennas are 5.696 GHz, 5.32 GHz, 5 GHz, 4.696 GHz, and 4.408 GHz, with return loss of 0.578 dB, 0.821 dB, 1.053 dB, 1.331 dB, and 1.562 dB, respectively. The notch bands have a 3 dB return loss bandwidth of 226 MHz, 210 MHz, 196 MHz, 187 MHz, and 176 MHz. Those correspond to quality factors of 25.24, 25.39, 25.56, 25.18, and 25.00 respectively. It is clear that when the length of slot increases, the band-rejection is getting worse. The loaded Q is very slightly increased when l_3 is changed from 1.2 mm to 3.2 mm but slightly decreasing when l_3 = 4.2 mm and 5.2 mm.
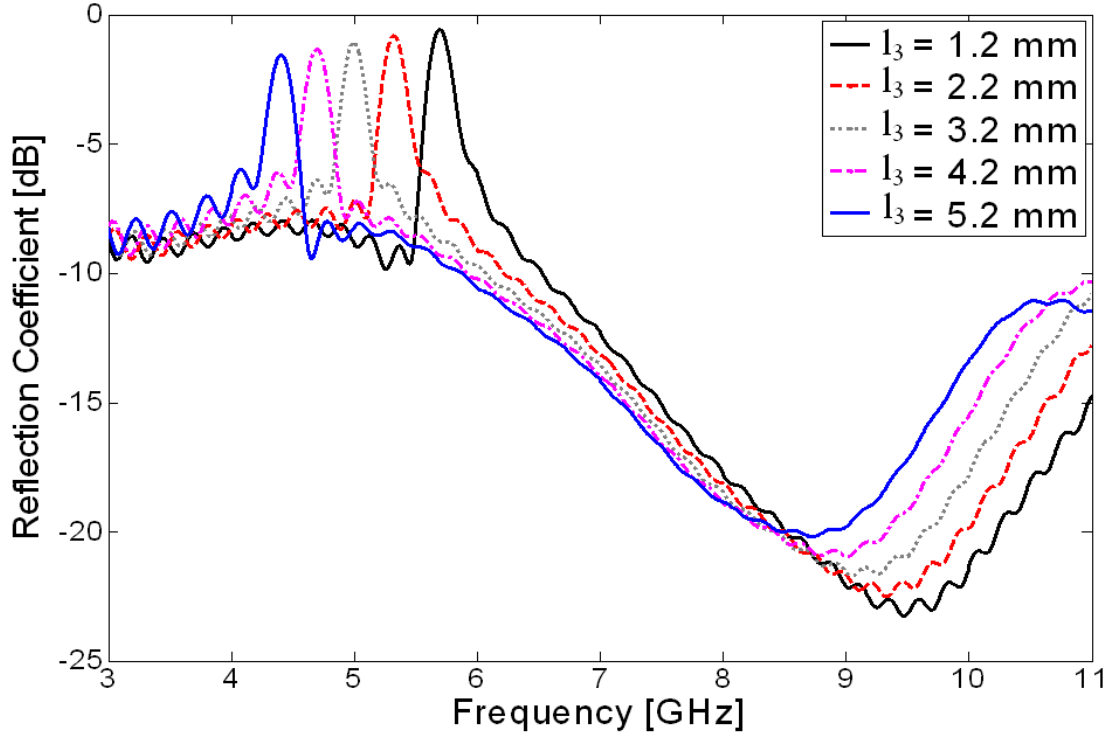
Fig. 5.39 Simulated reflection coefficient for antenna with 4 tilted-U-shaped slots with five different lengths of upper part slots, i.e. l_3 = 1.2, 2.2, 3.2, 4.2, and 5.2 mm (denoted as 'l_3' in Table 5.10)

For the size shown in Fig. 5.35(c), the C-shaped slots will overlap one another if the radius r (as shown in Table 5.10) is increased any further. In that case, the best way to reduce the notch band centre frequency is by increasing the length of U-shaped slot (i.e. 'l'). Fig. 5.40 illustrates the reflection coefficient for the slotted antennas with five different lengths of the upper section of the slot (i.e. U-shaped), which are l = 2 mm, 3 mm, 4 mm, 5 mm, and 6 mm, respectively. In all other respects these antennas are identical to that shown in Fig. 5.35(c). The notch band centre frequencies for those antennas are 7.000 GHz, 6.376 GHz, 5.832 GHz, 5.416 GHz, and 5.056 GHz, with return loss of 0.173 dB, 0.340 dB, 0.487 dB, 0.585 dB, and 0.945 dB, respectively. The notch bands have a 3 dB return loss bandwidth of 629 MHz, 500 MHz, 381 MHz, 308 MHz, and 260 MHz. Those correspond to quality factors of 11.14, 12.91, 15.35,

17.65, and 19.50 respectively. It is clear that when the length of slot increases, the quality factor also significantly increases but the band-rejection is getting worse.
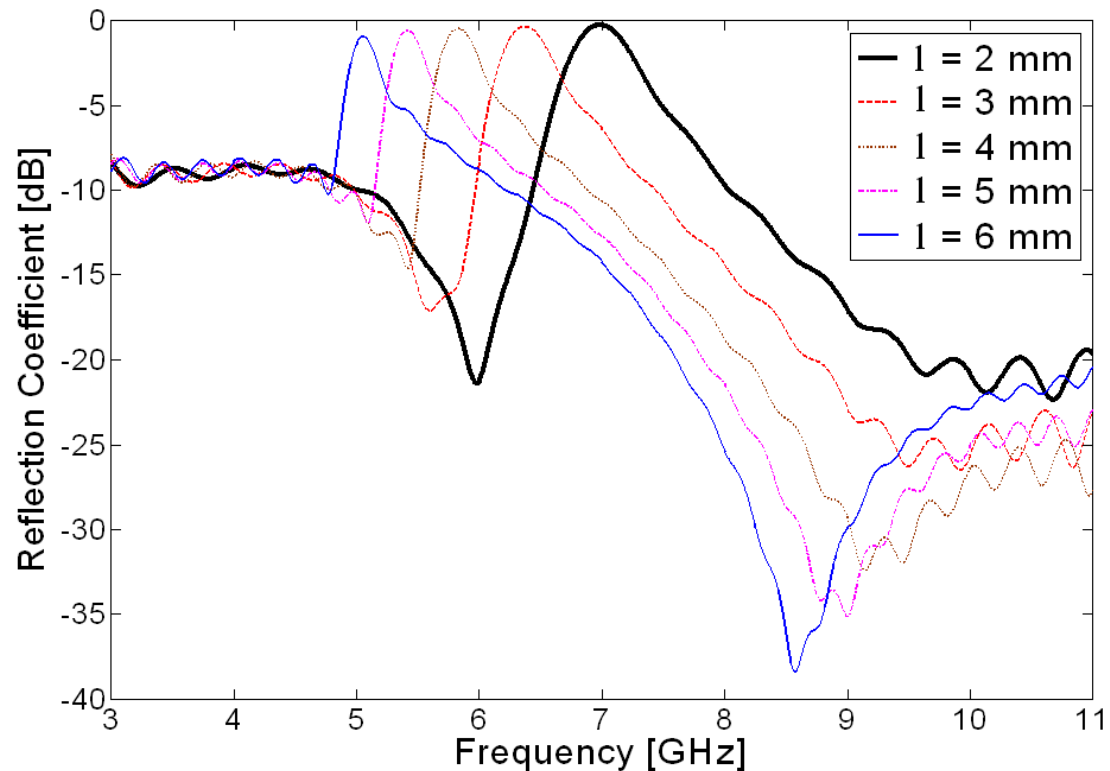
Fig. 5.40 Simulated reflection coefficient for antenna with 4 U-C-shaped slots with five different lengths of upper part slots, i.e. l = 2, 3, 4, 5, and 6 mm (denoted as 'l' in Table 5.10)

5.5. Equivalent Circuit Model for Wideband Antenna with Frequency Notch-Band

An equivalent circuit model has been created for the wideband conical monopole antenna with frequency notch-band. The study in this section has shown that the band-rejection can be improved by enhancing the coupling factor or by increasing the number of resonators. The analysis of relationship between quality (Q) factor and the coupling factor is also presented. The circuit simulations were performed using Advanced Design Studio (ADS).

5.5.1. Equivalent Circuit

Previous literature [10] proposed an equivalent circuit model to explain the resonant behaviour of a band-notched monopole UWB antenna, which was a fork-shaped antenna incoporating a open-looped resonator. However, the equivalent circuit model shown in ref. [10] only provided some simple parameter studies, which did not give sufficient information to explain the relationship between the antenna and the resonator. This is the first time in which an equivalent circuit model has been used to demonstrate how the band-rejection can be improved and also the relationship between the quality (Q) factor and the coupling factor in the notched band frequency.

A simple equivalent circuit model for the UWB antenna incorporating n slot resonators, coupled to a source impedance Z_o, is shown in Fig. 5.41(a). It can be seen that the combination of the LC series circuit and LCR parallel circuit is used to represent the UWB antenna [11] and LCR parallel circuits are used to represent the slot resonators [10]. If the antenna incorporates n similar slots then the n resonators should be connected in parallel. In Fig. 5.41(a), there is a transformer, denoted as 'T', connected between the antenna model and the resonators. The resonators are connected to the antenna through the magnetic coupling of the transformer, but there is no electrical connection between these two circuits. Because the ideal transformer, 'T', is lossless, all of the power delivered to the ideal transformer by the antenna circuit model is in turn delivered to the resonators circuit model by the ideal transformer. The transformer 'T' also represents how the resonators are coupled to the antenna. A generalized concept of the transformer has been given in ref. [12]. At the resonant frequency, the reactance should be zero. As shown in Fig. 5.41(a), the transformer can be represented, in terms of resistance, by the equation

$$r_A \big/ n^2 = Z_o + r_a \qquad\qquad (5.2)$$

in which, r_A is the resistive part of the number of parallel resonators. n is the turns

ratio of the transformer. r_a is the resistive part of the antenna circuit model, which can

be taken as the real part of $1 \big/ (\dfrac{1}{jw_o L_2} + jw_o C_2 + \dfrac{1}{R_1})$.

(a)

(b)
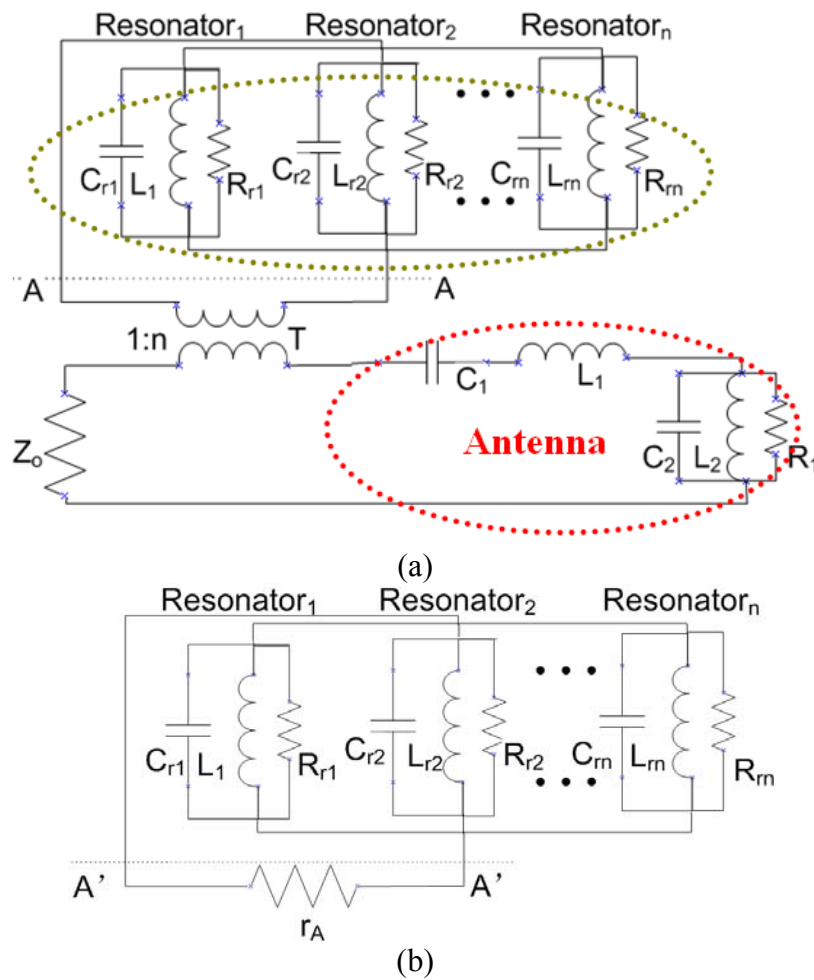
Fig. 5.41 (a) a completed equivalent circuit model for UWB antenna incorporating with number of resonators; (b) Equivalent circuit model for a number of parellel resonators coupled to r_A.

5.5.2. Number of Resonators

Fig. 5.42 illustrates the reflection coefficient for the equivalent circuit model (as shown in Fig. 5.41) incorporating 1, 2 and 4 resonators, respectively. From Fig. 5.42, it is clear that when the number of resonators increases, the band-rejection improves. However the bandwidth of the band-rejection will also be increased accordingly, as shown in Fig. 5.42.
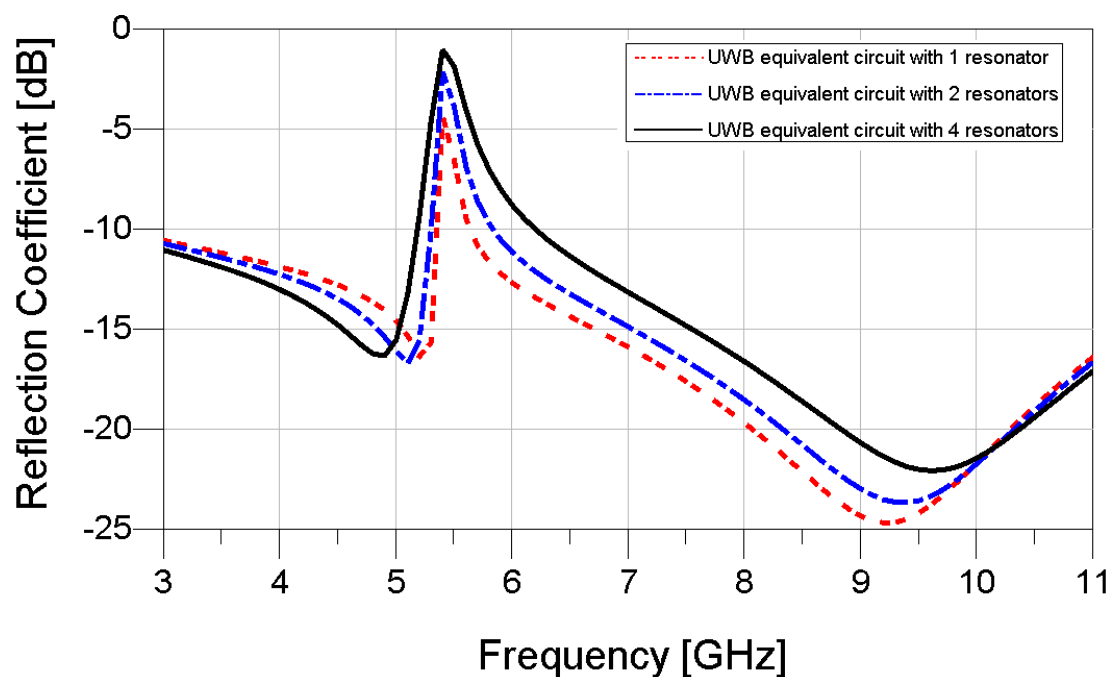
Fig. 5.42 Reflection coefficients for equivalent model (shown in Fig. 5.41) incorporating with 1, 2 and 4 resonators, respectively

5.5.3. Quality Factors and Coupling Factor

From Fig. 5.41, if the antenna incorporating n resonators is treated as one resonator (antenna) unit or load, then there will be an unloaded Q (denoted as 'Q_o') of the resonator. The conventional loaded Q (denoted as 'Q_L') of the frequency notch band is defined by the expression of [13]

$$\frac{1}{Q_L} = \frac{1}{Q_o} + \frac{1}{Q_e} \qquad (5.3)$$

or $$Q_L = \frac{Q_o}{1+\beta} \qquad (5.4)$$

From equation (5.4), it can be seen that the loaded Q (Q_L) of the frequency notch band

is depended on the unloaded Q (Q_o) of the resonators and the coupling factor β, which

can be defined as r/r_A or Q_o/Q_e [13], where Q_e is external Q factor and

$Q_o = r/(W_o L)$ and r is the resistance of the resonators. The increase in the coupling

factor (β) implies that the coupling gets stronger. There will be a progressive

improvement in the reflection coefficient at the notch centre if β increases. However,

when β increases, the quality factor (loaded Q) of rejection band gets lower.

5.5.3.1. Relationship between the Coupling Factor and the Transformer

By considering equation 5.2 and $\beta = r/r_A$, as mentioned earlier, the relationship

between the coupling factor β and the transformer 'T' with n turns ratio can be

expressed as

$$n = \sqrt{\frac{r}{\beta(Z_o + r_a)}} \qquad (5.5)$$

5.5.3.2. Determination of the Quality Factor and Coupling Factor from

   Measurement Results

For either elliptical cone antennas incorporating 4 tilted-U-shaped slots or 4 U-C-shaped slots in section 5.4, the loaded Q (Q_L) of the frequency notch band can be calculated at the -3 dB points of input reflection coefficient, as shown in Fig. 5.36. The unloaded Q (Q_o) can be calculated from equation 5.4, in which coupling factor β can be found from the return loss L_o of resonant frequency by, [14]

$$L_o(dB) = -20\log\left|\frac{1-\beta}{1+\beta}\right| \tag{5.6}$$

The unloaded Q (Q_o) of the whole antenna, in principle, is independent of either Q_L or β [14]. However, two situations, the over-coupled ($\beta>1$) and under-coupled ($\beta<1$) cases, need to be considered. There can be distinguished by inspecting the response circle in the Smith Chart from the simulation results. A large response circle enclosing the origin of the Smith Chart signifies an over-coupled case; for the under-coupling case, the response circle is small and excludes the origin [14]. Table 5.12 shows the values of Q_L, Q_o, β and return loss for both slotted antennas in simulation. The return loss performance of the antennas was simulated using the transient solver in CST Microwave Studio®. From Table 5.12, it can be seen that there is strong coupling for the 4-U-C-shaped, and it thus gives a better band-rejection but lower Q_L. Although the coupling, β, between the antenna and the resonators cannot be found easily, it can be determined by the location of the resonators. The parameters in Table 5.12 were considered when the slots were located at d = 2 mm (Tables 5.9 and 5.10) where d is the distance between the slot and the bottom of the cone. Different values of 'd' will introduce different coupling β, and thus give different Q_L.

Antenna with resonator	Frequency (GHz)	Q_L	Q_o	β	Return loss (dB) at the slot resonance
With 4 tilted-U-shaped	5.32	25.406	563.364	21.175	0.821
With 4 U-C-shaped	7	11.138	1128.200	100.297	0.173

Table 5.12 Q factors and coupling factors for the two antennas shown in Fig. 5.34

5.5.3.3. Coupling Factor Effect Reflection Coefficient and Quality Factors

Fig. 5.43 illustrates the reflection coefficient and coupling factor β for the antenna incorporating 4 U-C-shaped slots with different values of 'd', from 2 mm to 11 mm. Fig. 5.44 shows the unloaded Q (Q_o) and loaded Q (Q_L) of the antenna incorporating 4 U-C-shaped slots with different values of 'd' (i.e. from 2 mm to 11 mm). From Fig. 5.43, it can be seen that when 'd' increases, the reflection coefficient and coupling factor β decreased significantly, which are expected. As β decreased, the increase of loaded Q is expected, as shown in Fig. 5.44. Fig. 5.44 shows that the unloaded Q (Q_o) of the whole antenna is very high, and it implies that the resonator dominates rather than the antenna, and it has a low Q factor. From Figs. 5.43 and 5.44, it is clear that there is a trade-off to be made between the performance of band-rejection and the loaded Q of the band-notch.
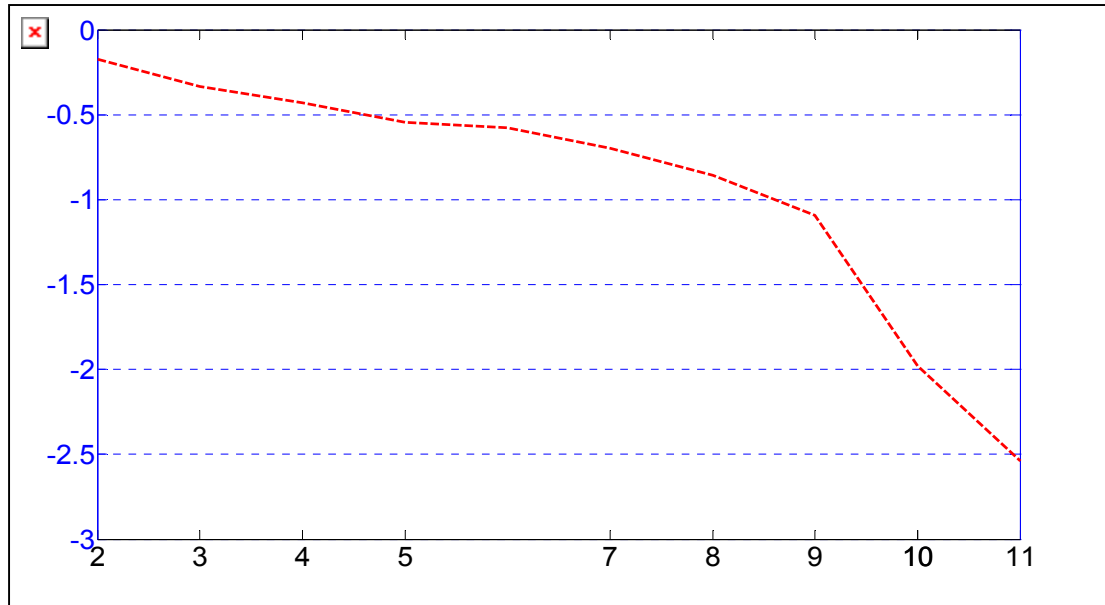
Fig. 5.43 Reflection coefficient and coupling coefficient for the antenna with 4 U-C-shaped slots with different 'd', which is the vertical distance from the bottom of the slot to the bottom of the conical antenna, as shown in Fig. 5.34(c).
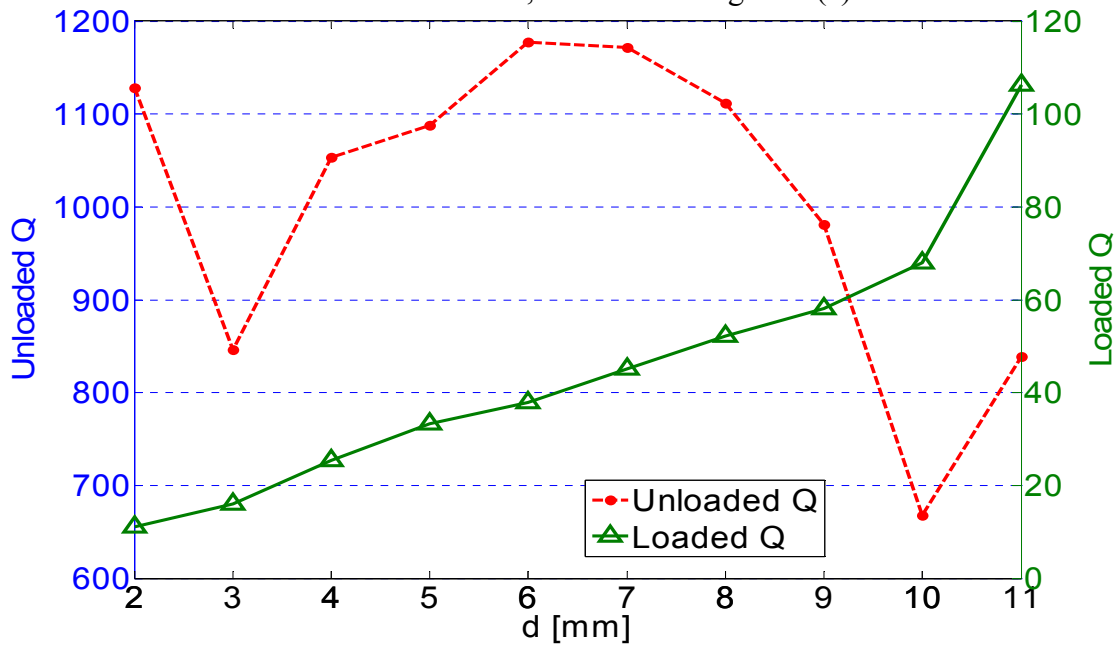
Fig. 5.44 Unloaded Q and Loaded Q for the antenna with 4 U-C-shaped slots with different 'd', which is the vertical distance from the bottom of the slot to the bottom of the conical antenna, as shown in Fig. 5.34(c).

5.5.4. Simulation Results

It is difficult to obtain accurate values of each component within the schematic equivalent circuit model. To tackle this problem, this section presents a methodology

to obtain the values and exam the performance of the equivalent circuit model. In order to determine the values of each component in the circuit model of Fig. 5.41 incorporating different number of resonators (or slots), several parameters need to be considered using the following sequence:

1) optimize the value of each antenna element (i.e. C_1, L_1, C_2, L_2 and R_1) to have the similar wideband performance;

2) determine the coupling condition (under- or over-coupled)

3) calculate the coupling parameter β;

4) calculate the resistance of the antenna model, i.e. r_a;

5) determine the resistance of the resonators, i.e. r;

6) calculate n, the turns ratio of ideal transformer 'T', from Equation (5.5);

7) optimize the value of each resonator element (i.e. C_r, L_r and R_r) to have the similar band-rejection performance.

5.5.4.1. Determination of the Resistance of the Resonators from Measurement

The resistance (r_1) of the single resonator in two cases, namely the tilted-U-shaped slot and U-C-shaped slot, can be found by simulating the antenna incorporating one tilted-U-shaped slot and U-C-shaped slot, respectively. In order to determine the Z parameters of the slot, a discrete port was placed in the bottom of the slot as shown in Fig. 5.45. Table 5.13 shows the Z parameters for the resonant frequency for each case. Thus, the resistance of four resonators (r) can be calculated by $r_1/4$.

<div align="center">(a)   (b)</div>
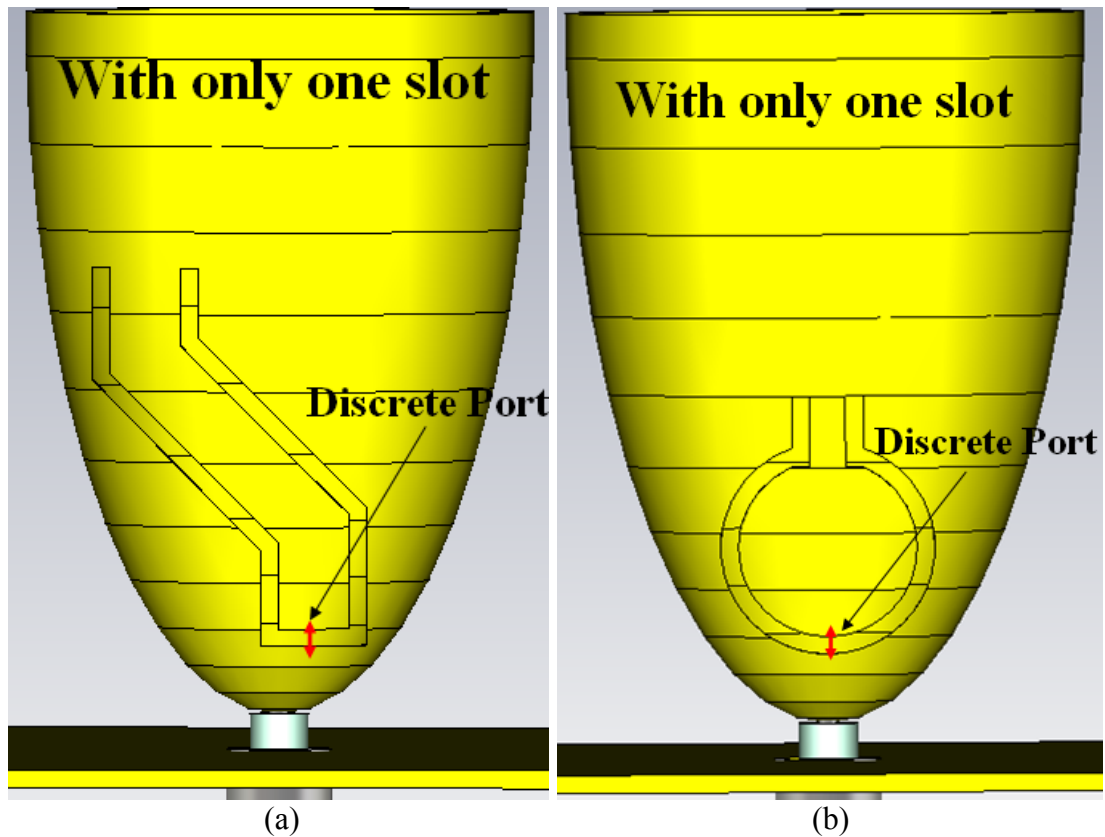
Fig. 5.45 Structure of the antenna with (a) one tilted-U-shaped slot and (b) one U-C-shaped slot.

Resonator	Frequency (GHz)	Real (ohm)	Imaginary (ohm)
4_tilted_U_shaped	5.2441	3158.7	0
4_U_C_shaped	6.9942	1949.1	0

Table 5.13 Complex Z parameters for the two slots shown in Fig. 5.45

5.5.4.2. Comparison between Equivalent Circuit Model and Prototype

The values of each component within the circuit model were adjusted within the Advanced Design System (ADS) environment, in order to optimize the impedance behaviour and shown in Table 5.14, for the two slotted antenna models, respectively. Fig. 5.46 illustrates the return loss for the simulated slotted antennas and the result obtained using the new equivalent circuit shown in Fig. 3.41(a). There is good agreement between them.

Antenna	C_1 (pF)	L_1 (nH)	C_2 (pF)	L_2 (nH)	R_1 (ohm)
	2.6280	0.9490	0.2459	4.8076	94.9500
Resonator	C_r (pF)	L_r (nH)	R_r (ohm)	**n**	
4_tilted_U_shaped	5.1100	0.1750	1019.6600	0.5131	
4_U_C_shaped	15.3985	0.0336	804.9000	0.2002	

Table 5.14 Parameters in the equivalent circuit model (see Fig. 5.41) representing the two slot antennas shown in Fig. 5.34, respectively
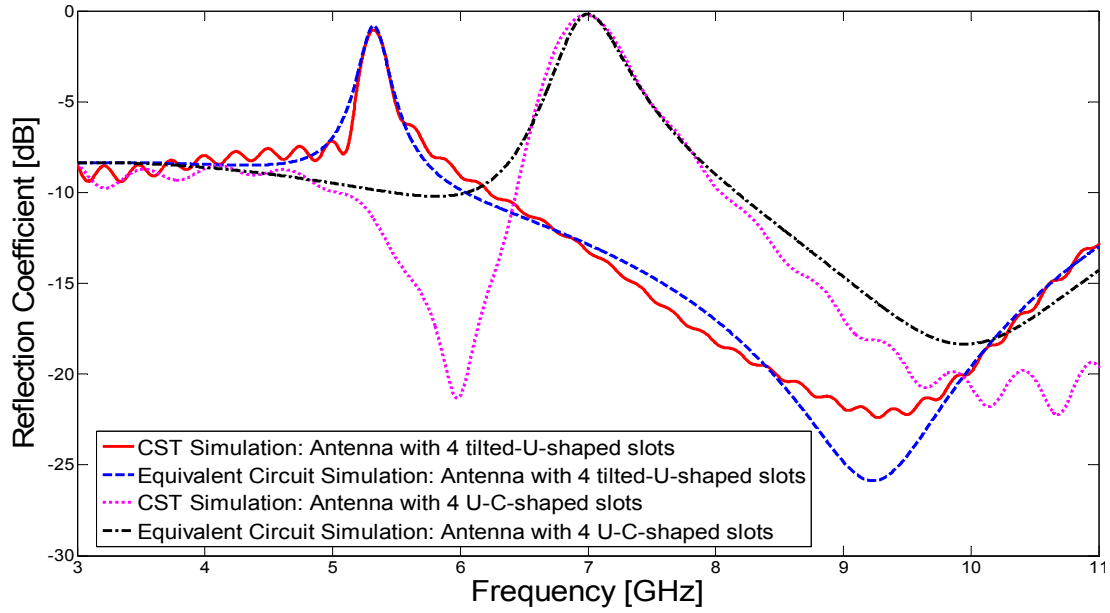
Fig. 5.46 Reflection Coefficient for both elliptical cone antenna with 4 tilted-U-shaped slots and 4 U-C-shaped slots (see in Fig. 5.34, section 5.4), in CST and equivalent circuit (see Fig. 5.41) simulations, respectively.

5.6. Comparison of Different Types of Slots

Table 5.15 shows the total efficiency and gain suppression for each type of slots, i.e. 2 C-shaped slots (section 5.1), 4 C-shaped slots (section 5.2), 4 U-shaped slots (section 5.3), 4 tilted U-shaped slots and 4 U-C-shaped slots (section 5.4). The antenna with 2 C-shaped slots provides 40.9 dB of gain suppression in null direction. However, it only provided 10.7 dB of gain suppression in the peak direction. When incorporating 4 slots, the peak gain suppression was improved, for example, the antenna with 4 C-

shaped slots can provide at least 28.8 dB of gain suppression. However, it lost the deep gain suppression in the null direction. The antenna with 4 U-shaped slots can prove high Q band-rejection, i.e. 34.5. However, it only provided 12.7 dB of peak gain suppression. When the peak gain suppression was improved, the bandwidth of the slotted antenna at the notched band was wider. For example, the antenna with 4 tilted U-shaped slots provided 19.7 dB of peak gain suppression, the notch band Q factor was reduced to 16.46 compared to the antenna with 4 U-shaped slots.

Resonator	Measured Notch Frequency (GHz)	Reflection Coefficient [dB]	Notch Band Q Factor [+]	Simulated Lowest Total Efficiency (dB)	Measured Peak Gain Suppression (dBi)
2 C-shaped	5.42	-0.63	6.70	-12.6	10.7
					40.9[*]
4 C-shaped	8.71	-0.10	5.58	-28.3	28.8
4 U-shaped	5.18	-1.30	34.50	-13.9	12.7
4 tilted U_shaped	5.35	-0.87	16.46	-15.6	19.7
4 U_C_shaped	7.41	-0.46	6.83	-25.0	25.0

Table 5.15 Total efficiency and gain suppression for each type of slots.
[+] at 6 dB return loss bandwidth;* null direction

It can be concluded that there is a trade-off between the gain suppression and the quality factor of the band-notch. Increasing the number of resonators will of course increase the band-rejection. However, it will also widen the bandwidth of the frequency notched band.

5.7. Manufacture and Stopband Frequency Control

The antenna was machined from solid, by first machining the outer shape from a stock copper rod, then drilling the centre hole using a CNC lathe. A small ball nose milling cutter on a CNC miller was then used to machine the internal shape of the

cone. The slots were machined individually using 0.5mm cutter with the blank cone mounted in a special fixture. Low cost production would depend on the intended frequency range and hence size. For smaller size the antennas could be die casting. Larger size could be produced by rapid prototyping. Alternately if the cone shape is altered at the expense of bandwidth several possibilities exist. A straight cone with circular cross section can be made by wrapping thin flexible PCB. A straight cone with square cross section can be made from four triangular printed circuit boards, as demonstrated in Chapter 6. The Chapter 6 proposes a novel pyramidal shaped monopole with four loop shaped slots and by loading each slot with a varactor diode, it is possible to tune the notch band centre frequency from 4.8 GHz to 7.472 GHz.

5.8. Summary

Section 5.1 introduced an elliptical cone antenna incorporating two C-shaped slots. Experimental results suggest that the antenna provides improved gain suppression (about 41.5 dB) in four specific directions and 11.3 dB of peak gain suppression in the vertical polarisation compared with planar antenna designs presented earlier in the literature. Analysis of simplified equivalent current sources associated with the slot and ground plane edge currents confirms that it is indeed radiation from those sources that give rise to these well defined patterns. The location of the band notch centre frequency can also be controlled by simply modifying the length of the C-shaped slot, as expected. The gain suppression in the null directions is affected by the distance between the C-shaped slots. If the direction of interferer changes, the antenna could be rotated using an electric motor. Alternatively one could effectively rotate the C-shaped slots by using a number of pin diode switches. The experimental results show

that the elliptical cone antenna with two C-shaped slots provides a high degree of gain reduction in the specified direction.

Section 5.2 proposed an elliptical cone antenna with four C-shaped slots. Experimental results show omni-directional radiation patterns with significantly improved gain suppression, at least 28.8 dB, compared with conventional band notched antenna designs. The antenna is also capable of pointing a pattern null towards any spatial directions within H-plane. The location of the band notch frequency can also be controlled by simply modifying the length of the C-shaped slot. This can be achieved by scaling antenna.

Section 5.3 proposed an elliptical cone antenna with four U-shaped slots. Experimental results show omni-directional radiation patterns are obtained along with good gain suppression, of at least 12.73 dB, in all directions around the H-plane, compared with conventional band notched antenna designs. The band notch frequency can be controlled by simply modifying the length of U-shaped slot. The proposed antenna also provided high Q notch-band performance. The quality factor can be adjusted by simply changing the width of the U-shaped slot.

Section 5.4 proposed two elliptical cone antennas incorporating two new types of slots, four tilted-U-shaped and four U-C-shaped slots. Experimental results suggest that both slotted antennas provide significantly improved gain suppression, such as 19.7 and 25 dB, in the vertical polarisation with high Q and low Q factor respectively. The central notched frequency may also be controlled simply by modifying the length

of the slot. Both antennas can provide stable omni-directional patterns at frequencies throughout the operating band, even at high frequency (i.e. 10 GHz).

The significant characteristics study of wideband antenna with notched-band behaviour using a simple equivalent circuit model has been introduced in section 5.5. There is a good agreement between the CST simulation and equivalent circuit simulation. Numerical results show that there is trade-off between the gain suppression and the quality factor of the band-notch. Increase the number of resonators and the coupling factor will of course increase the band-rejection. However, it will also widen the bandwidth of the frequency notched band.

Section 5.6 compared the conical monopole incorporating different type of slots with notch band Q factor, total efficiency and gain suppression.

Section 5.7 introduced the low cost production for this type of antenna and the way to control the stopband frequency.

The proposed antennas in this Chapter are promising candidates for use in wideband applications and if scaled down in frequency, for rural area networks (Cognitive Radio based) which will require omni-directional spectrum search antennas [15].

References:

[1]   Z. H. Hu, P. S. Hall, J. R. Kelly and P. Gardner, "Novel Wideband Conical Monopole Antenna with Frequency Band Notched Behaviour", *Electronics Letters*, vol. 46, Issue 23, 2010, pp. 1542-1543.

[2]   H. Kawakami and G. Sato, "Broad-band characteristics of rotationally symmetric antennas and thin wire constructs," *IEEE Trans. on Antennas and Propag.*, vol. 35, no. 1, Jan. 1987, 26-32.

[3]   J. Jamali, N. Tayarzade, and R. Moini, "Analyzing of conical antenna as an ultra-wideband antenna using finite difference time domain method," *Electromagnetics in Advanced Applications, 2007. ICEAA 2007. International Conference on 2007*, pp. 994-997.

[4]   S. Adachi, R. Kouyoumjian, and R. Van Sickle, "The finite conical antenna," *Antennas and Propagation, IRE Transactions* on vol. 7, 1959, pp. 406-411.

[5]   C. A. Balanis, Antenna Theory, 3rd edition, Analysis and Design, John Wiley & Sons, Inc, 2005, pp. 349-362.

[6]   Z. H. Hu, J. R. Kelly, P. Gardner, and P. S. Hall, "Pattern Reconfigurable Wideband Conical Monopole Antenna with frequency notch-band", *Second UK URSI Festival of Radio Science 2011*, University of Leicester, 12th Jan. 2011.

[7]   Z. H. Hu, P. S. Hall, J. R. Kelly and P. Gardner, "Improved band-notched wideband conical monopole antenna", Accepted by *Microwave and Optical Technology Letters*.

[8]   Z. H. Hu, P. S. Hall, J. R. Kelly and P. Gardner, "Wideband omni conical monopole antenna with high Q band-notched behaviour," Accepted by *IWAT 2011*.

[9] W-J. Lui, C-H. Cheng, and H-B. Zhu, "Improved frequency notched ultrawideband slot antenna using square ring resonator*," IEEE Antennas and Propag.*, vol. 55, issue 9, 2007, pp. 2445-2450.

[10] S.- J. Wu, C. – H. Kang, K. – H. Chen, and J. – H. Tarng, "Study of an ultrawideband monopole antenna with a band-notched open-looped resonator", *IEEE Transactions on Antennas and Propagation,*Vol. 58, No. 6, June 2010, pp. 1890-1897

[11] Y. Guo, Y. Zhang, A. Rasmita, and M. – S. Leong, "Equivalent circuit modelling of UWB antennas for system co-design", *Antennas and Propagation Society International Symposium (APSURSI), 2010 IEEE,* 11-17 July, 2010, pp. 1- 4

[12] R. C. Dorf and J. A. Svoboda, *Introduction to Electric Circuits,* 4th edition, John Wiley & Sons inc., 1999, pp. 551-555

[13] David M. Pozar, Microwave Engineering, John Wiley & Sons, Inc. 2nd edition, 1998, pp. 300-350.

[14] R. S. Kwok, and Ji-Fuh Liang, "Characterization of high-Q resonators for Microwave-filter applications", IEEE Transactions on Microwave Theory and Techniques, vol. 47, No. 1, 1january, 1999, pp. 111-114.

[15] IEEE 802.22 Wireless Regional Area Networks - Enabling rural broadband wireless access using cognitive radio technology, IEEE 802.22-10/0073r03, 2010-06-15.

CHAPTER VI

WIDEBAND PYRAMIDAL MONOPOLE ANTENNA WITH

WIDE TUNABLE FREQUENCY BAND-NOTCH

This chapter presents a square section pyramidal wideband monopole antenna incorporating four loop shaped slots [1-2]. Each slot is loaded with varactor diodes to provide a tunable notch-band. Simulation shows it is possible to tune the notch band centre frequency from 4.8 GHz to 7.472 GHz. Three prototypes, two incorporating both capacitors and varactors, and one reference antenna without slots, were fabricated and measured. Compared to previous work reported in the literature, the antenna provides good gain suppression in all horizontal directions in the vertical polarisation. It also yields stable omni-directional radiation patterns at frequencies throughout the operating band. To the best of my knowledge, this is the first time that a non-planar wideband antenna incorporating a tunable notch-band has been reported in the open literature.

All of the simulations presented in this chapter were performed using the transient solver in CST Microwave Studio®. Full equivalent circuits from the vendors' library in Microwave Office were used for the components, although these were not available for varactor diodes.

6.1. Simulated Pyramidal Monopole Antenna with Wide Tunable Frequency Band-Notch

6.1.1. Antenna Design and Structure

Fig. 6.1 illustrates the structure of the antenna. The band-notch is created by a loop shaped slot. A single slot is etched into each side of the pyramid. The pyramidal antenna was mounted above the centre of a flat 80×80 mm^2 copper ground plane, as shown in Fig. 6.1. This type of conical shaped antenna is inherently a wide band radiating element having an omni-directional radiation pattern [3]. For this reason it is well-suited for use in UWB systems [4-5]. By adjusting the height, flare angle as well as the distance between the base of the cone and the ground plane, it was possible to optimize the antenna's radiation pattern and input impedance [4]. The square section pyramidal monopole antenna was constructed by joining together four pieces of microwave substrate material, Taconic TLY-3-0450-C5. This material has a permittivity of 2.33, loss tangent of 0.0009, a thickness of 1.143 mm, and metal thickness of 0.01778 mm. The substrate was metalized on one side only. Each slot is loaded with a lumped capacitor or varactor diode. The resonant frequency of the embedded slot changes when the value of the capacitance changes. The quality (Q) factor associated with the notched band depends on the width of the upper part of the loop, which is denoted as 'w_u' in Fig. 6.1(b). Increasing the width of the slot reduces the Q factor. The vertical distance between the base of the slot and the bottom of the cone (1.62 mm) should be chosen to ensure that the maximum amount of current on the surface of the cone is intercepted by the slot. The antenna's dimensions are given in Table 6.1.
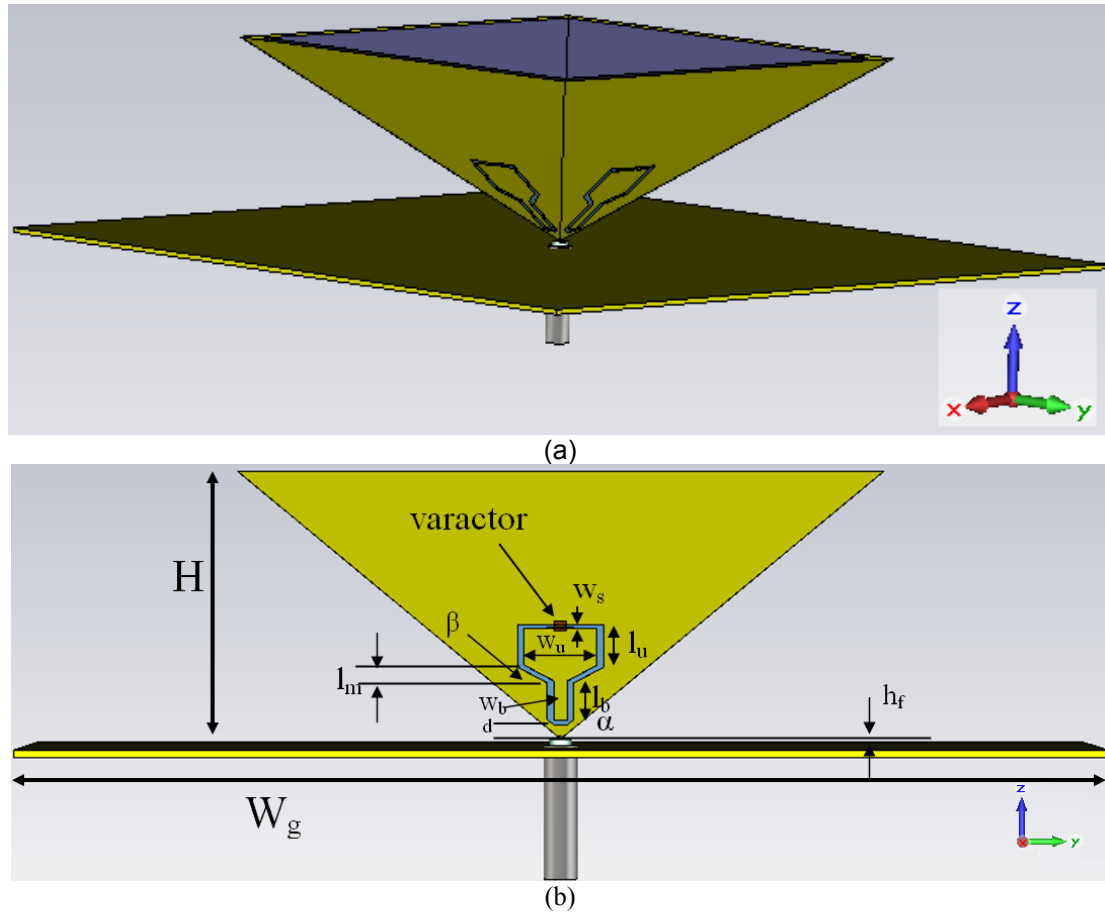
Fig. 6.1 (a) Structure of pyramidal antenna with four shaped loop slots; (b) dimensions of the slotted antenna

H	20.0 mm	g	1.0 mm
w_s	0.5 mm	h_f	0.5 mm
d	1.71 mm	w_u	5.4 mm
Wg	80.0 mm	w_b	1.0 mm
l_u	5.0 mm	l_m	2.88 mm
l_b	6.0 mm	α	40°
β	50°	-	-

Table 6.1 Antenna Dimensions

6.1.2. Simulation Results – Reflection Coefficient

Ideal components, without parasitics, were used in the simulation study. Fig. 6.2 shows the simulated reflection coefficient for the slotted antenna. The various curves

were obtained by altering the value of the capacitor within each slot from 0.1 pF to 10 pF. This causes the notch band centre frequency to vary from 4.8 GHz to 7.472. The instantaneous bandwidth of the notch-band is given in Table 6.2 for various different notch frequencies. Table 6.2 shows that the minimum bandwidth (96 MHz) occurs at 7.472 GHz. This corresponds to a Q factor of 77.83. The maximum bandwidth is 264 MHz. This occurs at 5.264 GHz and 4.888 GHz and corresponds to Q factors of 19.94 and 18.52, respectively.
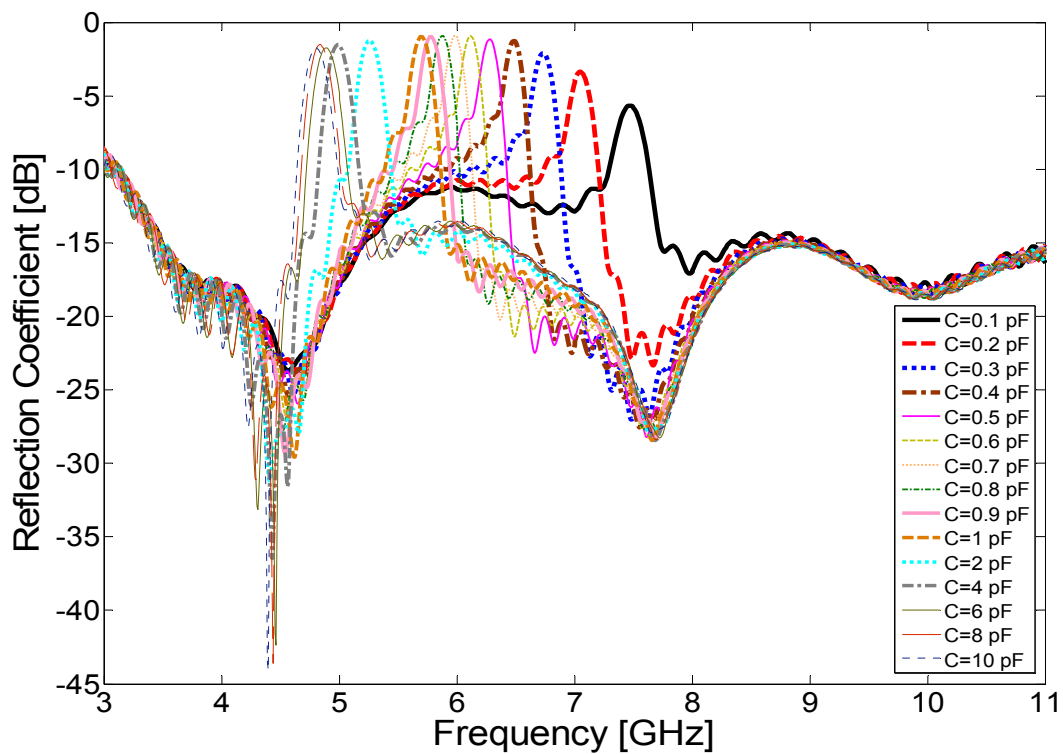
Fig. 6.2 Simulated reflection coefficient for slotted antennas with variable C (from 0.1 pF to 10 pF)

Capacitor (pF)	Freq. (GHz)	Refl. Coeff. (dB)	Band-rejection bandwidth@ 6 dB (MHz)	Q factor
0.1	7.472	-5.660	96	77.83
0.2	7.056	-3.361	208	33.92
0.3	6.736	-2.088	224	30.07
0.4	6.488	-1.255	232	27.97
0.5	6.280	-1.159	240	26.17
0.6	6.120	-0.942	248	24.68
0.7	5.984	-0.908	256	23.38
0.8	5.872	-0.919	256	22.94
0.9	5.776	-0.969	256	22.56
1	5.696	-0.980	256	22.25
2	5.264	-1.241	264	19.94
4	4.992	-1.508	256	19.50
6	4.888	-1.761	264	18.52
8	4.832	-1.537	256	18.88
10	4.800	-1.740	256	18.75

Table 6.2 Simulated reflection coefficient for the slotted antenna with capacitors varied from 0.1 pF to 10 pF, respectively

6.2. Prototype Incorporating Fixed Capacitors

Four prototypes incorporating fixed capacitors, i.e. 0.2 pF, 0.5 pF, 1 pF, 10 pF, have been fabricated, as shown in Fig. 6.3. A fifth square section pyramidal monopole, without slots, was also fabricated as a reference antenna.
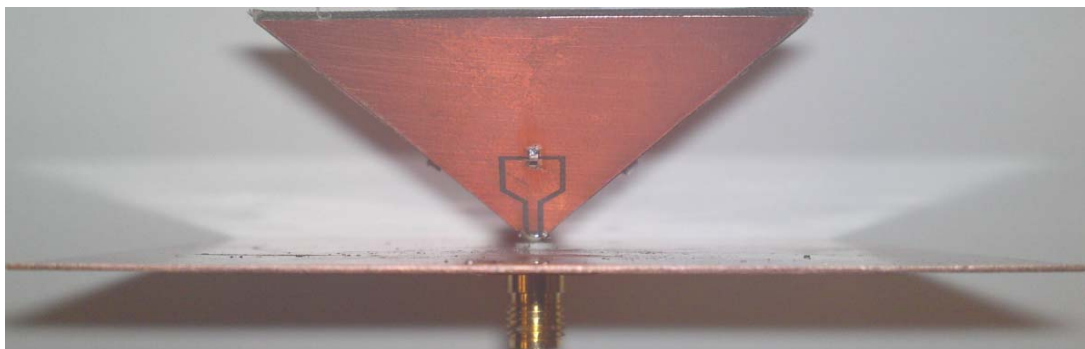
Fig. 6.3 Side view of the completed fabricated prototype

6.2.1. Reflection Coefficient

Fig. 6.4 shows the simulated and measured reflection coefficient of the proposed slotted antenna. In this case, a fixed 1 pF capacitor was connected across the slot. The band notch centre frequency is 5.304 GHz, and 5.04 GHz, according to simulation and measurement respectively. At this frequency the return loss is 1.01 dB and 2.84 dB, according to simulation and measurement respectively. The notch band frequency and return loss, obtained through simulation and measurement, differ by, at most, 1.83 dB and 264 MHz. These discrepancies are due to manufacturing tolerances and lumped element component parasitics. Fabricated slotted antennas incorporating four capacitively loaded slots are shown in Fig. 6.5 alongside the reference antenna. In total four prototypes were constructed, incorporating the following capacitor values 0.2 pF, 0.5 pF, 1 pF and 10 pF. The notch centre frequencies are 6.91 GHz, 5.76 GHz, 5.04 GHz and 4.195 GHz, with the return loss values of 3.89 dB, 2.42 dB, 2.84 dB, and 2.91 dB, respectively. Measured results also show that the notch bands for those capacitor values have 6 dB return loss bandwidths of 190 MHz, MHz, 140 MHz and 105 MHz, respectively. This corresponds to a quality factor of 36.4, 30.3, 36.0 and 40.0, respectively. In these simulations full models of the components, incorporating parasitics and dielectric losses, were used, represented by the manufacturers' models or s-parameters files.
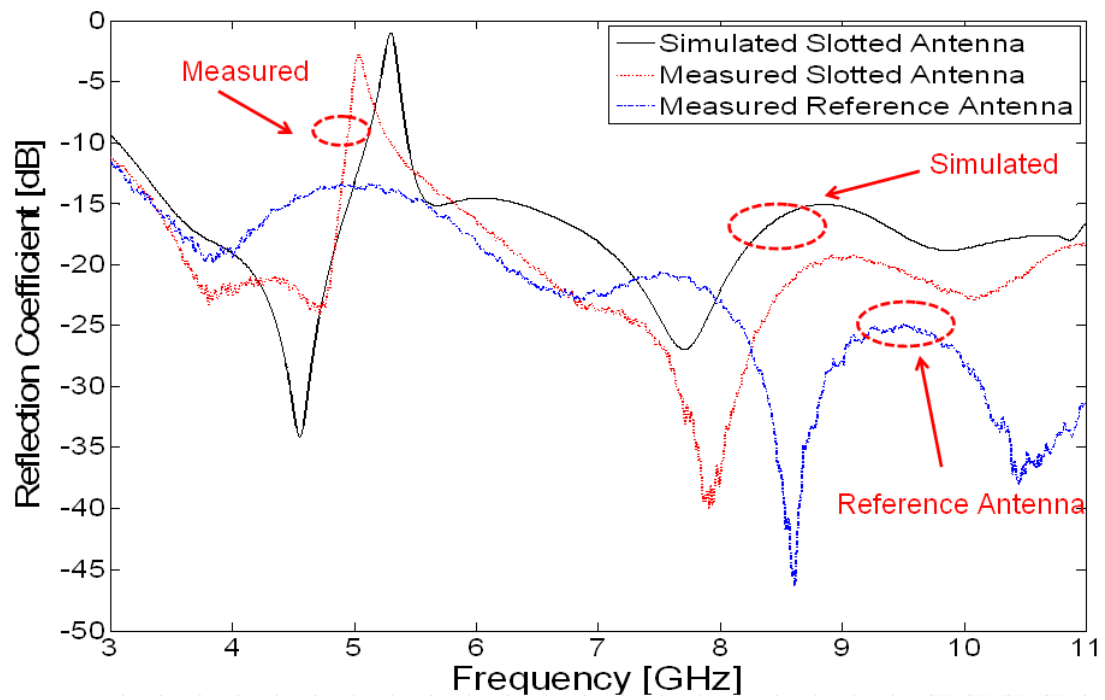
Fig. 6.4 Simulated and measured reflection coefficient for slotted antennas with four 1 pF capacitors (shown in Fig. 6.3) and the reference antenna
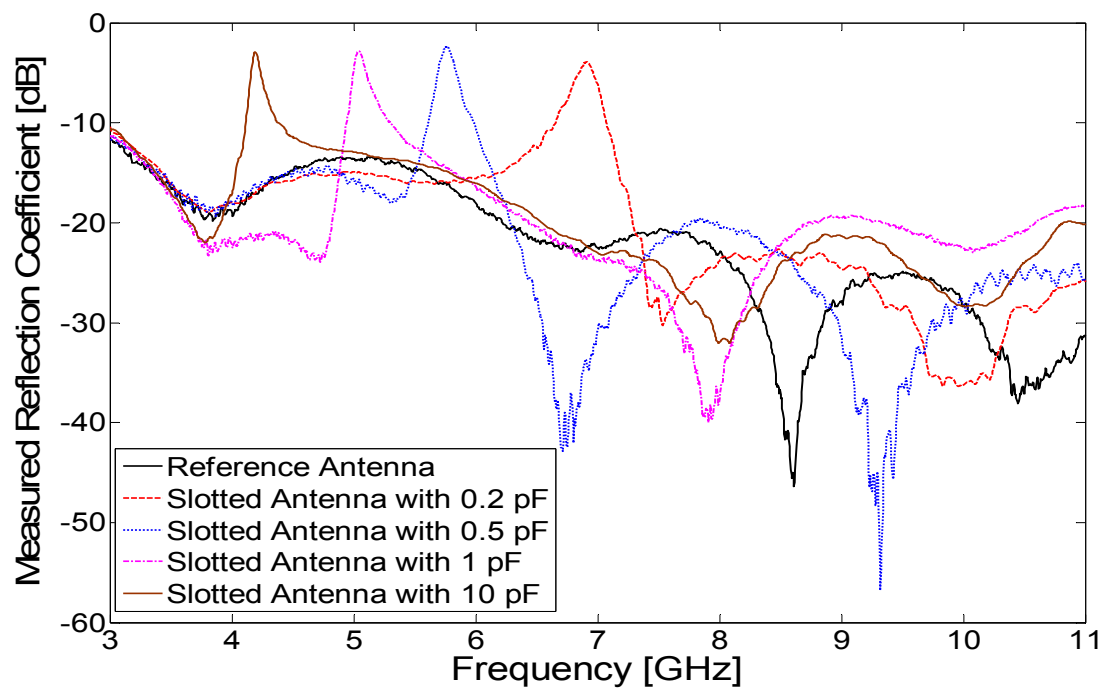
Fig. 6.5 Measured reflection coefficient for slotted antennas with four 0.2 pF, 0.5 pF, 1 pF and 10 pF capacitors, and the reference antenna, respectively

6.2.2. Radiation Patterns

Fig. 6.6 shows measured radiation patterns for the slotted antenna with four 1 pF capacitors at 5.04 GHz in both E-(zy-) and H-(xy-) planes. Measurement shows that the pattern maximum is directed towards at an angle of 85° in H-(xy-) plane, as shown in Fig. 6.6(b).

(a)   (b)
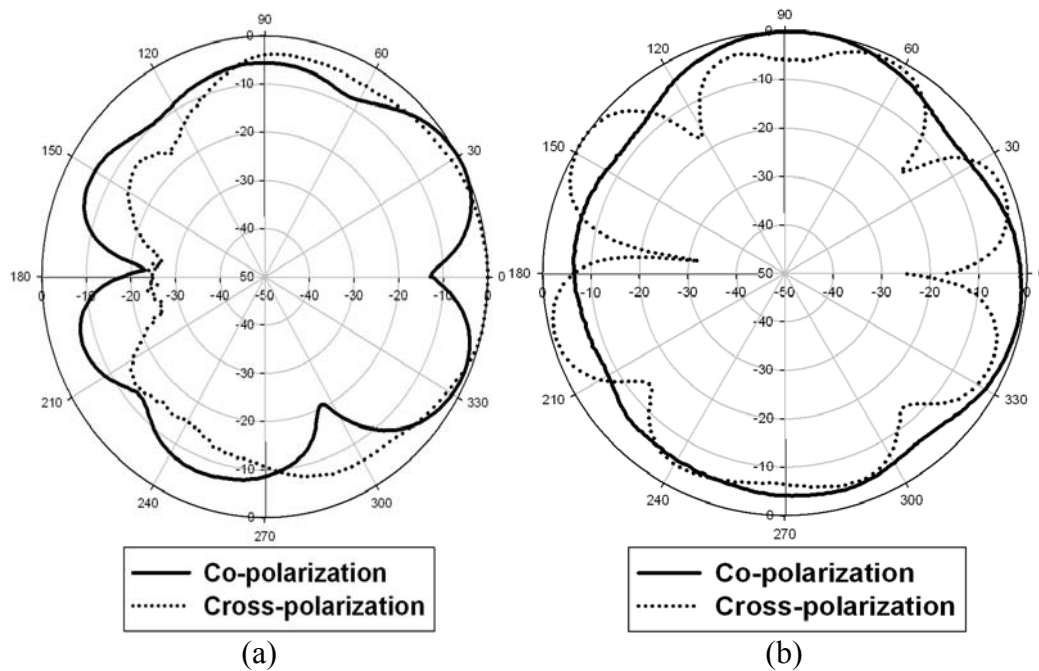
Fig. 6.6 Measured normalized radiation patterns for the slotted antennas incorporating four 1 pF capacitors at 5.04 GHz in (a) E-(zy-) plane; (b) H-(xy-) plane.

Measured both E-(zy-) plane and H-(xy-) plane patterns for a slotted antenna incorporating four 1 pF capacitors at other frequencies are presented in Fig. 6.7. The proposed antenna has a very stable omni-directional pattern even at high frequencies such as 10 GHz. Table 6.3 shows the values of standard deviation from omni-directional, for the slotted antenna incorporating four 1 pF capacitors, are 0.41 dB, 0.62 dB and 0.68 dB at 4 GHz, 8 GHz, and 10 GHz, respectively. The large cross-polar component, shown in Fig. 6.7, is due to the use of a square ground plane.

Simulations show that this component can be reduced by using a circular ground plane. For example a circular ground plane with a diameter of 40 mm reduces the cross polar at 4 GHz by at least 19 dB as shown in Fig. 6.8.
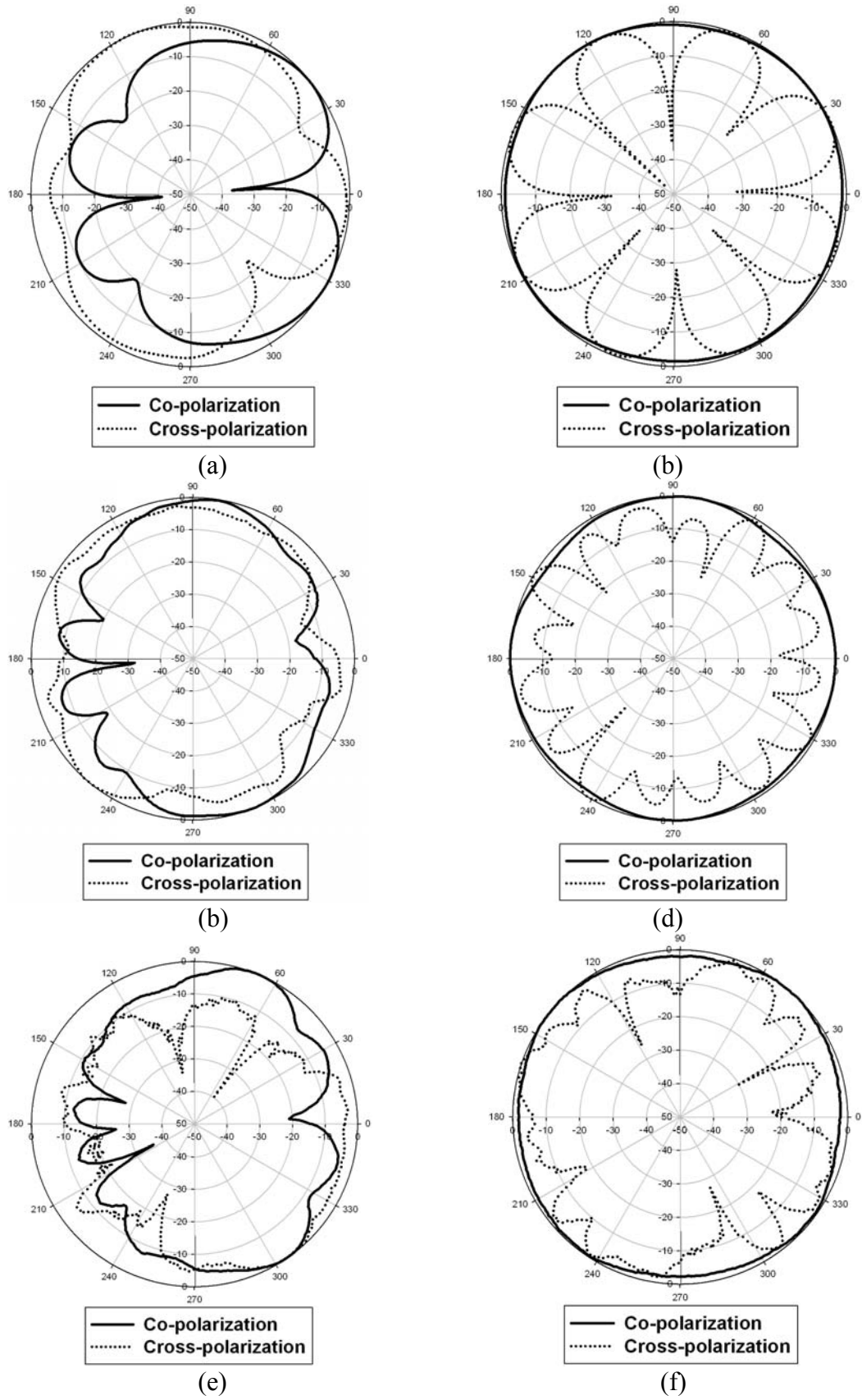
Fig. 6.7 Measured normalized radiation patterns for the slotted antennas incorporating four 1 pF capacitors (a) in E-(zy-) plane at 4 GHz ; (b) in H-(xy-) plane at 4 GHz; (c) in E-(zy-) plane at 8 GHz; (d) in H-(xy-) plane at 8 GHz; (e) in E-(zy-) plane at 10 GHz; (f) in H-(xy-) plane at 10 GHz

Frequency [GHz]	Standard deviation from Omni-directional (dB)
4	0.41
8	0.62
10	0.68

Table 6.3 Standard deviation in dB from omni-directional for the slotted antenna incorporating four 1 pF capacitors at 4, 8 and 10 GHz
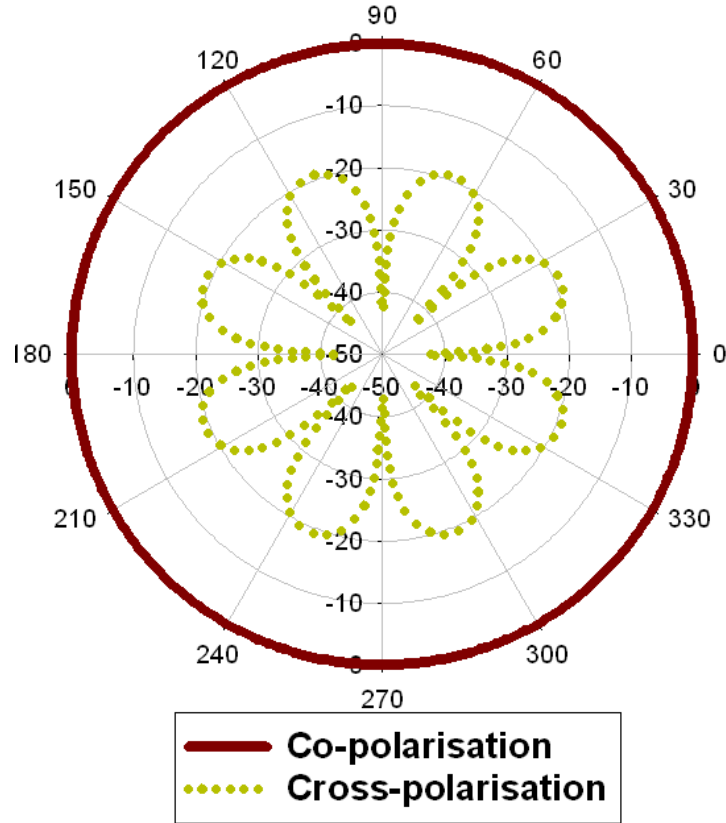
Fig. 6.8 Simulated normalized radiation patterns in H-(xy-) plane for the slotted antennas incorporating four 1 pF capacitors with a circular ground plane with a diameter of 40 mm at 4 GHz

6.2.3. Gain Suppression

Fig. 6.9 plots the measured azimuthal (i.e. xy-) plane gain in the peak direction for several different antennas. The gain for the slotted antenna incorporating four 1 pF capacitors, for example, is plotted in the direction of the main lobe in xy-plane (as shown in Fig. 6.6), which is $\phi = 85^{0}$. The slotted antennas, featured in Fig. 6.9, incorporate 0.2 pF, 0.5 pF, 1pF and 10 pF capacitors, respectively. At the band notch

the peak gain of the four antennas is reduced to -7.52 dBi, -8.79 dBi, -13.21 dBi and -9.28 dBi, respectively. The reference antenna has a gain of 0.5 dBi, -1.9 dBi, -3.2 dBi and -3.7 dBi, at each of these notch band centre frequencies, respectively. For a conventional monopole, a higher gain might be expected. Such a low gain is due to the small ground plane used and the fact that the maximum directivity is not in the H- (xy-) plane. It shows that there is approximately 8 dB, 6.9 dB, 10 dB and 5.6 dB of gain suppression in the peak directions for those slotted antennas, respectively.
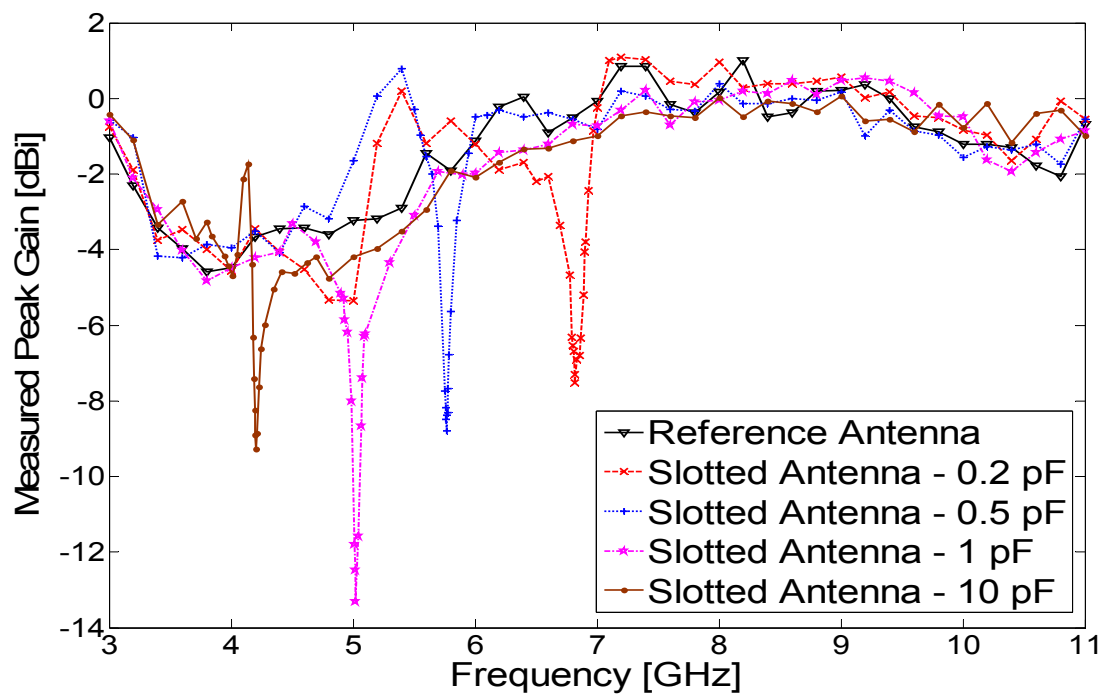
Fig. 6.9 Measured peak gain for the slotted antennas with four different values of capacitors (i.e. 0.2 pF, 0.5 pF, 1 pF and 10 pF) and the reference antenna

Fig. 6.10 shows the effect on the notch centre frequencies and the peak gain suppression when the capacitance varies from 0.1 pF to 10 pF in simulation and measurement.
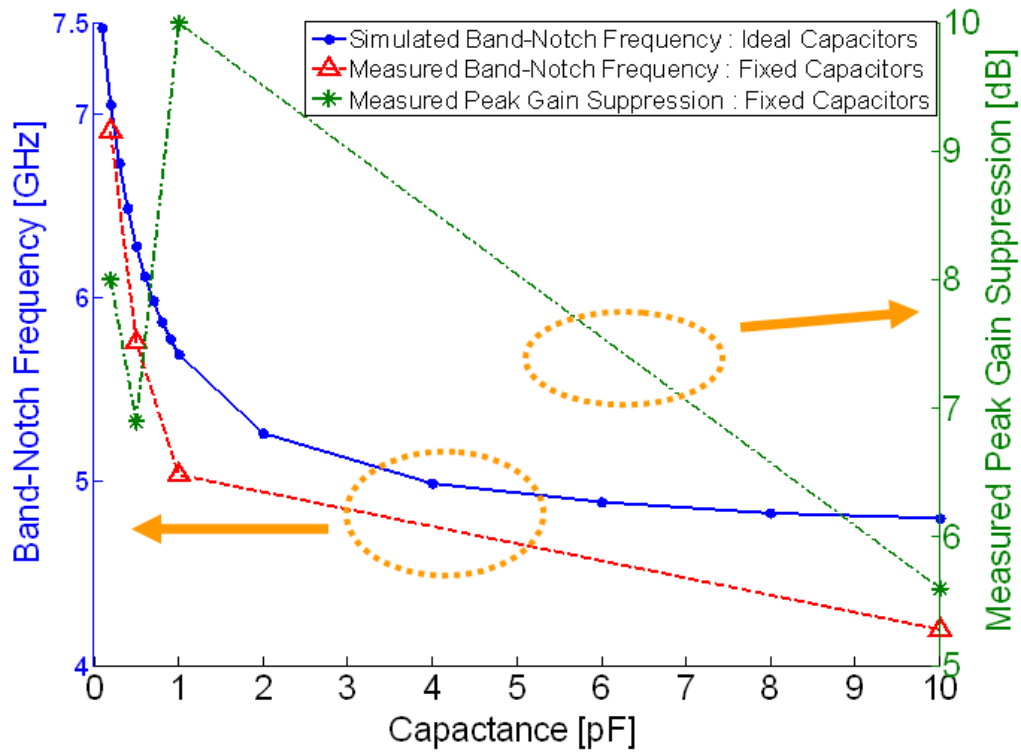
Fig. 6.10 Simulated, measured band-notch frequencies and measured peak gain suppression when the capacitors vary from 0.1 pF to 10 pF, respectively

6.3. Prototype Incorporating Varactors

Fig. 6.11 illustrates the structure of an antenna incorporating four varactor diodes, MV31009-150A, from Microsemi®. The capacitance of these varactors is variable from 0.946 pF to 21.982 pF for an applied voltage of 15 V to 0 V. A dc bias line, incorporating four 10 k Ω chip resistors, was attached to the anode of varactors to supply +ve voltage. The resistor is used to choke any residual RF signals appearing on the dc line. The −ve voltage is supplied from the inner conductor of the SMA connector by using a bias-tee (ZX85-122G-S+, from Mini-Circuits®).
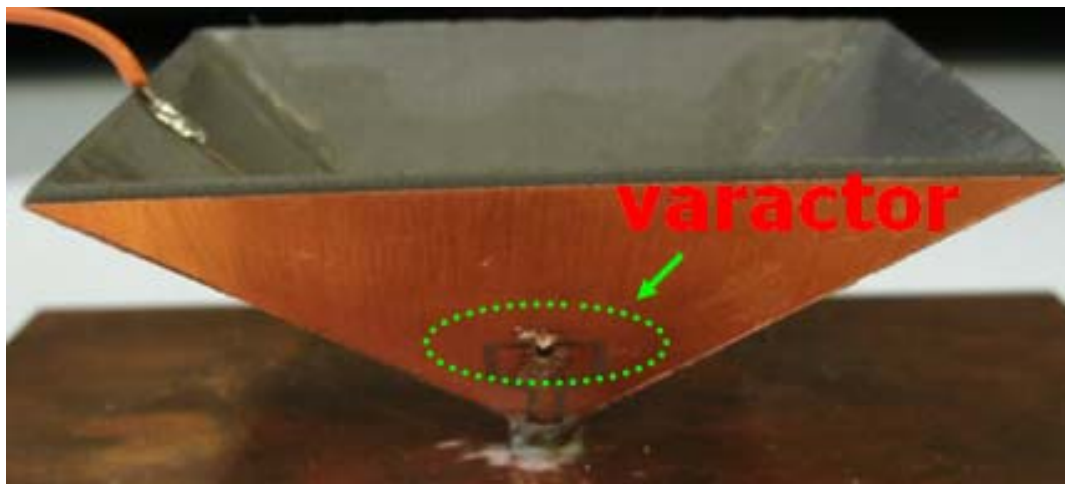
(a)
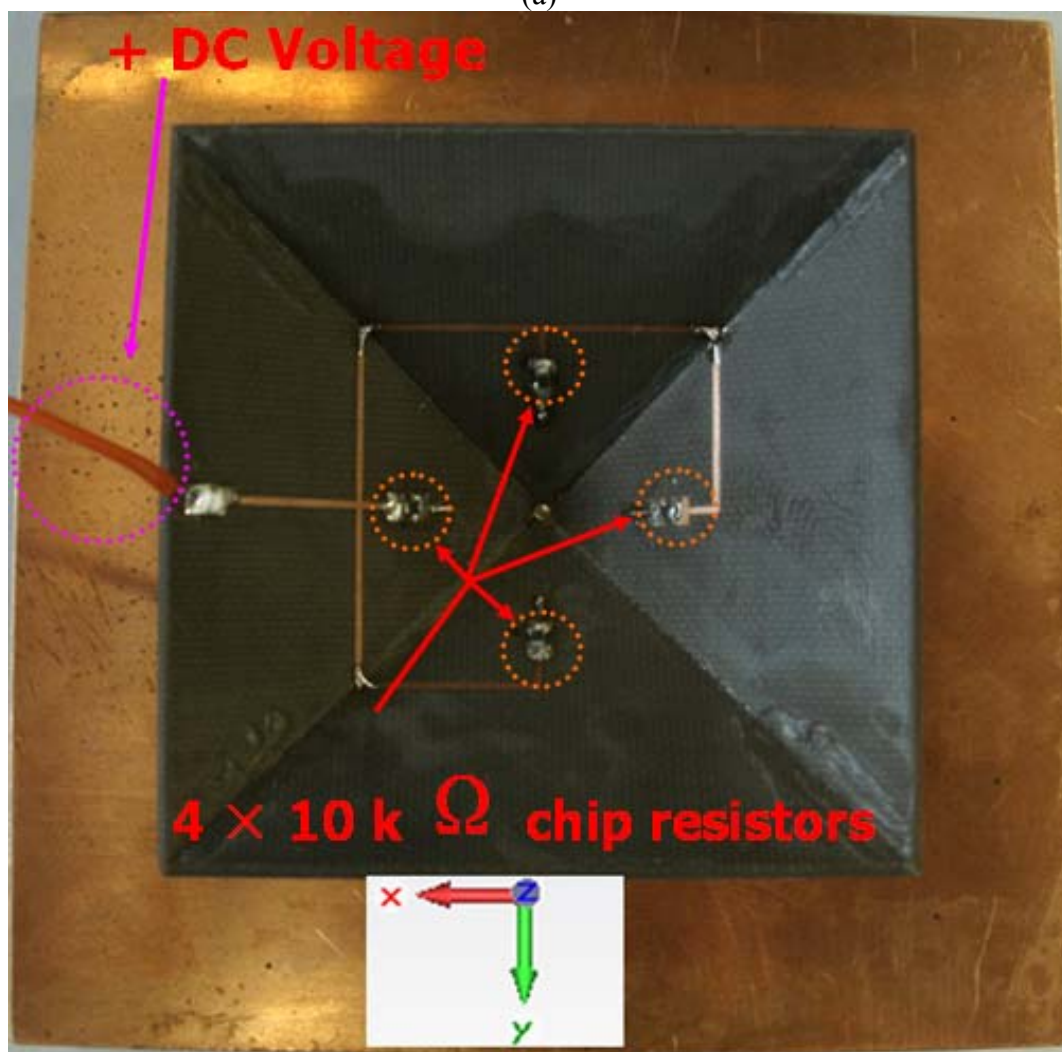
(b)

Fig. 6.11 The fabricated prototype with four varactors (a) side view; (b) top view

6.3.1. Reflection Coefficient and Gain Suppression

Fig. 6.12 shows the measured reflection coefficient of a slotted antenna incorporating four varactor diodes. The dc bias on the varactors was varied from 0 V to 15 V. This causes the notch band centre frequency to vary from 3.79 GHz to 4.885 GHz (as seen in Table 6.4), with a return loss from 7.63 dB to 4.96 dB. It is likely that the frequency tuning range could be increased, if the capacitance tuning range of the varactor was wider. The measured band-notch frequencies for the slotted antenna with four varactor diodes with applied voltage of 0 V to 15 V, is plotted in Fig. 6.14.
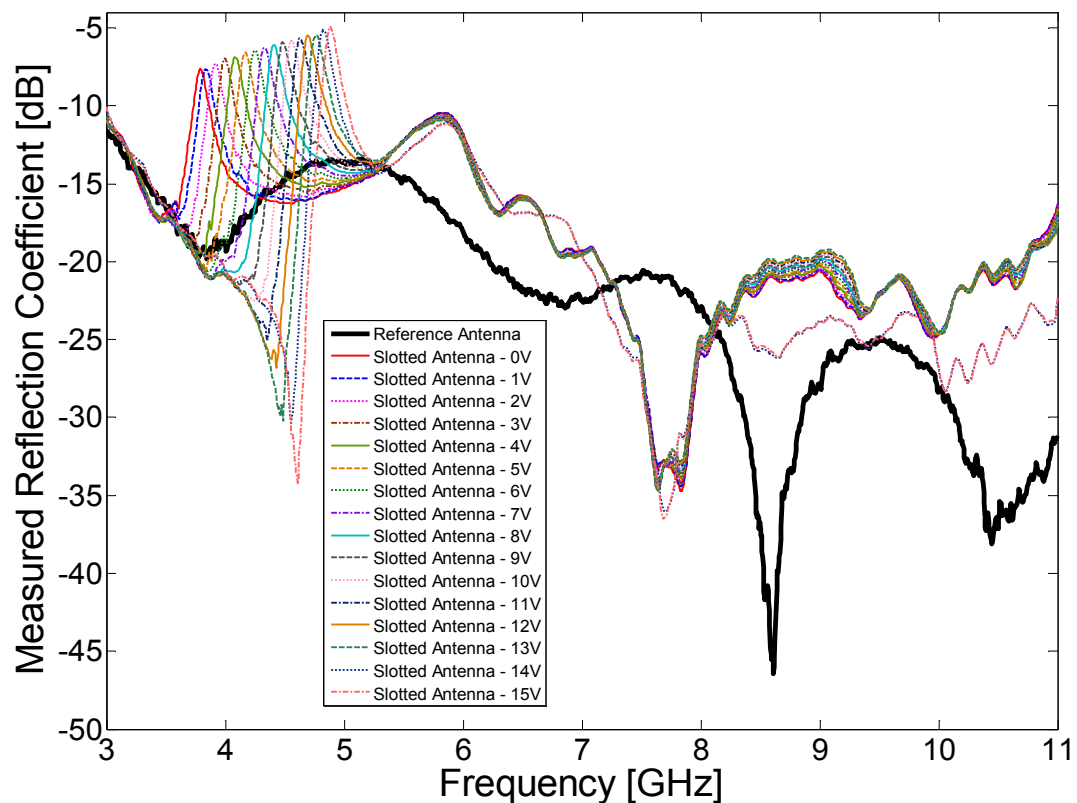
Fig. 6.12 Measured reflection coefficient for slotted antennas with four varactor diodes, and the reference antenna, respectively

Voltage (V)	Freq. (GHz)	Refl. Coeff. (dB)
0	3.790	-7.63
1	3.835	-7.65
2	3.920	-7.31
3	3.995	-6.96
4	4.085	-6.86
5	4.170	-6.56
6	4.250	-6.44
7	4.330	-6.26
8	4.405	-6.08
9	4.485	-5.92
10	4.560	-5.84
11	4.625	-5.70
12	4.695	-5.48
13	4.760	-5.46
14	4.825	-5.13
15	4.885	-4.96

Table 6.4 Measured reflection coefficient for slotted antennas with four varactor diodes, which are varied an applied voltage from 0 V to 15 V.

Fig. 6.13 illustrates the measured gain suppression in –x direction of H-(xy-) plane for the slotted antenna with four varactor diodes, with applied voltage of 0 V to 15 V, compared to reference antenna. Please note that such a low gain at higher frequencies is due to the small ground plane used and the fact that the maximum directivity is not in the H-(xy-) plane, as mentioned earlier. Fig. 6.14 shows how the gain suppression changes with four varactor diodes with applied voltage of 0 V to 15 V. From 4.14, it is clear that the minimum gain suppression, of only about 3 dB, was achieved with an applied voltage of 5 V and the maximum gain suppression, of about 8 dB, was achieved with an applied voltage of 14 V. The varactors, MV31009-150A, from Microsemi[®], used in Fig. 6.11 have a series resistance of 0.455 Ω when the applied voltage is set to 4 V.
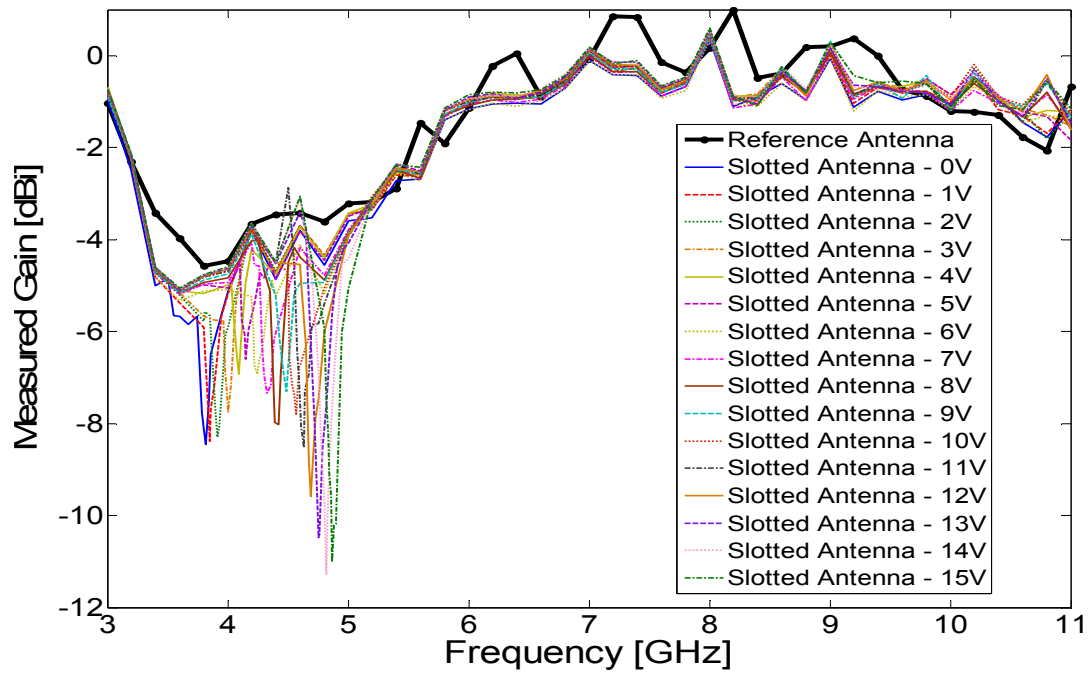
Fig. 6.13 Measured gain for the slotted antenna with four varactor diodes (shown in Fig. 6.11) and the reference antenna in the –x direction of the azimuthal (i.e. xy-) plane
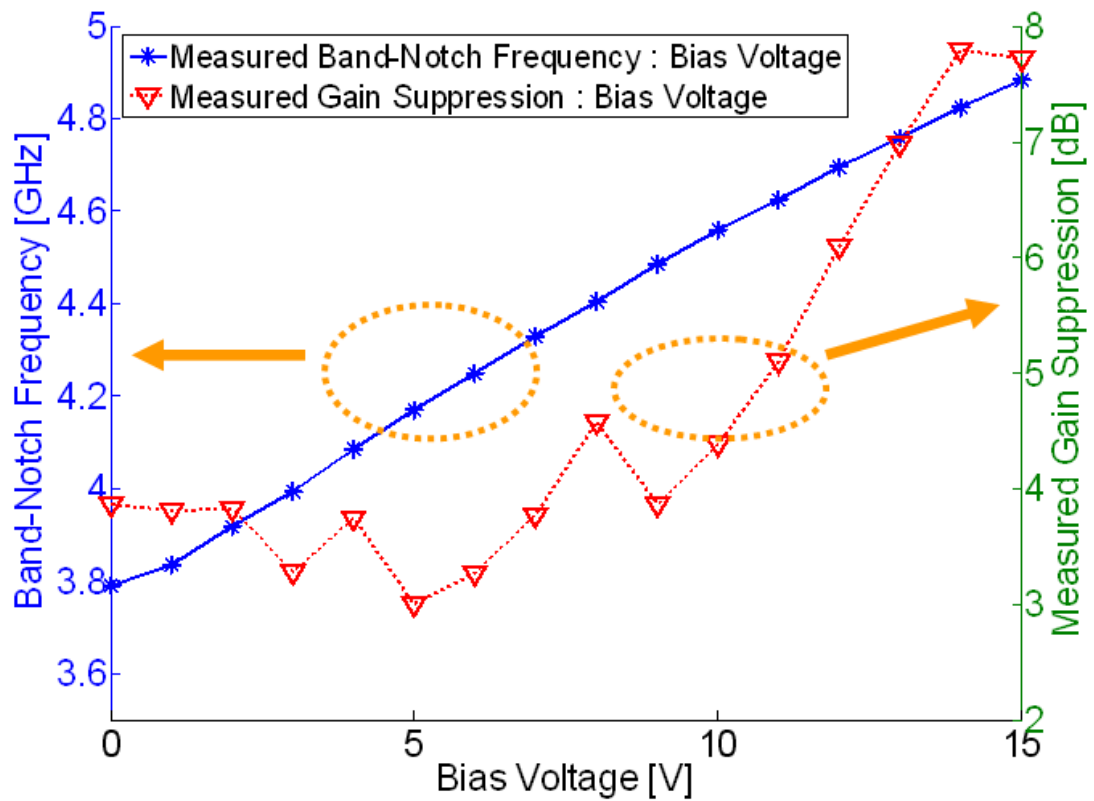
Fig. 6.14 Measured band-notch frequencies and gain suppression (in –x direction of xy-plane, see Fig. 6.11) for the slotted antenna with four varactor diodes with applied voltage of 0 V to 15 V, respectively

6.3.2. Radiation Patterns

Fig. 6.15 shows the measured H-(xy-) plane co-polar radiation patterns for a slotted antenna with four varactor diodes. The pattern was obtained at 10 GHz, for an applied voltage of 0 V, 8 V and 15 V, respectively. For conventional printed antennas, the patterns in H-plane become unstable at high frequencies. And it has been shown that the slotted antenna, incorporating four 1 pF capacitors, provides omni-directional patterns at 4, 8 and 10 GHz in section 5.2.2. Thus only radiation patterns in H-plane at 10 GHz are given in this section. It is clear that the proposed antenna has a very stable omni-directional pattern even at high frequencies such as 10 GHz. Table 6.5 shows the values of the standard deviation from omni-directional for the slotted antenna, incorporating four varactor diodes with applied voltage of 0 V, 8 V and 15 V, at 10 GHz, are 0.63 dB, 0.67 dB, and 0.66 dB, respectively.
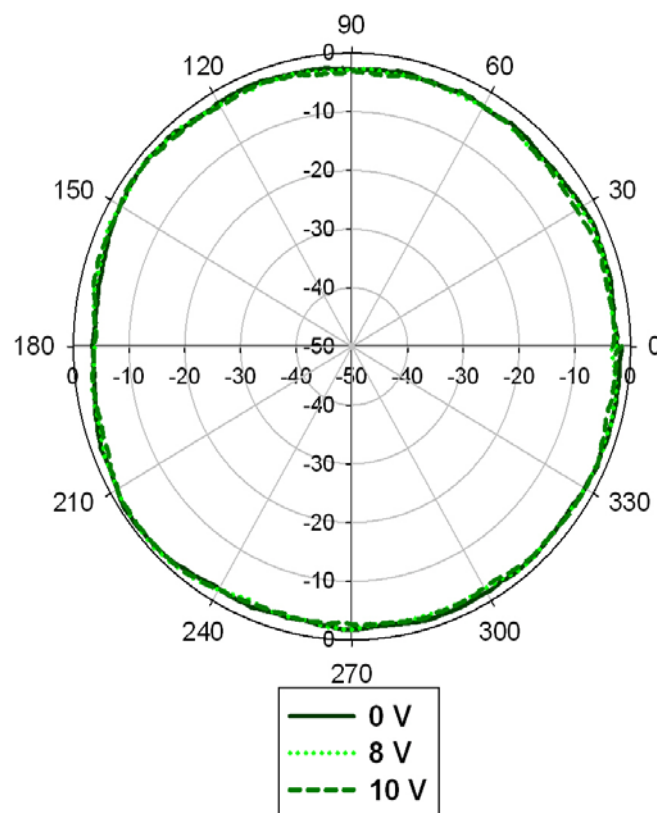
Fig. 6.15 Measured normalized xy-plane co-polarization radiation patterns for the slotted antennas with four varactors (shown in Fig. 6.11) at 10 GHz, with applied voltage of 0 V, 8 V and 15 V, respectively

Applied Voltage (V)	Frequency [GHz]	Standard deviation from Omni-directional (dB)
0	10	0.63
8	10	0.67
15	10	0.66

Table 6.5 Standard deviation in dB from omni-directional for the slotted antenna with four varactors at 10 GHz, with applied voltage of 0 V, 8 V, 15 V, respectively

6.3.3. Caparison between Capacitors and Varactors

Table 6.6 shows the comparison between the slotted antenna incorporating lumped capacitors and varactors. It shows that the frequency tuning range could be increased, if the capacitance tuning range of the varactor could be wider. It also shows that the gain suppression in the slotted antenna incorporating varactors is lower because of the much higher resistance compared to lumped capacitors. Thus, using varactors with lower resistance, or variable capacitance RF MEMS devices with very low resistance, will increase the gain suppression, thus improving the band-rejection.

	Lumped Capacitor	MV31009-150A Varactor
Capacitance [pF]	0.2 to 10	0.946 to 21.982
Bias voltage range	N/A	0 to 15 V
Resistance [Ω]	From 0.1 to 0.25	0.455 at 4 V
Notch frequency range [GHz]	4.195 to 6.91	3.79 to 4.885
Maximum gain suppression [dB]	10*	7.8[+]
Minimum gain suppression [dB]	5.6*	3[+]

Table 6.6 Comparison between the slotted antenna incorporating capacitors and the one incorporating varactors
* the peak direction in H-(xy-) plane; [+] -x direction in H-(xy-) plane

6.4. Design Guideline

The pyramidal monopole antenna is made from four triangular printed circuit boards and mounted above the centre of the ground plane, shown in Fig. 6.16. The first step is to optimize the antenna impedance to cover the required band, i.e. from 3 GHz to

11 GHz, by adjusting the height "H", flare angle "a" as well as the distance between the base of the cone and the ground plane "h_f". The second step is to consider how to get notched band. Any shape of slot would be etched into each side of the pyramid to achieve band-rejection. Due to the dielectric loss of the substrate, the distance between two arms of slot can not be too small in order to have certain Q and band-rejection. However, the bottom width of the slot needs to be small enough to locate close to the fed point in order to intercept the current to achieve high gain suppression within the notched band. For this pyramidal shape, a loop shaped slot, shown in Fig. 6.16, is designed. The whole length of the slot is about half wavelength and of course will be affected by the distance from the fed point. The bandwidth or Q factor associated with the notched band would be controlled by changing the width of the upper part of the loop "W_u". By loading with the lumped capacitor or varactor diode, the resonant frequency of the embedded slot would be adjusted and will changes with different value of capacitance. The higher notched band frequency is dependent on the maximum capacitance. For example, the notched band frequency of the pyramidal monopole antenna, with the dimension shown in Table 6.1, without loading capacitor, will be about 6.6 GHz and the notched band frequency will change to 4.8 GHz when loading with a 10 pF capacitor.
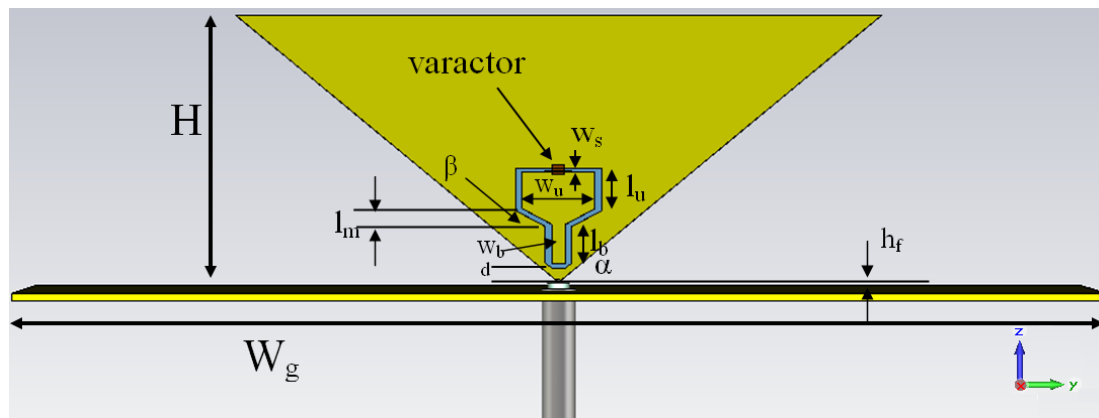
Fig. 6.16 Side view of pyramidal antenna with four shaped loop slots

6.5.   Summary

This chapter proposes a novel pyramidal monopole antenna with four loop shaped slots. Simulation shows that by loading each slot with a varactor diode, it is possible to tune the notch band centre frequency from 4.8 GHz to 7.472 GHz. The quality factor can be controlled by adjusting the width of the upper part of the slot. Prototypes with capacitors and varactors, respectively, were fabricated and measured.

Experimental results show the there is approximately 8 dB, 6.9 dB, 10 dB and 5.6 dB of gain suppression in the peak directions for those slotted antennas incorporating fix capacitors, such as 0.2 pF, 0.5 pF, 1 pF and 10 pF, respectively and they also provide stable omni-directional radiation patterns within the operating bands even at high frequencies, such as 10 GHz.

Measurements show that the reflection coefficient of a slotted antenna incorporating four varactor diodes. When the dc bias on the varactors was varied from 0 V to 15 V, this causes the notch band centre frequency to vary from 3.79 GHz to 4.885 GHz (as seen in Table. 4.3), with a return loss from 7.63 dB to 4.96 dB. It is likely that the frequency tuning range could be increased, if the capacitance tuning range of the varactor was wider.

Dynamic tuning is possible with electrically variable capacitance devices, such as varactors, although the parasitic resistance limits the band rejection levels. Alternative tuning devices such as MEMs variable capacitors may address this problem. The antenna is a promising candidate for use in wideband applications. If scaled down in

frequency it could also be used in IEEE 802.22, cognitive radio rural area networks [6], which require omni-directional spectrum search antennas.

References:

[1]   Z. H. Hu, P. S. Hall, J. R. Kelly and P. Gardner, "UWB pyramidal monopole antenna with wide tunable band-notched behaviour," *Electronic Letters,* vol. 46, Issue 24, 2010, pp. 1588-1590.

[2]   Z. H. Hu, P. S. Hall, J. R. Kelly and P. Gardner, "Novel wideband pyramidal monopole antenna with wide tunable band-notched," Accepted by *EUCAP 2011,* Roma, Italy.

[3]   H. Kawakami and G. Sato, "Broad-band characteristics of rotationally symmetric antennas and thin wire constructs," *IEEE Trans. On Antennas and Propag.,* vol. 35, no. 1, Jan. 1987, 26-32.

[4]   J. Jamali, N. Tayarzade, and r. Moini, "Analyzing of conical antenna as an ultra-wideband antenna using finite difference time domain method," *Electromagnetics in Advanced Applications,* 2007, pp. 994-997.

[5]   S. Adachi, R. Kouyoumjian, and R. Van Sickle, "The finite conical antenna," *Antennas and Propagation, IRE Transactions on* vol. 7, 1959, pp.406-411.

[6]   IEEE 802.22 Wireless Regional Area Networks - Enabling rural broadband wireless access using cognitive radio technology, IEEE 802.22-10/0073r03, 2010-06-15.

CHAPTER VII
CONCLUSIONS AND FUTURE WORK

7.1. Conclusions

This dissertation describes research into "Antennas with Frequency Domain Control for Future Communication Systems" and several novel antennas are shown, each of which address a specific issue for current and future communication systems, in terms of wideband coverage, channel capacity, antenna isolation and band-rejection. These antenna designs may be candidates for implementation in future multiband radios, and software defined radio (SDR) and cognitive radio (CR) systems, although it is evident that there are as yet no clear specifications for those future systems. Additionally, the reconfigurable two port chassis-antenna and reconfigurable balanced antenna have led to three patent applications.

7.1.1. Conclusions for Reconfigurable Two Port Chassis-Antenna

Future mobile devices might require an antenna that can operate in wide frequency range, which approximately covers FM radio broadcast, private mobile radio, radio microphones, TV broadcast, the current mobile phone bands, WiFi and other possible bands. In addition, supporting wideband radio links designed to handle large amounts of data will be expected in the next generation of mobile phones. It is therefore important to have an agile device that can cater for as wide a bandwidth as possible with the capability to provide operation in at least two bands simultaneously, to provide, for example cellular communications and wireless LAN connectivity.

Chapter 3 presents a novel two-port reconfigurable antenna, using a pair of coupling elements to excite resonant modes within the handset chassis. In this kind of resonant antenna-chassis combination, the coupling elements are typically located from the edge of the handset chassis, enabling the whole length of the chassis to be used as a radiating element. The larger element primarily excites modes within the lowermost band of frequencies, while the smaller one primarily excites modes within at the uppermost band of frequencies. Using a number of external matching circuits including switches and varactor diodes, the antenna can operate in either a narrowband or wideband mode.

The total tuning range is depended on the capacitance range of varactor diodes. Studies showed that the selection of a frequency in port 1 will restrict choice in port 2, and vice versa. The use of varactors and switches may lead to nonlinear effects, but these are beyond the scope of this study. Size investigation showed that the small size of the antenna will lead to low efficiency, which is expected from the Harrington-Chu limits. Measured results show that when the two resonant frequencies are close to one other, there will be strong coupling between the two ports. It could be reduced either by a decoupling network or an additional element, which should be investigated in future. This two port chassis antenna is also limited to a maximum of two simultaneous service accesses. Incorporating additional coupling elements should be help to alleviate this problem.

A new equivalent circuit for the chassis-antenna, with a single coupling element, was derived and shown to model the impedance of the antenna better than was previously achieved. For the chassis-antenna with two coupling elements, the equivalent circuit

model become more complex and an impedance inverter has been used to represent the coupling between two closely separate coupling elements. A further study needs to be continued in future to provide sufficient details to explain the coupling between the two close coupling elements.

7.1.2. Conclusions for Reconfigurable Balanced Antenna and Its MIMO Applications

In order to enhance communication performance in terms of improved signal quality and reliability, by use of multi-path propagation, without requiring additional spectrum bandwidth, a frequency agile MIMO antenna, with wide tuning range, will be demanded. Three different structures of wideband reconfigurable balanced antennas have been presented in Chapter 4, for use in current and future mobile wireless communication systems and for possible reconfigurable MIMO applications. To my best knowledge this is the first reconfigurable MIMO antenna with such a wide tuning range. The proposed MIMO antenna is potentially able to cover multiple wireless standards, such as the LTE 700, GSM850, PCN, GSM1800, GSM1900, PCS1900 and UMTS bands.

For the balanced antenna, two identical L-network matching circuits are connected to each leg, and then connected to an LC balun. To minimize the component count, the design of the matching network and the balun is co-optimized. Each matching circuit incorporates a single varactor diode together with a bank of fixed inductors. The number of resonant frequencies is dependent on the complexity or length of the dipole. For example, a small planar dipole only offers single resonant from 700 MHz to 3000 MHz; a dipole with 70 mm length of arms provides up to three resonant frequencies

which are controlled by the matching circuit. When the balanced antenna is combined with the two-port chassis-antenna, which also has a wide tuning range, it becomes a reconfigurable MIMO antenna for small terminals, and has good measured isolation, of at least 15 dB. By inserting a slot into the ground plane, it helps to isolate the two external matching circuits, that is to say, the matching circuit for balanced antenna and the matching circuit for chassis-antenna, so improving the gain of chassis-antenna. However, from a system integration point of view, this makes one part of the circuit board floating with respect to the reference common ground. A number of surface mount inductor across the slot, acting as a RF choke, could solve this problem.

The total tuning range is dependent on the capacitance range of varactor diodes and the size of the balanced element. The study of the balanced element shows that there is a trade-off between the tuning range, efficiency and size. Small dipole suffers low efficiency due to high dissipated loss on the lumped elements in the circuit. This problem can be solved either use low loss components (such as LTCC) or a bigger size of antenna element. The use of varactors may lead to nonlinear effects and a further investigation is required.

7.1.3. Conclusions for Conical Monopole Antenna Integrated with a Filter

For future communication systems which might require an antenna having as wide a bandwidth as possible while maintaining an omni-directional pattern, there is a need for stopband capabilities to avoid interfering with nearby narrow-band communication systems. Several designs of conical monopole antennas, incorporating with different types of slots to achieve good band-rejection behaviour, have been

proposed in Chapter 5. These were the 2 C-shaped, 4 C-shaped slots, 4 U-shaped slots, 4 tilted-U-shaped slots and 4 U-C-shaped slots. The total efficiency and gain suppression for each type of slots are summarised in Table 7.1. Those proposed wideband antennas with band-notch behaviour are promising candidates for use in wideband applications and if scaled down in frequency, for rural area networks (Cognitive Radio based) which will require omni-directional spectrum search antennas.

Resonator	Measured Notch Frequency (GHz)	Reflection Coefficient [dB]	Notch Band Q Factor $^+$	Simulated Lowest Total Efficiency (dB)	Measured Peak Gain Suppression (dBi)
2 C-shaped	5.42	-0.63	6.70	-12.6	10.7
					40.9*
4 C-shaped	8.71	-0.10	5.58	-28.3	28.8
4 U-shaped	5.18	-1.30	34.50	-13.9	12.7
4 tilted U_shaped	5.35	-0.87	16.46	-15.6	19.7
4 U_C_shaped	7.41	-0.46	6.83	-25.0	25.0

Table 7.1 Total efficiency and gain suppression for each type of slots.
$^+$at 6 dB return loss bandwidth;* null direction

The elliptical shaped antenna is inherently a wide band radiating element having an omni-directional radiation pattern even at a high frequency, and is therefore will suited for use in wideband systems. In this type of conical antenna the current is distributed evenly around the circumference, so that the slot can couple more strongly than other types, particularly planar types in which the current is concentrated along the edge. In addition, the bottom of an elliptical cone is larger than a V-shaped cone, which enables the slot to be located closer to the fed point, to further enhance coupling. The elliptical cone antenna has three parameters, namely the height of the cone, the flare angle, and the distance between the base of the cone and the ground

plane. By adjusting these parameters, it is possible to optimize the antenna's radiation pattern and input impedance. The different shaped slots offer a choice of narrow or wide rejection band (i.e. high Q or low Q). The total length of the slot is approximately half-a-wavelength at the notch-band frequency. Location of the slot will affect the resonant frequency. Increasing the slot length reduces the notch frequency. The study of wideband antennas with notched-band behaviour using a simple equivalent circuit model has been introduced in section 5.5. Numerical results show that there is a trade-off between the gain suppression and the quality factor of the band-notch. Increasing the number of resonators and the coupling factor will of course increase the band-rejection. However, it will also widen the bandwidth of the frequency notched band.

Table 7.1 shows that different shape of slot offers different bandwidth or Q factor and it shows that the U-shaped slot provides higher Q than other shapes, i.e. C-shaped. The effect on the Q factor might be due to the radiation loss, mutual coupling between the arms of the slots, or other potential reasons. It is necessary to investigate and find the physical explanation for the effect. Table 7.1 shows that the gain suppression of the tilted-U-shaped slotted antenna has been significantly improved when compared to that of the vertical U-shaped slotted antenna. This result implies that the mutual coupling of the slots or resonators will affect the band-rejection and a further investigation by using equivalent circuit model is necessary.

Low cost production would depend on the intended frequency range and hence size. For smaller size the antennas could be die casting. Larger size could be produced by rapid prototyping. Alternately if the cone shape is altered at the expense of bandwidth

several possibilities exist. A straight cone with circular cross section can be made by wrapping thin flexible PCB. A straight cone with square cross section can be made from four triangular printed circuit boards, as demonstrated in Chapter 6.

7.1.4. Conclusions for Pyramidal Monopole Antenna with Tunable Band-Notch

The notch band frequencies for the antennas proposed in Chapter 5 are fixed and can only be changed by modifying the length of slots prior to manufacture. To address this problem, a novel pyramidal monopole antenna, with four loop shaped slots, offering wide tunable band-notch, was proposed in Chapter 6.

To optimize the antenna impedance to cover the required band, i.e. from 3 GHz to 11 GHz, the height "H", flare angle "a" as well as the distance between the base of the cone and the ground plane "h_f" are needed to be adjusted. For this pyramidal shape, a loop shaped slot is etched on each side of pyramid antenna. The whole length of the slot is about half wavelength and of course will be affected by the distance from the fed point. The bandwidth or Q factor associated with the notched band would be controlled by changing the width of the upper part of the loop. By loading with the lumped capacitor or varactor diode, the resonant frequency of the embedded slot would be adjusted and will changes with different value of capacitance. The higher notched band frequency is dependent on the maximum capacitance. Prototypes with capacitors and varactors, respectively, were fabricated and measured. However, in demonstration, the frequency tuning range was limited by the capacitance tuning range of the varactor. It is likely that the frequency tuning range could be increased, if the capacitance tuning range of the varactor was wider. The measured results show

that the performance of band-rejection significantly relates to the loss of the components used. Higher performance of band-rejection requires lower loss of varactors or compactors, or alternatively increasing the upper part of the loop shaped slot for lower Q (wider bandwidth) of notched band to minimize the components loss effects.

7.2. Future Work

This work has shown that the reconfigurable chassis-antenna, reconfigurable balanced antenna and reconfigurable MIMO antenna give rise to many new features, such as wide continuous tuning range, improve channel capacity, high isolation etc. However, the potential trade-off is poor linearity due to the use of varactor diodes. In addition, there are some limitations for the two port chassis-antenna, as mentioned earlier, such as when two bands are operating close to each other then the coupling is increased. The antenna is also limited to a maximum of two simultaneous service accesses. Thus this antenna is not an ideal candidate for future communication system, if they require multiple services access with high isolation.

Some further investigations can be made in the future: -

1). A set of measurements for the MIMO antenna in a rich multipath environment to investigate the MIMO performance, in terms of correlation coefficient, power imbalance, diversity gain and average capacity increase;

2). Investigate whether either by circuit (for example, decoupling network) or additional element, the coupling between two close operating frequency bands can be reduced;

3). Study the complex coupling between two close coupling elements and provide physical explanations;

4). Investigate the use of more than two coupling elements to provide multiple bands operation and to optimize the element locations to have good tuning range and high isolation between each port;

5). Due to the small amount of space which is available for mobile terminals, more than two antenna elements may be not practical. Investigate the use of multiple matching circuits in the chassis antenna, to get multiple outputs, mimicking multiple antennas;

6). Linearization of non linear front end components is currently done. It may be possible to extend such techniques to allow the use of semiconductor based tuning elements, such as varactors, in antennas;

7). The trend to on-chip transceivers in software defined radio (SDR) and cognitive radio (CR) suggests that the integration of filtering into antennas will become important. Integrating a filter, using for example lump elements, with matching circuit to improve out of band-rejection, should be investigated.

8). Investigate the effect on Q factor with different shape of slots using the equivalent circuit model.

9). Study the mutual coupling between the slots or resonators using the equivalent circuit model to explain why enhancing the mutual coupling between slots or resonators will result in improvement of band-notched frequency.

APPENDIX A

GLOSSARY OF FREQUENCY RECONFIGURABLE ANTENNAS

SUMMARY

Table A.1 gives antennas incorporating different types of switches [1-39] and switching techniques and resulting their performance are noted. Table A.2 shows antennas incorporating varactor diodes [40-71]. Reconfigurations by other techniques [72-78] are listed in Table A.3.

The tables show that several designs have been proposed for reconfigurable balanced antennas namely dipole, folded loop, etc. Refs. [12, 16, 19, 36-39] introduce reconfigurable balanced antennas incorporating switches on each arm of the balanced elements while refs. [70-71] present the antennas incorporating varactor diodes, which were located on each arm of the balanced elements.

Those reconfigurable antennas [1-78] can be initially summarised as below:
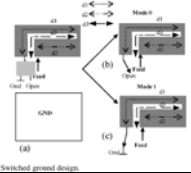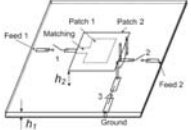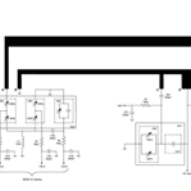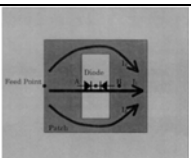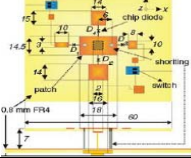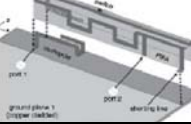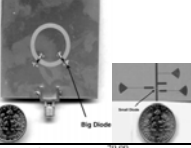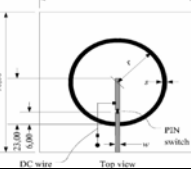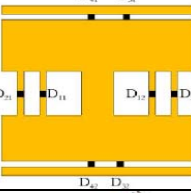
- ❖ Designed for handset: refs. [2, 4, 7, 13, 21, 24, 26-28, 32, 42, 48, 54-56, 58, 60-62, 64, 67, 69]
- ❖ Continuously cover most of DVB band (470 MHz to 862 MHz): refs. [12, 15, 26, 32, 40, 44, 54-56, 59, 61-63]
  - Designed for handset: refs. [26, 32, 54-56, 61-62]
- ❖ Continuously cover from GSM (850 MHz) to IMT2000 (2100 MHz): refs. [21, 26-28, 41-42, 48, 57-58]
  - Designed for handset: Refs. [21, 26-28, 42, 48, 58]
- ❖ Continuously cover from PCS (1850 MHz) to Wifi (2450 MHz): refs. [6, 11, 18, 26-29, 48, 57-58, 67]
  - Designed for handset: refs. [26-28, 48, 58, 67]
- ❖ Continuously cover from GSM (850 MHz) to Wifi (2450 MHz): refs. [26-28, 48, 57-58]
  - Designed for handset: refs. [26-28, 48, 58]
- ❖ Continuously cover from DVB (470 MHz) to GPS (1500 MHz): refs. [12, 26, 44]
  - Designed for handset: ref. [26]
- ❖ Continuously cover from DVB (470 MHz) to Wifi (2450 MHz): refs. [26]
  - Designed for handset: ref. [26]
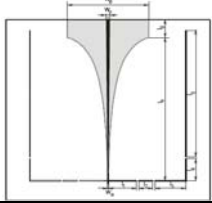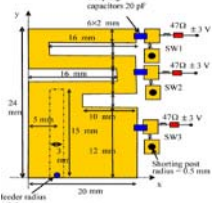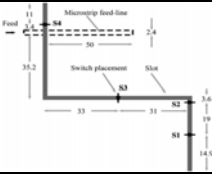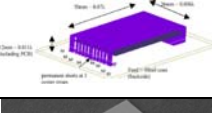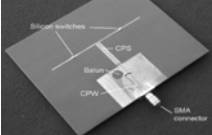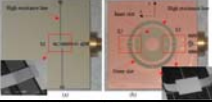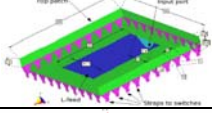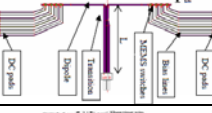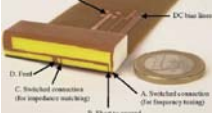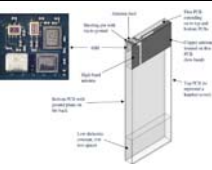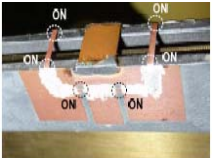
- ❖ Dual-band simultaneous operations (narrowband modes): refs. [7, 21, 27-28, 47, 52, 54, 61, 67, 69]
  - ● Designed for handset: refs. [7, 21, 27, 28, 54, 61, 67, 69]
- ❖ More than two bands simultaneous operations (narrowband modes): refs. [57, 60]
  - ● Designed for handset: ref. [60]
- ❖ Claim designing for cognitive radio or software defined radio: refs. [29, 31, 33-35, 76]
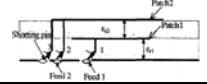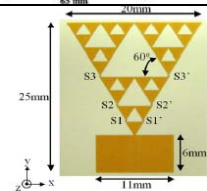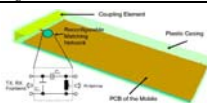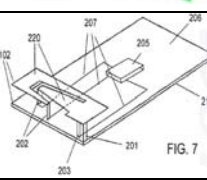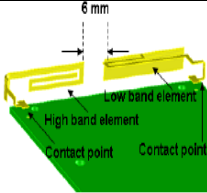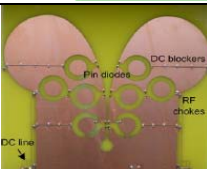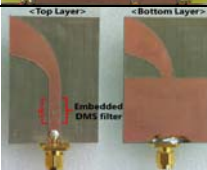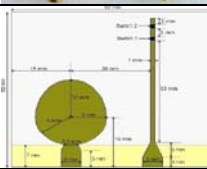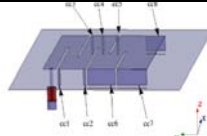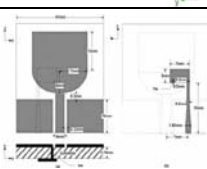
From the summary above, it shows that there are many antenna designs available for handset application in the open literature. However, in those literatures only the antenna in ref. [26] can cover from 470 MHz up to 2450 MHz. Only antenna designs in refs. [7, 21, 27, 28, 54, 61, 67, 69] can provide dual-band simultaneous operations and antenna in ref [60] can provide 5 bands simultaneous operations. Thus, there is no antenna with dual-band operations simultaneously to continuously cover from DVB (470 MHz) to Wifi (2450 MHz) Bands. Ref. [26] describes a single port chassis antenna, which has the widest coverage range. The antenna incorporates 17 matching circuits to cover from 76 MHz to 2500 MHz and 5 matching circuits to cover from 470 MHz to 2500 MHz. However, there are two disadvantages. Firstly the large number of switches will introduce significant losses and secondly the antenna is limited to one band at a time and is thus not suitable for terminals which require more than one simultaneous service access.

Table A.1 Reconfigurable antennas incorporating switches

Ref.	Antenna Figure	Antenna structure	Size (mm)	Switching band (GHz)	Frequency switching technique	Switch type	Number of switch
[1]		E-shaped patch antenna	21.7×13.2	State 1: 9.2-15 State 2: 7.5-10.7	Varying the width of E-shape.	Pin diode switch	19
[2]		PIFA	98×42	Mode 0: 0.85,0.92,1.8 Mode 1: 0.85,0.92,1.9, 2.05	Switched feed	Pin diode	2
						GaAs FET	1
						MEMs	1
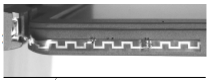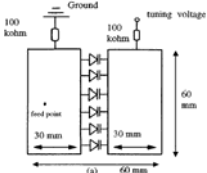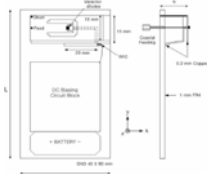
		PIFA	100.5×42	Mode 0: 0.85,0.9,1.8,1.9 Mode 1: 1.8,1.9,2.05,2.45	Switched ground	Pin diode	1
						GaAs FET	1
						MEMs	1
[3]		Stacked square microstrip patch	130×130	State 1: 1.75 State 2: 0.688	Switching from stacked square to PIFA type antenna	PIN diode	3
[4]		PIFA	100×40	Mode 1: 0.748-0.912 Mode 2: 1.84-2.151, 1.849-2.156, 1.901-2.185	Re-matching antenna externally	MEMS	4
[5]		Microstrip planar antenna with a rectangular slot	48×48	Mode1: 3.43 Mode2: 3.11	Controlling the effective path length	(Switching) Diode	2
[6]		Rectangular patch	120×120	Mode 1 to Mode 8 (1.82 – 2.48)	Varying the patch size	PIN diode	4
[7]		Two-port PIFA and monopole	150×40	Mode 1 : 0.75, 1.92, and 3.6 Mode 2 : 0.92 and 5.25	Two ports and switched length of PIFA	PIN diode	1
[8]		Annular slot antenna	50×50	Mode 1: 5.2 Mode 2: 5.8 Mode 3: 6.5	Reconfigure the impedance match	PIN diode	3
[9]		Annular slot antenna	70×70	Mode 1: 1.63 Mode 2: 2.34	Change the length of the microstrip feed	PIN diode	1
[10]		Aperture-coupled microstrip patch antenna	2.6×2.8	Mode 1 to Mode 5: 9.8 to 19	Change the coupling between the H-shape patch antenna and two parasitic elements	PIN diode	8
[11]		Integrated with 7 dipole elements	160×76	State 1: 0.8-0.9 State 2: 1.7-2.5 State 3: 3.3-3.6 State 4: 5.1-5.9	Switched between different size of dipole elemetns	MENS	4

Ref		Type	Size	States (GHz)	Mechanism	Switch	No.
[12]		Printed dipole	100×100	Mode 1 to Mode 4: 0.5 to 1.8	Switched to change the length of each dipole arm	GaAs FET	6
[13]		Slotted rectangular patch	24×20	State 1: 0.665 State 2: 0.85 State 3: 0.945 State 4: 1.175	Switched between different posts	PIN diode	3
[14]		Slot antenna	76.6×64	State 1: 0.561 State 2: 0.627 State 3: 0.711 State 4: 0.95	Switched to change the length of the slot	PIN diode	4
[15]		PIFA-as-a-Package	50×25	Cover from 0.4078 to 0.4631	Switched between 8 different short straps to ground	PIN diode GaAs FET CMOS or MENS	8
[16]		Printed dipole	about 90×90	State 1: 2.26 State 2: 2.7 State 3: 3.15	Changed the length of each dipole arm	Silicon photo switch	2
[17]		Annular slot antenna	about 25×25	State 1: 2.4 State 2: 5.3	Changed the length of feed line	MEMS	3
[18]		Patch antenna	30×30	Cover from 1.7 to 2.7	The use of switches connecting metal portions to the ground plane	Ideal (i.e. soldering)	8
[19]		Printed dipole	Not state	Cover from 8 to 12	Changed the length of each dipole arm	MEMS	8
[20]		Mini-nested patches antenna	23.05×21.55	State 1: 0.9 State 2: 1.57 State 3: 1.8 State 4: 2.4	Changed the size of patch	MEMS	4
[21]		PIFA	100×40	State 1: 0.824-0.96 State 2: 1.71-1.88 State 3: 1.85-1.99 State 4: 1.92-2.17	Switched connection for impedance matching	MEMS	2
		Two PIFAs	100×40	State 1: 0.824-0.849 State 2: 0.88-0.915 State 3: 0.925-0.960 State 4: 0.824-0.894 State 5: 1.710-1.785 State 6: 1.85-1.910 State 7: 1.85-1.99 State 8: 1.92-2.17	Switched connection for impedance matching	MEMS	8
[22]		E-shaped PIFA	40×20	State 1: 2.4-2.484 & 5.15-5.35 State 2: 3.3-3.6 & 5.15-5.35 State 3: 2.4-2.484 & 5.757-5.825 State 4: 3.3-3.6 & 5.775	Switched to change the structure	MEMS	6
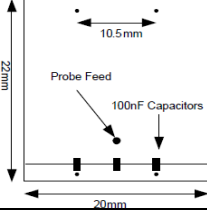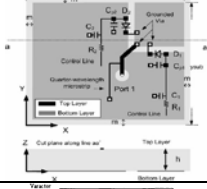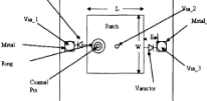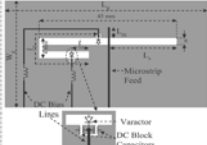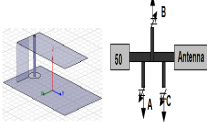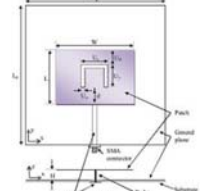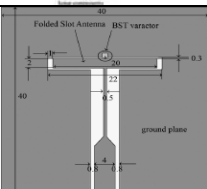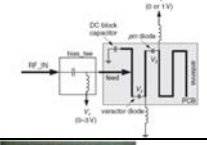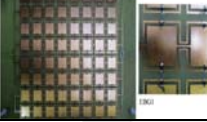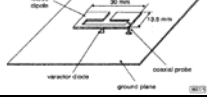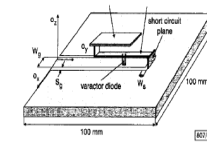
Ref		Antenna type	Size	States	Mechanism	Switch type	Number
[23]		Stacked patch antenna	38.8×38.8	State 1: 1.8-2.14 State 2: 0.6	Switched between two patches	PIN dipole	3
[24]		Rectangular patch and two parasitic folded dipole elements	100×65	State 1: 10 & 11 State 2: 5 & 15 State 3: 5 & 15 State 4: 14 & 15	Switching the patch and folded dipoles configuration	PIN dipole	4
[25]		Sierpinski antenna	25×20	State 1: 18 State 2: 9.4 State 3: 5.7 & 16.7 State 4: 2.4, 9 & 16.4	Switched to increase the number of radiating elements	MEMS	6
[26]		Chassis Antenna	Not state but handset size	State 1 to 17: 0.076 to 2.5	Incorporating 17 external matching circuits to cover the required bands	PIN diode GaAs FET CMOS or MENS	Large Number
[27]		PIFA type antenna	Not state but handset size	Not state But able to cover GSM, GPS, PCS, WiFi and etc	A leg is feed port, others are the tuning port, which are connected different reactive loads (matching circuits)	PIN diode GaAs FET CMOS or MENS	Large Number
[28]		Two-port Chassis antenna	110×50	**Port 1:** State 1: 0.824 to 0.901 State 2: 0.87 to 0.96 **Port 2**: 1.71-2.17	Low band element is incorporating two matching circuits and controlled by switch; high band element is incorporating a matching circuit	GaAs SPDT	1
[29]		Vivaldi Antenna	144×100	State 1 – 3: 1 to 3.2	Four pairs of switchable ring slots were introduced to change the wideband properties into narrower pass bands	PIN diode	8
[30]		UWB antenna with Defected microstrip structure (DMS) band pass filter	65×40	State 1: 7.4 State 2: 9.3 State 3: 10.8	The band pass filter is a reconfigurable T-shaped DMS structure, incorporating 9 switches to change the length of T-shaped slot	Ideal Switch (Copper)	9
[31]		Two printed microstrip-line-fed monopoles	50×50	Port 1: 3.1 to 10.6 Port 2: State 1: 5.5 and 9.15 State 2: 4.85 and 8.15 State 3: 4.4, 7.41 and 10.33	The wideband monopole operates from 3 to 11 GHz. The narrowband monopole has two switches to change the length	Ideal Switch (Copper)	2
[32]		Meander antenna	60×49	State 1 to 8: 0.47 to 0.702	The meander antenna uses PIN diodes inserted in different points of the radiating element	PIN diode	8
[33]		Two ports Printed monopole and PIFA	54×35	Port 1: 3 to 11 Port 2: 3 matching circuits to get 4, 8, and 10	Port 1 is wideband mode, and port 2 can be tuned be used different matching circuits	Not state	Not state
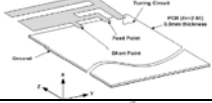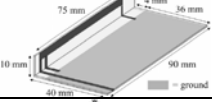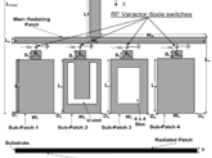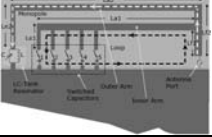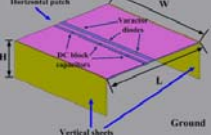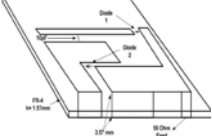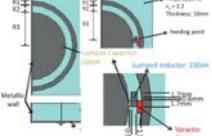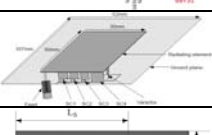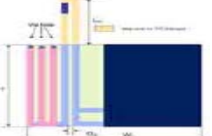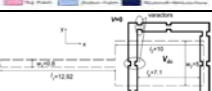
[34]		Slot antenna	Not state	Mode 1: 8.14 to 11 Mode 2: 2.56 to 11 Mode 3: 4.3 and 10.3	Using six switches to achieve three different operating modes	Ideal switch (coper)	6
[35]		Microstrip patch antenna	110×30	Mode 1: 3.6 to 11 Mode 2: 7.64	Using three switches to achieve two different operating modes	Ideal switch (coper)	3
		Microstrip patch antenna	110×30	Mode 1: 3.17 to 7.62 Mode 2: 4.18 to 7.84 Mode 3: 6 to 10.1	Using three switches to achieve three different wideband modes	Ideal switch (coper)	3
[36]		Dipole antenna	16×7	Mode 1: 8.98 Mode 2: 4.86	By operating the switches in the gap of each dipole arm	MEMS	2
[37]		Printed dipole antenna	62×62	Mode 1: 2.251 Mode 2: 2.517	Two optically activated silicon switches are placed on small gaps in the dipole arms	Silicon switches	2
[38]		CPW-fed folded dipole antenna	Not state	Mode 1: 5.1 Mode 2: 5.6	By changed the state of the switches, it is possible to discretely tune the resonate frequency	Ideal switch (coper)	3
[39]		Printed dipole antenna	64×64	State 1: 0.9 State 2: 1.05 State 3: 1.205 State 4: 1.46 State 5: 1.75 State 6: 2.05 State 7: 2.77	Incorporating six ideal switches on each dipole arm	Ideal switch (coper)	12

Table A.2 Reconfigurable antennas incorporating varactor diodes

Ref.	Antenna Figure	Antenna structure	Size (mm)	Tuning range (GHz)	Tuning technique	Varactor range (pF)	Number of varactor
[40]		Meander line antenna	Not state	0.415 to over 0.7	A single varactor was inserted in series with the upper and lower segments of the meander	Not state	1
[41]		Rectangular patch antenna	60×60	1.47 to 2.3	Varactor diodes are in parallel and connected two rectangular patch antenna	0.1 to 15	6
[42]		PIFA	80×40	1.64 to 2.05	A varactor diode is integrated between the slot and bias feeding strip line	0.2 to 1.15	1
[43]		Annular slot antenna	300×300	1.92 to 2.55	A varactor is located at the shorting pin and ground	1.44 to 21.6	1

[44]		Patch antenna with two shoring posts	80×40	0.55 to 1.5	Two varactors were placed in front of each shorting post to shift the resonant frequency	2 to 14	2
[45]		L-shaped slot	52×52	2.15 – 2.8	Changing the value of capacitors to reconfigure the slot	0.56 to 4.7	2
[46]		Patch antenna	44×44	1.6 to 1.8	Connecting the varactor diodes to alter the capacitance of the patch	1.02 to 7.37	2
[47]		Dual-band bent slot antenna	150×110	Band 1: 1.1 to 1.45 Band 2: 1.7 to 2.9	Dual-frequency operation is achieved by loading a slot antenna with two varactors placed in proper locations along the slot	0.5 to 2.25	2
[48]		PIFA with matching circuit	44×19.84	0.9 to 2.4	A matching circuit, including three capacitors, is connected to the PIFA externally	Capacitor 1: 0.6 to 2.089 Capacitor 2: 0.029 to 3.113 Capacitor 3: 0.334 to 3.467	3
[49]		Rectangular patch	77×57	2.6 to 3.35	The varactor is located on the back of the antenna and is soldered to the microstrip line at the position where the feeding probe is connecting to the microstrip line	0.4 to 1.5	1
[50]		Folded slot antenna	40×40	3.18 to 3.29	The resonant frequency of a slot/coplanar patch antenna is tuned using a discrete varactor component, which is placed over the radiating slot	1.05 to 1.5	1
[51]		Microstrip monopole antenna	24×12	State 1: 2.3 to 2.5 State 2: 5.15 to 5.35	1 PIN dipole switch and 1 varactor are located in the meander line to change the resonant frequency	14 to 36	1
[52]		Dual band EBG	Not state	Band 1: 0.7 to 1.2 Band 2: 1.7 to 2.6	A varactor diode soldered between each square patch and the DC bias line	0.6 to 4.5	128
[53]		Asymmetric folded dipole	100×100	2.7 to 3.5	A varactor diode was connected between the element and the ground plane	Not state	1
		Two opposite stacked quarter-wavelength elements	100×100	1.7 to 2.23	A varactor diode is placed between the radiating element and the CPW feed line	Not state	1

[54]		Two-port Chassis antenna	110×55	Band 1: 0.442 to 0.758 Band 2: 0.88 to 0.96	External matching circuit, contains an anti-series varactor pair A filter is added to the matching circuit to block EGSM TX to the DVB-H antenna	1.77 to 34.06	1
[55]		PIFA	100×60	0.47-0.77	Using a tuning circuit which consists of a varactor diode to adjust the impedances	0.8 to 8	1
[56]		IFA	90×40	0.47 to 0.688	A varactor loads the IFA element and thus enables it to resonate at different frequencies	0.1 to 1	1
[57]		5 Bands Patch antenna	50×50	5 tunable bands to cover 0.92 to 2.98	By placing a varactor diode at the input of the sub-patches to change the impedance matching frequency	2 to 14	4
[58]		Printed Loop-Monopole (Chassis-antenna)	Not state (handset size)	0.7 to 6	The monopole contributes tuning in the lower frequency bands by using an LC (Varactor)-tank resonating tuner while the loop contributes to a tuning in the upper frequency bands by using a bank of RF switches	0.18 to 3.81	1
[59]		Capacitively loaded loop (CLL)	50×50	0.4575 to 0.8945	Three varactor diodes and dc block capacitors mounted on the horizontal substrate, and thus tunable loaded capacitance of the radiating CLL	0.12 to 4	3
[60]		4 bands PIFA	Not state (handset size)	**Bnad 1:** 0.7 to 0.95 **Bnad 2:** 1.79 to 2.19 **Bnad 3:** 3.43 to 3.57 **Bnad 4:** 4.95 to 5.2	Two varactor diodes were located inside the PIFA to change the capacitance	1.2 to 7	2
[61]		Dual-band PIFA	36×18	Band 1: 0.34 to 0.84 Band 2: 2.2 to 2.3	The operation frequencies are tuned by the varactor diode, which was placed between the inner semicircular patch and the outer half-rings	1.5 to 19	1
[62]		PIFA	107×62	0.47 to 0.862	By combining the switching of 4 PIN diodes and the control of the varactor diode capacitance	5 to 40	1
[63]		Slot antenna	35×20	Mode 1: 0.42 to 0.96 Mode 2: 0.8 to 1.48	A PIN diode and a varactor diode are used in the structure, two modes were tuned	Not state	1
[64]		Meander-type stack antenna	Not state but should be small	2.17 to 2.56	Change the value of capacitor, but not clear the location of the capacitor	(Capacitor instead of varactor) 0 to 10 pF	1
[65]		Slot-loop antenna	40×38.97	2.34 to 4	By periodically loading the slot line with two varactor diodes at a 45° load period	Not state	2
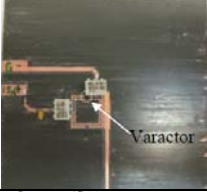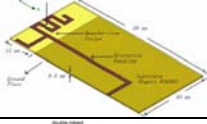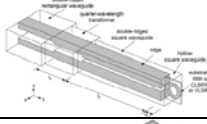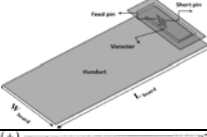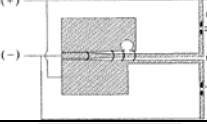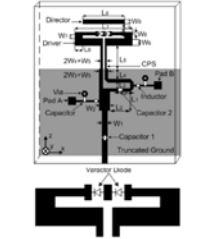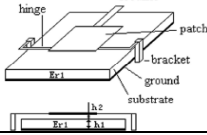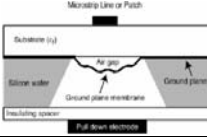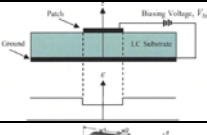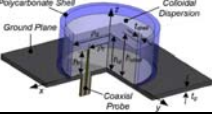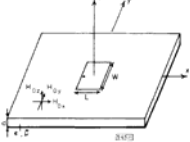
Ref.	Antenna Figure	Antenna structure	Size (mm)	Tuning range (GHz)	Tuning technique	Range	Technique
[66]		Split ring resonator antenna	80×80	1.81 t 2.14	By loading a reversely biased varactor diode which could offer variable capacitance into a SRR	0.79 to 4.15	1
[67]		Dual-band planar monopole antenna	80×40	Band 1: 1.9 to 2.6 Band 2: 3.5	A varactor capacitor is serially attached to one of the strips, which can tune the resonant frequency	0.1 to 3	1
[68]		Waveguide antenna with a varactor-loaded Split-Ring Resonator	465.2×30.62	1.96 to 2.36	The resonant frequency of a split-ring resonator is tuned by adjusting the capacitance of the gap	0.25 to 5	1
[69]		Dual-band PIFA	80×42	Band 1: 1.1 to 1.3 Band 2: 1.85 to 2.2	A varactor was inserted into the slot of the PIFA to change the antenna capacitance	1.5 to 4	1
[70]		CPW-fed CPS dipole antenna	50×30	Band 1: 2.065-2.365 Band 2: 3.955-3.505	Two varactors were located at the middle of each arm	Not state	2
[71]		Quasi-Yagi folded dipole antenna	Not state	6-6.6	A pair of varactor diodes loaded on the thin strip of the folded dipole	0.1 to 1	2

Table A.3 Reconfigurable antennas by other techniques

Other Reconfigurable Techniques						
Ref.	Antenna Figure	Antenna structure	Size (mm)	Tuning range (GHz)	Tuning technique	Reconfigurable Technique
[72]		Micromechanical patch antenna	2.2×2.2	38.8 to 46.3	The micromechanical patch is moving via electrostatic force. As the bias voltage between patch and antenna is changed, it makes the patch to move and the antenna operating frequency changes too.	Mechanical
[73]		Microstrip patch antenna	Not state	16.8 to 17.82	Electrostatic actuation of the membrane away from the substrate introduces a controllable air gap, and so lowers the substrate's effective dielectric constant in the membrane region	Mechanical
[74]		Patch antenna with a liquid crystal substrate	60×60	1.08 to 2.35	A liquid crystal substrate for a patch antenna whose frequency can be tuned by changing the biasing voltage across the substrate	Changing Substrate Characteristic
[75]		Rolled planar monopole antenna	100×100	2.9 to 15	By adjusting the degree of spiral tightness, a shift of the well-matched operating frequency range is achieved	Mechanical
[76]		Different shapes of printed monopoles	70×50	Antenna 1: 2 to 10 Antenna 2: 2 to 10	The five different patches were rotated to be reconfigured	Mechanical (motor)

[77]		Dielectric Resonator Antenna	100×100	2.5 to 4,5	The coaxial probe-fed structure has tunable impedance properties that are reversibly controlled by adjusting the columnar height of the dispersion	Mechanical
[78]		A microstrip antenna on a ferrite substrate	Not state	State 1: 4.6-5.5 State 2: 2.8-4.6	The rectangular microstrip antenna is printed on a ferrite substrate, which is magnetically biased along one of three possible principal axes. The resonant frequency can be tuned by varying the DC magnetic bias field applied to the substrate	Changing the Substrate Characteristic

References:

[1] B. Z. Wang, S. Xiao and J. Wang, "Reconfigurable patch-antenna design for wideband wireless communication systems", *IET Microwave Antennas Propagation*, Vol. 1, Issue 2, 2007, pp. 414-419

[2] A. C. K. Mak, C. R. Rowell, R. D. Murch, and C. – L. Mak, "Reconfigurable multiband antenna designs for wireless communication devices", *IEEE Transaction on Antennas and Propagation*, Vol. 55, Issue 7, 2007, pp. 1919-1928

[3] M. Ali, T. M. Sayem and V. K. Kunda, "A reconfigurable stacked microstrip patch antenna for satellite and terrestrial links", *IEEE Transactions on Vehicular Technology*, Vol. 56, Issue 2, 2007, pp. 426-435

[4] K. R. Boyle, and P. G. Steeneken, "A five-band reconfigurable PIFA for mobile phones", *IEEE Transactions on Antenna and Propagation*, Vol. 55, Issue 11, Part 2, 2007, pp. 3300-3309

[5] K. Sakamoto, E. Nishiyama and M. Aikawa, "Active microstrip planar antenna for frequency switching", *Electronics and Communications in Japan,* Part 1, Vol. 88, No. 11, 2005, pp. 1-8

[6] T. Y. Han and C. T. Huang, "Reconfigurable monopolar patch antenna", *Electronics Letters*, Vol. 46, Feb. 4 2010, pp. 199-200

[7]   J. Cho, C. W. Jung, and K. Kim, "Frequency-reconfigurable two-port antenna for mobile phone operating over multiple service bands", *Electronics Letters*, Vol. 45, Sep. 24 2009, pp. 1009-1010

[8]   N. Symeon, R. Bairavasubramanian, C. Jr. Lugo, I. Carrasquillo, D. C. Thompson, G. E. Ponchak, J. Papapolymerou, and M. M. Tentzeris, "Pattern and frequency reconfigurable annular slot antenna using PIN diodes", *IEEE Trans. Antennas and Propag.,* vol. 54, Feb. 2006, pp. 439-448.

[9]   M. Berg, M. Komulainen, E. Salonen, and H. Jantunen, "Frequency reconfigurable microstrip-fed annular slot antenna", *Antennas and Propag., 2006, EuCAP 2006, First European Conference* on 6-10 Nov. 2006, pp.1-6.

[10]   L. Le Garrec, R. Sauleau, and M. Himdif, "A 2:1 band frequency-agile active microstrip patch antenna", *Antennas and Propag., 2007, EuCAP 2007, The Second European Conference* on 11-16 Nov. 2007, pp. 1-6.

[11]   T. Wu, R. L. Li, S. Y. Eom, K. Lim, S. I. Jeon, J. Laskar, and M. M. Tentzeris, "A multiband/scalable reconfigurable antenna for cognitive radio base station", *Antennas and Propag. Society International Symposium, 2008, AP-S 2008, IEEE,* 5-11 July 2008, pp. 1-4.

[12]   A. Cidronali, L. Lucci, G. Pelosi, P. Samori, and S. Selleri, "A reconfigurable printed dipole for quad-band wireless applications", *Antennas and Propag. Society International Symposium 2006, IEEE,* 9-14 July 2006, pp. 217-220.

[13]   A. –F. Sheta, and S. F. Mahmoud, "A widely tunable compact patch antenna", *Antennas and Wireless Propag. Letters, IEEE,* vol. 7, 2008, pp. 40-42.

[14]   D. Peroulis, K. Sarabandi, and L. P. B. Katehi, "Design of reconfigurable slot antennas", *Antennas and Propag., IEEE Transactions* on vol. 53, Feb. 2005, pp. 645-654.

[15] L. M. Feldner, C. T. Rodenbeck, C. G. Christodoulou, and N. Kinzie, "Electrically small frequency-agile PIFA-as-a-package for portable wireless devices", *Antennas and Propag., IEEE Transactions* on vol. 55, part2, Nov. 2007, pp. 3310-3319.

[16] C. J. Panagamuwa, A. Chauraya, and J. C. Vardaxoglou, "Frequency and beam reconfigurable antenna using photoconducting switches", *Antennas and Propag., IEEE Transactions* on vol. 54, Feb. 2006, pp. 449-454.

[17] B. A. Cetiner, Q. Xu, and L. Jofre, "Frequency reconfigurable annular slot antenna", *Antennas and Propag. International Symposium, 2007 IEEE,* 9-15 June 2007, pp. 5845-5848.

[18] J. L. A. Quijano, and G. Vecchi, "Optimization of an innovative type of compact frequency-reconfigurable antenna", *Antennas and Propag., IEEE Transactions* on vol. 57, Jan. 2009, pp. 9-18.

[19] C. G. Christodoulou, L. F. Feldner, V. Zachou, and D. Anagnostou, "Planar reconfigurable antennas", *Antennas and Propag., 2006, EuCAP 2006, First European Conference* on 6-10 Nov. 2006, pp. 1-7.

[20] C. Zhang, S. Yang, H. K. Pan, A. E. Fathy, S. El-Ghazaly, and V. Nair, "Reconfigurable antenna for simultaneous multi-service wireless applications", *Radio and Wireless Symposium, 2007, IEEE,* 9-11 Jan. 2007, pp. 543-546.

[21] K. R. Boyle, P. G. Steeneken, Z. Liu, Y. Sun, A. Simin, T. Huang, E. Spits, O, Kuijken, T. Roedle, and F. Van Straten, "Reconfigurable antennas for SDR and cognitive radio", *Antennas and Propag., 2007, EuCAP 2007, The Second European Conference* on 11-16 Nov. 2007, pp. 1-6.

[22] J. Guterman, A. A. Moreira, C. Peixeiro, and Y. Rahmat-Samii, "Reconfigurable E-shaped patch antennas", *Antenna Technology, 2009, iWAT 2009, IEEE International Workshop* on 2-4 March 2009, pp. 1-4.

[23] V. K. Kunda, and M. Ali, "Reconfigurable stacked patch antenna for satellite and terrestrial applications", *Wireless Communication Technology, 2003, IEEE Topical Conference* on 15-17 Oct. 2003, pp. 152-153.

[24] E. Palantei, D. V. Thiel, and S. G. O'Keefe, "Rectangular patch with parasitic folded dipoles: a reconfigurable antenna", *Antenna Technology: Small Antennas and Novel Metamaterials, 2008, iWAT 2008, International Workshop* on 4-6 March 2008, pp. 251-254.

[25] N. Kingsley, D. E. Anagnostou, M. Tentzeris, and J. Papapolymerou, "RF MEMS sequentially reconfigurable sierpinski antenna on a flexible organic substrate with novel DC-Biasing technique", *Journal of Microelectromechanical Systems,* vol. 16, Oct. 2007, pp. 1185-1192.

[26] D. Manteuffel, M. Arnold, "Considerations for reconfigurable multi-standard antennas for mobile terminals", Antenna Technology: Small Antennas and Novel Metamaterials, 2008, iWAT 2008. International Workshop in 2008, pp. 231-234

[27] G. G. Bit-Babik, C. D. Nallo, and A. Faraone, "Multi-frequency conductive-strip antenna system", U.S. Patent, US 7928914 B2, Apr. 19, 2011

[28] P. Bahramzy, and M. Sager, "Dual-feed ultra-compact reconfigurable handset antenna for penta-band operation", *Antennas and Propagation Society International Symposium (APSURSI), 2010 IEEE*, pp. 1-4

[29] M. R. Hamid, P. S. Hall, P. Gardner, and F. Ghanem, "Frequency reconfigurable Vivaldi antenna", *Antennas and Propagation (EuCAP), 2010 Proceedings of the Fourth European Conference in 2010*, pp. 1-4

[30] M. Zamudio, Y. Tawk, J. Costantine, J. Kim, and C. G. Christodoulou, "Integrated cognitive radio antenna using reconfigurable band pass filters", *Antennas and Propagation (EuCAP), 2011 Proceedings of the 5th European Conference in 2011* pp. 2108-2112

[31] M. Al-Husseini, Y. Tawk, C. G. Christodoulou, K. Y. Kabalan, and A. El Hajj, "A reconfigurable cognitive radio antenna design", *Antennas and Propagation Society International Symposium (APSURSI), 2010 IEEE*, pp. 1-4

[32] F. Canneva, J. −M, Ribero, and R. Staraj, "Reconfigurable meander antenna for DVB-H band", *Antenna Technology (iWAT), 2010 International Workshop*, pp. 1-4

[33] E. Ebrahimi, J. Kelly, and P. S. Hall, "A reconfigurable narrowband antenna integrated with wideband monopole for cognitive radio applications", *Antennas and Propagation Society International Symposium, 2009, APSURSI 2009 IEEE*, pp. 1-4

[34] J. R. Kelly, and P. S. Hall, "Reconfigurable slot antenna for cognitive radio", *Antennas and Propagation Society International Symposium, 2009, APSURSI 2009 IEEE*, pp. 1-4

[35] J. R. Kelly, P. S. Hall, and P. Gardner, "Integrated wide-narrow abnd antenna for switched operation", *Antennas and Propagation, 2009, EuCAP 2009, 3rd European Conference*, pp. 3757-3760

[36] J. Kiriazi, H. Ghali, H. Ragaie, and H. Haddara, "Reconfigurable dual-band dipole antenna on silicon using series MEMS switches", *2003 IEEE Antennas*

and *Propagation Society International Symposium,* vol. 1, 22-27 June 2003, pp. 403-406

[37]   C. J. Panagamuwa, and J. C. Vardaxoglou, "Optically reconfigurable balanced dipole antenna", *Antennas and Propagation, 2003, (ICAP 2003). Twelfth International Conference on (Conf. Publ. No. 491),* Vol. 1, 2003, pp. 237-240

[38]   G. H. Huff, and J. T. Bernhard, "Frequency reconfigurable CPW-fed hybrid folded slot/slot dipole antenna", *Wireless Communications and Applied Computational Electromagnetics, 2005, IEEE/ACES International Conference in* 2005, pp. 574-577

[39]   A. Mirhamali, P. S. Hall, and M. Soleimani, "Wideband reconfigurable printed dipole antenna with harmonic trap", *Antenna Technology Small Antennas and Novel Metamaterials, 2006, IEEE International Workshop in* 2006, pp. 188-191

[40]   R. J. DeGroot, D. P. Gurney, K. Hutchinson, M. L. Johnson, S. Kuffner, A. Schooler, S. D. Silk, and E. Visotsky, "A cognitive-enabled experimental system", *New Frontiers in Dynamic Spectrum Access Networks, 2005, DySPAN2005, 2005 First IEEE International Symposium* on 8-11 Nov. 2005, pp.556-561.

[41]   N. Fayyaz, S. Safavi-Naeini, E. Shin, and N. Hodjat, "A novel electronically tunable rectangular patch antenna with one octave bandwidth", *Electrical and Computer Engineering, 1998, IEEE Canadian Conference* on vol. 1, 24-28 May 1998, pp. 25-28.

[42]   Se-Keun Oh, Yong-sun Shin, and Seong-ook Park, "A novel PIFA type varactor tunable antenna with U-shaped slot", *Antennas, Propag. & EM*

*Theory, 2006, ISAPE '06. 7*th *International Symposium* on 26-29 Oct. 2006, pp. 1-3.

[43] P. R. Urwin-Wright, G. S. Hitton, I. K. Graddock, and P. N. Fletcher, "A reconfigurable electrically-small antenna operating in the 'DC' mode", *Vehicular Technology Conference, 2003, VTC 2003-Spring, The 57*th *IEEE Semiannual*, vol. 2, 22-25 April 2003, pp. 857-861.

[44] J. A. Zamrnit, and A. Muscat, "A small tunable antenna using multiple shorting posts and varactor diodes", *Communications, Control and Signal Processing, 2008, ISCCSP 2008, 3*rd *International Symposium* on 12-14 March 2008, pp. 83-86.

[45] M. –I. Lai, T. –Y. Wu, J. –C. Hsieh, C. –H. Wang, and S. –K. Jeng, "Design of reconfigurable antennas based on an L-shaped slot and PIN diodes for compact wireless devices", *IET Microwaves, Antennas & Propagation,* vol. 3, Feb. 2009, pp. 47-54.

[46] J. Kishor, P. Kumar, and A. K. Shrivastav, "Designing of varactor tuned microstrip patch antenna", *Recent Advances in Microwave Theory and Applications, 2008, MICROWAVE 2008, International Conference* on 21-24 Nov. 2008, pp. 907-909.

[47] N. Behdad, and K. Sarabandi, "Dual-band reconfigurable antenna with a very wide tunability range", *Antennas and Propag., IEEE Transactions* on vol. 54, Feb. 2006, pp. 409-416.

[48] B. K. Fankem, K. L. Melde, and Z. Zhen, "Frequency reconfigurable planar inverted F antenna (PIFA) with software-defined match control", *Antennas and Propag. Society International Symposium, 2007, IEEE,* 9-15 June 2007, pp. 81-84.

[49]   S. L. S. Yang, A. A. Kishk, and K. F. Lee, "Frequency reconfigurable U-slot microstrip patch antenna", *IEEE Antennas and Wireless Propagation Letters*, Vol. 7, 2008, pp. 127-129

[50]   V. K. Palukuru, M. Komulainen, T. Tick, J. Perantie, and H. Jantunen, "Low-sintering-temperature ferroelectric-thick films RF properties and an application in a frequency-tunable folded slot antenna", *Antennas and Wireless Propag. Letters, IEEE,* vol. 7, 2008, pp. 461-464.

[51]   W. J. Chang, J. K. Yong, K. Ilkyu, and E. K. Young, "Macro-micro frequency reconfigurable antenna", *Antennas and Propag. International Symposium, 2007, IEEE,* 9-15 June 2007, pp. 5853-5856.

[52]   J. H. Lee, L. Liu, K. L. Ford, and R. J. Langley, "Reconfigurable antennas and band gap materials", *Cognitive Radio and Software Defined Radios: Technologies and Techniques, 2008 IET Seminar* on 18 Sept. 2008, pp. 1-5.

[53]   J. M. Carrere, R. Staraj, and G. Kossiavas, "Small frequency agile antennas", *Electronics Letters*, vol. 37, 7 Jun 2001, pp. 728-729.

[54]   L. Huang, and P. Russer, "Tunable antenna design procedure and harmonics suppression methods of the tunable DVB-H antenna for mobile applications", *Wireless Technologies, 2007 European Conference* on 8-10 Oct. 2007, pp. 304-307.

[55]   H. Mi, and Z. Feng, "A novel compact varactor-tunable PIFA antenna for ISDB-T application", *Microwave Conference, 2007, APMC 2007, Asia-Pacific*, pp. 1-4

[56]   M. Berg, M. Komulainen, V. Palukuru, H. Jantunen, and E. Salonen, "Frequency-tunable DVB-H antenna for mobile terminals", *Antennas and Propagation Society International Symposium, 2007 IEEE*, pp. 1072-1075

[57] H. F. Abutarboush, R. Nilavalan, K. M. Nasr, H. S. Al-Raweshidy and D. Budimir, "Widely tunable multiband reconfigurable patch antenna for wireless applications", *Antennas and Propagation (EuCAP), 2010 Proceedings of the Fourth European Conference in 2010,* pp.1-3

[58] M. G. S. Hossain, and T. Yamagajo, "Reconfigurable printed antenna for a wideband tuning", *Antennas and Propagation (EuCAP), 2010 Proceedings of the Fourth European Conference in 2010*, pp. 1-4

[59] Y. Yu, J. Xiong, H. Li, and S. He, "An electrically small frequency reconfigurable antenna with a wide tuning range", *Antennas and Wireless Propagation Letters, IEEE*, Vol. 10, 2011, pp. 103-106

[60] H. F. AbuTarboush, R. Nilavalan, and T. Peter, "PIFA based reconfigurable multiband antenna for wireless applications", *Electromagnetics in Advanced Applications (ICEAA), 2010 International Conference,* pp. 232-235

[61] M. Ng Mou Kehn, O. Quevedo-Teruel, and E. Rajo-Iglesias, "Reconfigurable loaded planar inverted-F antenna using varactor diodes", *Antennas and Wireless Propagation Letters, IEEE*, Vol. 10, 2011, pp. 466-468

[62] F. Canneva, F. Ferrero, J. M Ribero, and R. Staraj, "Reconfigurable miniature antenna for DVB-H standard", *Antennas and Propagation Society International Symposium (APSURSI) 2010, IEEE*, pp. 1-4

[63] H. Li, J. Xiong, Y. Yu, and S. He, "A simple compact reconfigurable slot antenna with a very wide tuning range", *Antennas and Propagation, IEEE Transactions*, Vol. 58, Issue, 11, 2010, pp. 3725-3728

[64] J. Yoon, Y. C. Rhee, S. M. Lee, and W. S. Kim, "Tunable meander-type antenna integrated with a Bluetooth module in PCB board", *Microwave Conference Proceedings (APMC), 2010 Asia-Pacific, 2010*, pp. 1985-1988

[65]   P. –L. Chi, R. Waterhouse, and T. Itoh, "Compact and tunable slot-loop antenna", *Antennas and Propagation, IEEE Transactions* on Vol. 59, Issue 4, 2011, pp. 1394-1397

[66]   X. Cheng, D. E. Senior, J. J. Whalen, and Y. –K, Yoon, "Electrically small tunable split ring resonator antenna", *Antennas and Propagation Society International Symposium (APSURSI), 2010, IEEE*, pp. 1-4

[67]   S. Liu, Q. Feng, and Z. Wu, "Design of a frequency-tunable dual-band planar monopole antenna for handheld terminals", *Wireless And Optical Communications Networks (WOCN) 2010 Seventh International Conference in 2010*, pp. 1-3

[68]   W. –K. Park, S. –S. Oh, Y. –H. Lee, and H- D. Park, "Frequency-tunable waveguide antenna with miniaturized aperture using a varactor-loaded split-ring resonator", *Antennas and Wireless Propagation Letters, IEEE*, Vol. 9, 2010, pp/ 1233-1236

[69]   I. T. E. Elfergani, S. H. Abubakar, R. A. Abd-Alhameed, C. H. See, H. I. Hraga, M. S. Bin-Melha, P. S. Excell, and J. Rodriguez, "A dual-band frequency tunable planar inverted F antenna", *Antennas and Propagation (EuCAP), 2010 Proceedings of the 5th European Conference in 2011,* pp.223-227

[70]   A. T. Kolsrud, Ming-Yi Li, and K. Chang, "Frequency tunable CPW-fed CPS dipole antenna using varactors", *Antennas and Propagation Society International Symposium, 1998, IEEE,* Vol. 1, 1998, pp. 308-311

[71]   Pei-Yuan Qin, A. R. Weily, Y. J. Guo, T. S. Bird, and Chang-Hong Liang, "Frequency reconfigurable quasi-yagi folded dipole antenna", *Antennas and Propagation, IEEE Transactions on* Vol. 58, Issue 8, 2010, pp. 2742-2747

[72]   H. Chen, Z. Shi, L. Wu, and D. Guo, "Frequency reconfigurable antenna with micromechanical patch", *Anti-counterfeiting, Security, Identification, 2007 IEEE International Workshop* on 16-18 April 2007 pp. 18-22.

[73]   C. Shafai, L. Shafai, R. Al-Dahleh, D. D. Chrusch, and S. K. Sharma, "Reconfigurable ground plane membranes for analog/digital microstrip phase shifters and frequency agile antenna", *MEMS, NANO and Smart Systems, 2005, Proceedings, 2005 Internation Conference* on 24-27 July 2005, pp. 287-289.

[74]   R. Bose, and A. Sinha, "Tunable patch antenna using a liquid crystal substrate", *Radar Conference, 2008, RADAR '08, IEEE,* 26-30 May 2008, pp. 1-6.

[75]   G. Ruvio, M. J. Ammann, and C. N. Zhi, "Wideband reconfigurable rolled planar monopole antenna", *Antennas and Propag., IEEE Transactions* on vol. 55, June 2007, pp. 1760-1767.

[76]   Y. Tawk, J. Costantine, and C. G. Christodoulou, "A rotatable reconfigurable antenna for cognitive radio applications", *Radio and Wireless Symposium (RWS), 2011 IEEE*, pp. 158-161

[77]   G. H. Huff, D. L. Rolando, P. Walters, and J. McDonald, "A frequency reconfigurable dielectric resonator antenna using colloidal dispersions", *Antennas and Wireless Propagation Letters, IEEE, Vol.* 9, 2010, pp. 288-290

[78]   D. M. Pozar, and V. Sanchez, "Magnetic tuning of a microstrip antenna on a ferrite substrate", *Electronics Letters,* Vol. 24, Issue 12, 9th June 1988, pp. 729-731

APPENDIX B

MATCHING CIRCUIT DESIGN

The objective of this appendix is to explain the design of a matching circuit, incorporating a varactor, for the chassis-antenna, with a single coupling element, as seen in Fig. B.1, to achieve wide tuning range with minimum components.
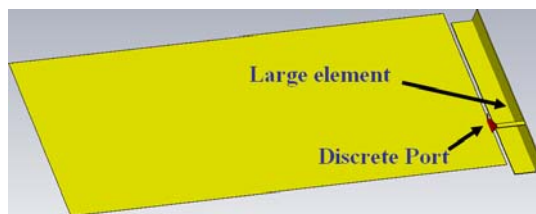
Fig. B.1 The structure of one port chassis-antenna
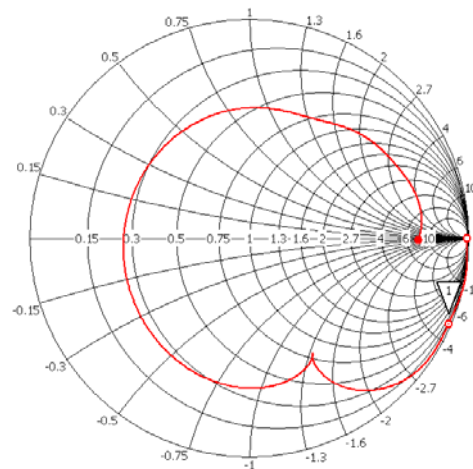
Fig. B.2 Input impedance for the chassis-antenna with one single element on the Smith Chart (from 50 MHz to 3 GHz)

Fig. B.2 shows the input impedance for the chassis-antenna with a single coupling element. It is clear that the antenna provides capacitive susceptance in the low frequencies and inductive susceptance at high frequencies. From basic principle, adding one inductor or capacitor can match any low frequency or high frequency, respectively. For example, the circuit incorporating an inductor, shown in Fig. B.3, can rotate the frequency of 1140 MHz, from the mismatched point close to the centre of the Smith Chart, as shown in Fig. B.4. Similarly the circuit incorporating a capacitor shown in Fig. B.5, can rotate the frequency of 2442 MHz, from the mismatched point to the centre, as shown in Fig. B.6.
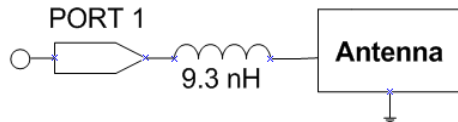
Fig. B.3 The matching network incorporating an inductor
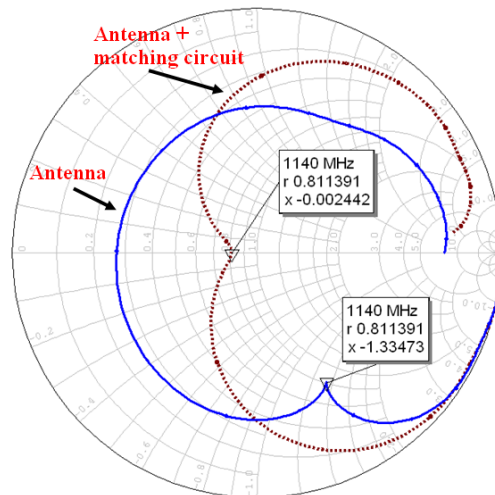
Fig. B.4 Input impedance on the Smith Chart for for the antenna itself and the antenna with matching circuit (from 50 MHz to 3 GHz)
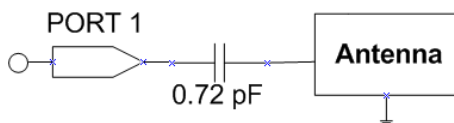
Fig. B.5 The matching network incorporating a capacitor
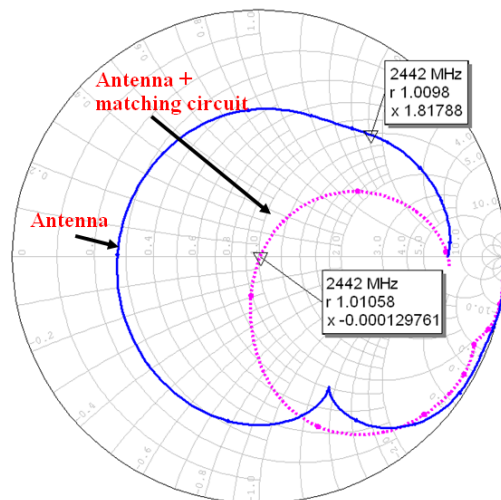
Fig. B.6 Input impedance on the Smith Chart for for the antenna itself and the antenna with matching circuit (from 50 MHz to 3 GHz)

It is clear that by changing the value of inductor or capacitor, can move any low frequency or high frequency close to the matching point. Thus an LC series network, as shown in Fig. B.7, would cover both low and high bands. In the series network, increasing the inductance or capacitance could move the frequency clockwise as shown in Fig. B.8.
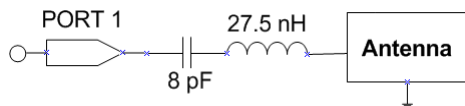
Fig. B.7 The matching network incorporating a series inductor and a series
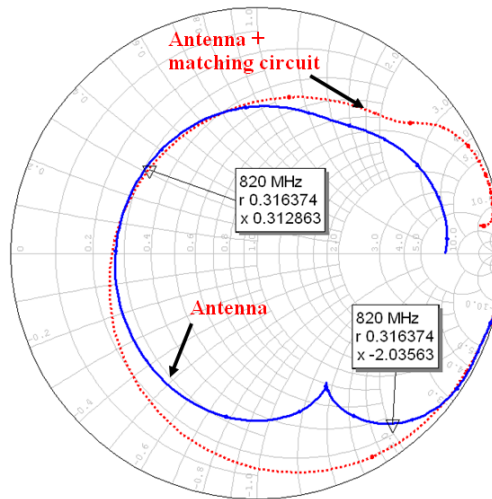
Fig. B.8 Input impedance on the Smith Chart for the antenna itself and the antenna with matching circuit (from 50 MHz to 3 GHz)

Reducing the capacitance will move the frequency anti-clockwise, thus moving the frequency close to the centre. However, the resonant frequency of 820 MHz, in Fig. B.8, still not well matched. The third component, a shunt inductor, is needed as shown in Fig. B.9. By incorporating a shunt inductor, it is possible to counter-clockwise move the frequencies which are capacitive on the chart until the desired impedance is achieved, as shown in Fig. B.10.
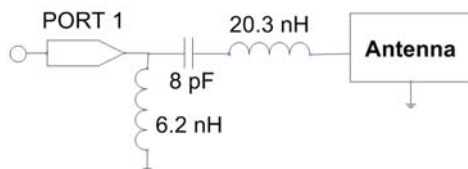
Fig. B.9 The matching network incorporating a series inductor, a series capacitor and a shunt inductor
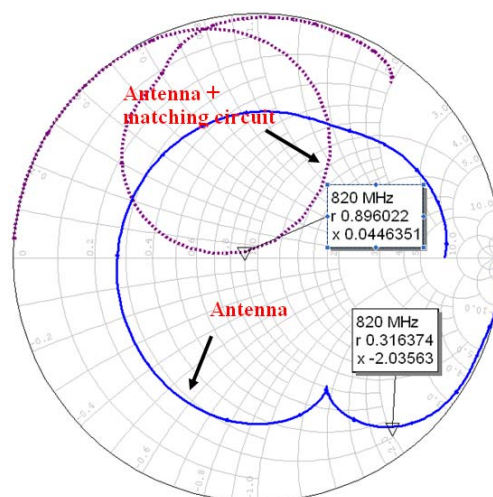
Fig. B.10 Input impedance on the Smith Chart for the antenna itself and the antenna with matching circuit (from 50 MHz to 3 GHz)

Thus, optimising the three components, namely the series inductor, series capacitor and shunt inductor, it is possible to cover a wide tuning range. The series inductor determines the lowest resonant frequency, a capacitor which can be replaced by a varactor tunes the resonant frequency, and the shunt inductor match at the resonant frequency. The values of the components within each of the matching circuits were calculated using standard formulas available within the literature [1]. Microwave Office, from Applied Wave Research, was then used to adjust the value of each inductor in order to optimise the return loss performance of the antenna.

References:

[1]   C. Bowick, RF Circuit Design, Newnes, 1997, pp. 66 – 97.

APPENDIX C

SIMPLE ARRAY ANALYSIS

Extraction of the surface currents on the antenna and ground plane of the conical antenna with 2 C-shaped slots, at 5.41 GHz, indicated the presence of strong currents on the top of the slots, and on the ground plane edges (Chapter 5, Section 5.1). Fig. C.1 shows the relative locations of these current concentrations. To enable a first order analysis of the likely radiation pattern of these current sources, it is assumed that there are strong vertical components of the currents at these locations, either across the metal bridge at the top of the C slots, or on the ground plane edge. Two tools were used to do simple array analysis on these currents.

1) Matlab

2) CST array tools in CST Microwave Studio®
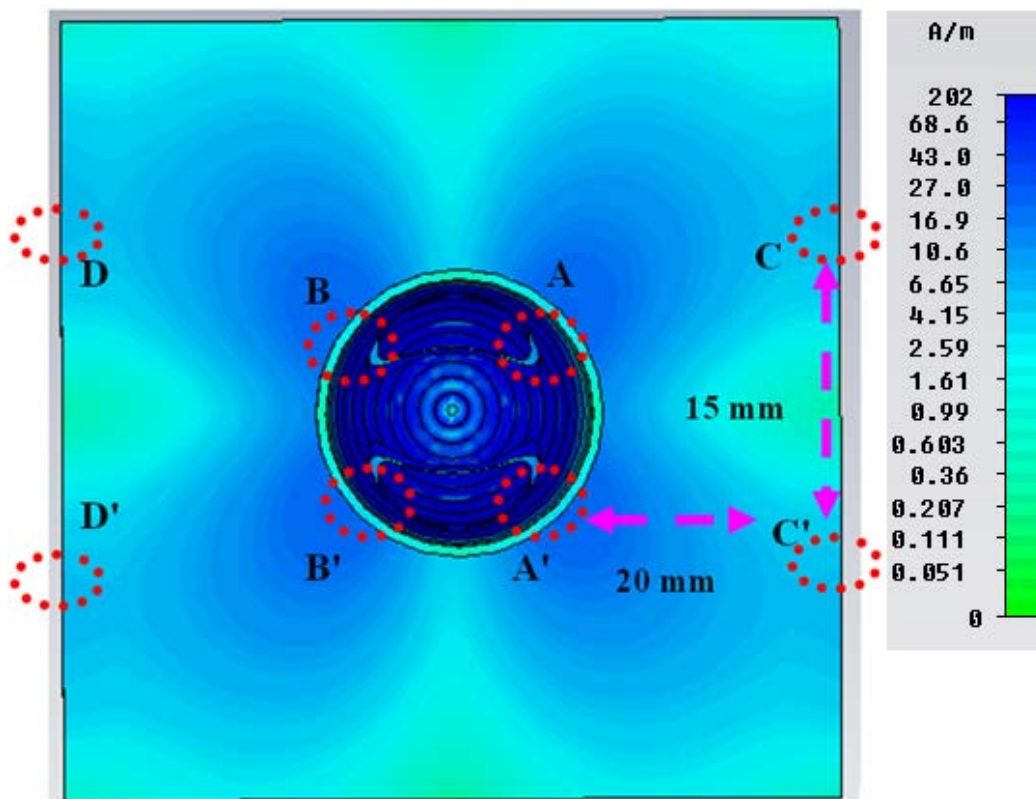
Fig. C.1 The relative locations of those current concentration on the cone and ground plane (conical antenna with 2 C-shaped slots, details can be referred to Chapter 5, Section 5.1)

C.1. Matlab

For a simple calculation, it is firstly assumed that there are strong vertical components of the currents at these locations, either across the metal bridge at the top of the C slots, or on the ground plane edge, and that secondly the currents are of equal magnitude. A simple array analysis using the equation [1] as below:

$$AF = \sum_{n=1}^{N} I_{1n} \left[\sum^{M} I_{m1} e^{j(m-1)(kd_x \sin\theta\cos\phi + \beta_x)} \right] e^{j(n-1)(kd_y \sin\theta\sin\phi + \beta_y)}$$
(C.1)

in which, m=2 and n=4 in the x and y directions with distances d_x=15mm and d_y=20mm. ϕ has a range from 0° to 360° and θ is fixed at 90°. Both values of phase shift (i.e. β_x and β_y) are 0.

The Matlab code for this calculation follows. The function referred to 'polar_dB.m' is used to plot the radiation patterns in polar coordinates [2]:

```
fi=linspace(0,360,361); %the range for fi is from 0 degree to 360 degree
the=90;%linspace(0,360,361); %the range for fi is from 0 degree to 360 degr
Fre = input('Enter your frequency in GHz: ');
phax = input('Enter the phase difference in x direction: ');
phay = input('Enter the phase difference in y direction: ');
dx = input('Enter the distance difference in x direction in mm: ');
dy = input('Enter the distance difference in y direction in mm: ');
f=Fre*1e9; %change frequency into Hz
lam=3e8./f; %wavelength
k=2*pi./lam; %wavenumber k
DX=dx./1000; % change to meter
DY=dy./1000; % change to meter
%6 array element 2x3 as planar array
Sx1=1;
Sy1=1;
FI=fi.*pi./180;
THE=the.*pi./180;
phaX=phax.*pi./180;
phaY=phay.*pi./180;
Sx2=exp(1j.*(k.*DX.*sin(THE).*cos(FI)+phaX));
%Sx3=exp(2j.*(k.*DX.*sin(THE).*cos(FI)+phaX));
Sy2=exp(1j.*(k.*DY.*sin(THE).*sin(FI)+phaY));
Sy3=exp(2j.*(k.*DY.*sin(THE).*sin(FI)+phaY));
Sy4=exp(3j.*(k.*DY.*sin(THE).*sin(FI)+phaY));
AF=(Sx1+Sx2).*(Sy1+Sy2+Sy3+Sy4);
theta=fi;
rho=10*log10(abs(AF));
rmin=min(rho);
rmax=max(rho);
rticks=std(0.001);
hpol = polar_dB(theta,rho,rmin,rmax,rticks,'--r');
clear phaX phaY dx dy f lam k DX DY Sx1 Sy1 Sx2 Sy2 Sy3 Sy4 Fre FI THE
clear rmin rmax rticks hpol fi the
```

C.2. CST Array Tools

The Matlab code provided in the previous section was assumed that the elements, in x and y directions, had identical amplitude, distance and phase difference, respectively. When the values of amplitude, distance and phase difference of the elements are different, the equation needs to be modified and becomes complex. Alternatively, CST array tools can be used. The steps for the array analysis are as follows:

1) Design a simple dipole antenna which can operate at the required frequency, for example 5.41 GHz, as shown in Fig. C.2;

2) Created a far field monitor at the required frequency, for example 5.41 GHz, as shown in Fig. C.3;

3) After the transient solver simulation, then clink the 'Properties' for 'Antenna array' in 'Farfield Plot', as shown in Fig. C.4;

4) Then enter the details for the antenna arrays, such as number of elements in each direction, spaceshift and phaseshift for each element, as shown in Fig. C.5. (please note that, in this condition, the values of current amplitude, spacesshift and phaseshift for each elements are equal);

5) For different values of current amplitude, spacesshift or phaseshift, the 'Edit antenna list' can be selected, as shown in Fig. C.5.
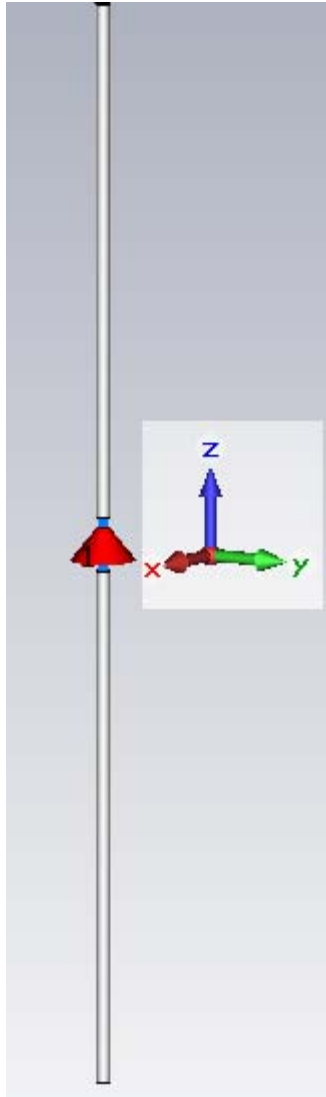
Fig. C.2 The structure of dipole antenna

Fig. C.3 Created a farfield monitor at the requited frequency, for example 5.41 GHz
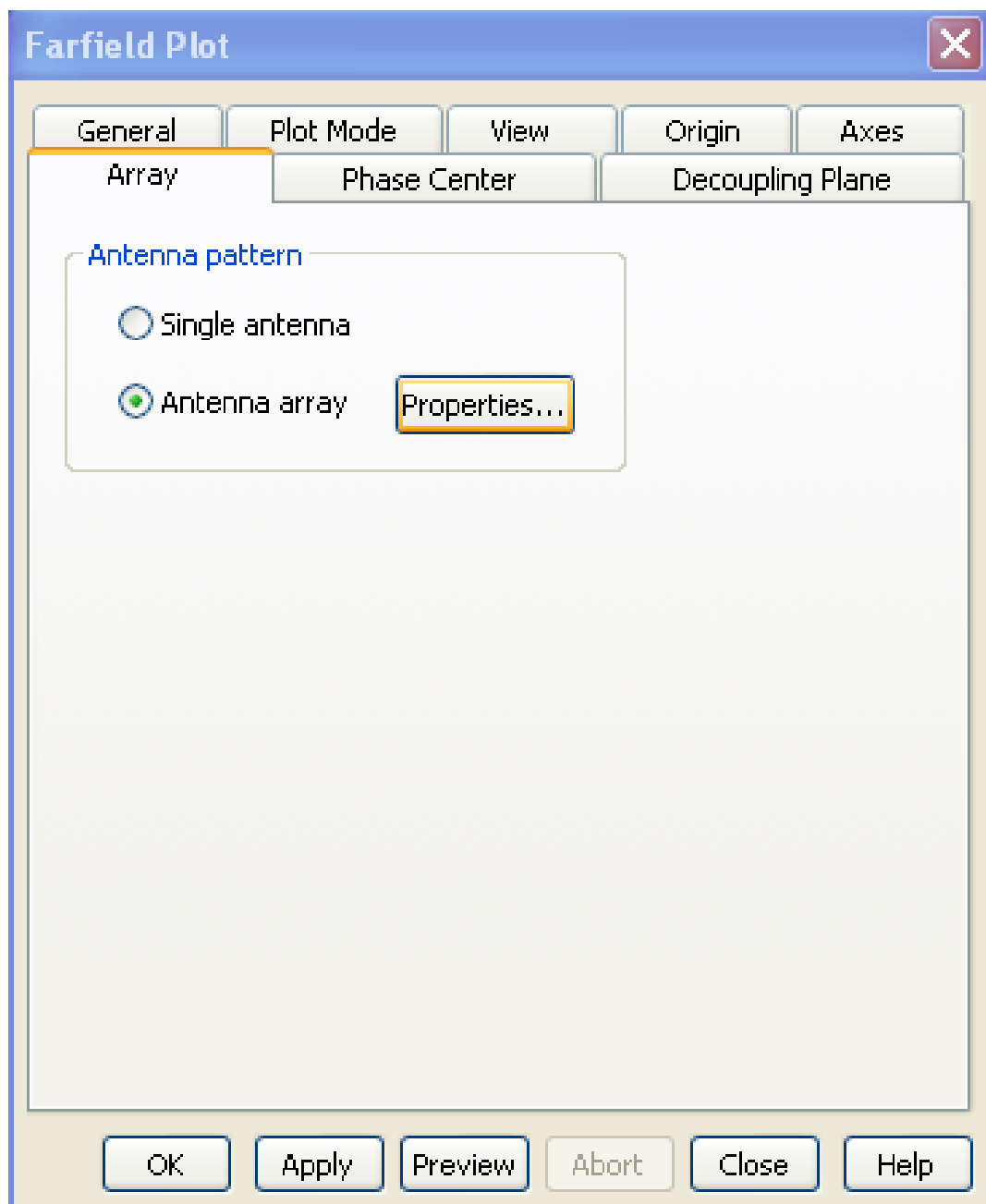
Fig. C.4 Antenna array properties in Farfield Plot

Fig. C.5 Edit parameters for antenna array

References:

[1]   C. A. Balanis, Antenna Theory, 3rd edition, Analysis and Design, John Wiley & Sons, Inc, 2005, pp. 349-362.

[2]   C. A. Balanis, Antenna Theory, 3rd edition, Analysis and Design, John Wiley & Sons, Inc, 2005. CD-ROM.

APPENDIX D

CST MICROWAVE STUDIO®

CST Microwave Studio® is software that is used for simulating high frequency three dimensional problems. The main features of CST are the frequency domain solver, modal analysis, fast, accurate and memory efficient finite integral method, far-field calculation, broadband S-parameter calculation and solution of antenna problems. The versions used during the PhD research study were 2009, 2010 and 2011.

D. 1. Instruction to Use CST Microwave Studio®

CST model allows very simple to model creation, as a number of templates have been specified for antenna design. For instance, the template of an antenna for a mobile phone, as shown in Fig. D.1, is chosen to design a two port chassis-antenna. This template specifies the units, background, boundaries and bounding box.
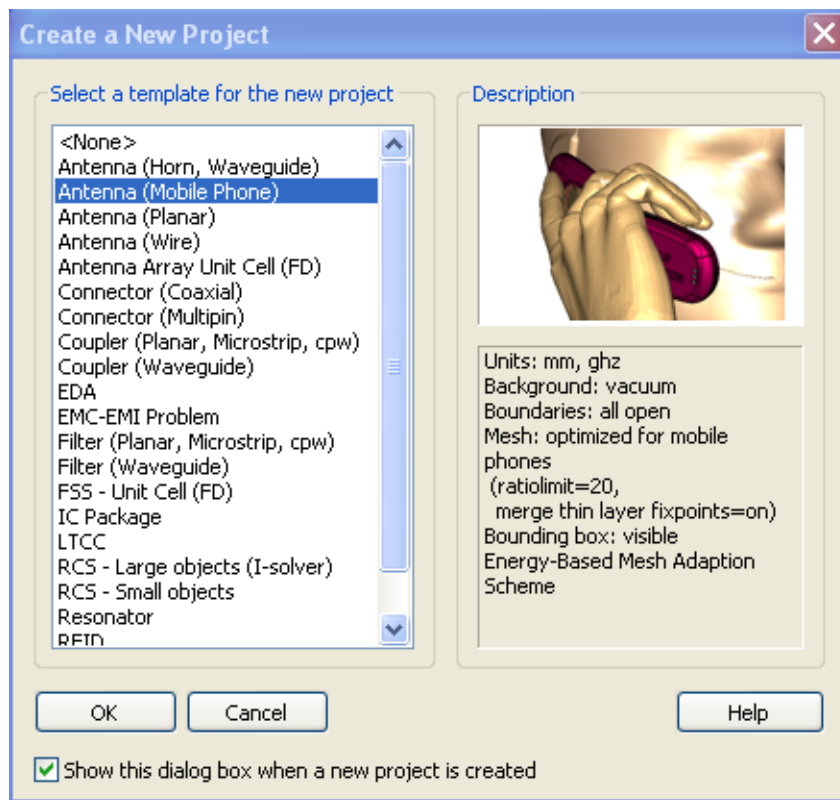
Fig. D. 1 Template of the project (Antenna for Mobile Phone)

As CST applies very high quality of graphic user interface (GUI) as shown in Fig. D.2, this feature makes it easy to use. The antenna is constructed using the polygons. The units, background properties, material, frequency, boundary condition, waveguide port, field monitor and transient solver parameters can be obtained from the "Solver" menu. For a two port chassis-antenna, the background properties are chosen to be normal, units are in mm and GHz, frequency from 0 to 3 GHz, and the boundary condition is set as "open (add space)" for all directions. These are shown in Fig. D.3(a-d).
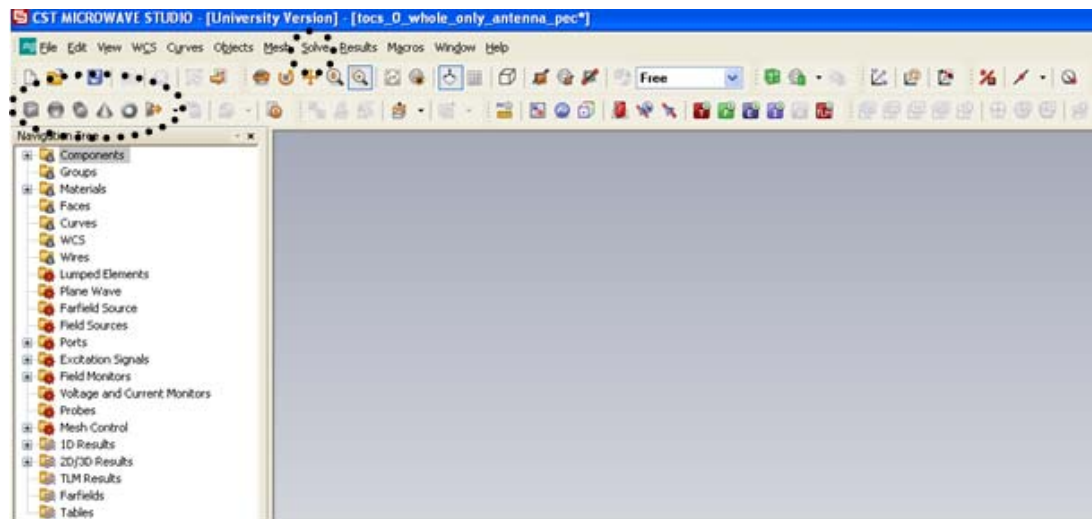
Fig. D. 2 GUI of the project
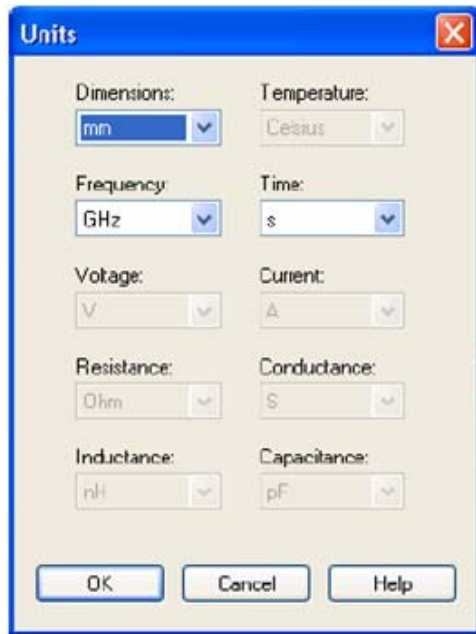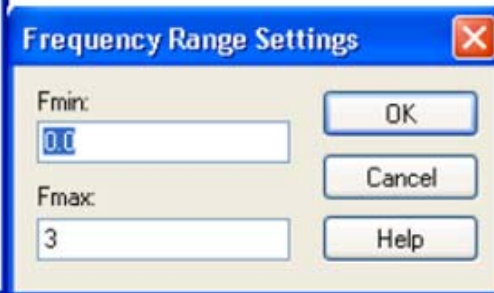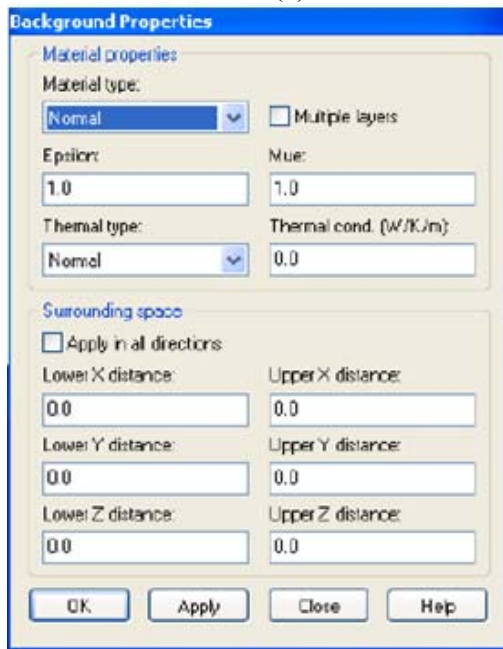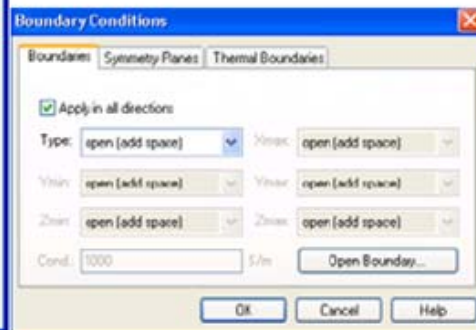
Fig. D. 3 (a) Units; (b) Frequency; (c) Background Properties; and (d) Boundary
Conditions

APPENDIX E

MICROWAVE OFFICE FROM AWR

Microwave Office RF/microwave design software encompasses all the tools essential for high frequency IC, PCB and module design, including:

- Linear circuit simulators

- Non-linear circuit simulators

- Electromagnetic (EM) analysis tools

- Integrated schematic and layout

- Statistical design capabilities

- Parametric cell libraries with built-in design-rule check (DRC)

. The versions used during this PhD research study were 2009 and 2010.

E. 1. Instruction to use Microwave Office from AWR

Microwave Office has simple interface. The linear circuit simulator is the main tool used for this work. The first step is to create "New Schematics", shown in Fig. E.1. The second step is to check the units setting in "Project Options" in "Options", as shown in Fig. E.2.
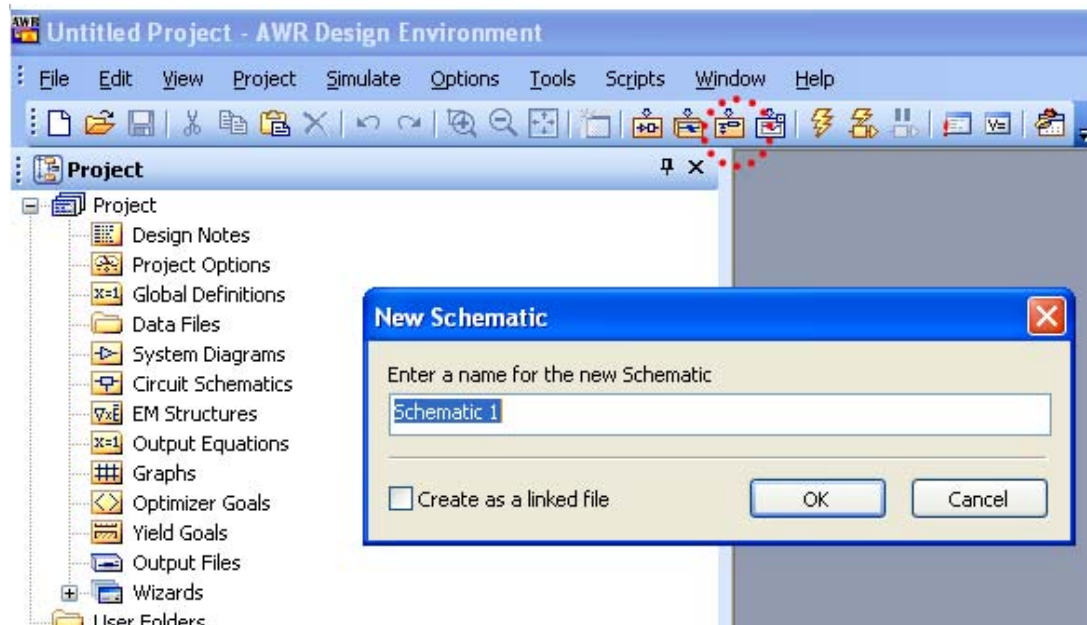
Fig. E. 1 Add a new schematic
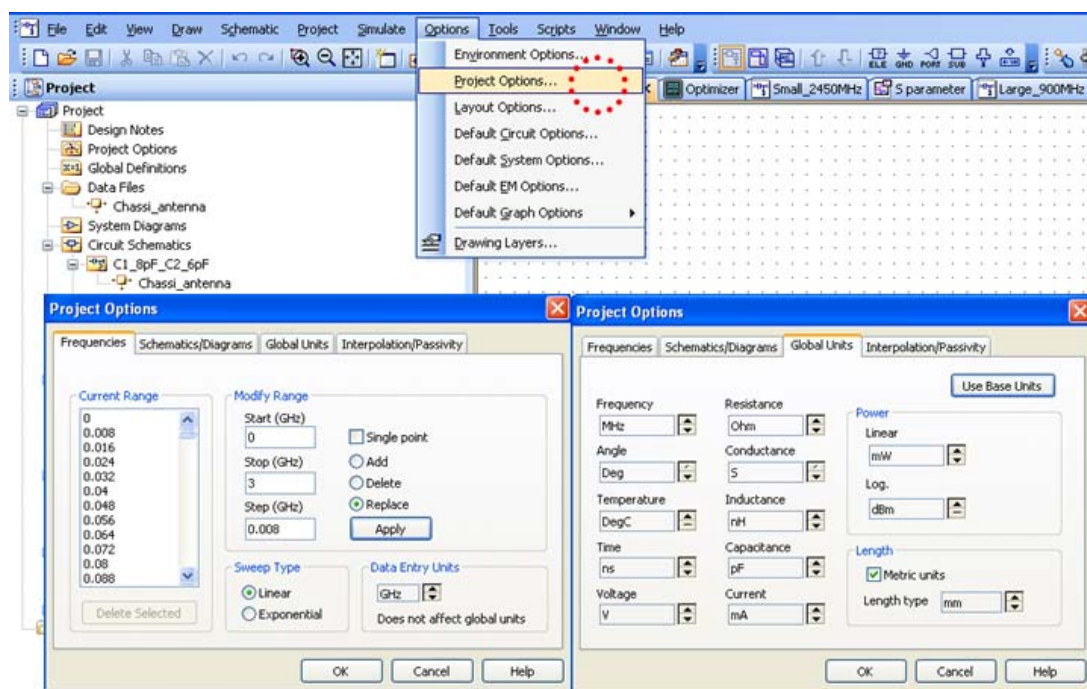
Fig. E. 2 Check units setting

Both "Optimizer", shown in Fig. E.3, and "Tune", shown in Fig. E. 4, are very helpful

tools for designing a circuit in Microwave Office.
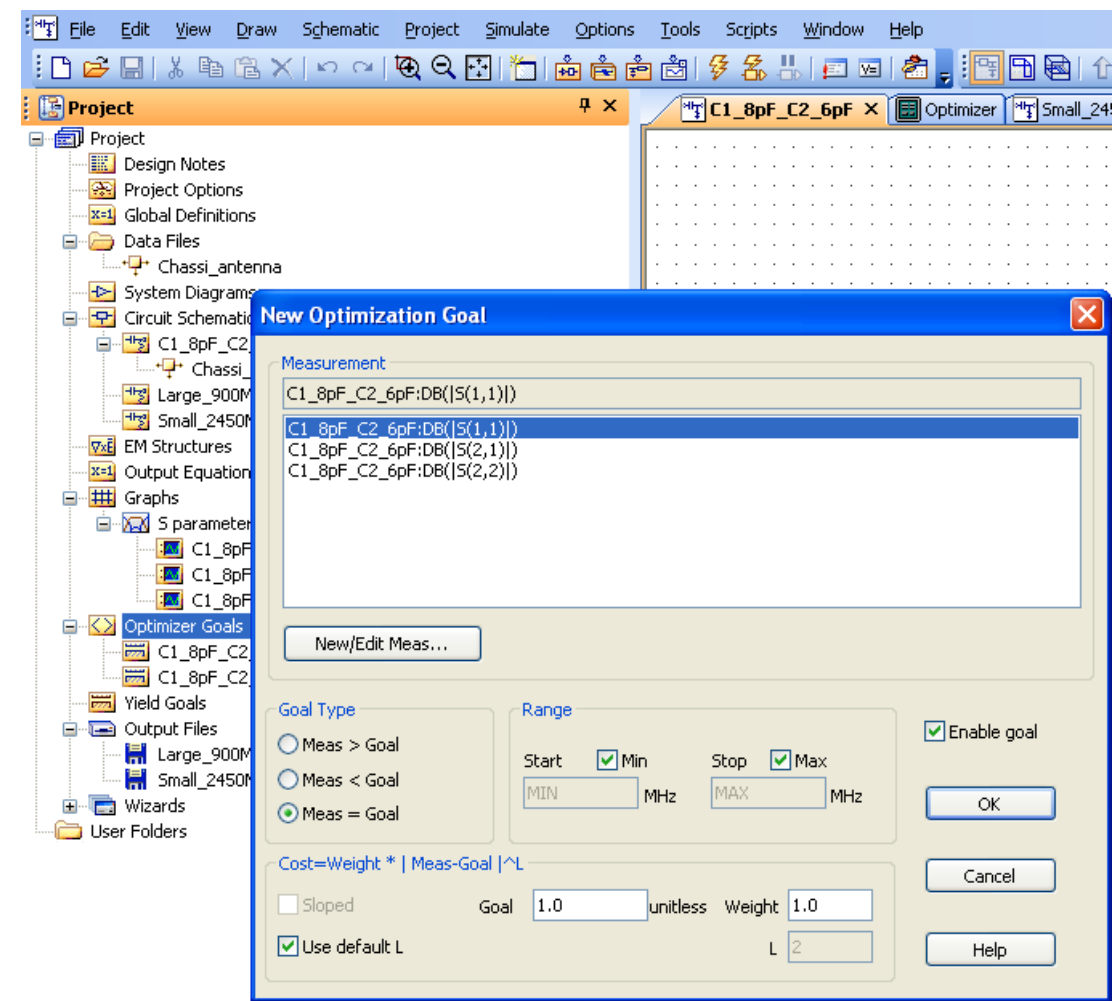
Fig. E. 3 Optimizer goals setting
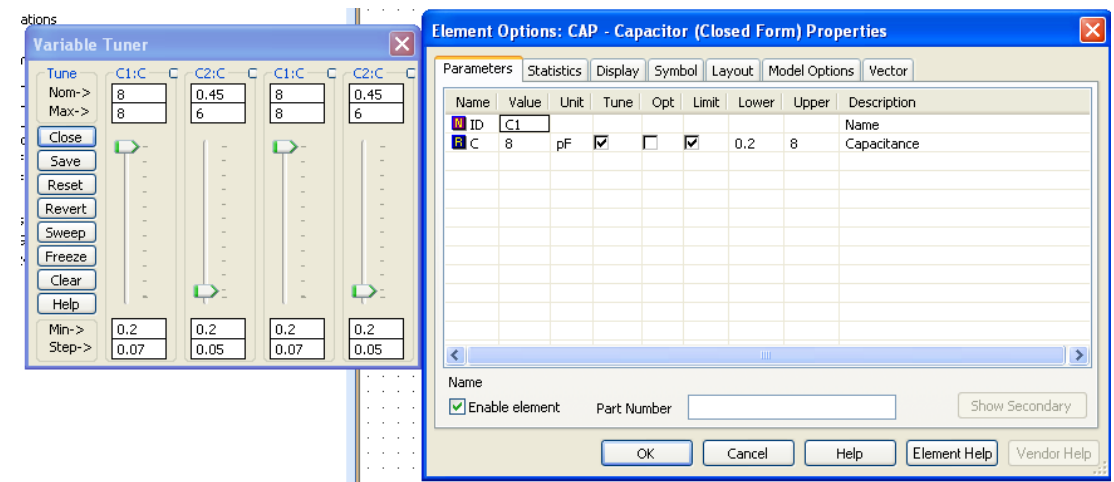
Fig. E. 4 Tuner setting

Microwave Office not only provides simulation on ideal lumped elements, but also

provides S parameters files for popular components from manufacturers, such as

different types of capacitors, inductors, resistors, etc, shown in Fig. E.5.
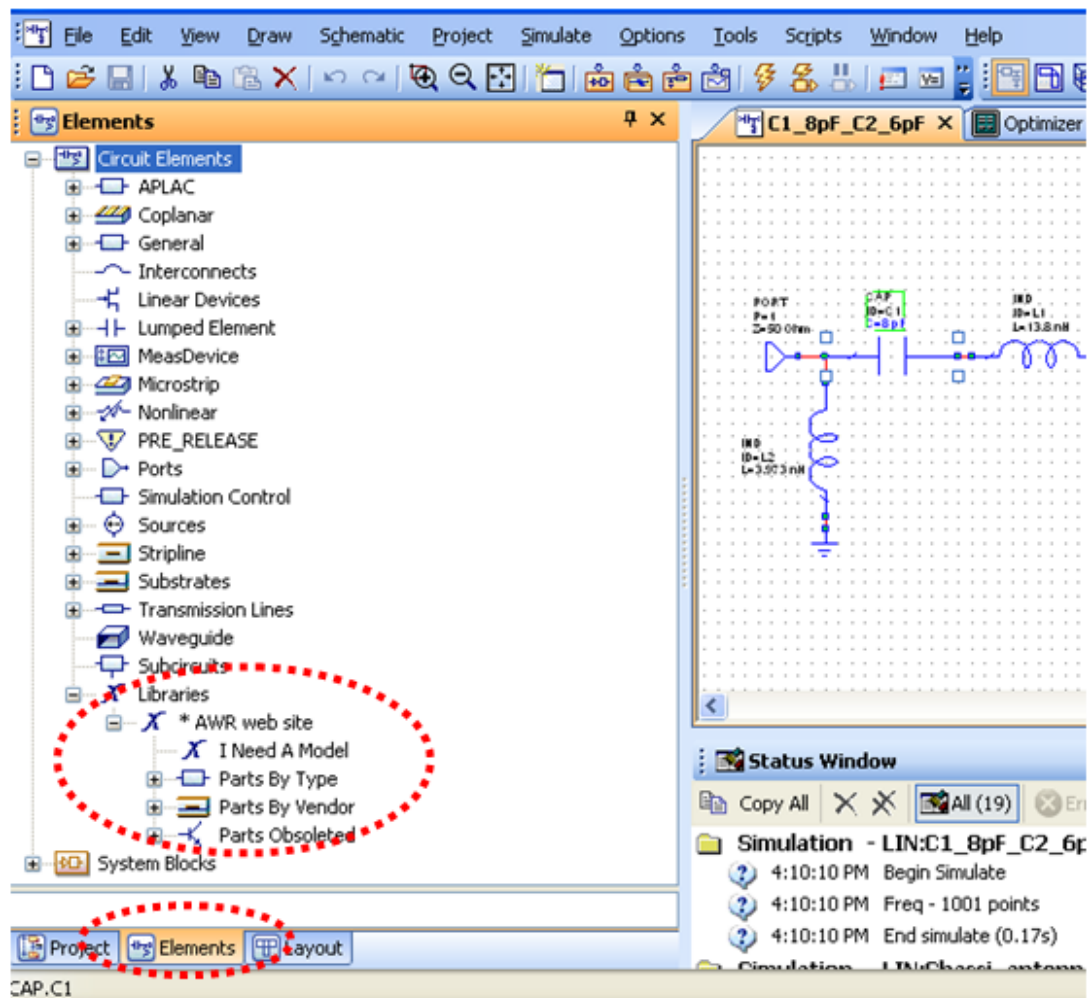
Fig. E. 5 S parameters files from manufacturers in Microwave Office Libraries

APPENDIX F

ANTENNA PARAMETERS AND MEASUREMENT EQUIPMENT

Antenna measurement is an important part of evaluating and verifying an antenna's performance during the design procedure. There are several important parameters affecting an antenna's performance, such as S parameters, radiation pattern, gain, antenna efficiency, and polarization, etc. All of these parameters can be measured by the use of the proper techniques and equipment.

F.1. S Parameters

S parameters, or scattering parameters [1], are the reflection and transmission coefficients between the incident and reflection voltage waves mostly operating at radio frequency and microwave frequencies. S parameters change with frequency and each parameter is typically characterized by a magnitude and a phase.

F.2. Radiation Pattern

An antenna radiation pattern or antenna pattern is defined as "a mathematical function or a graphical representation of the radiation properties of the antenna as a function of space coordinates. In most cases, the radiation pattern is determined in the farfield region and is represented as a function of the directional coordinates. Radiation properties include power flux density, radiation intensity, field strength, directivity, phase or polarization." [2].

The space surrounding an antenna is usually subdivided into three regions: (a) reactive near-field, (b) radiating near-field (Fresnel) and (c) far-field (Fraunhofer) regions [2]. Only within the far-field regions, the angular field distribution is

independent of the distance from the antenna. The far-field region is commonly taken to exist at distances greater than $2D^2/\lambda$ from the antenna, where D is the maximum overall dimension of the antenna and λ is the wavelength. In general, the radiation pattern is determined by the far-field radiation properties and is represented as a function of the directional coordinates.

The radiation pattern is three-dimensional, and can be displayed in a meaningful manner by 2D cuts or planes. For a linearly polarized antenna, performance is often described in terms of its principal E- and H-plane patterns. The E-plane is defined as "the plane containing the electric-field vector and the direction of maximum radiation," and the H-plane as "the plane containing the magnetic-field vector and the direction of maximum radiation." [2]

F.3. Gain and Efficiency

Three gains can be defined. The first one is referred to as directivity, D, the second one as antenna gain, G, and the third one as absolute gain or realized gain, $G_{abs.}$

Directivity is defined as "the radio of the radiation intensity in the peak intensity direction to the averaged radiation intensity in all other directions." [2]. It can be expressed as,

$$D(\theta,\phi) = \frac{power\_radiated\_per\_unit\_solid\_angle}{average\_power\_radiated\_per\_unit\_solid\_angle} \qquad (F.1)$$

However, in IEEE standard definitions of terms for antennas [3], Directivity is defined as "the ratio of the radiation intensity in a given direction from the antenna to

the radiation intensity averaged over all directions." and "if the direction is not specified, the direction of maximum radiation intensity is implied." [3]

Gain is defined as "the ratio of the intensity, in a given direction, to the radiation intensity that would be obtained if the power accepted by the antenna were radiated isotropically." [2]. In equation form this can be expressed as:

$$G(\theta, \phi) = \frac{power\_radiated\_per\_unit\_solid\_angle}{total\_input\_(accepted)\_power} \tag{F. 2}$$

or $G(\theta, \phi) = e_{cd} D(\theta, \phi)$ (F.3)

where e_{cd} is antenna radiation efficiency, which includes conduction efficiency and dielectric efficiency. According to the IEEE Standards [3], this gain does not include losses arising from impedance mismatches and polarization mismatches; if the direction is not specified then the direction of maximum radiation intensity is implied.

The other gain, named as "absolute gain" or "realized gain", takes into account the reflection/mismatch losses, and it can be written as,

$G_{abs}(\theta, \phi) = e_o D(\theta, \phi)$ (F.4)

where e_o is antenna total efficiency, which includes reflection efficiency and radiation efficiency and can be expressed as $e_r e_{cd}$. Please note that the realized gain does not include losses due to polarization mismatch between two antennas in a complete system [3].

F.4. Polarisation

Polarization is "the sum of the electric field (E-plane) orientations over time projected onto an imaginary plane perpendicular to the direction of motion of the radio wave",

[2]. There are three polarisation, which are linear polarisation, circular polarisation and elliptical polarisation. The polarisation is expressed with reference to the electric field. "Co-polarisation represents the polarization the antenna is intended to radiate (receive) while cross-polarisation represents the polarisation orthogonal to a specified polarization, which is usually the co-polarization." [2]

F.5. Measurement Equipments

S parameters can be measured using vector network analyzer (VNA), shown in Fig. F.1.

Fig. F. 1 Picture of vector network analyzer

The radiation patterns (amplitude and phase), polarization, and gain of antenna, which are used to characterize the radiation capabilities of an antenna, are measured using the typical instrumentation, shown in Fig. F. 2. Such an antenna range instrumentation must be designed to cover a wide range of frequency operation band, and it usually can be classified into five categories [4] as below:

1. source antenna and transmitting system

2. receiving system

3. positioning system

4. recording system

5. data-processing system

For all the antennas design during this work, their radiation patterns and gain were measured inside an anechoic chamber in N510, School of Electronic, Electrical and Computer Engineering, University of Birmingham.

F.6. Gain Measurement

In this research study, the gain measurement method is three-antenna method [2]. Except the unknown antenna, denoted as "*uk*", the other two known antennas are denoted as "A" and "B". The external dimension of the used anechoic chamber for the antenna gain measurement is 4L*3W *2H m^3. The antennas were located almost 2 m from each other. Equation (F.5) and (F.6), based on Friis formula, is used to calculate the realised gain of the antenna.

$$(G_A)_{dB} + (G_B)_{dB} = 20\log_{10}\left(\frac{4\pi R}{\lambda}\right) + (S_{21,BA})_{dB} \tag{F.5}$$

$$(G_A)_{dB} + (G_{uk})_{dB} = 20\log_{10}\left(\frac{4\pi R}{\lambda}\right) + (S_{21,ukA})_{dB} \tag{F.6}$$

where G_A and G_B are gain for the two known antennas and G_{uk} is gain for the unknown antenna. λ is the wavelength of the frequency measurement and R is the distance between two antennas. $S_{21,BA}$ and $S_{21,ukA}$ are the transmission losses which are available from the measurements. By calculating (F.6) and substituting it in (F.5), the gain of the unknown antenna can be determined as (F.7):

$$\left(G_{uk}\right)_{dB} = \left(S_{21,ukA}\right)_{dB} - \left(S_{21,BA}\right)_{dB} + \left(G_{B}\right)_{dB} \qquad \text{(F.7)}$$
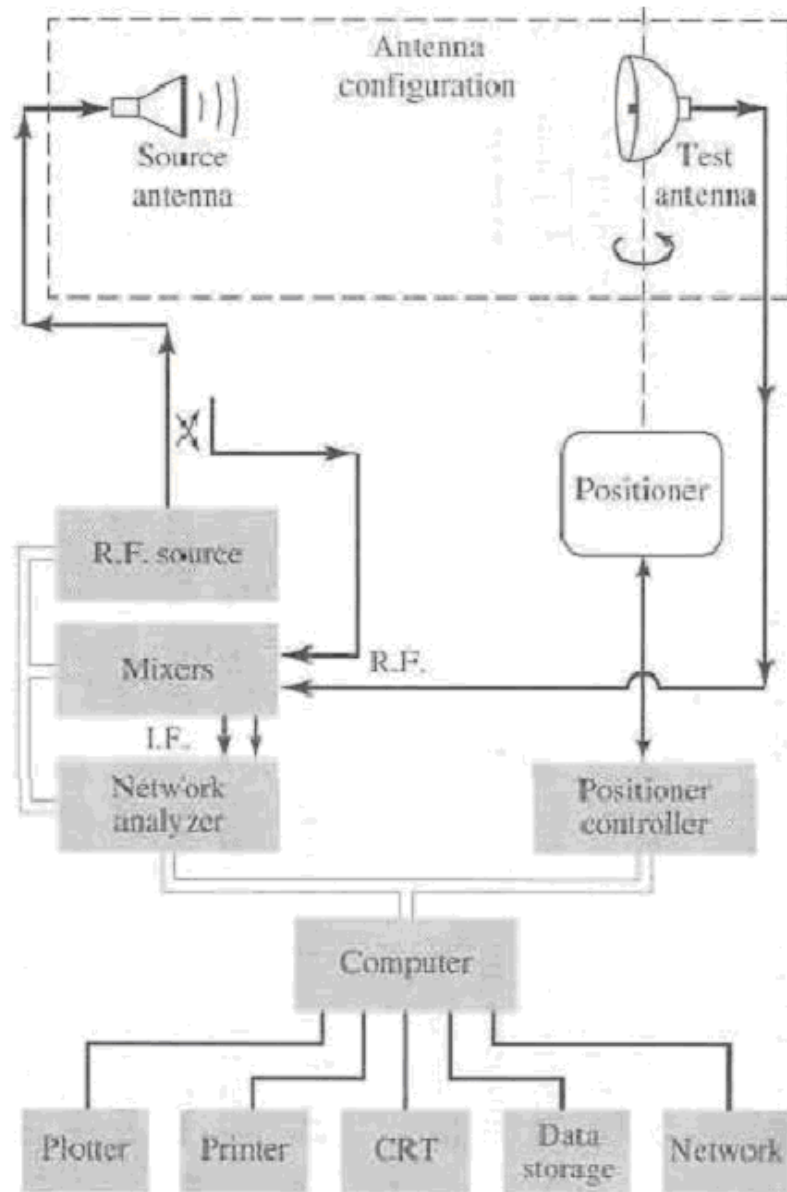
Fig. F. 2 Block diagrams of typical instrumentations for measuring antenna patterns [2]

References:

[1]   D. M. Poza, *Microwave Engineering*, 2nd ed: John Wiley & Sons, Inc, 1998

[2]   C. A. Balanis, *Antenna Theory, Analysis and Design*, 3rd ed: John Wiley & Sons, Inc, 2005

[3]   IEEE Stantard Definitions of Terms for Antennas, *IEEE Std 145-1983*, *Published by IEEE, Inc.,* 1983.

[4]   IEEE Standard Test Procedures for Antennas*, IEEE Std 149-1979, Published by IEEE, Inc.*, 1979, Distributed by Wiley-Interscience.

APPENDIX G

MANUFACTURE OF ANTENNAS

G.1. Printed Circuit Broad (PCB)

In recent times, printed antennas have attracted increasing interest due to their simple manufacture. The most economic way to build a printed circuit broad (PCB) is photoengraving, which uses a photomask and etchant to selectively remove a photoresist coating. The remaining photoresist protects the copper foil. Subsequent etching removes the unwanted copper. If you are using "Pre Coated FR4" as the PCB material, then you will need to create a "Photo Positive" master. However, if you use "Duroid" or a similar uncoated substrate, then the process to coat this material is different, in that a "Photo Negative" artwork is required and you will need to ensure you design your layout accordingly.

G.2. 3D Antenna Manufacture

In this thesis, a series of 3D conical monopole antennas have been demonstrated. Those antennas were machined from solid, by first machining the outer shape from a stock copper rod, then drilling the centre hole using a CNC lathe. A small ball nose milling cutter on a CNC miller was then used to machine the internal shape of the cone. The antenna slots were machined individually using 0.5mm cutter with the blank cone mounted in a special fixture. Low cost production would depend on the intended frequency range and hence size. For smaller size the antennas could use die casting. Larger size could be produced by rapid prototyping. Alternately if the cone shape is altered at the expense of bandwidth several possibilities exist. A straight cone with circular cross section can be made by wrapping thin flexible PCB over a former. A straight cone with square cross section can be made from four triangular printed

circuit boards, as demonstrated in Chapter 6. This then allows simple loading of each

slot with a varactor diode and other components.

APPENDIX H

COMPONENTS DATA SHEETS

H.1. Microwave Substrate Material – Taconic TLY-3-450-C5

TLY-5 TYPICAL VALUES					
Property	**Test Method**	**Units**	**Value**	**Units**	**Value**
Dielectric Constant @ 10 GHz	IPC-TM 650 2.5.5.5		2.20		2.20
Dissipation Factor @ 10 GHz	IPC-TM 650 2.5.5.5		0.0009		0.0009
Moisture Absorption	IPC-TM 650 2.6.2.1	%	<0.02	%	<0.02
Dielectric Breakdown	IPC-TM 650 2.5.6	kV	>60	kV	>60
Volume Resistivity	IPC-TM 650 2.5.17.1	Mohm/cm	10^7	Mohm/cm	10^7
Surface Resistivity	IPC-TM 650 2.5.17.1	Mohm	10^7	Mohm	10^7
Arc Resistance	IPC-TM 650 2.5.1	seconds	>180	seconds	>180
Flexural Strength Lengthwise	IPC-TM 650 2.4.4	lbs./in.	>12,000	N/mm²	>83
Flexural Strength Crosswise	IPC-TM 650 2.4.4	lbs./in.	>10,000	N/mm²	>69
Peel Strength (1oz copper)	IPC-TM 650 2.4.8	lbs./linear in.	12.0	N/mm	2.1
Thermal Conductivity	ASTM F 433	W/m/K	0.22	W/m/K	0.22
x-y CTE	ASTM D 3386 (TMA)	ppm/°C	20	ppm/°C	20
z CTE	ASTM D 3386 (TMA)	ppm/°C	280	ppm/°C	280
UL-94 Flammability Rating	UL-94		V-0		V-0

Type		Dk
TLY-5A		2.17
TLY-5		2.20
TLY-3		2.33
TLT-0	TLX-0	2.45
TLT-9	TLX-9	2.50
TLT-8	TLX-8	2.55
TLT-7	TLX-7	2.60
TLT-6	TLX-6	2.65
TLE-95		2.95
TLC-27		2.75
TLC-30		3.00
TLC-32		3.20
RF-30		3.00
RF-35	RF-35P	3.50
RF-60		6.15
CER-10		10

ELECTRICAL PROPERTIES PTFE/E GLASS

LOSS vs. FREQUENCY

DIELECTRIC CONSTANT vs. FREQUENCY
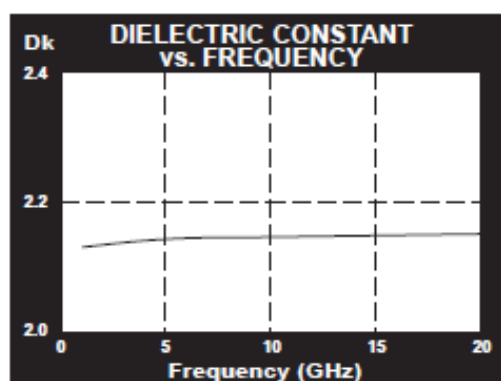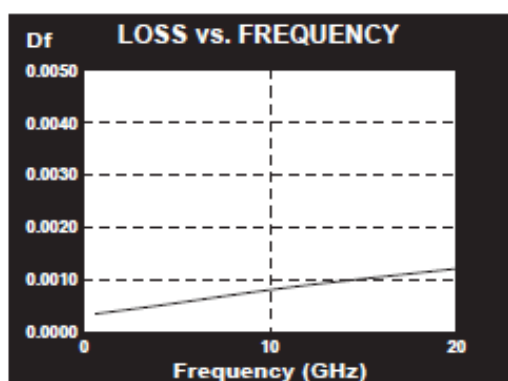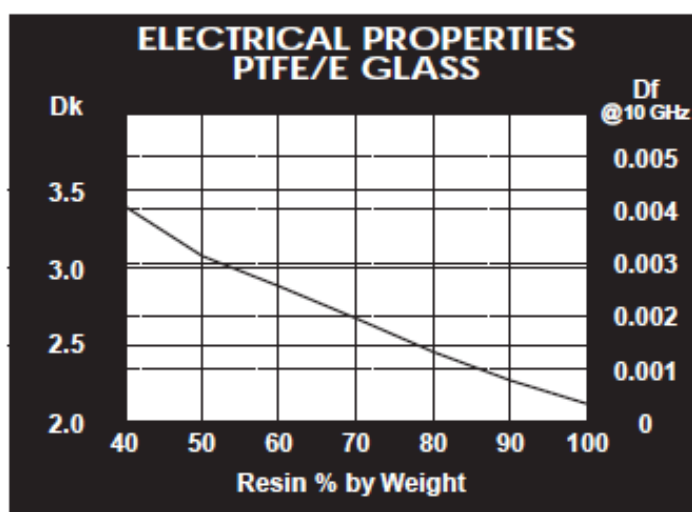
Designation	Dielectric Constant	Dielectric Thickness	Dielectric Thickness
TLY - 5A	2.17 +/– .02	.0310"	0.78mm
TLY - 5	2.20 +/– .02	.0050"	0.13mm
TLY - 3	2.33 +/– .02	.0050"	0.13mm

Standard sheet size is 36″ x 48″ (914mm x 1220mm). Please contact our Customer Service Department for the availability of other sizes and claddings.

TLY can be ordered with the following electrodeposited copper:

Designation	Weight	Copper Thickness	Copper Thickness
CH	1/2 oz./sq. ft.	~ .0007"	~18 μm
C1	1 oz./sq. ft.	~ .0014"	~ 35 μm
C2	2 oz./sq. ft.	~ .0028"	~ 70 μm

Panels may be ordered cut to size

Typical Panel Sizes	
12" x 18"	304mm x 457mm
16" x 18"	406mm x 457mm
18" x 24"	457mm x 610mm
16" x 36"	406mm x 914mm
24" x 36"	610mm x 914mm
18" x 48"	457mm x 1220mm

An example of our part number is: TLY-5-0100-CH/CH-18" x 24" (TLY-5-0100-CH/CH-457mm x 610mm)

H.2. Chip Capacitor – 0603 from AVX

C0G (NP0) Dielectric

General Specifications
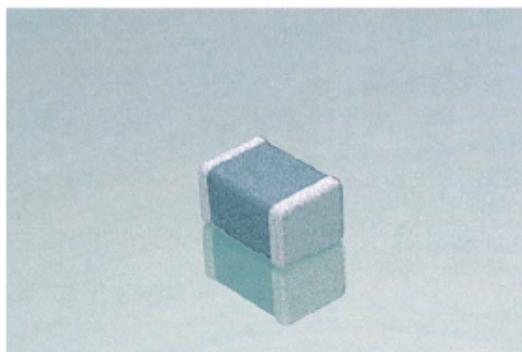
C0G (NP0) is the most popular formulation of the "tempera-ture-compensating," EIA Class I ceramic materials. Modern C0G (NP0) formulations contain neodymium, samarium and other rare earth oxides.

C0G (NP0) ceramics offer one of the most stable capacitor dielectrics available. Capacitance change with temperature is 0 ±30ppm/°C which is less than ±0.3% Δ C from -55°C to +125°C. Capacitance drift or hysteresis for C0G (NP0) ceramics is negligible at less than ±0.05% versus up to ±2% for films. Typical capacitance change with life is less than ±0.1% for C0G (NP0), one-fifth that shown by most other dielectrics. C0G (NP0) formulations show no aging characteristics.

PART NUMBER (see page 2 for complete part number explanation)

0805	5	A	101	J	A	T	2	A

Size (L* x W*)

Voltage
6.3V = 6
10V = Z
16V = Y
25V = 3
50V = 5
100V = 1
200V = 2
500V = 7

Dielectric
C0G (NP0) = A

Capacitance Code (In pF)
2 Sig. Digits + Number of Zeros

Capacitance Tolerance
B = ±.10 pF (<10pF)
C = ±.25 pF (<10pF)
D = ±.50 pF (<10pF)
F = ±1% (≥ 10 pF)
G = ±2% (≥ 10 pF)
J = ±5%
K = ±10%

Failure Rate
A = Not Applicable

Terminations
T = Plated Ni and Sn
7 = Gold Plated

Contact Factory For
1 = Pd/Ag Term

Packaging
2 = 7" Reel
4 = 13" Reel
7 = Bulk Cass.
9 = Bulk

Contact Factory For Multiples

Special Code
A = Std. Product

NOTE: Contact factory for availability of Termination and Tolerance Options for Specific Part Numbers.
Contact factory for non-specified capacitance values.

Temperature Coefficient

Δ Capacitance vs. Frequency

Insulation Resistance vs Temperature

Variation of Impedance with Cap Value
Impedance vs. Frequency
0805 - C0G (NP0)
10 pF vs. 100 pF vs. 1000 pF

Variation of Impedance with Chip Size
Impedance vs. Frequency
1000 pF - C0G (NP0)

Variation of Impedance with Ceramic Formulation
Impedance vs. Frequency
1000 pF - C0G (NP0) vs X7R
0805

4

AVX

- 280 -

C0G (NP0) Dielectric

Specifications and Test Methods

Parameter/Test		NP0 Specification Limits	Measuring Conditions	
Operating Temperature Range		-55°C to +125°C	Temperature Cycle Chamber	
Capacitance		Within specified tolerance	Freq.: 1.0 MHz ± 10% for cap ≤ 1000 pF	
Q		<30 pF: Q≥ 400+20 x Cap Value ≥30 pF: Q≥ 1000	1.0 kHz ± 10% for cap > 1000 pF Voltage: 1.0Vrms ± .2V	
Insulation Resistance		100,000MΩ or 1000MΩ - µF, whichever is less	Charge device with rated voltage for 60 ± 5 secs @ room temp/humidity	
Dielectric Strength		No breakdown or visual defects	Charge device with 300% of rated voltage for 1-5 seconds, w/charge and discharge current limited to 50 mA (max) Note: Charge device with 150% of rated voltage for 500V devices.	
Resistance to Flexure Stresses	Appearance	No defects	Deflection: 2mm Test Time: 30 seconds	
	Capacitance Variation	±5% or ±.5 pF, whichever is greater		
	Q	Meets Initial Values (As Above)		
	Insulation Resistance	≥ Initial Value x 0.3		
Solderability		≥ 95% of each terminal should be covered with fresh solder	Dip device in eutectic solder at 230 ± 5°C for 5.0 ± 0.5 seconds	
Resistance to Solder Heat	Appearance	No defects, <25% leaching of either end terminal	Dip device in eutectic solder at 260°C for 60 seconds. Store at room temperature for 24 ± 2 hours before measuring electrical properties.	
	Capacitance Variation	≤ ±2.5% or ±.25 pF, whichever is greater		
	Q	Meets Initial Values (As Above)		
	Insulation Resistance	Meets Initial Values (As Above)		
	Dielectric Strength	Meets Initial Values (As Above)		
Thermal Shock	Appearance	No visual defects	Step 1: -55°C ± 2°	30 ± 3 minutes
	Capacitance Variation	≤ ±2.5% or ±.25 pF, whichever is greater	Step 2: Room Temp	≤ 3 minutes
	Q	Meets Initial Values (As Above)	Step 3: +125°C ± 2°	30 ± 3 minutes
	Insulation Resistance	Meets Initial Values (As Above)	Step 4: Room Temp	≤ 3 minutes
	Dielectric Strength	Meets Initial Values (As Above)	Repeat for 5 cycles and measure after 24 hours at room temperature	
Load Life	Appearance	No visual defects	Charge device with twice rated voltage in test chamber set at 125°C ± 2°C for 1000 hours (+48, -0). Remove from test chamber and stabilize at room temperature for 24 hours before measuring.	
	Capacitance Variation	≤ ±3.0% or ± .3 pF, whichever is greater		
	Q (C=Nominal Cap)	≥ 30 pF: Q≥ 350 ≥10 pF, <30 pF: Q≥ 275 +5C/2 <10 pF: Q≥ 200 +10C		
	Insulation Resistance	≥ Initial Value x 0.3 (See Above)		
	Dielectric Strength	Meets Initial Values (As Above)		
Load Humidity	Appearance	No visual defects	Store in a test chamber set at 85°C ± 2°C/ 85% ± 5% relative humidity for 1000 hours (+48, -0) with rated voltage applied. Remove from chamber and stabilize at room temperature for 24 ± 2 hours before measuring.	
	Capacitance Variation	≤ ±5.0% or ± .5 pF, whichever is greater		
	Q	≥ 30 pF: Q≥ 350 ≥10 pF, <30 pF: Q≥ 275 +5C/2 <10 pF: Q≥ 200 +10C		
	Insulation Resistance	≥ Initial Value x 0.3 (See Above)		
	Dielectric Strength	Meets Initial Values (As Above)		

C0G (NP0) Dielectric

Capacitance Range

PREFERRED SIZES ARE SHADED

SIZE	0201			0402			0603				0805					1206					
Soldering	Reflow Only			Reflow Only			Reflow Only				Reflow/Wave					Reflow/Wave					
Packaging	All Paper			All Paper			All Paper				Paper/Embossed					Paper/Embossed					
(L) Length MM (in.)	0.60 ± 0.03 (0.024 ± 0.001)			1.00 ± 0.10 (0.040 ± 0.004)			1.60 ± 0.15 (0.063 ± 0.006)				2.01 ± 0.20 (0.079 ± 0.008)					3.20 ± 0.20 (0.126 ± 0.008)					
(W) Width MM (in.)	0.30 ± 0.03 (0.011 ± 0.001)			0.50 ± 0.10 (0.020 ± 0.004)			0.81 ± 0.15 (0.032 ± 0.006)				1.25 ± 0.20 (0.049 ± 0.008)					1.60 ± 0.20 (0.063 ± 0.008)					
(t) Terminal MM (in.)	0.15 ± 0.05 (0.006 ± 0.002)			0.25 ± 0.15 (0.010 ± 0.006)			0.36 ± 0.15 (0.014 ± 0.006)				0.50 ± 0.25 (0.020 ± 0.010)					0.50 ± 0.25 (0.020 ± 0.010)					
WVDC	10	16	25	16	25	50	6.3	25	50	100	16	25	50	100	200	16	25	50	100	200	500
Cap (pF) 0.5			A	C	C	C	G	G	G	G	J	J	J	J	J	J	J	J	J	J	J
1.0			A	C	C	C	G	G	G	G	J	J	J	J	J	J	J	J	J	J	J
1.2			A	C	C	C	G	G	G	G	J	J	J	J	J	J	J	J	J	J	J
1.5	A	A	A	C	C	C	G	G	G	G	J	J	J	J	J	J	J	J	J	J	J
1.8	A	A	A	C	C	C	G	G	G	G	J	J	J	J	J	J	J	J	J	J	J
2.2	A	A	A	C	C	C	G	G	G	G	J	J	J	J	J	J	J	J	J	J	J
2.7	A	A	A	C	C	C	G	G	G	G	J	J	J	J	J	J	J	J	J	J	J
3.3	A	A	A	C	C	C	G	G	G	G	J	J	J	J	J	J	J	J	J	J	J
3.9	A	A	A	C	C	C	G	G	G	G	J	J	J	J	J	J	J	J	J	J	J
4.7	A	A	A	C	C	C	G	G	G	G	J	J	J	J	J	J	J	J	J	J	J
5.6	A	A	A	C	C	C	G	G	G	G	J	J	J	J	J	J	J	J	J	J	J
6.8	A	A	A	C	C	C	G	G	G	G	J	J	J	J	J	J	J	J	J	J	J
8.2	A	A	A	C	C	C	G	G	G	G	J	J	J	J	J	J	J	J	J	J	J
10	A	A	A	C	C	C	G	G	G	G	J	J	J	J	J	J	J	J	J	J	J
12	A	A	A	C	C	C	G	G	G	G	J	J	J	J	J	J	J	J	J	J	J
15	A	A	A	C	C	C	G	G	G	G	J	J	J	J	J	J	J	J	J	J	J
18	A	A	A	C	C	C	G	G	G	G	J	J	J	J	J	J	J	J	J	J	J
22	A	A	A	C	C	C	G	G	G	G	J	J	J	J	J	J	J	J	J	J	J
27	A	A	A	C	C	C	G	G	G	G	J	J	J	J	J	J	J	J	J	J	J
33	A	A	A	C	C	C	G	G	G	G	J	J	J	J	J	J	J	J	J	J	J
39	A	A	A	C	C	C	G	G	G	G	J	J	J	J	J	J	J	J	J	J	J
47	A	A	A	C	C	C	G	G	G	G	J	J	J	J	J	J	J	J	J	J	J
56	A	A	A	C	C	C	G	G	G	G	J	J	J	J	J	J	J	J	J	J	J
68	A	A	A	C	C	C	G	G	G	G	J	J	J	J	J	J	J	J	J	J	J
82	A	A	A	C	C	C	G	G	G	G	J	J	J	J	J	J	J	J	J	J	J
100	A	A	A	C	C	C	G	G	G	G	J	J	J	J	J	J	J	J	J	J	J
120				C	C	C	G	G	G	G	J	J	J	J	J	J	J	J	J	J	J
150				C	C	C	G	G	G	G	J	J	J	J	J	J	J	J	J	J	J
180				C	C	C	G	G	G	G	J	J	J	J	J	J	J	J	J	J	J
220				C	C	C	G	G	G	G	J	J	J	J	J	J	J	J	J	J	M
270							G	G	G	G	J	J	J	J	M	J	J	J	J	J	M
330							G	G	G	G	J	J	J	J	M	J	J	J	J	J	M
390							G	G	G		J	J	J	J	M	J	J	J	J	J	M
470							G	G	G		J	J	J	J	M	J	J	J	J	J	M
560							G	G	G		J	J	J	J	M	J	J	J	J	J	M
680							G	G	G		J	J	J	J		J	J	J	J	J	P
820							G	G	G		J	J	J	J		J	J	J	J	M	
1000							G	G	G		J	J	J	J		J	J	J	J	Q	
1200											J	J	J			J	J	J	J	Q	
1500											J	J	J			J	J	J	M	Q	
1800											J	J	J			J	J	M	M		
2200											J	J	M			J	J	M	P		
2700											J	J	M			J	J	M	P		
3300																J	J	M	P		
3900																J	J	M	P		
4700																J	J	M	P		
5600																J	J	M			
6800																M	M				
8200																M	M				
Cap (µF) 0.010																M	M				
0.012																					
0.015																					
0.018																					
0.022																					
0.027																					
0.033																					
0.039																					
0.047																					
0.068																					
0.082																					
0.1																					
WVDC	10	16	25	16	25	50	6.3	25	50	100	16	25	50	100	200	16	25	50	100	200	500
SIZE	0201			0402			0603				0805					1206					

Letter	A	C	E	G	J	K	M	N	P	Q	X	Y	Z
Max. Thickness	0.33 (0.013)	0.56 (0.022)	0.71 (0.028)	0.86 (0.034)	0.94 (0.037)	1.02 (0.040)	1.27 (0.050)	1.40 (0.055)	1.52 (0.060)	1.78 (0.070)	2.29 (0.090)	2.54 (0.100)	2.79 (0.110)
	PAPER					EMBOSSED							

C0G (NP0) Dielectric

Capacitance Range

PREFERRED SIZES ARE SHADED

SIZE	1210					1812					1825			2220			2225		
Soldering	Reflow Only					Reflow Only					Reflow Only			Reflow Only			Reflow Only		
Packaging	Paper/Embossed					All Embossed					All Embossed			All Embossed			All Embossed		
(L) Length MM (in.)	3.20 ± 0.20 (0.126 ± 0.008)					4.50 ± 0.30 (0.177 ± 0.012)					4.50 ± 0.30 (0.177 ± 0.012)			5.70 ± 0.40 (0.225 ± 0.016)			5.72 ± 0.25 (0.225 ± 0.010)		
(W) Width MM (in.)	2.50 ± 0.20 (0.098 ± 0.008)					3.20 ± 0.20 (0.126 ± 0.008)					6.40 ± 0.40 (0.252 ± 0.016)			5.00 ± 0.40 (0.197 ± 0.016)			6.35 ± 0.25 (0.250 ± 0.010)		
(t) Terminal MM (in.)	0.50 ± 0.25 (0.020 ± 0.010)					0.61 ± 0.36 (0.024 ± 0.014)					0.61 ± 0.36 (0.024 ± 0.014)			0.64 ± 0.39 (0.025 ± 0.015)			0.64 ± 0.39 (0.025 ± 0.015)		
WVDC	25	50	100	200	500	25	50	100	200	500	50	100	200	50	100	200	50	100	200
Cap (pF) 0.5																			
1.0																			
1.2																			
1.5																			
1.8																			
2.2																			
2.7																			
3.3																			
3.9																			
4.7																			
5.6																			
6.8																			
8.2																			
10					J														
12					J														
15					J														
18					J														
22					J														
27					J														
33					J														
39					J														
47					J														
56					J														
68					J														
82					J														
100					J														
120					J														
150					J														
180					J														
220					J														
270					J														
330					J														
390					M														
470					M														
560	J	J	J	J	M														
680	J	J	J	J	M														
820	J	J	J	J	M														
1000	J	J	J	J	M	K	K	K	K	M	M	M	M				M	M	P
1200	J	J	J	M		K	K	K	K	M	M	M	M				M	M	P
1500	J	J	J	M		K	K	K	K	M	M	M	M				M	M	P
1800	J	J	J	M		K	K	K	K	M	M	M	M				M	M	P
2200	J	J	J	Q		K	K	K	K	P	M	M	M				M	M	P
2700	J	J	J	Q		K	K	K	P	Q	M	M	M				M	M	P
3300	J	J	J			K	K	K	P	Q	M	M	M			X	M	M	P
3900	J	J	M			K	K	K	P	Q	M	M	M			X	M	M	P
4700	J	J	M			K	K	K	P	Q	M	M	M	X	X	X	M	M	P
5600						K	K	M	P	X	M	M	M	X	X	X	M	M	P
6800						K	K	M	X		M	M	M	X	X	X	M	M	P
8200						K	M	M			M	M		X	X	X	M	M	P
Cap (µF) 0.010						K	M	M			M	M		X	X	X	M	M	P
0.012						K	M				M	M		X	X	X	M	M	P
0.015						M	M				M	M		X	X	X	M	M	Y
0.018						M	M				P	M		X	X	X	M	M	Y
0.022						M	M				P			X	X		M	Y	Y
0.027														X	X		P	Y	Y
0.033														X	X				
0.039																			
0.047																			
0.068																			
0.082																			
0.1																			
WVDC	25	50	100	200	500	25	50	100	200	500	50	100	200	50	100	200	50	100	200
SIZE	1210					1812					1825			2220			2225		

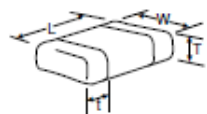| Letter	A	C	E	G	J	K	M	N	P	Q	X	Y	Z
Max. Thickness	0.33 (0.013)	0.56 (0.022)	0.71 (0.028)	0.86 (0.034)	0.94 (0.037)	1.02 (0.040)	1.27 (0.050)	1.40 (0.055)	1.52 (0.060)	1.78 (0.070)	2.29 (0.090)	2.54 (0.100)	2.79 (0.110)
	PAPER					EMBOSSED							

H.3. Chip Inductor – 0402 CS Series (1005) from Coilcraft

Chip Inductors - 0402CS Series (1005)

Continuing in our long tradition of innovation and leadership, Coilcraft introduced the industry's first 0402 wirewound inductor.

This series shares all of the characteristics of Coilcraft's other ceramic inductors: exceptionally high Q factors, especially at use frequencies; outstanding self-resonant frequency; tight inductance tolerance; and excellent batch-to-batch consistency.

Coilcraft **Designer's Kits C128A** and **C128B** contain samples of 5% inductance tolerance parts. Kits with 2% tolerance are also available. To order, contact Coilcraft or visit **http://order.coilcraft.com**.

Terminal wraparound: approx 0.007/0,18 both ends
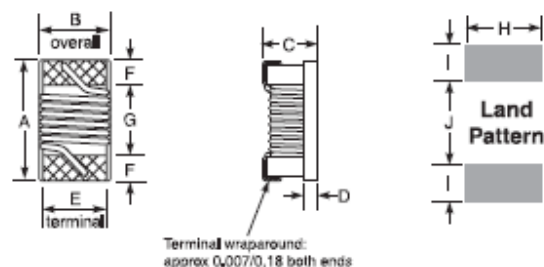
A max	B max	C max	D ref	E	F	G	H	I	J
0.047	0.025	0.026	0.010	0.020	0.009	0.022	0.026	0.014	0.018
1,19	0,64	0,66	0,25	0,51	0,23	0,56	0,66	0,36	0,46

Parts/reel: 7" 2000   Tape width: 8 mm
For packaging data see Tape and Reel Specifications section.

TYPICAL L vs FREQUENCY

Inductance (nH) vs Frequency (MHz)

27 nH
19 nH
12 nH
5.6 nH
1 nH

TYPICAL Q vs FREQUENCY

Q Factor vs Frequency (MHz)

12 nH
5,6 nH
19 nH
27 nH
1 nH
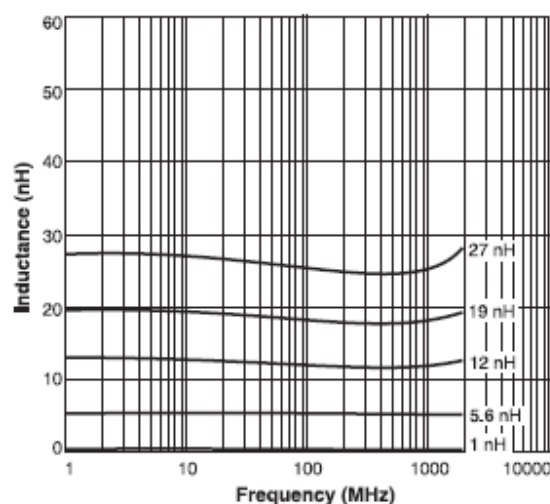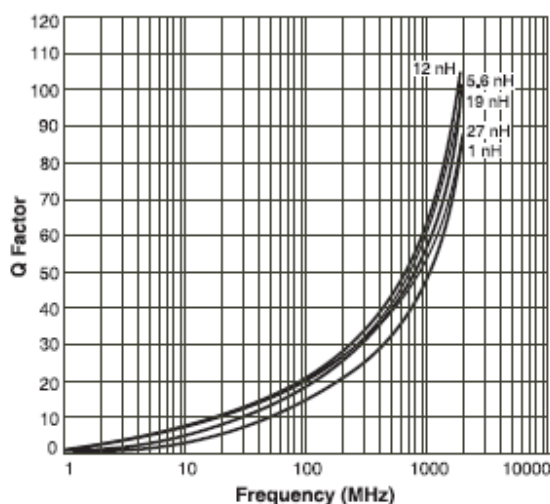
0402CS Series (1005)

Part number[1]	Inductance[2] (nH)	Percent tolerance[3]	Q min[4]	SRF min[5] (MHz)	DCR max[6] (Ohms)	I_{DC} max[7] (mA)	900 MHz		1.7 GHz	
							L typ	Q typ	L typ	Q typ
0402CS-1N0X_B_	1.0	10,5	16	>6000	0.045	1360	1.02	77	1.02	69
0402CS-1N9X_B_	1.9	10,5	16	>6000	0.070	1040	1.72	68	1.74	82
0402CS-2N0X_B_	2.0	10,5	16	>6000	0.070	1040	1.93	54	1.93	75
0402CS-2N2X_B_	2.2	10,5	19	>6000	0.070	960	2.19	59	2.23	100
0402CS-2N4X_B_	2.4	10,5	15	>6000	0.068	790	2.24	51	2.27	68
0402CS-2N7X_B_	2.7	10,5	16	>6000	0.120	640	2.23	42	2.25	61
0402CS-3N3X_B_	3.3	10,5,2	19	>6000	0.066	840	3.10	65	3.12	87
0402CS-3N6X_B_	3.6	10,5,2	19	>6000	0.066	840	3.56	45	3.62	71
0402CS-3N9X_B_	3.9	10,5,2	19	5800	0.066	840	3.89	50	4.00	75
0402CS-4N3X_B_	4.3	10,5,2	18	>6000	0.091	700	4.19	47	4.30	71
0402CS-4N7X_B_	4.7	10,5,2	15	4775	0.130	640	4.55	48	4.68	68
0402CS-5N1X_B_	5.1	10,5,2	20	4800	0.083	800	5.15	56	5.25	82
0402CS-5N6X_B_	5.6	10,5,2	20	4800	0.083	760	5.16	54	5.28	81
0402CS-6N2X_B_	6.2	10,5,2	20	4800	0.083	760	6.16	52	6.37	76
0402CS-6N8X_B_	6.8	10,5,2	20	4800	0.083	680	6.56	63	6.93	78
0402CS-7N5X_B_	7.5	10,5,2	22	4800	0.10	680	7.91	60	8.22	88
0402CS-8N2X_B_	8.2	10,5,2	22	4400	0.10	680	8.50	57	8.85	84
0402CS-8N7X_B_	8.7	10,5,2	18	4100	0.20	480	8.78	54	9.21	73
0402CS-9N0X_B_	9.0	10,5,2	22	4160	0.10	680	9.07	62	9.53	78
0402CS-9N5X_B_	9.5	10,5,2	18	4000	0.20	480	9.42	54	9.98	69
0402CS-10NX_B_	10.0	10,5,2	21	3900	0.20	480	9.8	50	10.10	67
0402CS-11NX_B_	11.0	10,5,2	24	3680	0.12	640	10.7	52	11.20	78
0402CS-12NX_B_	12.0	10,5,2	24	3600	0.12	640	11.9	53	12.70	71
0402CS-13NX_B_	13.0	10,5,2	24	3450	0.21	440	13.4	51	14.63	57
0402CS-15NX_B_	15.0	10,5,2	24	3280	0.17	560	14.6	55	15.50	77
0402CS-16NX_B_	16.0	10,5,2	24	3100	0.22	560	16.6	46	18.86	47
0402CS-18NX_B_	18.0	10,5,2	25	3100	0.23	420	18.3	57	20.28	62
0402CS-19NX_B_	19.0	10,5,2	24	3040	0.20	480	19.1	50	21.10	67
0402CS-20NX_B_	20.0	10,5,2	25	3000	0.25	420	20.7	52	23.66	53
0402CS-22NX_B_	22.0	10,5,2	25	2800	0.30	400	23.2	53	26.75	53
0402CS-23NX_B_	23.0	10,5,2	22	2720	0.30	400	23.8	49	26.90	64
0402CS-24NX_B_	24.0	10,5,2	25	2700	0.30	400	25.1	51	29.50	50
0402CS-27NX_B_	27.0	10,5,2	24	2480	0.30	400	28.7	49	33.50	63
0402CS-30NX_B_	30.0	10,5,2	25	2350	0.30	400	31.1	46	38.50	39
0402CS-33NX_B_	33.0	10,5,2	24	2350	0.30	400	34.9	31	41.74	32
0402CS-36NX_B_	36.0	10,5,2	24	2320	0.44	320	39.5	44	48.40	53
0402CS-39NX_B_	39.0	10,5,2	25	2100	0.55	200	41.7	47	50.23	45
0402CS-40NX_B_	40.0	10,5,2	24	2240	0.44	320	39.0	44	47.40	33
0402CS-43NX_B_	43.0	10,5,2	25	2030	0.81	100	45.8	46	61.55	34
0402CS-47NX_B_	47.0	10,5,2	20	2100	0.83	150	50.0	38	–	–
0402CS-51NX_B_	51.0	10,5,2	25	1750	0.82	100	56.6	40	–	–
0402CS-56NX_B_	56.0	10,5,2	22	1760	0.97	100	62.8	42	–	–
0402CS-68NX_B_	68.0	10,5,2	22	1620	1.12	100	78.19	36	–	–

1. When ordering, please specify tolerance and packaging codes:

Inductance tolerance code:
Table above shows stock tolerances in bold.
G= ±2%, J= ±5%, K= ±10%

0402CS-68NX_B_

Packaging code:
W= 7" machine-ready reel   EIA RS-481 punched paper tape. 2000 per full reel.
U= Less than full reel   Not machine ready. May be on multiple reels. To have a leader and a trailer added ($25 charge), use code letter W instead.

2. Inductance measured at 250 MHz using Agilent/HP16193 test fixture in Agilent/HP4286 impedance analyzer with Coilcraft-provided correlation pieces. For recommended test procedures, contact Coilcraft.
3. Tolerances in bold are stocked for immediate shipment.
4. Q measured using Agilent/HP4291A with Agilent/HP16193 test fixture.
5. SRF measured using Agilent/HP8753D network analyzer and Coilcraft SMD-D test fixture.
6. DCR measured on micro-ohmmeter.
7. For 15°C rise.
8. Operating temperature range –40°C to +125°C.
9. Electrical specifications at 25°C.
10. For environmental data see Product Specifications section.
11. For part marking data see Color Coding section.

H.4. Varactor Diodes – from Microsemi

H.4.1. MV31009-150A

Varactor Calculator

MDT Varactor Part Number MV31009 ▾   Package Style M46   Package Capacitance **0.100** pf

Note: P2713 is the package for flip chips:
MV39001,MV39002, and MV39003.

Varactor Specifications		Calculations			Reverse Voltage	Ct
Gamma	1.25	Cj@0V	21.882 pF		V	pF
Ct@4V	3.6 pF	Rs@4V	0.455 Ω (Derived from varactor Q)		0	21.982
Vb@10uA	15 V	Ct2V/Ct12V	5.470		1	10.358
Q@50MHz,4V	2000				2	6.521
					3	4.671
					4	3.600
					5	2.909
					6	2.430
					7	2.081
					8	1.815
					9	1.608
					10	1.441
					11	1.305
					12	1.192
					13	1.097
					14	1.016
					15	0.946

Total Capacitance vs Reverse Voltage

(Graph: Total Capacitance(pF) on y-axis from 0.0 to 25.0; Reverse Voltage(V) on x-axis from 0 to 15)

H.4.2. MV34003-150A

Varactor Calculator

MDT Varactor Part Number MV34003   Package Style M46   Package Capacitance **0.100** pf

Varactor Specifications		Calculations		Note: P2713 is the package for flip chips:
Gamma	1.5	Cj@0V	15.335 pF	MV39001,MV39002, and MV39003.
Ct@4V	1.8 pF	Rs@4V	0.749 Ω (Derived from varactor Q)	Reverse Voltage
Vb@10uA	15 V	Ct2V/Ct12V	6.960	
Q@50MHz,4V	2500			

Reverse Voltage	Ct
V	pF
0	15.435
1	6.278
2	3.622
3	2.442
4	1.800
5	1.406
6	1.143
7	0.958
8	0.822
9	0.719
10	0.638
11	0.573
12	0.520
13	0.477
14	0.440
15	0.409